Tailor made organic molecules for electronic applications

Inauguraldissertation

zur

Erlangung der Würde eines Doktors der Philosophie

vorgelegt der

Philosophisch-Naturwissenschaftlichen Fakultät

der Universität Basel

Von

Manuel Hellstern

aus Basel (BS), Schweiz

Basel, 2019

Genehmigt von der Philosophisch-Naturwissenschaftlichen Fakultät

auf Antrag von

Prof. Dr. Marcel Mayor

Prof. Dr. Oliver Wenger

Basel, den 17. Oktober 2017

<div align="right">

Prof. Dr. Martin Spiess

Dekan

</div>

Acknowledgments

Summary

Within this thesis, the synthesis of functional molecules with specific characteristics and a wide application spectrum was of major interest. Due to the nature of their applications, it is rather difficult to categorize all the designed molecules within one general topic. For the purpose of a clearly represented structure, this work is divided in three individual chapters, each treating one independent topic by its own introduction, synthetic strategy, results and conclusion.

Chapter 1 - Surface Functionalization
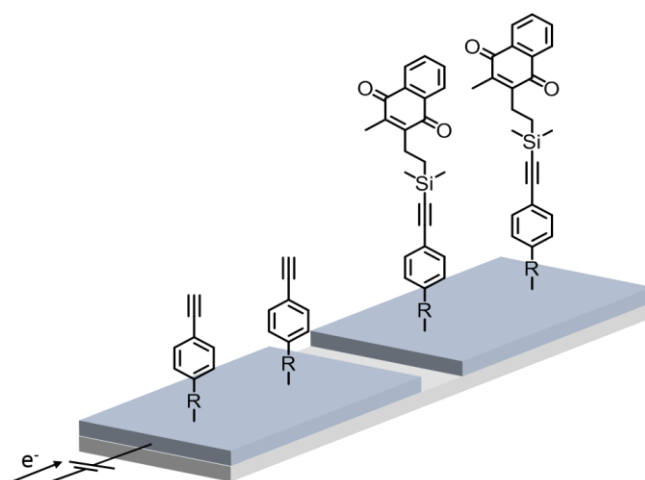
Protection groups for alkynes, representing structural building blocks in various chemical applications, are sensitive to a fluoride source or basic conditions. The synthetic accessibility and efficient functionalization by click chemistry of the alkyne moiety makes them interesting target structures in surface functionalization approaches. A main challenge is the site-selective functionalization of a surface. To address this challenge, an electrochemically cleavable protecting group for alkynes was developed. The immobilization of the designed molecules on TiO_2 surfaces was achieved with an EDTA based anchoring group, linked by a phenyl ethylene moiety to the protected alkyne. Upon reduction of the naphthoquinone based protecting group, an intramolecular ring formation forces the release of the alkyne moiety, which remains immobilized on the TiO_2 surface. The site-selectivity was achieved by dividing a wafer into electronically separated sections. By applying a potential of -0.9 V vs. SCE on individual areas of the wafer, selective deprotection was achieved. The received free alkyne moieties were further functionalized with naphthalene diimide based azide dyes by copper catalyzed 1,3-dipolar Huisgen cycloaddition reactions. To confirm the individual steps of the procedure, solid-state UV-Vis measurements were performed.

Chapter 2 - Molecular Wires

The scientific challenge to build electronic circuits by bottom-up approaches in a nanometer scale appealed generation of chemists. With organic synthetic techniques, an atomic precision in the structural design is achievable and enables the creation of identical molecules in large quantities. The understanding of structural and electronical characteristics and their influences on the behavior of molecules in electronic circuits has risen during the last decade. As consequence, molecules acting as molecular wires, rectifiers, switches or memory elements have been developed.

Most of the conformation effects contributing to the conductivity of molecular wires were investigated with rather short molecules. By elongate the molecular wires, a change in the transport mechanism was reported in literature from a tunneling to a hopping process. Therefore, new molecules were designed with a length within the determined mechanism changing range. The molecular design was based on already investigated biphenyl structures with defined inter-plane angles, to determine if the same conformation effects were observable in the elongated analogues.
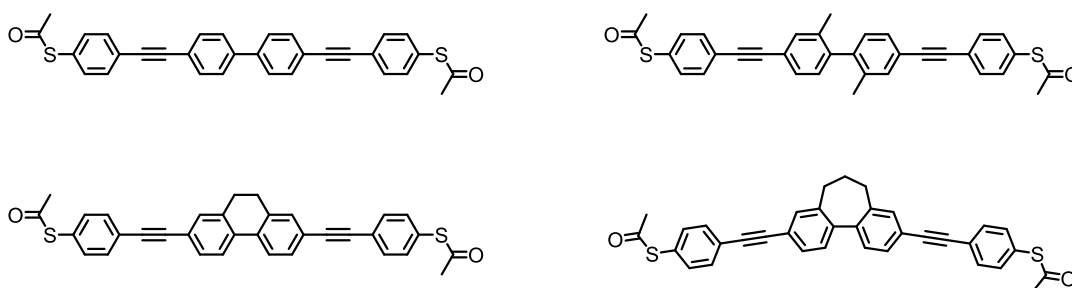
The second part of this chapter is based on an earlier study with a bipyridyl derivative[1], which has shown a switch between an "on" state of higher conductance and "off" state with lower conductance in break junction measurements. The switching was achieved by applying a positive or negative voltage in the range of ± 0.9 V. The state of the molecule was readable by the conductance difference of both states at an applied potential, lower than the required switching potential. To further investigate this phenomenon, biphenyl derivatives with electron withdrawing and electron donating moieties were synthesized. The resulting intrinsic dipole moment of the molecules is considered crucial for the switching behavior.
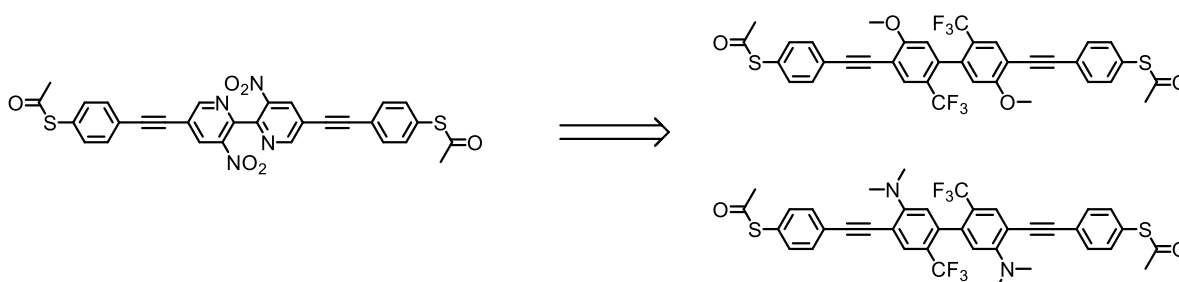
Chapter 3 - High-Triplet State Energy Materials

Used as building blocks for organic light emitting diodes (OLED), 4,4'-dicarbazole-1,1'-biphenyl (CBP) derivatives are of major interest in the field of electrophosphorescence.[2] Carbazole moieties in CBP provide a high triplet energy state and thereby enable the use as matrix materials with an efficient energy transfer to a phosphorescence light emitting dye.[3] For an efficient triplet energy transfer, especially for deep blue light emitting dyes, the triplet energy state of the matrix material should be higher than 2.7 eV.
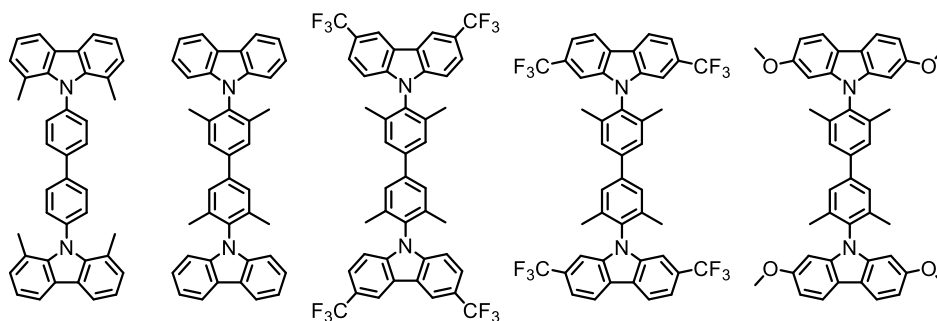
Five new CBP derivatives were synthesized by introducing sterically demanding substituents to the carbazole subunit in 1,8-position or to the biphenyl backbone. With these modifications, a perpendicular alignment between the carbazole subunit and the biphenyl backbone was achieved, resulting in a decreased π-conjugation through the molecule and therefore an increased triplet state energy. Furthermore, by introducing electron withdrawing and electron donating groups at the carbazole subunit, a shift of the HOMO / LUMO level was achieved.[4]

Table of Contents

Chapter 1 - Surface Functionalization

Introduction

Surface Modification

Surface modification is an enormous topic with a countless amount of different applications. It is used in a wide scope of applications from chemical, electronical to biomedical aspects or even in textile, automotive and constructions industries. The techniques, used to obtain the desired properties of the surface, are highly diverse. Therefore, we can categorize different surface modifications based on the used techniques. A major difference exists between the top down processes of roughening or patterning an original structure and chemical / physical modifications and further functionalization by attaching suitable molecules.[5]
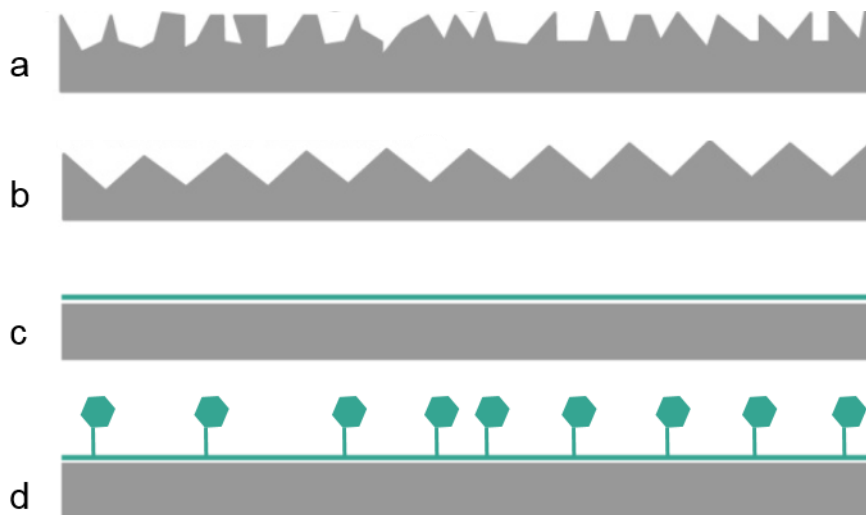
Figure 1. Schematic illustration of surface roughening (a), patterning (b), chemical modification (c), and attaching functional molecules (d).

During the latter two processes, a new layer is deposited on top of a surface to alter the surface characteristics. Examples for the chemical modifications include chemical vapor deposition (CVD), physical vapor deposition (PVD), adsorption from solution or vapor-phase adsorption.[6] Chemical modification can further be distinguished in the binding mode of the molecules on the surface, from adsorption to covalently bound molecules. However, the distinctions are diffuse and a clear assignment is difficult in some cases. For our work, the modification by chemisorption from a solution is of mayor interest. This technique is mainly used to form self-assemble mono layers (SAM). SAMs are the spontaneous assembly of molecules in repetitive arrays on a surface.[7,8] The molecules consist of a head group with a specific affinity for the particular surface. One of the most investigated SAMs are alkanethiols, absorbed on different

metal surfaces, such as gold,[9,10] silver[11,12] and platinum[13] among others. Other common SAM formation schemes are based on carboxylic or phosphoric acid groups interacting with metal oxide surfaces[14–16] and silicon based interaction on silica.[17,18]

Aside from the head group and its responsibility for the binding to the surface, the organic molecules used for the modification of surfaces consist on two additional parts: a terminal functional group and in between, a spacer as connection to the head group.[8] The terminal functional group determines the obtained surface characteristics after the SAM formation or presents functional groups for further functionalization. A variety of surface terminal groups including alkyl,[7,15] amino,[19,20] azide[21–23] and alkyne[21–23] functionalities can be designed by this approach. Thereby obtained functionality can be used for further functionalization by chemical reactions and allows the attachment of almost every thinkable molecule to the surface.

Click Chemistry based Surface Functionalization

A major tool in the surface functionalization is the "click chemistry". The term click chemistry is commonly used for an azide-alkyne 1,3-dipolar cycloaddition. Originally, click chemistry was introduced to the chemical world by Hartmuth C. Kolb, M. G. Finn and K. Barry Sharpless in their review article 2001 about the future of the natural product synthesis and active pharmaceutical ingredient research.[24] The vision behind the concept of a new reaction-type was to overcome existing problems in the natural products synthesis, which were based on imitating carbonyl-based chemistry to from new C-C bonds as found in natural bio-synthesis. The authors defined several criteria to be fulfilled by this reactions as *be modular*, *wide in scope*, give *very high yields*, generate only *inoffensive byproducts,* and be *stereospecific*. To achieve these requirements, a high thermodynamic driving force usually higher than 20 kcal/mol is necessary. This represents a tremendous increase compared to typical aldol reactions, which are often energetically favored by less than 3 kcal/mol.[25] Next to the mentioned 1,3-dipolar cycloaddition, Diels-Alder reactions, nucleophilic substitutions mainly focused on strained-ring opening, and oxidation of unsaturated carbon-carbon bonds are included in the term of "click chemistry" to name the most important.

From a surface functionalization point of view, the Huisgen dipolar cycloaddition of azides and alkynes[26,27] are of huge interest. The advantages rely on several points: (i) often quantitative yields, (ii) a high tolerance of functional groups, (iii) an insensitivity of the reaction to solvents and (iv) reaction at various types of interfaces, such as solid/liquid, liquid/liquid or solid/solid inferfaces.[24,28,29] The purely thermal 1,3-dipolar cycloaddition was not stereospecific regarding the 1,4-triazole and the 1,5-triazole formation and the high activation barrier (for instance 105

2

kJ/mol for the reaction between methylazide and propyne[30]) demands for increased reaction temperatures.[31] Independently, the research groups of Fokin and Sharpless[32], and of Meldal[33] developed an Cu(I) catalyzed mechanism. The metal salt catalyzed 1,3-dipolar cycloaddition enables the reaction at room temperature and in a stereo specific manner. Beside the most important Cu(I), other less efficient catalyst are used including Pd^{2+}, Ni^{2+}, Pt^{2+} [34]34 and Au^{2+} salts.[34,35] This improvement was critical and led to a broad application of the Cu(I)-Catalyzed Azide-Alkynes Cycloaddition (CuAAC), not only in surface functionalization, but as well in organic chemistry and for drug discovery and bio labeling.

Huisgen's 1,3-dipolar cycloaddition
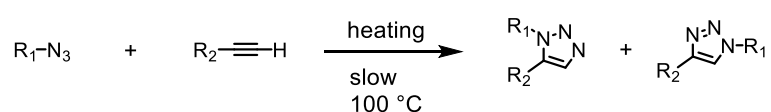
CuAAC reaction
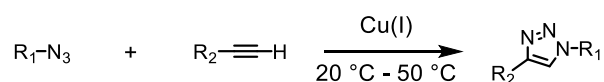
Figure 2. The Huisgen's 1,3-dipolar cycloaddition is depended on high temperatures and is not stereospecific. The Cu(I)-Catalyzed Azide-Alkynes Cycloaddition results only in the 1,4-triazole product and proceeds at moderate temperatures.

For the use of the CuAAC in surface functionalization approaches, the high reactivity in heterogeneous reaction systems is crucial.[28] The first example of a SAM further functionalized by a CuAAC reaction was described by Collman et al.[22] in 2004. The azido-functional SAM was obtained by the adsorption of a mixture containing 11-azidoundecanthiol and undecanethiol on a gold surface. The click reaction was performed in a 2:1 mixture of water and methanol and Cu(II)SO$_4$ / sodium ascorbate was used as catalytic system. A ferrocene-alkyne was used for the functionalization and an almost quantitative conversion was observed.
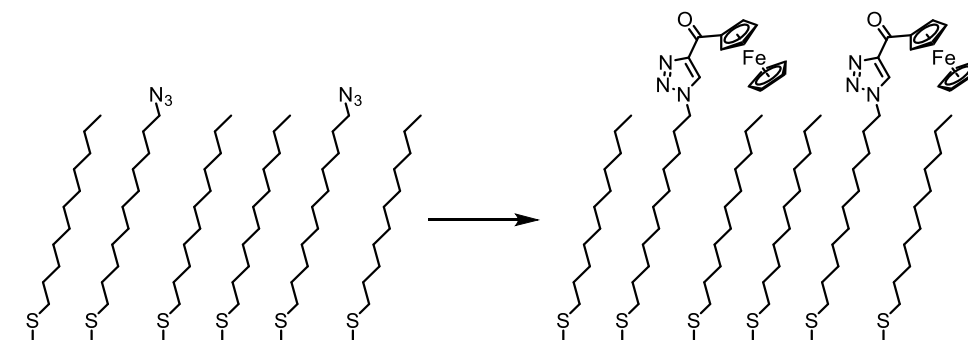
Figure 3. First surface functionalization by click chemistry. A SAM provided the azide functionality for the CuAAC with a ferrocene-alkyne.

Since this first successful functionalization of a SAM modified surface, several additional approaches were published. Some highlights are shown in **table 1**. Gold is still the most used surface due to the well-understood gold-thiol interaction. However, SiO$_2$ and Si(111) surfaces were successfully modified with an azide or alkyne terminal group and further functionalized.

Table 1. Example of SAM's functionalized by click chemistry.

Entry	Surface	Surface Structure	Catalytic System	Reference
1	Au	⌇S−(CH$_2$)$_{11}$−N$_3$	CuSO$_4$ · H$_2$O /sodium ascorbate / H$_2$O/ EtOH	Collman *et al.*[22]
2	SiO$_2$	⌇Si−(CH$_2$)$_4$−N$_3$	Thermal / 70 °C / neat	Lummerstorfer *et al.*[36]
3	Au	⌇Si−(CH$_2$)$_{11}$−(OCH$_2$CH$_2$)$_3$O⟍	CuSO$_4$ · H$_2$O / sodium ascorbate / H2O/ EtOH	Lee *et al.* [37]
4	Au	⌇S−(CH$_2$)$_4$−N$_3$	CuSO$_4$ · H$_2$O / sodium ascorbate, (Ph$_3$)$_3$Cu(I)Br / H$_2$O/ EtOH	Zirbs *et al.*[38]
5	SiO$_2$	⌇O-Si−(CH$_2$)$_{11}$−N$_3$	No catalyst / RT	Rozkiewicz *et al.*[39]
6	Si(111)	⌇≡−H	CuSO$_4$ / sodium ascorbate / DMF / RT	Rohde *et al.* [40]
7	Porous Si	⌇⟋⟍≡	CuSO$_4$ / sodium ascorbate, MeCN / tris-buffer /pH = 8.0 / RT	Meng *et al.* [41]
8	Au	⌇S−(CH$_2$)$_{10}$−NH−C(O)≡	CuSO$_4$ · H$_2$O / sodium ascorbate / H$_2$O / EtOH	Zhang *et al.*[42]

Another advantage of the CuAAC for the surface functionalization is the readily access to azide or alkyne molecules. A large diversity of azide marker molecules are commercial available including fluorescent dyes, biotin-azide, desthiobiotin-azide, and polyethylene glycol chains. Especially biochemistry pushed for the use of azide functionalized biomolecules, like amino acids, nucleotides, nucleosides and monosaccharides. This diversity of azide reagents allows a wide scope of applications for the click chemistry in surface functionalization. An overview of specific application is shown in **table 2**. The use of water or polar solvents, not generating

4

offensive byproduct and a high selectivity are the main advantage for the field of biochemistry and allowed even the immobilization of proteins on surfaces (entry 5 and entry 6, **table 2**) or the fluorescence labeling of antibodies (entry 7**, table 2**). The modification of gold nanoparticles for example, is possible (entry 11, **table 2**).

Table 2. Overview of azide functionalized molecules and their application in surface functionalization by CuAAC.

Entry	Azide compound	Application	Ref
1	Galactosyl azide	Labelling oligonucleotides with carbohydrates	Moses et al.[43]
2	Toluoyl protected 1-azido-2-deoxyribofuranose	Coupling to nucleobase analogues as antiviral agents	Moses et al.[43]
3	Oligonucleotide –Azid-3'-Azidothymidin	Ligation of DNA	Moses et al.[43]
4	Biotin – PEG	Labeling of molecules by affinity of biotin to streptavidin-FITC	Sun et al.[44]
5	(S-Tag)-Thrombomodulin-Azide	Immobilization of a protein on a surface	Sun et al.[44]
6	Green fluorescent protein	Control of site specifically surface functionalization	Lin et al. [45]
7	Antibody (rabbit IgG)- Z_{32}BPA	Fluorescent labeling of an antibody	Perols et al. [46]
8	Steroids	Synthesis of peptide and steroid conjugates	Echemendia et al.[47]
9	5-Fluorescein	Fluorescent labeling of DNA	Gramlich et al.[48]
10	Cyclodextrin	Porphyrin and Cyclodextrin Arrays	Liu et al. [49]
11	Au-Nanoparticles-Thiolalkylazid	Functionalization of Au Nanoparticles with fluorescence dye	Fleming et al.[50]

As shown in **table 2**, a broad diversity of azide compounds were used in CuAAC click chemistry. The readily available azide group has a high stability and is unaffected in a wide scope of reaction conditions. Therefore, it enables the synthesis of almost all molecular classes

functionalized with an azide group and thereby contributes to the success story of the CuAAC click chemistry in surface functionalization chemistry.

Site-Selective Functionalization of Surfaces

A drawback of the in solution chemical modification and functionalization of surfaces is the nature of the application technique. The surface is dipped into a solution or reaction mixture to obtain the desired effect, either the adsorption of molecules on the surface or a reaction with immobilized functional groups. Thereby, the entire surface is in contact with the same homogenous solution and it cannot be distinguished between different sections of the surface. So far, to achieve a selective modification or functionalization, physical techniques are necessary as for example photolithography.[51] In order to obtain a site-specific functionalization with an in solution chemical approach, it would be necessary to either immobilize different molecules on different sections of the surface or immobilize molecules with a protected reactive moiety and, primary to the functionalization, perform a site-selective deprotection.

Regarding the CuAAC click chemistry, either the alkyne or the azide group can be immobilized on the surface. For the azide functionality, no protecting group exists. The use of alkyl halogen or similar good leaving groups could be used to immobilize a masked azide moiety on the surface and install the azide by a simple S_N2 type reaction if desired. However, the site-selective conversion to the azide is so far not accessible without physical barriers to prevent the contact of the surface with the reaction solution on the unaddressed areas. A similar challenge reveals the inverse situation with the immobilized alkyne on the surface. Commonly used alkyne protecting groups are trialkyl silanes.[52] The deprotection proceeds by treatment with basic conditions or a fluoride source. The selective deprotection of defined parts on a surface remains challenging due to all-over contact of the surface with the reaction solution. To overcome this challenge, the used deprotection condition is not allowed to initiate the deprotection without an additional, site dependent impulse. Gchneidtner and Moth-Poulson published a strategy of a photolabile alkyne protecting group.[53] The combination of a tertiary propargyl alcohol with an *o*-nitrobenzyl alcohol resulted in the corresponding ether. This propargyl ether is stable under strong alkaline conditions in contrast to the alcohol where the free alkyne is released. Upon irradiation, the photolabile *o*-nitrobenzene forms the propargyl alcohol and it is further deprotected under strong alkaline conditions.

6
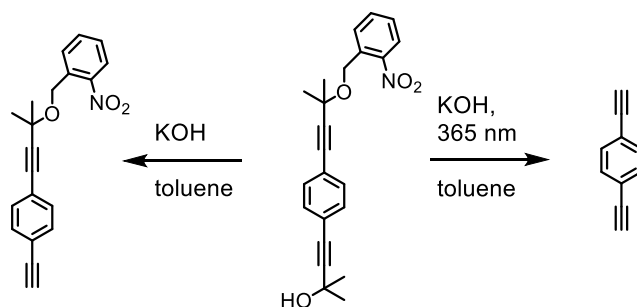
Figure 4. Photolabile alkyne protecting group based on the irradiation labile *o*-nitrobenzyl moiety.[53]

Next to the photolabile protecting groups, the deprotection can be initiated by electrochemistry. Due to the mild conditions of electrochemistry and the absence of strong offensive chemicals, an electrochemical deprotection attracted the scientific field for years. Example for the electrochemical deprotection are known for functional groups like alcohols[54,55], ketones[56], aldehydes[57], carboxylic acids[58], amines[59–61] and phosphoric acids[62]. The research group of Thompson immobilized a 1,4-dimethoxybenzene moiety by a phosphoric acid anchoring group on In_2O_3 nanowires.[63] After electrochemical reductive demethylation to the corresponding benzoquinone species, a functionalization by a 1,4-addition of a thiol-fluorescence marker was successfully demonstrated. Another example of electrochemical induced surface modification was shown by Jung and coworkers.[61] After immobilization of 3-(4-(phenyldiazonyl)-phenoxy)propane-1-thiol on a gold surface the azobenzene moiety was reduced to the hydroazobenzene and further decomposed to yield the free aniline functionality. The site-selective functionalization was achieved by a partial immersion of the wafer into the electrolyte solution.
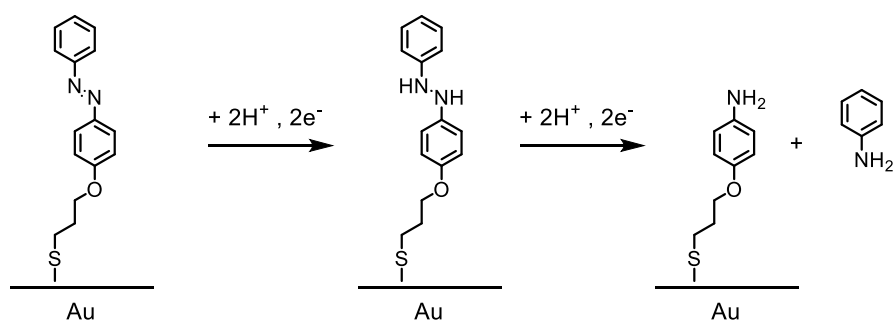
Figure 5. Electrochemical cleavage mechanism of the azobenzene moiety and release of the free aniline.

Aim of the Work

Functionalization of surfaces can be performed with different approaches. For example, synthesizing a molecule with the desired functionality installed is followed by the immobilization to obtain a homogenous layer. Another approach includes the use of a general building block for the immobilization process. In a subsequent step, this main building block can be further functionalized. For the latter approach, a readily functionalized reactive moiety has to be implemented on the core building block. As consequence of the anticipated high reactivity for the effective functionalization, this reactive moiety has to be protected during the immobilization step and deprotected ahead of the functionalization. Most of the deprotection methods in organic chemistry are based on the interaction with chemical reagents. Whereas the needed deprotection condition defines and excludes tolerated functional groups within the immobilized core building block, another challenge is the site-specific application. By performing chemistry in solution, all molecules immobilized of the surface get in contact with the reaction mixture for the deprotection of the reactive moiety, and therefore will be affected. A separation in different areas on the surface and a selective deprotection of a defined area is not possible by in solution chemistry without physically separating the areas by covering, walls or equal constructs.

The aim of this work was to develop a surface functionalization technique which allows a modular approach for the site-selective surface functionalization. The specification of the designed molecule has to fulfill the following requirements: (i) a strong adhesion to the surface, (ii) an effective deprotection mechanism under mild conditions, (iii) a deprotection mechanism for the site-specific deprotection of defined areas on the surface.

Regarding the immobilization of the molecules, a wide variety of surface - anchoring group combinations are known in literature. Therefore, our main focus was concentrated on the deprotection mechanism. The first inspiration was received by the work of Vasella and co-workers in 1995.[64]
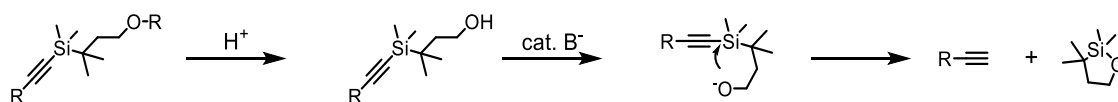
Scheme 1. Vasella's approach of a base labile acetylene protecting group. Upon deprotonation of the hydroxyl group, an intramolecular attack releases the alkyne by the formation of a five - membered 1,2-oxasilolane ring.[64]

The releasing mechanism is based on the concept of a Brook rearrangement.[65] After exposing the hydroxy group to a catalytic amount of base in an aprotic solvent, the intramolecular ring formation is induced. The nucleophilic attack of the deprotonated oxygen at the silicon atom

forms the five - membered ring and in a concerted mechanism, the silicon-acetylene bond breaks and releases the negative charged alkyne. The selectivity of the alkyne-silicon bond cleavage over the other three competing carbon-silicon bonds can be explained by the better stabilization of the negative charge on the sp-hybridized carbon atom. With the hydroxyl protecting group in place, the methyl groups at the silicon atom and at the alpha - carbon of the propyl chain increases the sterical hindrance for the deprotection under classical condition with K_2CO_3 in methanol. Vasella and co-worker showed the orthogonal deprotection in presence of a trimethylsilyl protected acetylene.[64]

Another inspiring work was published by Carpino *et al.*[66] After reducing of a quinone moiety to the correlating hydroquinone, an intramolecular lactone formation was used to release an alcohol or amine moiety. The reductive lactonization was performed using sodium dithionite in diethyl ether. Whereas the reduction proceeded instantaneously, the cyclization occurred with varying rates constants, taking between 15 min. and up to 4.25 hours.
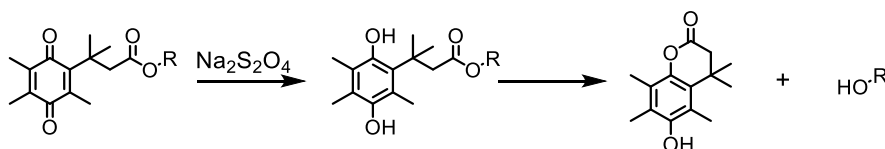
Scheme 2. Reduction of the quinone system to the hydroquinone induces the intramolecular lactone formation and release of the alcohol.

The combination of those two approaches published by Vasella and Carpino leads to the consequence of achieving an alkyne deprotection by electrochemistry. The concept of this project was to design a quinone system immobilized on a surface, which after site-selective electrochemical reduction performs a Brook type rearrangement and promotes the release of a free alkyne, as shown in **figure 6.**
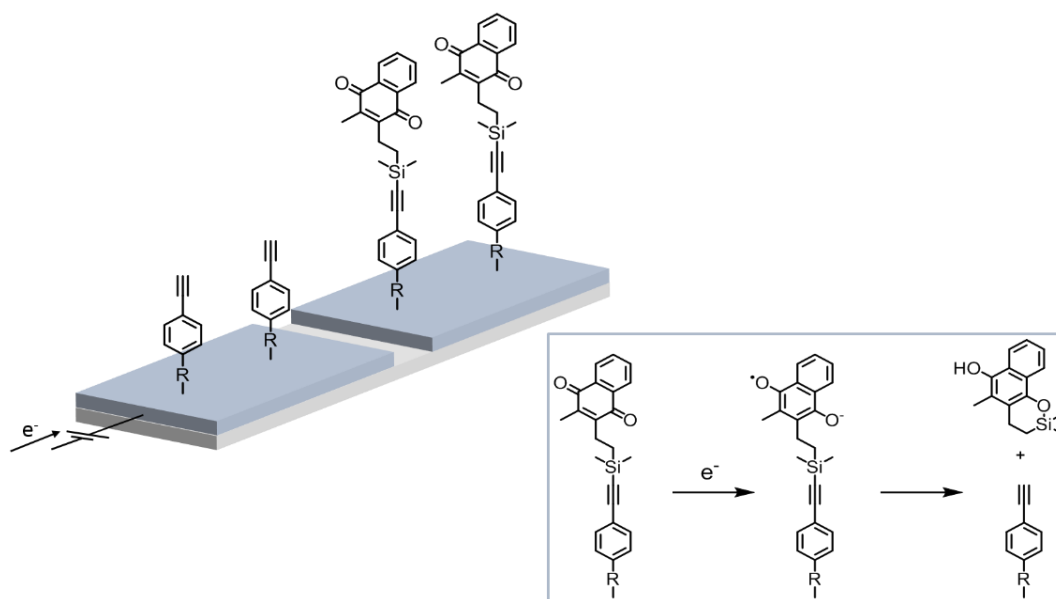
Figure 6. Schematic concept of the designed protecting group. By applying a potential to a selected area of the surface, the immobilized quinone is reduced and releases the free alkyne moiety.

For the electrochemical addressability of the system, the protected acetylene is chemisorbed on a conductive surface, and the whole acts as the working electrode. Electrically independent sections can be obtained by cutting through the conductive layer of the substrate, making them addressable sequentially. By applying a reductive potential on one of these sections, only the molecules immobilized in this area are addressed. Therefore, the reduction of the quinone and the subsequent acetylene release can only occur at molecules immobilized on the electrochemically addressed section, even the complete surface is within the electrolyte solution. Post deprotection, the released acetylene can be functionalized with a suitable azide-containing molecule by click chemistry. Repeating the deprotection and functionalization cycle, every section of the surface can be specifically functionalized in a modular approach.

A Test System in Solution

Molecular Design

To investigate the working principle of the alkyne deprotection by electrochemistry, a test system was designed to work first in solution. The fundamental part of the molecule was the quinone building block. The quinone moiety provides the key characteristic of transforming a non-nucleophilic group into a good nucleophile upon electrochemical reduction. Considering 1,4-benzoquinone, the free positions can be functionalized either to fine tune the redox potential and therefore to provide a mild and efficient electrochemical reduction or to reduce the reactivity of the highly reactive system.[67] All unfunctionalized positions of a 1,4-benzoquinone structure are activated for a 1,4-addition with soft nucleophiles.[68] Furthermore, spontaneous dimerization and Diels-Alder reaction are possible.[69] However, the redox potential of naphthoquinone derivatives are well documented and in a reasonable range with values lower than -1.0 V vs SCE.[70] As consequence Menadione (**5**, E° = -0.71 V/SCE in acetonitrile[71]) was chosen as quinone building block, providing a high chemical stability. For the concept of the release mechanism, it was crucial that the 1,4-naphthoquinone had to be linked by an ethyl bridge to the silicon atom, to obtain a six-membered ring after the intramolecular attack of the hydroquinone oxygen. The preorganized and thermodynamically favored six-membered ring[66] is the driving force for the irreversible nucleophilic attack and key step of the desired electrochemically induced alkyne release. As part of the protected alkyne in the test system, 4-*tert*-butylphenylacetylene (**4**) was selected. The commercial available building block has a high chemical stability due to a lack of additional functional groups and allows an effective deprotonation to form the alkyne - silicon bond. Additionally, the small building block is readily detectable after deprotection by several analytical techniques like TLC, GCMS, NMR-, and UV-Vis- spectroscopy to confirm a successful deprotection.
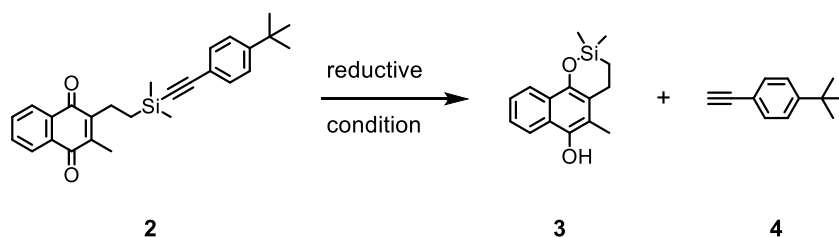
Scheme 3. Concept of the designed test system.

Synthetic Strategy
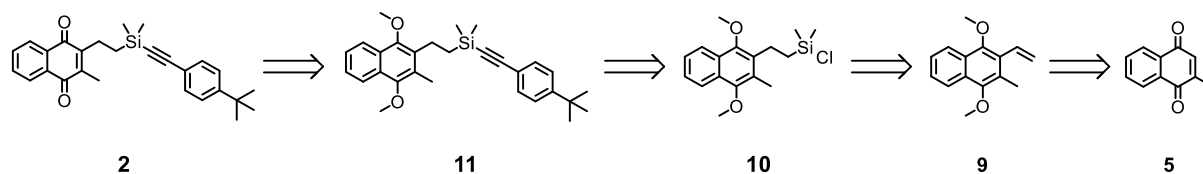
Scheme 4. Retrosynthetic analysis of the designed test system **2.**

The synthetic strategy of the designed test system **2** consisted of two main challenges: to functionalize the naphthoquinone with the ethyl linker and to connect the ethyl linker to the silicon atom. In literature, the protection of alkynes uses different, mostly commercially available, silyl chlorides and takes place by the deprotonation of the alkyne followed by an S_N2 type reaction at the silyl chloride, releasing the chloride as leaving group. The high efficiency of these reactions leads to the implementation of this principle in our synthetic approach. Therefore, silyl chloride **10** was required as a key precursor. The functionalization of 2-methyl-1,4-naphthoquinonen (**5**) is well known in literature due its use as core building block of different vitamin K derivatives.[72–74] Menadione **5** is converted into the dimethoxynaphthalene analogue to avoid complications with the reactive quinone system. After a formylation of the naphthalene's 3-position, the corresponding alkene **9** is accessible by a Wittig reaction. The regioselective hydrosilylation is the key step, avoiding a challenging mono functionalization of dichlorodimethylsilane by a feasible nucleophile like a Grignard reagent. As last step, the installation of the quinone system is implemented into the strategy by an oxidative demethylation reaction.

Synthesis of the Test System
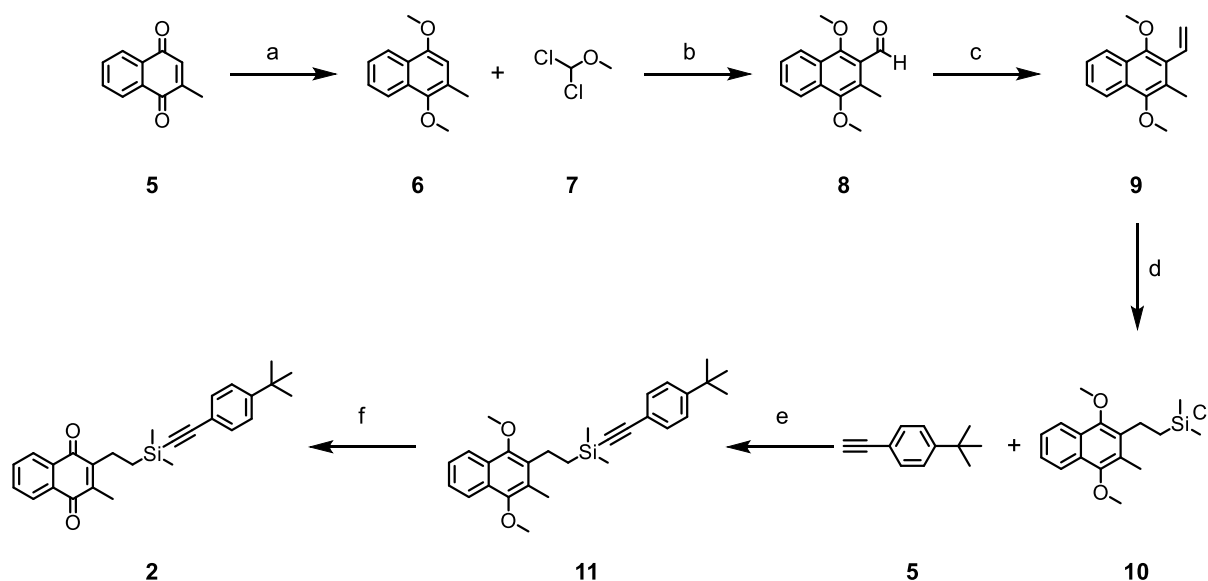
Scheme 5. Synthesis of the test system **2**. Reaction conditions: a) SnCl₂, HCl, MeOH, RT, 1 h; then K₂CO₃, dimethyl sulfate, acetone, reflux, 4 h, 68 %; b) TiCl₄, DCM, 0 °C, 3 h, 90 %; c) MeP(Ph)₃Br, *n*-BuLi, THF, 0 °C → RT, 3 h, 90 %; d) Karstedt's catalyst, chlorodimethylsilane, 34 °C, 3 h, 75 %; e) *n*-BuLi, THF, -78 °C, 1 h, 86 %; f) CAN, MeCN / H₂O (2:1), RT, 1 h, 90 %.

The synthesis of the test system **2** started from commercial available 2-methyl-1,4-napthaquinone (**5**). Reduction of the quinone moiety with tin(II) chloride and HCl in methanol at room temperature followed by the methylation with dimethyl sulfate in refluxing acetone, resulted 2-methyl-1,4-dimethoxynaphtalene (**6**) in 68 % yield over two steps.[75] The intermediate hydroquinone was precipitated out of water and used without further purification. The Rieche formylation in ortho position of the methoxy group was carried out with TiCl₄ and dichloromethyl methyl ether (**7**) in dichloromethane at 0 °C.[76] After the following Wittig reaction with methyltriphenylphosphonium bromide, all carbon atoms for the designed intramolecular ring formation and acetylene release mechanism were installed. As a key step, the formation of the silyl chloride **10** was achieved by a hydrosilylation reaction catalyzed by Karstedt's catalyst as Pt(0) source, in a regioselective manner. The reaction was performed directly in 1.5 equivalents of chlorodimethylsilane as solvent. After addition of the Karstedt's catalyst, an immediate color change initiated the strong exothermic reaction process. Reaction control by GC-MS showed a quantitative conversion to the silyl chloride **10.** After distillation of the excessive chlorodimethylsilane under argon atmosphere, the air and moisture sensitive silyl chloride **10** was isolated in high vacuum at 180 °C by bulb to bulb distillation in 75 % yield. A fast hydrolysis was observed during further handling of the compound or storage not under strict exclusion of air. Test reactions performing the oxidative demethylation to the corresponding quinone with the alkene derivative **9**, and handling the hydrosilylation with the quinone moiety in place, let to undesired functionalization of the carbonyl group instead of the

alkene. Furthermore, the oxidation of the silyl chloride **10** to the corresponding quinone was not possible due to the aqueous reaction condition of the oxidation or the formation of the hydroquinone intermediate.

However, with silyl chloride **10** in hands, the further functionalization to the test system **2** was achieved by a S_N2 type reaction with ^{t}butylphenylacetylene (**4**). Alkyne **4** was deprotonated with n-BuLi at -78 °C followed by the addition of the silyl chloride **10** at room temperature to obtain dimethoxynaphthalene **11** in a good yield of 86 %. The final step was the oxidative demethylation to the quinone **2** with ammoniumcer(IV)-nitrat (CAN) in a water / acetonitrile solvent mixture, resulting in 90 % yield after purification by column chromatography. The test system **2** was obtained as a slightly yellow oil and did not shown decomposition during several days under air. The target molecule and all precursor were fully characterized by ^{1}H- and ^{13}C-NMR and high resolution mass spectroscopy.

Chemical Deprotection

In a first step, the chemical reduction of the test system **2** was investigated in solution. The reduction was performed with 25 equivalents of sodium dithionite in various solvent mixtures (see **table 3**). The reduction of the quinone moiety and subsequent release of the alkyne **4** was monitored by TLC and GC-MS analysis. Kinetic studies of CAN reduction reactions has shown that the active reductant is obtained after dissociation in water to the radical SO^{2-}.[77] The calculated redox potential for the active redox couple SO^{2-} / HSO^{3-} was found to be E° = -0.66 V vs. SCE. Quinone **2** was dissolved in the organic solvent followed by the addition of sodium dithionite and water. The reaction in dichloromethane and acetonitrile showed no conversion to the free alkyne **4** according to TLC and GC-MS analysis. However, using aprotic polar solvents as acetone and dimethylformamide resulted in a quantitative conversion. The GC-MS analysis revealed exclusively the formation of oxasilinane **3** and the alkyne **4** (see **figure 7**). In the case of DMSO as organic solvent, a small quantity of start material was observed after 30 minutes reaction time by GC-MS. The isolation of the oxasilinane **3** has not been achieved despite intensive efforts due to the fast hydrolysis to the 1,4-dihydroxynaphthalene species.

Table 3. Screening of chemical deprotection condition in different solvent mixtures.

Entry	Solvent / Water (2:1)	Temperature [°C]	Time [h]	Conversion [a] [%]
1	Diethyl ether	25	0.5	50
2	DCM	25	0.5	-
3	Acetone	25	0.5	100
4	MeCN	25	0.5	-
5	DMF	25	0.5	100
6	DMSO	25	0.5	90

[a] Determined by GC-MS

Further investigations showed that the reaction time for the reduction and the following intramolecular ring formation is shorter than 1 minute when using acetone or DMF as the organic solvent. The short reaction time can be attributed to a fast reduction process and the preorganized arrangement for the intramolecular attack. Furthermore, aprotic polar solvents favor S_N2 type reactions.
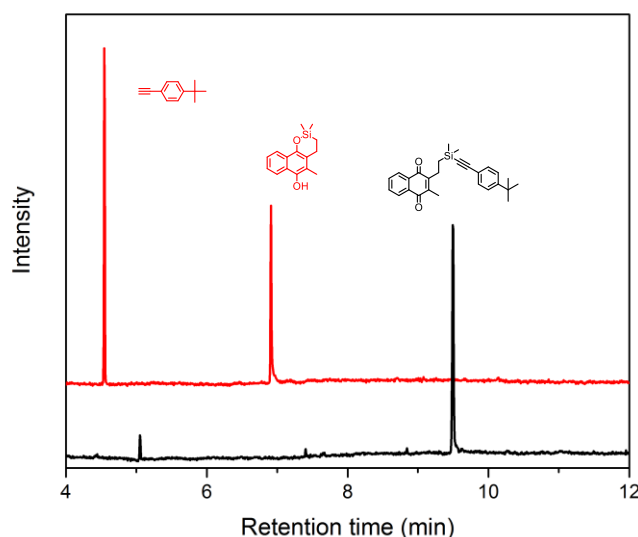
Figure 7. GC trace of the chemical deprotection of test system **2** in acetone. The black trace shows the starting material **2** as reference. The red trace shows the reaction control after 30 min. Only the free alkyne **4** and the formed oxasilinane **2** were detected.

Electrochemical Deprotection

For the electrochemical deprotection, the electrochemical properties of the test system **2** were investigated. A conventional three electrode set up was used consisted of a glassy carbon disk (2mm diameter) as working electrode, a Pt wire as counter electrode, and a saturated potassium chloride calomel electrode (SCE) as reference, using a 0.1 M Et_4NBF_4 acetonitrile solution as electrolyte. The experiment was recorded with an Autolab PGSTAT302 potentiostat. First, a cyclic voltammetry (CV) measurement was performed of a 1 mM solution of quinone **2**.
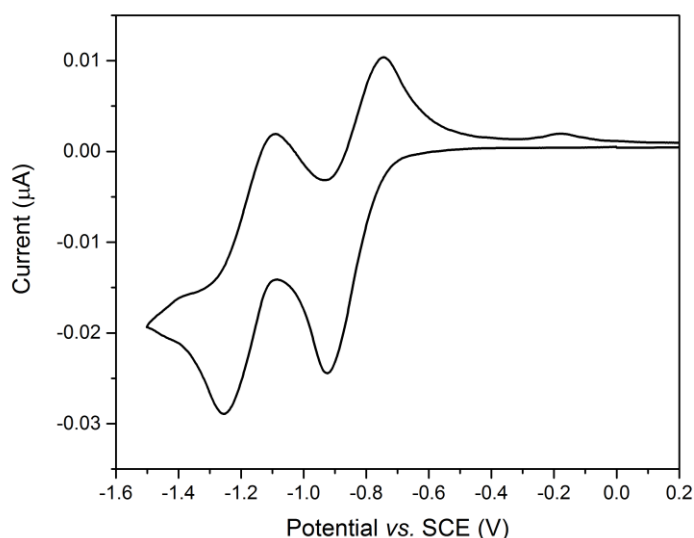
Figure 8. CV voltammogram of 1 mM quinone **2** in acetonitrile using 0.1 M Et_4NBF_4 as electrolyte and a scan rate of 100 mV/s.

The potential was applied relative to the electrochemical potential of SCE with a scan rate of 100 mV/s. Quinone **2** showed two successive one-electron reduction steps at -0.84 V and -1.27 V, respectively. The first reduction step correlates to the formation of the semiquinone $Q^{\bullet-}$ while the second reduction step is the formation of the quinone dianion Q^{2-}.[67,78] In the timescale of the CV experiment, the reoxidation of the hydroquinone species was observable indicating a slow release of the free alkyne. For further investigation spectroelectrochemical measurements were performed.
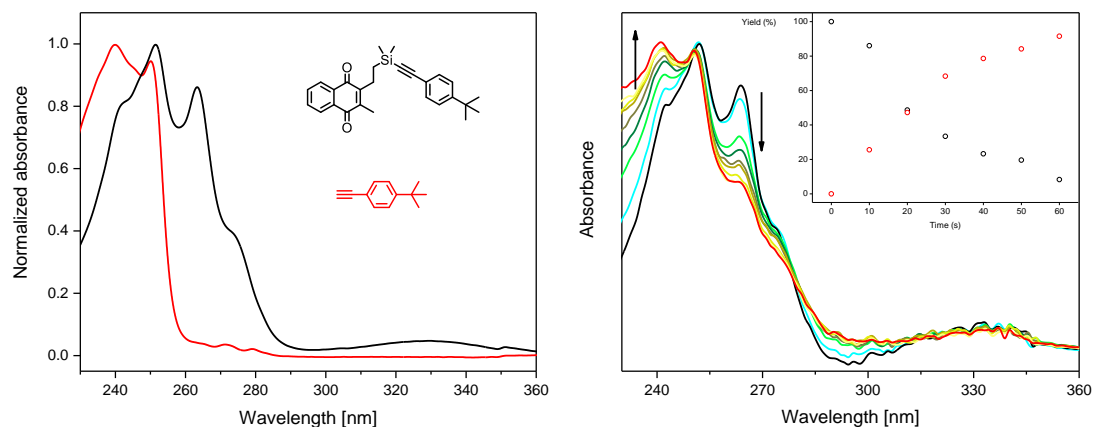
Figure 9. Left: UV-Vis absorbance measurement of test system **2** and 4-*t*butylphenylacetylene (**4**). Right: Spectroelectrochemical measurement of a 10^{-5} M solution of quinone **2** in acetonitrile containing 0.1 M Et$_4$NBF$_4$ as electrolyte. A potential of E° = -0.9 V vs. SCE was applied and the absorbance spectra was measured continuously every 10 seconds (black to red line). The yield corresponds to relative intensities at peak maxima λ_{max} = 263 nm (quinone, black circle) and λ_{max} = 240 nm (acetylene, red circle).

As references, the absorbance spectra of the quinone **2** and 4-*t*butylphenylacetylene (**4**) were measured (see **figure 9**). The alkyne **4** had the highest absorbance band at λ_{max} = 240 nm with a second band at λ = 250 nm. The absorbance spectra of quinone **2** consist of two main bands: (i) the benzene located transition at λ_{max} = 252 nm and (ii) the quinone located transition at λ = 263 nm.[79]

The spectroelectrochemical measurement was recorded on a Cary 5000 UV/Vis/NIR spectrometer from Varian. As electrochemical cell set up, a platinum mesh with an active surface of 0.25 cm^2 served as working electrode in combination with a platinum wire as counter electrode and a SCE reference electrode. The spectra were recorded with a starting concentration of 10^{-5} M quinone **2** in acetonitrile containing 0.1 M Et$_4$NBF$_4$ as electrolyte. At a potential of E° = 0 V vs. SCE, the recorded absorbance spectra was identical with the reference of quinone **2**. After applying a potential of E° = -0.9 V vs. SCE, the absorbance was measured repetitively every 10 seconds indicated in **figure 9** by the black to red lines. Due to the applied potential, the reduction of the quinone to the semiquinone proceeded and the subsequent intramolecular ring formation released the free alkyne **4**. As consequence, the quinone located absorbance band at λ = 263 nm decreased with the quantity of reduced species. Furthermore, the increase of the absorbance band at λ = 240 nm indicated the formation of the free alkyne **4**. After 80 seconds, no further changes in the absorbance spectra were observed. The difference of the spectra obtained after 80 seconds to the absorbance spectra of the pure alkyne **4** can be explained by the formation of the naphthalene compound **3** and its absorbance in this specific wavelength range. The proposed mechanism of the alkyne release is shown in **scheme 6**.
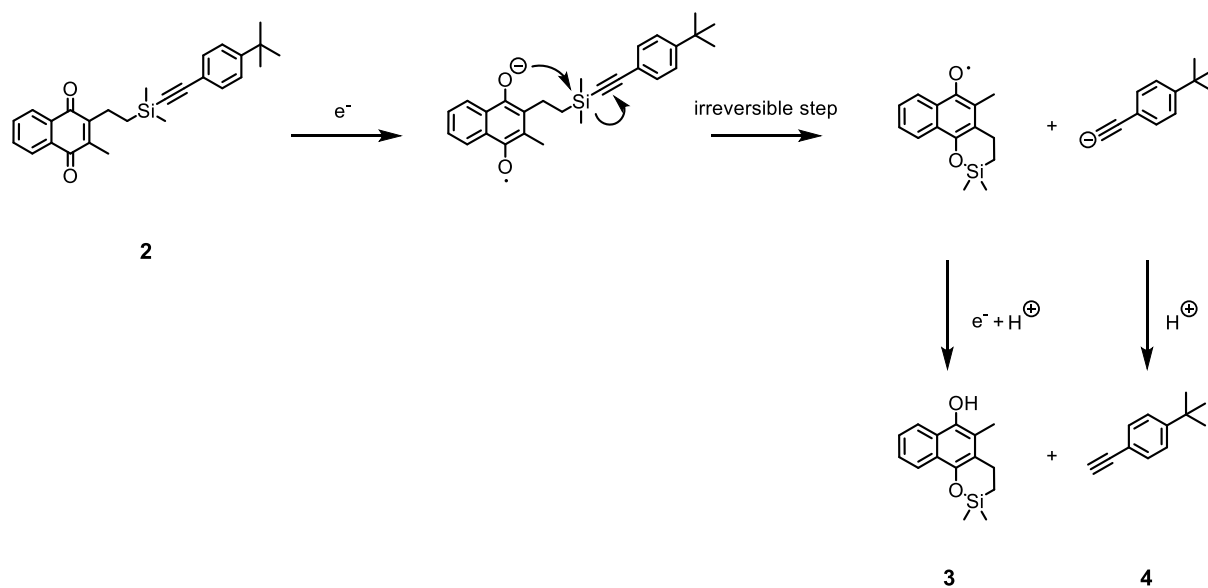
Scheme 6. Proposed mechanism of the reductive cleavage. One electron reduction to the semiquinone followed by the intramolecular attack induces the irreversible release of the alkyne **4** and the formation of the oxasilinane **3**.

After the reduction of the quinone **2** to the semiquinone, the negative charged oxygen can attack the silicon atom in a S$_N$2 type reaction and release the negative charged acetylene moiety. During work up, the subsequent protonation lead to the alkyne **4** and the oxasilinane **3**.

Surface Functionalization

Molecular Design
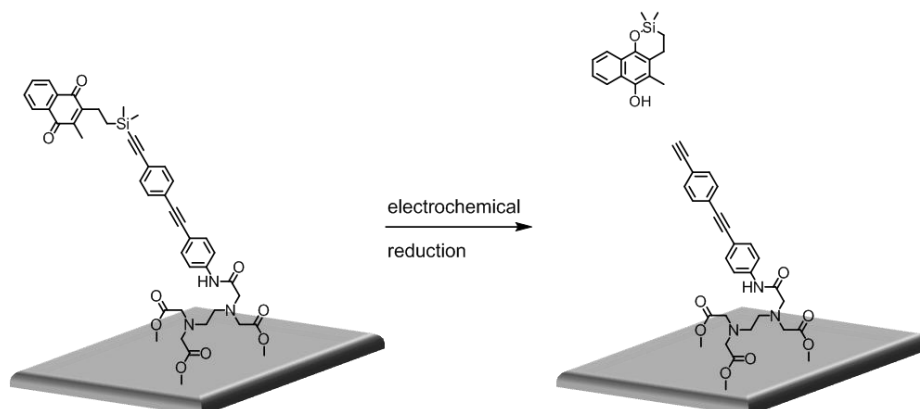
Figure 10. Schematic illustration of the molecular design for the surface functionalization.

The designed molecule for the surface functionalization consisted of three units: (i) the anchoring group for the immobilization on the surface, (ii) a linker to a silane protected acetylene, and (iii) the quinone building block for the electrochemical addressing and releasing mechanism.

For the quinone part of the molecule, the same 1,4-naphtaquinone based structure as used in the test system **2** was implemented. Although the planned variation of the molecular structure, influences regarding the electrochemical behavior and the function of the release mechanism were not expected.

The linker between the silane protected acetylene and the EDTA can consist of either a single phenyl ring, or a longer repetitive oligo phenyl ethylene linker. The function of the linker unit is to guarantee the unhindered accessibility of the free alkyne group attached to the surface for further functionalization by copper catalyzed click chemistry. The amine moiety at the end of the linker ensures the formation of the strong amid bond with the EDTA anchoring group.

The EDTA functionality was chosen as anchoring group because of its strong and well understood binding behavior to TiO_2 surfaces.[80–82] The three carboxylic acids form a tripodal structure on the surface by covalent bond formation or adhesion to the titanium centers. Simultaneously, the flexibility due to the sp^3 hybridized -CH_2 segments allows the linker to point away from the surface. TiO_2 surfaces are of high interest in solar cell applications, making them a well understood material for surface modification and consist of high stable nanoparticles without stabilizing ligands.[83–86] The commercial availability of glass substrates topped with a conductive ITO layer and a defined TiO_2 surface area, favors the EDTA - TiO_2 combination and in general EDTA as the anchoring group.

Synthetic Approach

The retrosynthetic analysis of the designed target molecule **1** revealed several challenges. The handling and more specific the purification of EDTA derivatives is challenging due to their high polarity. Furthermore, the strong chelating EDTA moiety is an element of uncertainly for a wide range of chemical reaction conditions. The design of the target molecule **1** allows the introduction of the EDTA moiety in the last step by the selective opening of the monoanhydride EDTA **16**. Additional the approach relied on the same silyl chloride **10** as synthesized for the test system **2**.
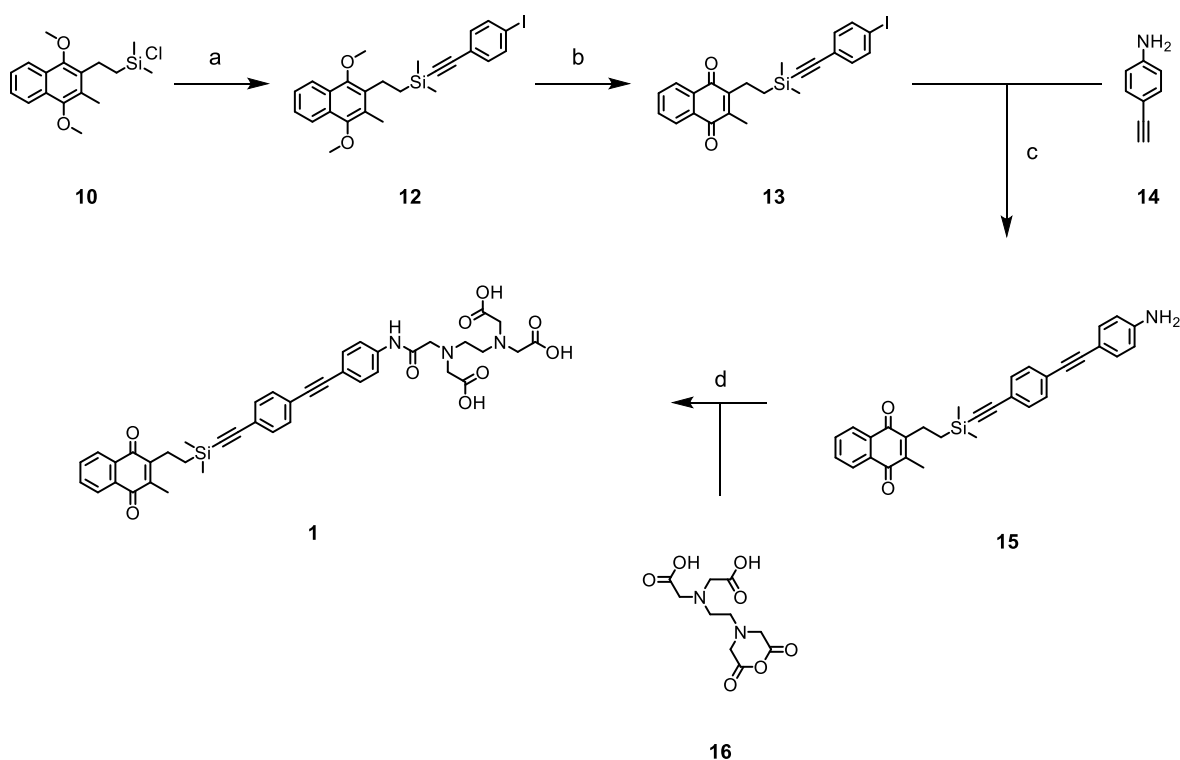
Scheme 7. Synthesis of target molecule **1**. Reaction condition: a) KHB base, 4-iodophenylacetylene, THF, 0 °C, 1 h, 73 %; b) CAN, MeCN / H$_2$O (2:1), RT, 1 h, 94 %; c) Pd(PPh$_3$)$_4$, CuI, Et$_3$N, RT, 16 h, 91 %; d) DMF, 60 °C, 16 h, 49 %.

The functionalization of silyl chloride **10** was achieved with 4-iodophenylacetylene, which was synthesized according literature known procedure.[87] For the deprotonation of the acetylene, the sterical hindered piperidinylmagnesium chloride based Knochel-Hauser base was used to prevent a lithium halogen exchange as side reaction.[88] The direct functionalization of the silyl chloride **10** with an aniline derivative was considered challenging hence an efficient protection and deprotection of the amine would be necessary. With dimethoxy compound **12** in hand, the oxidative demethylation was performed to the corresponding quinone **13** under the same condition as used in the synthetic approach of the test system **2** with CAN as the active oxidant.

20

To introduce the required terminal amine moiety, a Sonogashira cross-coupling with 4-aminophenylacetylene (**14**) was performed to obtain the amine precursor in excellent yield. First tries with Pd(PPh$_3$)$_2$Cl$_2$ in different THF / amine base mixtures were not successful. The change to Pd(PPh$_3$)$_4$ as Pd(0) source and to use exclusively EtN$_3$ as solvent leaded to a quantitative conversion. The amine **15** was thoroughly purified by column chromatography before the final step. A direct monoanhydride formation from EDTA was not possible in good yields. Therefore, the commercially available EDTA was suspended in pyridine and acetic anhydride to form the di anhydride species, followed by the hydrolysis with one equivalent of water in DMF to obtain monoanhydride **16**.[89] The selective anhydride opening to the target compound **1** was performed in DMF at 60 °C. The purification of EDTA derivative **1** was challenging due to an overall bad solubility. Best results were achieve by repetitively suspending and decantation with acetone to remove unreacted amine precursor **15** followed by the same procedure in diethyl ether to wash off excessive EDTA residues. Even after multiple purification cycle, a residual amount of EDTA was confirmed by ^{1}H-NMR spectroscopy. However, 2D NMR spectroscopy allowed all the observed signals in the ^{1}H- and ^{13}C-NMR spectra to be fully assigned. For the further purpose, residual EDTA decreases the packing density of the compound on the TiO$_2$ surface, but will not have an influence during the consequent functionalization.

As a reference, the free alkyne **21** was synthesized in four steps starting from the commercially available 1,4-diiodebenzene (**17**). Subsequent Sonogashira cross-coupling reaction with TMS-acetylene and 4-ethynylaniline lead to aniline **19**. After cleaving of the trimethylsilane protecting group under standard conditions, alkyne **20** was used for the condensation with EDTA monoanhydride **6** to obtain the desired reference structure **21**.
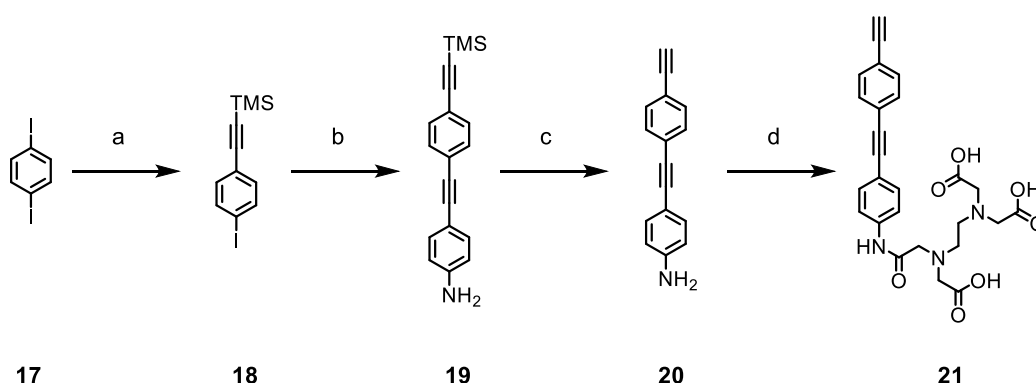
Scheme 8. Synthesis of reference alkyne **21**. Reaction condition: a) TMS-acetylene, Pd(PPh$_3$)$_2$Cl$_2$, CuI, NEt$_3$, THF, RT, 7h, 54 %; b) 4-ethylenylaniline, Pd(PPh$_3$)$_2$Cl$_2$, CuI, NEt$_3$, THF, RT, 4 h, quant.; c) TBAF, THF, RT, 1 h, 95 %; d) EDTA monoanhydride, DMF, 60 °C, 12 h, 49 %.

To later prove the successful reduction and deprotection of the immobilized molecules, the functionalization of the released free acetylene by click chemistry with detectable markers was developed. As a simple marker system, dyes of different color functionalized with an azide moiety were selected. Fluorescent markers are widely used in biochemical click chemistry applications. However, the detection rely mostly on fluorescence microscopy. Additional, the commercially available azide-dyes are mostly based on polar structures like fluorescein and cyanine, interlinked with polyethylene glycol (PEG) chains to an azide group. The polar design is mainly focused for the use in biochemistry suitable water based click chemistry. However, to avoid the adsorption of the dye marker directly on the TiO_2 surface and obtaining false positive results as consequence, nonpolar structures as dyes were favored.

Naphthalene diimide (NDI) based dyes are known for their high molar extinction coefficient above 350 nm and furthermore, the color can be readily defined by different substituents on the naphthalene core. Two different NDI-azide dyes were synthesized by substitution of the NDI core either by two thiol alkyl chains to obtain the red dye **26**, or with two alkyl amine chains for the blue azide-dye **27** showed in **scheme 9**.
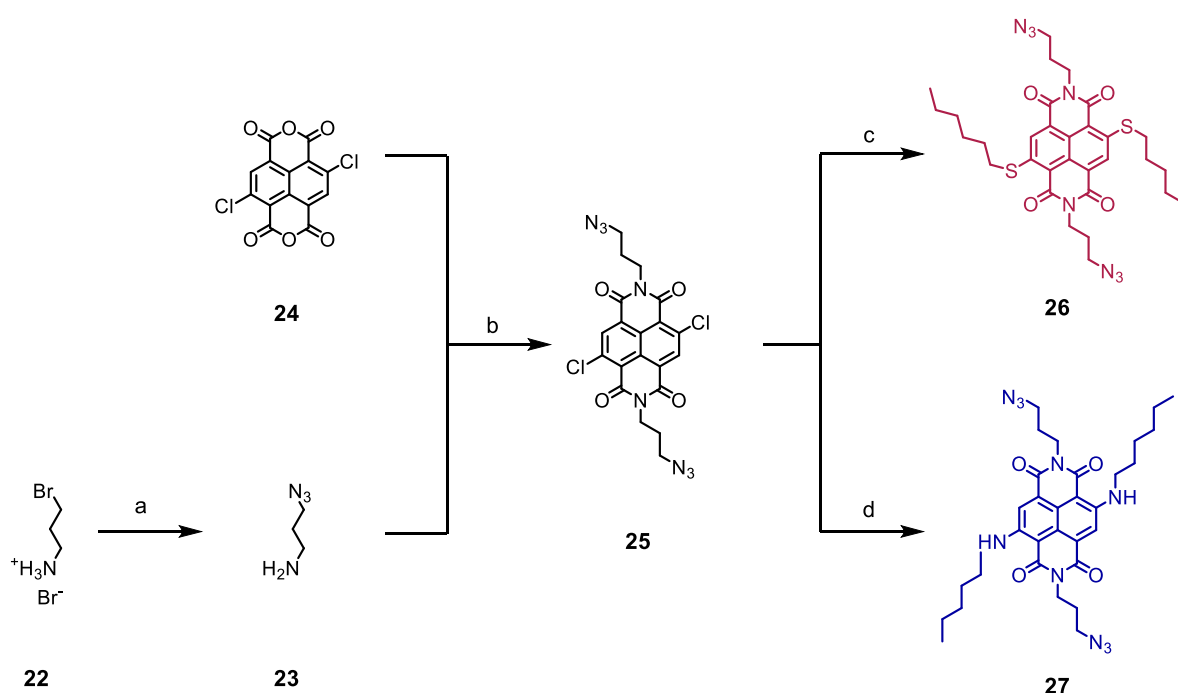
Scheme 9. Synthesis of NDI-azide dyes **26** and **27**. Reaction conditions: a) NaN_3, H_2O, 100 °C, 16 h, 94 %; b) AcOH, 120 °C, 16 h; c) 1-hexanthiol, K_2CO_3, DMF, RT, 30 min, 25 %; d) hexylamine, K_2CO_3, THF, 60 °C, 3 days, 54 %.

For the synthesis of both azide-dyes **26** and **27**, respectively, the main building block **25** was obtained by the condensation of naphthalene dianhydride **24** with 3-azidopropan-1-amine (**23**) in acetic acid at 120 °C. By using acidic conditions, the anhydride acts as a Lewis base and is

protonated. The obtained activated carboxyl group facilitated the amide formation. Additional, due to the shift of the equilibrium between the free amine and the ammonium species, the nucleophilic character of the 3-azidopropan-1-amine (**23**) is under acidic conditions not sufficient for the nucleophilic aromatic substitution of the chlorine at the naphthalene core. Strong π – π stacking decreased the solubility of azide **25** and made the purification challenging. As consequence, the azide **25** was used directly after work up for the following S$_N$Ar without further purification. The reaction of NDI **25** with 1-hexanethiol in dimethylformamide and potassium carbonate as base resulted in 25 % yield for the red azide-dye **26**. Reaction control by MALDI-TOF and TLC showed an almost quantitative conversion to the desired product. However, the purification by column chromatography leaded to a tremendous loss of compound. Using the same reaction conditions for the substitution with the amine analogue leaded to the undesired substitution of the chlorine group with dimethylamine as byproduct. As consequence, the reaction was performed in THF as solvent. Moreover, increased reaction temperature and time were necessary due to the stronger +M - effect of the first amine inserted at the NDI core, compared to the thiol functional group. The enhanced electron density within the aromatic system hindered the substitution of the second chlorine. The blue NDI-azide dye **27** was obtained in 54 % yield after purification. Both azide-dyes **26** and **27**, respectively, are bench stable over several weeks.

The insertion of two azide moieties was due to the synthetic pathway. A statistical reaction with a mixture of 3-azidopropan-1-amine (**23**) and the corresponding propyl amine would lead to a mixture of all three possible products. Whereas the almost quantitative twofold insertion of 3-azidopropan-1-amine (**23**) allowed to proceed without the challenging purification of NDI **25**. The UV-Vis spectra of both azide-dyes **26** and **27**, respectively, are shown in **figure 16.**

Immobilization on the TiO₂ Surface

For the attachment of the quinone **1** to the TiO$_2$ surface, an EDTA moiety with three free carboxylic acids groups was linked to the quinone protected alkyne by an amide bond connected phenyl ethylene linker. Several examples of TiO$_2$ surfaces functionalization with organic molecules by carboxylic acid based anchoring groups are known in literature.[90–92] The absorption mechanism of carboxylic acid groups to the TiO$_2$ surface was investigated from multiple research groups, obtaining a nanoparticle size-depending adsorption behavior.[80–82] The adsorption can take place in different forms, either by chelating to the titanium centers in different geometries, or formation of a covalent ester bonds having free hydroxyl groups on the surface acting as nucleophiles. However, in all cases, a mixture of the different binding possibilities was observed.
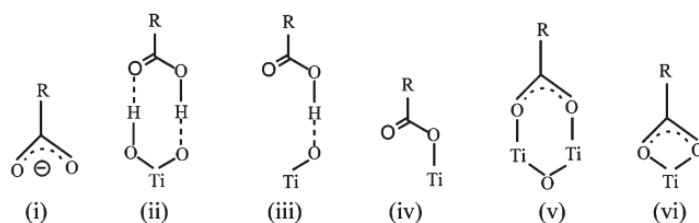
Figure 11. Adsorption of carboxylic acid groups on a TiO$_2$ surface. (i) Electrostatic attraction; (ii) and (iii) H-Bonding; (iv) Monodentate (ester-like linkage); (v) Bidentate bridging; (vi) Bidentate chelating. Reprinted with permission from Qu *et al.*[93]

The used wafer were purchased from SOLARNIX. The glass substrate has a square shape with a side length of 20 mm and a thickness of 2 mm. One side of the glass substrate is topped with a conductive fluorine-doped tin oxide (FTO) layer. On top of the FTO layer, a 10 - 12 µm thick TiO$_2$ nanoparticle film is deployed with the dimension of 6 x 6 mm. The particle size of the TiO$_2$ nanoparticles are in the range of 15 - 20 nm. Stable absorption to the TiO$_2$ surface was achieved by dip coating the wafer into a bath consisting of a 3 x 10^{-4} M solution of quinone **1** in methanol for 4 hours. Afterwards, the wafer was rinsed with methanol and sonicated in methanol for two minutes to wash of unabsorbed material. After absorption, the TiO$_2$ surface showed a yellow coloring indicating the successful immobilization (see **figure 15**).

Electrochemical Deprotection

To compare the electrochemical features of quinone **1** with the test molecule **2**, cyclic voltammetry measurements were first performed in solution. The voltammogram was obtained from a 1 mM solution in DMF and $LiCF_3SO_3$ was used as electrolyte in a 1 M concentration.[94] Li^+ ions containing electrolyte was chosen to govern the flat band energy of the TiO_2 surface and enable the theoretical reversible operation in later experiments with the immobilized system.[94,95] The electrode set up consisted of a platinum disk (2 mm diameter) as working electrode, platinum wire as counter electrode and a SCE reference electrode. The experiment was run with a scan rate of 100 mV/s.
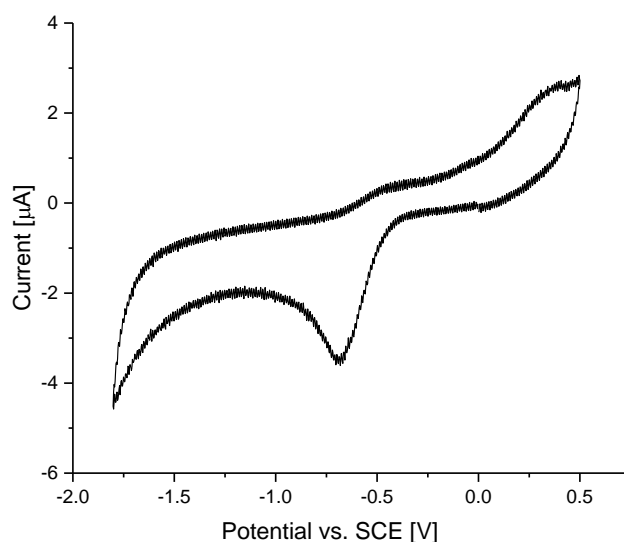
Figure 12. Cyclic voltammetry of 1 mM quinone **1** in DMF containing 0.1 M $LiCF_3SO_3$ as electrolyte. Scan rate: 100 mV/s.

The CV shows the first reduction step at -0.68 V vs. SCE correlating to the semiquinone $Q^{\bullet-}$ formation. A second reduction step was not observed within the measured voltage area (**figure 12**). Remarkably, in contrast to the CV of the test system **2** (see **figure 8)**, the reoxidation was not observed revealing a non-reversible system. This can be again attributed to the solvent choice. The same trend was observed during the chemical deprotection, where the reactions performed in DMF, DMSO, and acetone showed a quantitative deprotection of the acetylene in contrast to the reaction in acetonitrile (see **table 3**). Furthermore, the experiment supported the proposed deprotection mechanism where the semiquinone performs the intramolecular attack on the silicon atom and the reduction to the dianion species is not required.

As next step, the reductive cleavage of the quinone protecting group with the molecule immobilized on the TiO2 surface was investigated. We applied as similar condition as for the CV experiment in solution. The functionalized TiO_2 chip with the conductive ITO layer intended as working electrode during the experiment and was combined with a SCE reference electrode and platinum wire as counter electrode in an argon-purged 0.1 M $LiCF_3SO_3$ / DMF solution as electrolyte. The CV of quinone **1,** immobilized on the surface, showed a shift of the reduction peak to 0.79 vs. SCE. The current flow was significantly increased up to 400 µA due to the larger electrode surface. In the second cycle, the reduction peak was no longer observable, indicating the reduction of all immobilized quinone molecules during the first measured cycle.
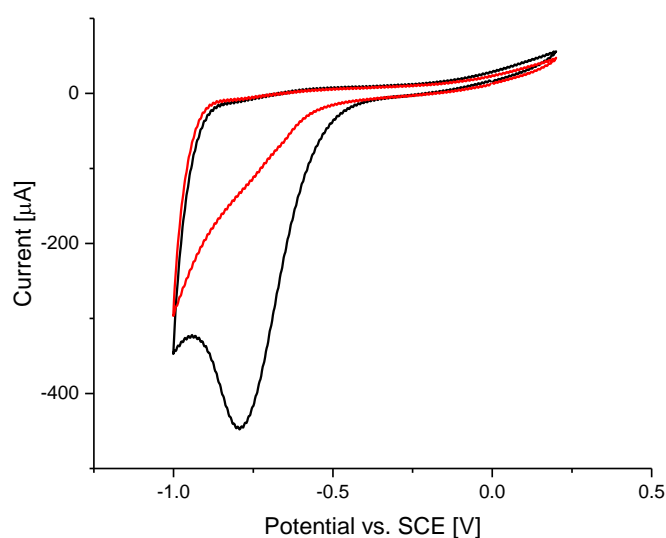
Figure 13. Cyclic voltammetry of quinone **1** immobilized on the TiO_2 surface. Black: First measured cycle. Red: Second measured cycle.

The reduction and deprotection could also be achieved by applying a constant potential of -0.90 V for 10 sec. Considering the obtained reduction potential of -0.68 V from the CV measurements of quinone **1** in solution, the reduction and deprotection takes place within seconds by applying a potential of -0.90 V. A longer exposure time was unnecessary due to the very fast reduction process and the pre-aligned intramolecular ring closure. The choice of DMF as solvent was crucial as the electrochemical deprotection on the surface in acetonitrile showed no success. The deprotection of the acetylene was verified by the absorbance spectrum in a solid state UV-Vis experiment.

Solid State UV-Vis Absorbance

For the investigation of the immobilized species on the TiO$_2$ surface, solid state UV-Vis measurements were performed. The absorption values were recorded relative to the absorption of a blank TiO$_2$ surface. The cutoff for the measurement caused by strong absorption of the TiO$_2$ layer was at a wavelength of 350 nm. For the quinone **1** functionalized surface, an absorption band in the range of 370 nm was observed (see **figure 14).**

For the immobilization of the free alkyne **21** as reference, the same condition were used as for the quinone **1**. The glass substrate was dipped into a 3 x 10^{-4} M solution in methanol for 4 hours. The solid-state UV-Vis absorbance measurements of the free alkyne **21** showed no absorption band in the measurable range. As consequence, the presence of the free alkyne species after deprotection could not be confirmed by using solid state UV-Vis experiments, but only the absence of the quinone moiety.
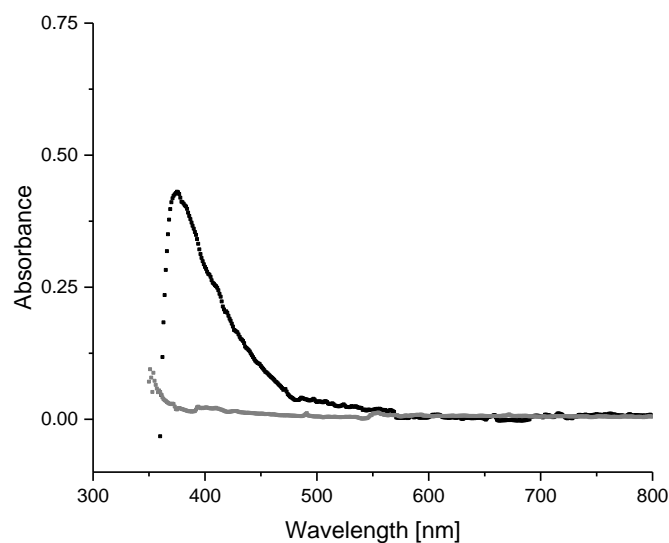
Figure 14. Solid state UV-Vis measurement of quinone **1** (black) and reference acetylene compound **21** (grey) on TiO$_2$ surface. Absorbance was measured relative to a blank TiO$_2$ surface.

Cu(I)-Catalyzed Click Chemistry Functionalization

For the development of the click chemistry system, conditions were screened using a wafer with the free alkyne **21** immobilized on the TiO$_2$ surface. Using directly the free alkyne **21** had the advantage of excluding reductive deprotection related factors. We tested different conditions successfully used in literature for surface functionalization by click chemistry.[28,90,96,97]

Table 4. Screening of click chemistry conditions with the free alkyne compound **21** immobilized on a TiO$_2$ surface.
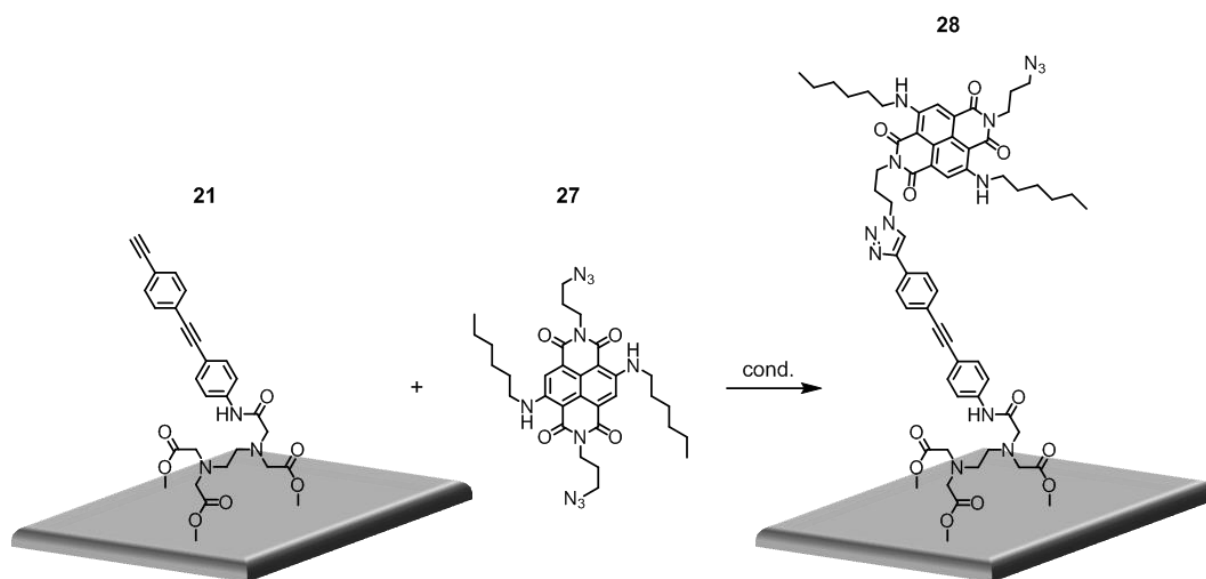
Entry	Copper source eq.	Ligand eq.	Reagent eq.	Solvent Ratio	Result
1	CuI	Hünig's Base	Acetic acid	DCM	-
	0.02	0.04	0.04		
2	Cu(MeCN)$_4$PF$_6$	TBTA	-	^{t}BuOH / H$_2$0	-
	0.10	0.10		2:1	
3	CuI	-	Ascorbic acid	MeCN / H$_2$O	-
	0.20		0.4	1:1	
4	CuI	PMDTA	-	THF	Blue
	1.0	1.0			
5	Cu(MeCN)$_4$PF$_6$	TBTA	-	THF	Blue
	1.0	1.0			
6	Cu(MeCN)$_4$PF$_6$	TBTA	-	MeCN	-
	1.0	1.0			

All reactions were performed at RT for 4 h.

As Cu(I) source, either copper(I)iodide or the stabilized tetrakis(acetonitrile)copper(I) hexafluorophosphate was used.[98] All reactions were performed at room temperature and the wafer was dipped into the reaction solution for 4 hours. The combination of CuI with PMDTA as ligand in THF resulted in a blue colored surface, indicating a successful click reaction (entry 4, **table 4**). The reaction solution turned from blue to green and a precipitation was observed indicating the oxidation of the Cu(I) to Cu(II) during the reaction time. To obtain a more stable system, the copper source was changed to $Cu(MeCN)_4PF_6$ and TBTA was used as a ligand (entry 5, **table 4**).[99] The reaction mixture showed a higher stability combined with an increased blue color intensity of the surface. By using the same catalyst system in acetonitrile instead of THF, no visible color change of the surface was observed (entry 6, **table 4**).
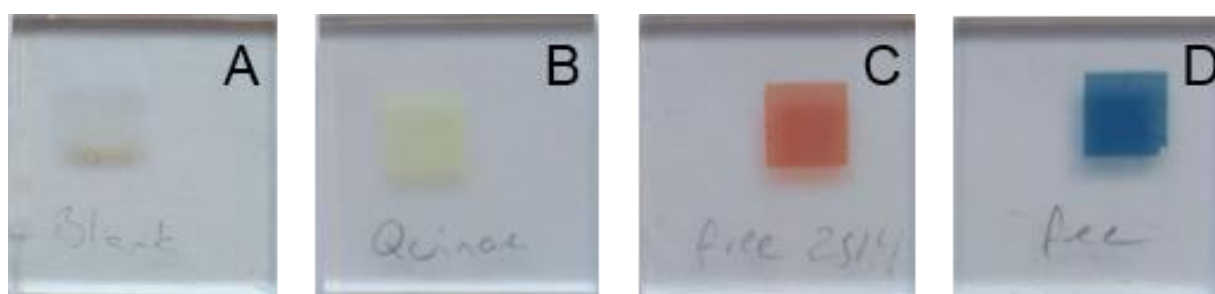
Figure 15. Illustration of different wafer. (A) Blank TiO_2 surface on the glass substrate; (B) The immobilized quinone **1**; (C) With red NDI-azide dye **26** functionalized surface; (D) With blue NDI-azide dye **27** functionalized surface.

To achieve a more specific analysis of the surface, solid state UV-Vis measurements were performed. The references for the solid state absorption was obtained by in solution UV-Vis absorption measurements of the azide-dyes **26** and **27**, respectively. The absorption spectra of the red azide-dye **26** showed characteristic bands around 350 nm with electronic transition typical for the NDI core.[100–102] The S_0-S_1 absorption band exhibits a maximum at 529 nm.[102] The blue azide-dye **27** showed a similar absorption spectra. The electronic transition was minimally blue shifted but of major interest was the bathochromic shift of the S_0-S_1 transition to a maximum at 619 nm. This shift of 90 nm allowed to distinguish the absorbance and to proof that the solid state UV-Vis showed a dye specific absorbance.
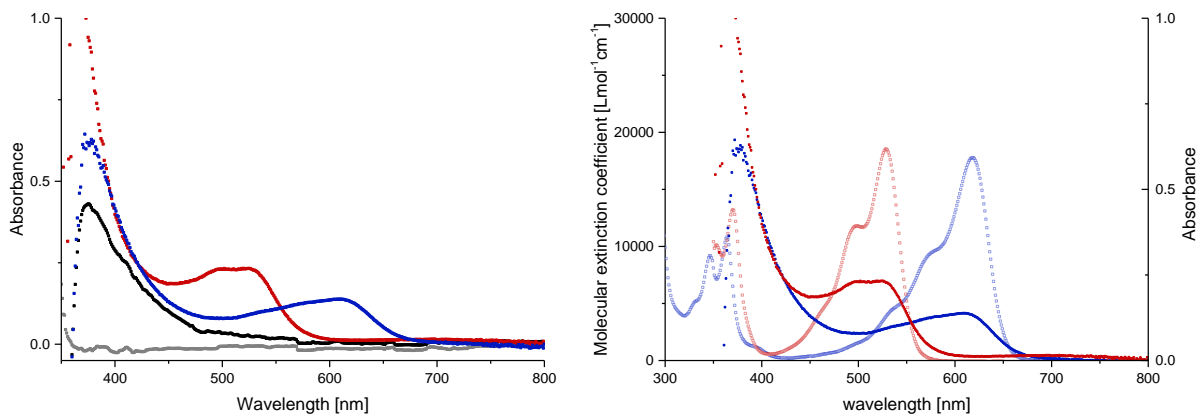
Figure 16. Left: Solid state UV-Vis absorbance measurement. Free alkyne **21** (■), quinone **1** (■), functionalized with the blue NDI-azide dye **27** (■) and functionalized with the red NDI-azide dye **26** (■). Right: In solution UV-Vis spectra of the NDI-azide dyes (red dye □; blue dye □) compared with the solid state measurement (red dye ■; blue dye ■).

Comparing the solid state absorption spectra with the corresponding spectra obtained from in solution measurements revealed a high degree of conformance. Mainly the S_0-S_1 absorption band was located at the same wavelength maximum for both, the in solution and solid state systems. The structural information of the S_0-S_1 absorption band was not distinct in the same resolution for the dyes immobilized on the surface. Furthermore, the absorbance in the solid state experiment was strongly increased in the range lower than 450 nm for both, the red and blue azide-dye functionalized systems. This effect was already observed with the immobilized quinone **1**. Overall, the solid state UV-Vis measurements clearly confirmed the functionalization of the free acetylene with the azide-dyes **26** and **27**, respectively.

To obtain an idea about the reaction kinetics of the functionalization by click chemistry, the absorbance was measured as a function of the reaction time (see **figure 17,** left). The immobilization and reductive deprotection of four individual wafers was performed as identical as possible. After deprotection, all wafers were exposed to the same click chemistry reaction solution, but for a different time period (0.5 hours, 1 hours, 2 hours, and 3 hours). Considering the λ_{max} values from the S_0-S_1 transition at 525 nm, the solid state absorption measurements showed a proportional increase of the absorbance dependent on the reaction time. These results indicate a highly reproducible process over all the different working steps including immobilization, electrochemical reduction, cleaving of the protection group, and functionalization, despite the enormous amounts of variable factors, starting already at the beginning with the non-homogenous TiO_2 surface. Furthermore, the continuous increase of

the absorbance indicates a rather slow reaction of the click reaction on the surface. However, a significant coloring was already observable after 30 min.
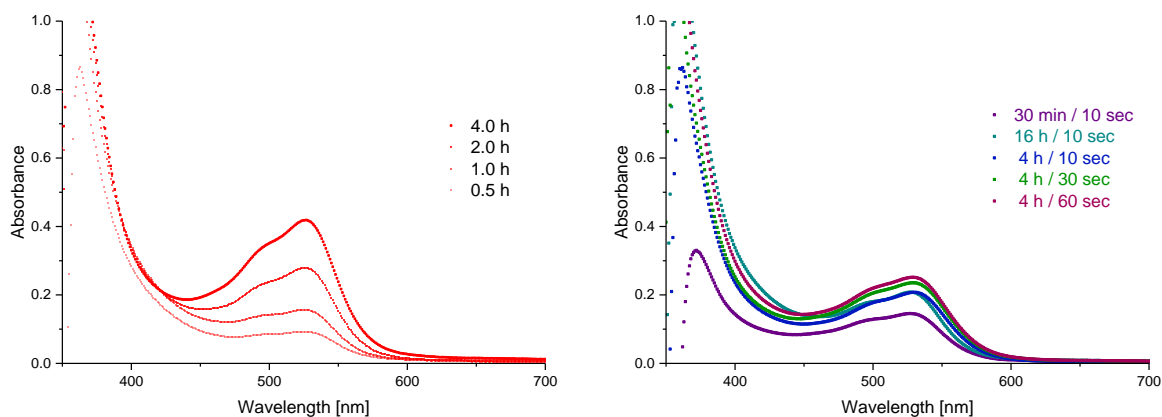
Figure 17. Left: Solid state absorbance measurements after various reaction times. Right: Absorbance dependent of immobilization time (30 min., 4 h, or 16 h) or time suspended to the electrochemical reductive condition (10 sec., 30 sec., or 60 sec.). The click reaction duration was 2 h for all waver.

Furthermore, dependency of the immobilization time was investigated (see **figure 17**, right). The immobilization time of quinone **1** was altered from 0.5 h to 4 h and 16 h. The deprotection was performed with an applied potential of -0.9 V vs. SCE for 10 sec. and the wafer was dipped into the click chemistry solution for 2 h. The solid state absorbance measurement showed an increase compared the wafer with 4 h immobilization time to the wafer with 0.5 h. A further increase for the wafer placed 16 h into the quinone **1** solution was not observable. In a next step, the duration of the electrochemical deprotection was examined. The immobilization time was kept at 4 h and the click chemistry at 2 h for all three wafers, whereas the applied potential of -0.9 V vs. SCE was held for 10 sec., 30 sec. or 60 sec. for each wafer. An small increase in absorption was observed after reacting the deprotected surface with the dye **26** when the deprotection condition were applied for 30 sec. compared to the wafer which was deprotected for 10 sec. A prolonged deprotection time of 60 seconds showed only a minimal increase in intensity.

Surface Functionalization – A Site-Selective Approach

To further prove the concept of an electrochemically induced deprotection, the surface of the wafer was divided in four electronically separated sections. By applying a voltage exclusively to one isolated section of the wafer, a site-selective deprotection of the immobilized molecule **1** on the TiO$_2$ surface was achieved. As a result, the consequent click chemistry based functionalization with the NDI-azide dyes occurred mainly on the deprotected part of the wafer. A minimal coloring of the electrochemical unaddressed sections was observed, even though the distance between the immobilized molecules of the non-addressed sections and the electrode with the applied potential is too large to cause a direct reduction. Therefore, it is more likely that the hydroxyl group of the obtained naphthalene derivative **3** (see **scheme 3**) can deprotect a second alkyne moiety. A direct immobilization or decomposition of the azide-dyes on the surface can be excluded. Negative tests with the blank TiO$_2$ surface, or with the immobilized quinone, showed no coloring after exposure to an NDI-azide dye solution for several hours. However, through repetitively applying of deprotection and consequent functionalization, a modular approach to functionalize different surface areas is possible as shown in **figure 18**. For this modular approach, the selected section was reductively deprotected with an applied voltage of -0.9 V over 10 seconds. After washing the wafer with THF, it was dipped into the click chemistry solution for 2 hours. By repeating the procedure for four cycles, a checkered pattern was achieved.
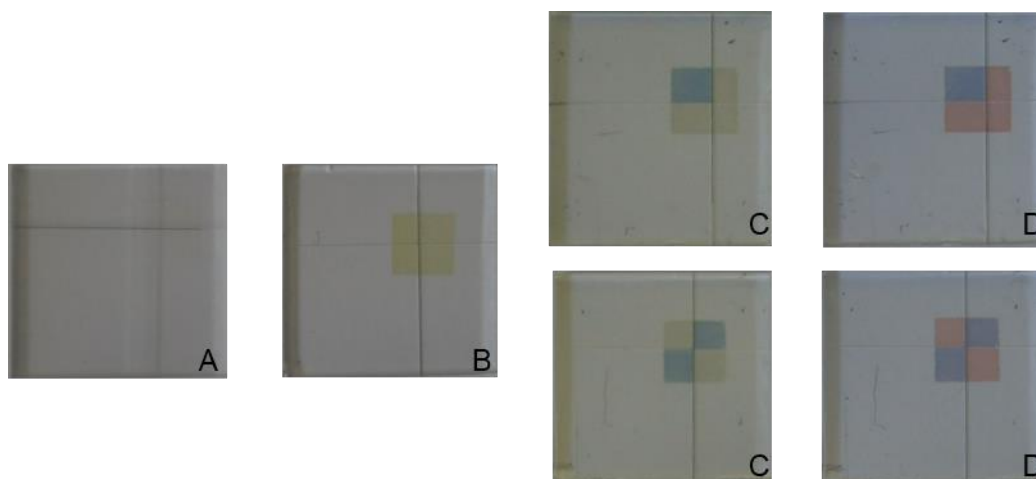
Figure 18. Site selective functionalization by repetitive electrochemical deprotection and functionalization with an NDI-azide dye. The cross lines on the wafer are the cutting sites for obtaining electrically isolated sections. (A) Blank TiO$_2$ surface on the glass substrate; (B) The immobilized quinone **1**; (C) After onefold or two fold deprotection and subsequent functionalization with the blue NDI-azide dye **27.** (D) Deprotection and functionalization of the remaining sections with the red NDI-azide dye **26**.

Conclusion and Future Prospects

The successful synthesis of a test system to investigate the working principle of an electrochemically cleavable alkyne protecting group has been shown. The test system contains of a naphthoquinone moiety for the electrochemical addressability and is linked to a silyl protected alkyne. The synthesis consist of seven steps with an overall yield of 32 %. The key step of the synthesis was the hydrosilylation of a terminal alkene in a regioselective manner to obtain the silyl chloride **10**, which can be further functionalized by a wide range of alkynes. For the test system, 4-^{t}butylphenylacetylene (**4**) was used due to its verifiability after the successful deprotection. The effective deprotection was first shown in a chemical manner with sodium dithionite as reducing agent. The reduction and the following intramolecular nucleophilic attack of the obtained negative charged oxygen at the silane atom leaded to a break of the silane-alkyne bond, and released the alkyne in a quantitative manner. The release of the alkyne **4** was verified by TLC, GC-MS, and UV-Vis measurements. The electrochemical properties of test system **2** were investigated by cyclic voltammetry techniques, revealing an one-electron reduction step from the quinone to the semiquinone at -0.84 V vs. SCE and a second one-electron reduction step at -1.27 V vs. SCE to form the dianion species. Furthermore, with spectroelectrochemical experiments we were able to demonstrate the electrochemical induced deprotection. After applying a potential of -0.9 V vs SCE, the characteristic absorption band at λ = 263 nm of the quinone moiety decreased in the same quantity as the absorption band at λ = 240 nm of the free alkyne compound **4** increased.

For the site-selective functionalization of a surface, target structure **1** was designed and successful synthesized. Whereas the naphthoquinone structure was adopted from the test system **2**, the silyl protected alkyne was interlinked by a phenyl ethynyl moiety to the EDTA based anchoring group. For the synthesis, the silyl chloride **10** was functionalized with 4-iodophenylacetylene. The iodine provided the required functionality for the insertion of an amine moiety and in the same time didn't influenced the oxidative demethylation to the quinone **13**. A Sonogashira cross-coupling reaction to extend the system by a 4-ethynylaniline building block installed the amine for the final selective anhydride opening of EDTA-monoanhydride **16**, to obtain the mono functionalized EDTA target compound **1** in nine consecutive steps with an overall yield of 13 %. All compounds have been fully characterized. The EDTA moiety as anchoring group was chosen because its strong absorption of the three carboxylic acid groups to the TiO$_2$ surface. The electrochemical behavior of the target compound **1** was investigated by CV measurements revealing a non-reversible reduction at -0.68 V vs. SCE in solution, whereas the reduction step shifted to -0.79 V vs. SCE while immobilized on the TiO$_2$ surface. To prove the electrochemically induced cleavage of the protecting group immobilized on the surface, a click chemistry approach, using Cu(MeCN)$_4$PF$_6$ / TBTA catalyst system, was investigated to attach a NDI-azide dye marker to the free alkyne moiety. The functionalization

was proven optically and by solid state UV-Vis absorbance measurements. In a next step, a mechanically, in different electrical nonconductive sections, divided surface was site-selective deprotected by applying a potential of -0.9 V vs. SCE on selected areas. After the selective deprotection, the affected area was functionalized by the NDI-azide dye with the developed click chemistry approach. By repetitive application of the site-selective deprotection and functionalization, a checkered color pattern was realized on the surface. As result, an electrochemical cleavable alkyne protecting group was developed and successfully used for the site-selective surface functionalization. This is the first example of an alkyne release induced by electrochemistry.

Even though investigations showed a high reproducibility of the deprotection and functionalization procedure, further optimization regarding the enormous amount of individual parameters are desirable. Particular further analyzing the deprotection of the electrochemical unaddressed sections is important to avoid undesired functionalization.

As future prospects the insertion of different anchoring groups would be very appealing. The exchange of the iodine into an S-acetyl moiety would allow to form stable mono layers on gold electrodes. Alternatively, the conversion of the amine **15** into the corresponding diazonium salt **30** allows the grafting on different surfaces including carbon[103], semiconductors (Si, GaAs)[104,105], gold and platinum[106].

Scheme 10. Possible transformation to introduce a thiol or diazonium salt based anchoring group.

Experimental Section

General Remarks

Reagent and Solvents: All chemical were used as received without any further purification unless explicitly stated otherwise. Dry Solvents were purchased from *Fluka* or *Accros*. NMR solvent were obtained from *Cambridge Isotope Laboratories, Inc.* (Andover, MA,USA).

[1]H Nuclear Magnetic Resonance (NMR): Bruker DPX-NMR (400 MHz) instrument was used to record all spectra. All chemical shifts are reported relative to trimethylsilane (TMS) or the used solvent. The measurements were performed at room temperature. The multiplicities are written as: s = singlet, d = doublet, t = triplet, dd = doublet of doublets and m = multiplet.

[13]C Nuclear Magnetic Resonance (NMR): Bruker DPX-NMR (101 MHz) instrument was used to record all spectra. All chemical shifts are reported relative to the used solvent. The measurements were performed at room temperature.

GC/MS: For GC/MS analysis a *Shimadzu* GCMS-QP2010 SE gas chromatograph system, with a Zebron 5 MS Inferno column (30 m x 0.25 mm x 0.25 mm), at 1 mL/min He-flow rate (split = 20:1) with a *Shimadzu* mass detector (EI 70 eV) was used.

Mass spectroscopy (MS): MALDI-TOF analyses were performed on a Burker microflex system.

High-resolution mass spectra (HRMS): HR-ESI-ToF-MS were measured with a Maxis 4G instrument from Bruker with the addition of NaOAc.

Column Chromatography: For column chromatography SiliaFlash® P60 from *SILICYCLE* was used with a particle size of 40-63 µm (230-400 mesh), , and TLC was performed on silica gel 60 F254 glass plates with a thickness of 0.25 mm purchased from Merck.

UV-Vis Spectroscopy: The UV-Vis spectra were recorded on a *Shimadzu* UV spectrometer UV-1800 at room temperature in dichloromethane.

Solid state Spectroscopy: The solid state absorption measurements were performed with a Cary 5000 UV/Vis/NIR spectrometer Varian from Agilent. All results are measured relative to the absorption of a blank TiO_2 surface.

Electrochemistry: The electrochemical measurements were performed with an AutoLab PGSTAT302 potentiostat-galvanostat controlled by resident NOVA 9.1 software using a conventional single-compartment three-electrode cell. Unless explicitly stated otherwise, a Pt disk of 2 mm ø served as working electrode, as auxiliary a Pt wire was used and the reference electrode was a saturated potassium chloride calomel electrode (SCE). The supporting electrolyte was 0.1 M Et_4NBF_4 in MeCN or 0.1 M $LiCF_3SO_3$ in DMF. All potentials are quoted

relative to SCE. In all the experiments the scan rate was 100 mV/s for cyclic voltammetry. The surface deprotection was performed using the same set up, but the working electrode was replaced by the functionalized wafer.

Synthetic Procedures

1,4-Dimethoxy-2-methylnaphthalene (6)
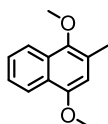
Menadione (4.99 g, 29.0 mmol, 1.0 eq.) was suspended in methanol (80 mL) in a 50 mL round-bottom flask. A solution of tin(II) chloride (22.0 g, 116 mmol, 4.0 eq.) in conc. HCl (37 %, 19 mL) was added dropwise over 30 min. After addition, the reaction mixture was stirred at room temperature for 30 minutes. The methanol was evaporated under reduced pressure and the residue was poured into water (33 mL). The precipitation was filtered off, diluted in acetone (66 mL) and dried over $MgSO_4$. K_2CO_3 (30.1 g, 218 mmol, 7.5 eq.) and dimethyl sulfate (15.3 mL, 160 mmol, 5.5 eq.) was added to the solution and the suspension was refluxed for 4 h. The insoluble components were filtered off and the filtrate was concentrated under reduced pressure. The residue was diluted in diethyl ether (20 mL) and aq. NaOH (20 %, 20 mL). The organic layer was washed with brine, dried over $MgSO_4$ and concentrated under reduced pressure. The crude product was purified by column chromatography (SiO_2, toluene). 1,4-Dimethoxy-2-methylnaphthalene (**6**, 3.97 g, 19.6 mmol, 68 %) was obtained as white crystals.

^{1}H-NMR (CDCl$_3$, 400 MHz) δ (ppm): 8.19 (dd, $^3J_{H.H}$ = 8.4 Hz, 1H), 8.03 (dd, $^3J_{H.H}$ = 8.4 Hz, 1H), 7.51 (dd, $^3J_{H.H}$ = 8.3 Hz, $^3J_{H.H}$ = 6.8 Hz, 1H), 7.42 (dd, $^3J_{H.H}$ = 8.2 Hz, $^3J_{H.H}$ = 6.8 Hz, 1H), 6.61 (s, 1H), 3.97 (s, 3H), 3.87 (s, 3H), 2.45 (s, 3H).

^{13}C-NMR (CDCl$_3$, 101 MHz) δ (ppm): 151.7, 147.1, 128.8, 126.6, 125.7, 125.4, 124.7, 122.3, 121.6, 107.0, 77.5, 77.4, 77.2, 76.8, 61.4, 55.8, 16.4.

MS (EI, 70 eV): m/z (%) = 202.0 (55), 187.0 (100), 188.0 (12.8), 159.1 (30.9), 144.1 (16.2), 128.1 (12.6), 115.0 (21.4).

HRMS (ESI): m/z calcd for [C$_{13}$H$_{14}$O$_2$+H]$^+$ 203.1067; found: 203.1067.

TLC (SiO_2, Toluene, UV): R$_f$ = 0.64.

1,4-Dimethoxy-3-methyl-2-naphthaldehyde (8)
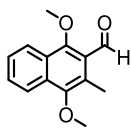
1,4-Dimethoxy-2-methylnaphthalene (**6**, 3.90 g, 19.3 mmol, 1.0 eq.) was dissolved in dry dichloromethane (28 mL) under argon atmosphere. A solution of $TiCl_4$ (1 M in dichloromethane, 21.6 mL, 21.6 mmol, 1.1 eq.) was added dropwise at 0 °C followed by 1,1-dichloromehtyl methyl ether (1.93 mL, 21.6 mmol, 1.1 eq.). The reaction mixture was stirred for 3 h at 0 °C, afterwards poured into ice and extracted with ethyl acetate. The combined organic layers were washed with brine, dried over $MgSO_4$ and concentrated under reduced pressure. The crude product was purified by column chromatography (SiO_2, cyclohexane / ethyl acetate 10:1). 1,4-Dimethoxy-3-methyl-2-naphthaldehyde (**8**, 4.01 g, 17.4 mmol, 90 %) was obtained as white crystals.

^{1}H-NMR ($CDCl_3$, 400 MHz) δ (ppm): 10.73 (s, 1H), 8.20 (d, $^3J_{H.H}$ = 8.4 Hz, 1H), 8.11 (d, $^3J_{H.H}$ = 8.4 Hz, 1H), 7.66 (dd, $^3J_{H.H}$ = 8.4 Hz, $^3J_{H.H}$ = 6.9 Hz, 1H), 7.55 (dd, $^3J_{H.H}$ = 8.2 Hz, $^3J_{H.H}$ = 6.8 Hz, 1H), 4.07 (s, 3H), 3.87 (s, 3H), 2.65 (s, 3H).

^{13}C-NMR ($CDCl_3$, 101 MHz) δ (ppm): 192.5, 160.3, 150.8, 132.1, 129.6, 122.2, 126.4, 126.2, 125.2, 123.3, 122.7, 65.6, 61.6, 13.2.

MS (EI, 70 eV): m/z (%) = 230.1 (100), 215.0 (78.8), 200.0 (47.5), 187.0 (13.1), 172.0 (30.4), 144.1 (24.2), 128.1 (23.8), 115.1 (49.4), 77.1 (11.7).

HRMS (ESI): m/z calcd for $[C_{14}H_{14}O_3+H]^+$ 231.1016; found: 231.1017.

TLC (SiO_2, Cyclohexane / ethyl acetate 10:1, UV): R_f = 0.53.

1,4-Dimethoxy-2-methyl-3-vinylnaphthalene (9)
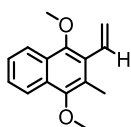
Methyltriphenylphosphonium bromide (698 mg, 1.91 mmol, 1.1 eq.) was suspended in dry THF (8 mL) under argon atmosphere. The suspension was cooled to 0 °C and n-BuLi (1.2 mL, 1.6 M in hexane, 1.91 mmol, 1.1 eq.) was added dropwise. The solution was stirred for 1 h at 0 °C. A solution of 1,4-dimethoxy-3-methyl-2-naphthaldehyde (**8**, 401 mg, 1.74 mmol, 1.0 eq.) in dry THF (4 mL) was added and the cooling bath was removed. After stirring 3 h at room temperature, the reaction was quenched by adding an aq. HCl solution (2M, 10 mL) and the mixture was extracted with ethyl acetate. The combined organic layers were dried over $MgSO_4$ and concentrated under reduced pressure. The crude product was purified by column chromatography (SiO_2, toluene). 1,4-Dimethoxy-2-methyl-3-vinylnaphthalene (**9**, 359 mg, 1.57 mmol, 90 %) was obtained as a colorless oil.

^{1}H-NMR ($CDCl_3$, 400 MHz) δ (ppm): 8.13 – 8.03 (m, 2H), 7.52 – 7.44 (m, 2H), 6.89 (dd, $^2J_{H.H}$ = 17.9 Hz, $^3J_{H.H}$ = 11.7 Hz, 1H), 5.79 (dd, $^2J_{H.H}$ = 18.0 Hz, $^3J_{H.H}$ = 2.0 Hz, 1H), 5.65 (dd, $^2J_{H.H}$ = 11.7 Hz, $^3J_{H.H}$ = 2.1 Hz, 1H), 3.88 (s, 3H), 3.84 (s, 3H), 2.44 (s, 3H).

^{13}C-NMR ($CDCl_3$, 101 MHz) δ (ppm): 150.2, 150.0, 131.4, 128.1, 128.0, 127.5, 126.1, 125.7, 125.5, 122.6, 122.0, 120.5, 61.3, 60.9, 13.6.

MS (EI, 70 eV): m/z (%) = 228.1 (100), 213.0 (68.1), 198.0 (48.0), 182.1 (36.70), 152.1 (18.7), 141.1 (28.8), 115.1 (25.2), 76.0 (18.2).

HRMS (ESI): m/z calcd for $[C_{15}H_{16}O_2+H]+$ 229.1223; found:.229.1223.

TLC (SiO_2, Toluene, UV): R_f = 0.66.

Chloro(2-(1,4-dimethoxy-3-methylnaphthalen-2-yl)ethyl)dimethylsilane (10)
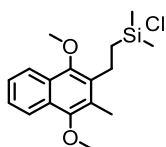
1,4-Dimethoxy-2-methyl-3-vinylnaphthalene (**9**, 890 mg, 3.90 mmol, 1.0 eq.) was placed in a 5 mL flask under argon atmosphere. Chlorodimethylsilane (651 µL, 5.85 mmol, 1.5 eq.) was added followed by the careful dropwise addition of the Karstedt's catalyst (780 µL, 0.1 M in xylene, 0.078 mmol, 0.02 eq.). The reaction mixture was stirred at 34 °C for 3 h. After cooling to room temperature, the mixture was dissolved in dry dichloromethane and filtered over a $MgSO_4$ plug directly into a bulb to bulb distillation flask under argon atmosphere. Dichloromethane and xylene was distilled off by a normal distillation under argon atmosphere. The crude product was purified by bulb to bulb distillation at 190 °C under high vacuum. Chloro(2-(1,4-dimethoxy-3-methylnaphthalen-2-yl)ethyl)dimethylsilane (**10**, 943 mg, 2.92 mmol, 75 %) was obtained as a colorless oil.

¹H-NMR (CDCl₃, 400 MHz) δ (ppm): 8.10 – 7.98 (m, 2H), 7.52 – 7.42 (m, 2H), 3.92 (s, 3H), 3.87 (s, 3H), 2.95 – 2.87 (m, 2H), 2.42 (s, 3H), 1.18 – 1.08 (m, 2H), 0.51 (s, 6H)

MS (EI, 70 eV): m/z (%) = 322.0 (100), 307.0 (63.4), 292.0 (48.3), 257.0 (14.2), 183.0 (15.8), 155.1 (25.2), 141.1 (11.8), 128.1 (15.7), 115.1 (12.6), 93.0 (48.7).

((4-(*tert*-Butyl)phenyl)ethynyl)(2-(1,4-dimethoxy-3-methylnaphthalen-2-yl)ethyl)dimethylsilane (11)
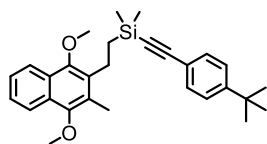
4-*tert*-Butylphenylacetylene (**4**, 0.572 mL, 3.05 mmol, 1.05 eq.) was dissolved in dry THF (9 mL), cooled to -78 °C and *n*-BuLi (2.08 mL, 1.6 M in hexane, 3.33 mmol, 1.15 eq.) was added dropwise. After stirring for 1 h at -78 °C, the reaction mixture was added dropwise to a solution of chloro(2-(1,4-dimethoxy-3-methylnaphthalen-2-yl)ethyl)dimethylsilane (**10**, 936 mg, 2.90 mmol, 1 eq.) in dry THF (13.5 mL) at room temperature and stirred for 30 min. The reaction was quenched with sat. aq. NH$_4$Cl solution and extracted with TBME. The combined organic layers were dried over MgSO$_4$, filtered and concentrated under reduced pressure. The crude product was purified by column chromatography (SiO$_2$, cyclohexane / ethyl acetate, 20:1). ((4-(*tert*-butyl)phenyl)ethynyl)(2-(1,4-dimethoxy-3-methylnaphthalen-2-yl)ethyl)dimethyl-silane (**11**, 1.10 g, 2.90 mmol, 86 %) was obtained as a colorless oil.

^{1}H-NMR (CDCl$_3$, 400 MHz) δ (ppm): 8.08 – 8.01 (m, 2H), 7.48 – 7.42 (m, 4H), 7.34 (d, $^3J_{H.H}$ = 8.6 Hz, 2H), 3.94 (s, 3H), 3.88 (s, 3H), 3.00 – 2.92 (m, 2H), 2.46 (s, 3H), 1.32 (s, 9H), 1.04 – 0.96 (m, 2H), 0.34 (s, 6H).

^{13}C-NMR (CDCl$_3$, 101 MHz) δ (ppm): 152.1, 150.3, 149.4, 134.4, 131.9, 127.5, 127.4, 126.3, 125.4, 125.4, 122.3, 122.3, 120.2, 106.4, 92.2, 77.2, 62.4, 61.4, 35.0, 31.3, 21.6, 17.6, 12.3, -1.7.

MS (EI, 70 eV): m/z (%) = 444.2 (15.3), 313.1 (12.1), 271.2 (24.6), 235.9 (19.5), 207.1 (20.7), 158.2 (15.5), 143.2 (50.9), 128.1 (18.4), 115.2 (33.3), 78.1 (100), 57.1 (22.7), 51.1 (25.6).

HRMS (ESI): m/z calcd for [C$_{29}$H$_{36}$O$_2$Si+K]$^+$ 483.2116; found: 483.2116.

TLC (SiO$_2$, Cyclohexane / ethyl acetate 15:1, UV): R$_f$ = 0.65.

2-(2-(((4-(*tert*-Butyl)phenyl)ethynyl)dimethylsilyl)ethyl)-3-methylnaphthalene-1,4-dione (2)
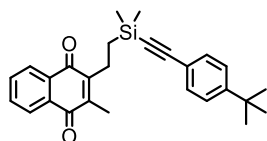
Dimethoxy compound **11** (80.5 mg, 0.181 mmol, 1.0 eq.) was dissolved in acetonitrile (3 mL) and water (1.5 mL). To the solution, ammonium cerium(IV) nitrate (257 mg, 0.462 mmol, 2.55 eq.) was added. The mixture was stirred for 1 h at room temperature followed by the extraction with dichloromethane. The combined organic layers were washed with brine, dried over $MgSO_4$ and concentrated under reduced pressure. The crude product was purified by column chromatography (SiO_2 cyclohexane / ethyl acetate, 20:1). 2-(2-(((4-(*tert*-Butyl)phenyl)-ethynyl)dimethylsilyl)ethyl)-3-methylnaphthalene-1,4-dione (**2**, 67.3 mg, 0.181 mmol, 90 %) was obtained as a slightly yellow oil.

¹H-NMR (CDCl$_3$, 400 MHz) δ (ppm): 8.10 – 8.03 (m, 2H), 7.70 – 7.64 (m, 2H), 7.37 (d, $^3J_{H.H}$ = 8.3 Hz, 2H), 7.31 (d, $^3J_{H.H}$ = 8.3 Hz, 2H), 2.82 – 2.70 (m, 2H), 2.22 (s, 3H), 1.30 (s, 9H), 0.92 – 0.82 (m, 2H), 0.31 (s, 6H).

¹³C-NMR (CDCl$_3$, 101 MHz) δ (ppm): 187.4, 186.4, 153.8, 151.4, 144.0, 135.1, 135.09, 134.2, 134.1, 133.6, 128.1, 128.0, 127.1, 121.7, 108.4, 93.5, 79.2, 78.9, 78.6, 36.7, 33.0, 23.2, 17.7, 14.2, 1.9.

HRMS (ESI): m/z calcd for [C$_{27}$H$_{30}$O$_2$Si+Na]$^+$ 437.1907; found: 437.1910.

TLC (SiO_2, Cyclohexane / ethyl acetate 15:1, UV): R$_f$ = 0.38.

(2-(1,4-Dimethoxy-3-methylnaphthalen-2-yl)ethyl)((4-iodophenyl)ethynyl)dimethylsilane (12)
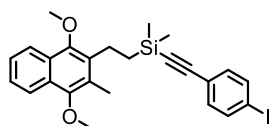
1-Ethynyl-4-iodobenzene (648 mg, 2.84 mmol, 1.0 eq.) was dissolved in dry THF (5 mL) under argon atmosphere. A solution TMPMgCl•LiCl in THF (1.0 M, 3.32 mL, 3.32 mmol, 1.2 eq.) was added at 0 °C and the reaction mixture was stirred for 1 h. A solution of chloro(2-(1,4-dimethoxy-3-methylnaphthalen-2-yl)ethyl)dimethylsilane (**10**, 917 mg, 2.84 mmol, 1.0 eq.) in dry THF (5 mL) was added. The ice bath was removed and the mixture was stirred for 16 h at room temperature. The reaction was quenched with sat. aq. NH_4Cl solution and extracted with ethyl acetate. The combined organic layers were washed with brine, dried over $MgSO_4$ and concentrated under reduced pressure. The crude product was purified by column chromatography (SiO_2, cyclohexane / ethyl acetate 20:1). (2-(1,4-Dimethoxy-3-methylnaphthalen-2-yl)ethyl)((4-iodophenyl)ethynyl)dimethylsilane (**12**, 1.33 g, 2.58 mmol, 91 %) was obtained as a colorless oil.

^{1}H-NMR (CDCl$_3$, 400 MHz) δ (ppm): 8.08 – 7.99 (m, 2H), 7.66 (d, $^3J_{H.H}$ = 8.6 Hz, 2H), 7.48 – 7.42 (m, 2H), 7.20 (d, $^3J_{H.H}$ = 8.4 Hz, 2H), 3.92 (s, 3H), 3.87 (s, 3H), 2.99 – 2.89 (m, 2H), 2.44 (s, 3H), 1.03 – 0.95 (m, 2H), 0.33 (s, 6H).

^{13}C-NMR (CDCl$_3$, 101 MHz) δ (ppm): 150.4, 149.4, 137.6, 134.1, 133.6, 127.5, 126.2, 125.4, 122.7, 122.3, 122.3, 105.0, 94.9, 94.7, 62.4, 61.4, 21.5, 17.4, 12.3, -1.9.

HRMS (ESI): m/z calcd for [C$_{25}$H$_{27}$IO$_2$Si+Na]$^+$ 537.0726; found: 537.0717.

TLC (SiO$_2$, Cyclohexane / ethyl acetate 20:1, UV): R$_f$ = 0.48.

2-(2-(((4-Diodophenyl)ethynyl)dimethylsilyl)ethyl)-3-methylnaphthalene-1,4-dione (13)
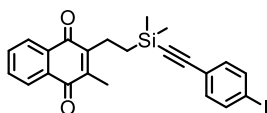
Dimethoxy compound **12** (520 mg, 1.01 mmol, 1 eq.) was dissolved in acetonitrile (8 mL) and water (4 mL). Ammonium cerium(IV) nitrate (1.41 g, 2.58 mmol, 2.55 eq.) was added and the mixture was stirred for 2 h at rt. The reaction was quenched with water and extracted with dichloromethane. The combined organic layers were washed with brine, dried over $MgSO_4$ and concentrated under reduced pressure. The crude product was purified by column chromatography (SiO$_2$, cyclohexane / ethyl acetate 10:1). 2-(2-(((4-Diodophenyl)ethynyl)dimethylsilyl)ethyl)-3-methylnaphthalene-1,4-dione (**13**, 444 mg, 0.917 mmol, 91 %) was obtained as a yellow solid.

^{1}H-NMR (CDCl$_3$, 400 MHz) δ (ppm): 8.09 – 8.05 (m, 2H), 7.69 – 7.65 (m, 2H), 7.62 (d, $^3J_{H.H}$ = 8.4 Hz, 2H), 7.14 (d, $^3J_{H.H}$ = 8.4 Hz, 2H), 2.79 – 2.70 (m, 2H), 2.21 (s, 3H), 0.93 – 0.82 (m, 2H), 0.31 (s, 6H).

^{13}C-NMR (CDCl$_3$, 101 MHz) δ (ppm): 185.6, 184.67, 149.4, 142.3, 137.6, 133.5, 133.5, 133.4, 132.4, 132.3, 126.3, 126.3, 122.5, 105.3, 94.8, 94.4, 21.4, 15.7, 12.5, -1.9.

HRMS (ESI): m/z calcd for $[C_{23}H_{21}IO_2Si+H]^+$ 485.0431; found: 485.0428.

TLC (SiO$_2$, Cyclohexane / ethyl acetate 10:1, UV): R$_f$ = 0.61.

2-(2-(((4-((4-Aminophenyl)ethynyl)phenyl)ethynyl)dimethylsilyl)ethyl)-3-methylnaphthalene-1,4-dione (15)
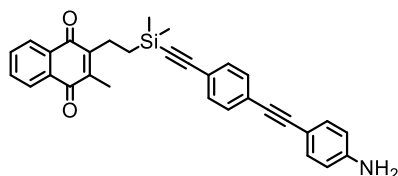
Quinone **14** (260 mg, 0.537 mmol, 1.0 eq.) was dissolved in dry Et_3N (11 mL) under argon atmosphere. The solution was degassed for 10 min. with argon, followed by the addition of 4-ethynylaniline (71.3 mg, 0.591 mmol, 1.1 eq.), $Pd(PPh_3)_4$ (31 mg, 0.027 mmol, 0.05 eq.) and CuI (6.1 mg, 0.032 mmol, 0.06 eq.). The reaction mixture was stirred over night at room temperature. The reaction mixture was extracted with ethyl acetate, washed with brine, dried over $MgSO_4$ and concentrated under reduced pressure. The crude product was purified by column chromatography (SiO_2, toluene / ethyl acetate 3:1). 2-(2-(((4-((4-Aminophenyl)ethynyl)phenyl)ethynyl)dimethylsilyl)ethyl)-3-methylnaphthalene-1,4-dione (**15**, 250 mg, 0.528 mmol, 98 %) was obtained as a yellow solid.

¹H-NMR (CDCl₃, 400 MHz) δ (ppm): 8.11 – 8.02 (m, 2H), 7.70 – 7.64 (m, 2H), 7.44 – 7.34 (m, 6H), 6.76 (d, $^3J_{H.H}$ = 8.0 Hz, 2H), 2.80 – 2.73 (m, 2H), 2.22 (s, 3H), 0.91 – 0.84 (m, 2H), 0.32 (s, 6H).

¹³C-NMR (CDCl₃, 101 MHz) δ (ppm): 185.6, 184.7, 149.5, 142.3, 133.5, 133.4, 133.2, 132.4, 132.3, 132.0, 131.3, 126.3, 126.3, 124.2, 122.2, 116.0, 113.9, 106.1, 94.4, 87.7, 21.4, 15.8, 12.5, -1.8.

HRMS (ESI): m/z calcd for $[C_{31}H_{27}NO_2Si+H]^+$ 474.1887; found: 474.1884.

TLC (SiO_2, Toluene / ethyl acetate 3:1, UV): R_f = 0.60.

2,2'-((2-((Carboxymethyl)(2-((4-((4-((dimethyl(2-(3-methyl-1,4-dioxo-1,4-dihydronaphthalen-2-yl)ethyl)silyl)ethynyl)phenyl)ethynyl)phenyl)amino)-2-oxoethyl)amino)ethyl)azanediyl)diacetic acid (1)
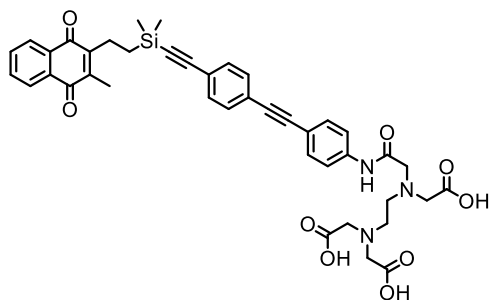
EDTA-monohydrate (**16,** 187 mg, 0.682 mmol, 1.0 eq.) and aniline **15** (323 mg, 0.682 mmol, 1.0 eq.) were dissolved in dry DMF (60 mL) under argon atmosphere. The reaction mixture was stirred at 60 °C for 12 h and afterwards was concentrated under reduced pressure. The crude product was suspended in acetone and after sedimentation, the acetone was decanted. The precipitation was washed 3 times with diethyl ether. 2,2'-((2-((Carboxymethyl)(2-((4-((4-((dimethyl(2-(3-methyl-1,4-dioxo-1,4-dihydronaphthalen-2-yl)ethyl)silyl)ethynyl)phenyl)ethynyl)phenyl)amino)-2-oxoethyl)amino)ethyl)azanediyl)diacetic acid (**1**, 251 mg, 0.336 mmol, 49 %) was obtained as a yellow solid.

^{1}H-NMR (Methanol-d_4, 400 MHz) δ (ppm): 8.08 – 8.03 (m, 1H), 8.02 – 7.97 (m, 1H), 7.57 – 7.69 (m, 4H), 7.47 (d, $^3J_{H.H}$ = 8.7 Hz, 2H), 7.42 (d, $^3J_{H.H}$ = 8.4 Hz, 2H), 7.32 (d, $^3J_{H.H}$ = 8.3 Hz, 2H), 3.94 (s, 4H), 3.75 (s, 2H), 3.64 (s, 2H), 3.38 (t, $^3J_{H.H}$ = 5.6 Hz 2H), 3.21 (t, $^3J_{H.H}$ = 5.6 Hz, 2H), 2.84 – 2.80 (m, 2H), 2.22 (s, 3H), 0.95 – 0.91 (m, 2H), 0.31 (s, 6H).

^{13}C-NMR (Methanol-d_4, 101 MHz) δ (ppm): 186.5, 185.7, 173.9, 171.1, 170.4, 150.3, 143.6, 140.0, 134.6, 134.5, 133.6, 133.5, 133.2, 132.9, 132.4, 127.1, 127.0, 125.1, 123.8, 121.1, 119.7, 106.9, 95.4, 92.3, 89.2, 59.1, 56.9, 56.2, 53.8, 51.7, 22.1, 16.3, 12.6, -1.9.

MS (MALDI-TOF): m/z = 748.5 ([M]$^+$)

HRMS (ESI): m/z calcd for [C$_{41}$H$_{42}$N$_3$O$_9$Si+H]$^+$ 748.2685; found: 748.2681.

((4-Iodophenyl)ethynyl)trimethylsilane (18)
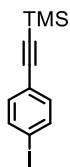
1,4-Diiodobenzene (4.00 g, 12.1 mmol, 1.0 eq.), $Pd(PPh_3)_2Cl_2$ (111 mg, 0.157 mmol, 0.013 eq.) and CuI (60.3 mg, 0.315 mmol, 0.026 eq.) were dissolved in dry THF (50 mL) under argon atmosphere. Afterwards, dry triethylamine (0.8 mL) was added and the reaction mixture was degassed for 10 min with argon. A solution of trimethylsilylacetylene (1.07 mL, 7.26 mmol, 0.6 eq.) was added dropwise over 1 h at room temperature. After 6 h, the reaction was stopped and diluted with dichloromethane. The crude mixture was filtered over a celite plug and concentrated under reduced pressure. The crude product was purified by column chromatography (SiO_2, cyclohexane). ((4-Iodophenyl)ethynyl)trimethylsilane (**18**, 1.95 g, 6.50 mmol, 54 %) was obtained as an off white solid.

^{1}H-NMR (CDCl$_3$, 400 MHz) δ (ppm): 7.63 (d, $^3J_{H,H}$ = 8.4 Hz, 2H), 7.18 (d, $^3J_{H,H}$ = 8.4 Hz, 2H), 0.24 (s, 9H).

^{13}C-NMR (CDCl$_3$, 101 MHz) δ (ppm): 137.5, 133.6, 122.8, 104.1, 96.0, 95.0, 0.0.

MS (EI, 70 eV): m/z (%) = 299.9 (41.2), 284.9 (100), 158.1 (29.2), 143.0 (24.2), 117.1 10.6), 79.1 (16.7).

TLC (SiO_2, Cyclohexane, UV): R_f = 0.58.

4-((4-((Trimethylsilyl)ethynyl)phenyl)ethynyl)aniline (19)
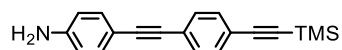
(4-Iodophenylethynyl)trimethylsilane (**18**, 659 mg, 2.13 mmol, 1.0 eq.), Pd(PPh$_3$)$_2$Cl$_2$ (74.8 mg, 0.107 mmol, 0.05 eq.) and CuI(40.6 mg, 0.213 mmol, 0.1 eq.) was placed in a dry flask under argon atmosphere. THF (8.5 mL) and triethylamine (2.5 mL) was added followed by 4-ethynylaniline (300 mg, 2.56 mmol, 1.2 eq.). The reaction mixture was degassed for 10 min. with argon and was stirred at room temperature for 4 h. Afterwards the mixture was diluted with dichloromethane and filtered over a silica plug. No further purification was performed.

^{1}H-NMR (CDCl$_3$, 400 MHz) δ (ppm): 7.41 (s, 4H), 7.33 (d, $^3J_{H,H}$ = 8.5 Hz, 2H), 6.64 (d, $^3J_{H,H}$ = 8.5 Hz, 2H), 3.95 (s, 2H), 0.25 (s, 9H).

^{13}C-NMR (CDCl$_3$, 101 MHz) δ (ppm): 146.8, 133.2, 132.0, 131.2, 124.2, 122.3, 115.0, 112.6, 105.0, 96.0, 92.3, 87.3, 0.1.

MS (EI, 70 eV): m/z (%) = 289.3 (100), 274.2 (88.0), 137.1 (22.6).

TLC (SiO$_2$, Cyclohexane / dichloromethane 1:5, UV): R$_f$ = 0.54.

4-((4-Ethynylphenyl)ethynyl)aniline (20)
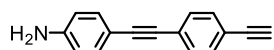
4-((4-((Trimethylsilyl)ethynyl)phenyl)ethynyl)aniline (**19**, 359 mg, 1.24 mmol, 1.0 eq.) was dissolved in dry THF (10 mL) under argon atmosphere and a TBAF solution in THF (1M, 1.24 mL, 1.24 mmol, 1.0 eq.) was added dropwise. The reaction mixture was stirred for 1 h at room temperature. The reaction was quenched with water and extracted with dichloromethane. The combined organic layers were dried over $MgSO_4$ and concentrated under reduced pressure. The crude product was purified by column chromatography (SiO_2, cyclohexane / dichloromethane 1:5). 4-((4-Ethynylphenyl)ethynyl)aniline (**20**, 257 mg, 1.18 mmol, 95 %) was obtained as a slightly yellow solid.

^{1}H-NMR (CDCl$_3$, 400 MHz) δ (ppm): 7.44 (s, 4H), 7.34 (d, $^3J_{H,H}$ = 8.6 Hz, 2H), 6.64 (d, $^3J_{H,H}$ = 8.6 Hz, 2H), 3.84 (s, 2H), 3.15 (s, 1H).

^{13}C-NMR (CDCl$_3$, 101 MHz) δ (ppm): 147.0, 133.2, 132.1, 131.3, 124.7, 121.3, 114.9, 112.4, 92.5, 87.1, 83.6, 78.7.

MS (EI, 70 eV): m/z (%) = 217.1 (100), 189.2 (12.7), 108.6 (8.4).

TLC (SiO_2, Cyclohexane / dichloromethane 1:5, UV): R_f = 0.48

48

2,2'-((2-((Carboxymethyl)(2-((4-((4-ethynylphenyl)ethynyl)phenyl)amino)-2-oxoethyl)amino)ethyl)azanediyl)diacetic acid (21)
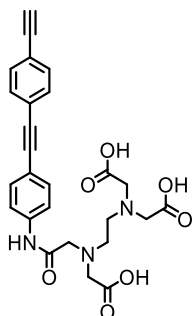
EDTA-monohydrate (**16**, 63.1 mg, 0.230 mmol, 1.0 eq.) and 4-((4-ethynylphenyl) ethynyl)aniline (**20**, 50.0 mg, 0.230 mmol, 1.0 eq.) were dissolved in dry DMF (15 mL) under argon atmosphere. The reaction mixture was stirred at 60 °C for 12 h. The mixture was concentrated under reduced pressure. The crude product was suspended in acetone and after sedimentation, the acetone was decanted followed by washing the precipitation 3 times with diehtylether. 2,2'-((2-((Carboxymethyl)(2-((4-((4-ethynylphenyl)ethynyl)phenyl)amino)-2-oxo ethyl)amino)ethyl)azanediyl)diacetic acid (**21**, 251 mg, 0.336 mmol, 49 %) was obtained as a yellow solid.

3-Azidopropan-1-amine (23)
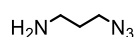
3-Bromopropylamine hydrobromide (3.28 g, 15.0 mmol, 1.0 eq.) was dissolved in water (10 mL). A solution of sodium azide (3.25 g, 50.0 mmol, 3.3 eq.) in water (15 mL) was added and the mixture was heated to reflux and stirred for 16 h. After cooling to room temperature, diethyl ether (50 mL) was added. The solution was cooled with an ice-water bath and KOH pellets (4.0 g) were added, holding the temperature below 10 °C. The mixture was extracted twice with diethyl ether and the combined organic layers were dried over $MgSO_4$. The diethyl ether was carefully distilled of. 3-Azidopropan-1-amine (**23**, 1.24 g, 12.4 mmol, 83 %) was obtained as a colorless volatile oil.

¹H-NMR (CDCl₃, 400 MHz) δ (ppm): 3.37 (t, $^3J_{H,H}$ = 6.7 Hz, 2H), 2.80 (t, $^3J_{H,H}$ = 6.8 Hz, 2H), 1.73 (p, $^3J_{H,H}$ = 6.7 Hz, 2H). 1.45 (brs, 2H).

2,7-Bis(3-azidopropyl)-4,9-dichlorobenzo[lmn][3,8]phenanthroline-1,3,6,8(2H,7H)-tetraone (25)
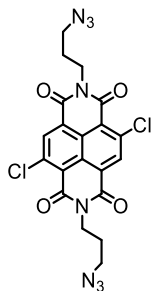
3,7-Dichloro-1,4,5,8-naphthalenetetracarboxylic dianhydride (**24**, 213 mg, 0.632 mmol, 1.0 eq.) was suspended in acetic acid (12 mL). 3-Azidopropan-1-amine (**23**, 248 µL, 2.53 mmol, 4.0 eq.) was added and the reaction mixture was heated to 120 °C and stirred for 3 h. After cooling to room temperature, the precipitation was filtered off and washed with ice cold water. The product was dried in high vacuum. No further purification was performed. 2,7-Bis(3-azidopropyl)-4,9-dichlorobenzo[lmn][3,8]phenanthroline-1,3,6,8(2H,7H)-tetraone (**25**, 198 mg, 0.395 mmol, 63 %) as a brown solid.

MS (MALDI-TOF): m/z = 500.3 ([M]$^-$)

2,7-Bis(3-azidopropyl)-4,9-bis(hexylthio)benzo[lmn][3,8]phenanthroline-1,3,6,8(2H,7H)-tetraone (26)
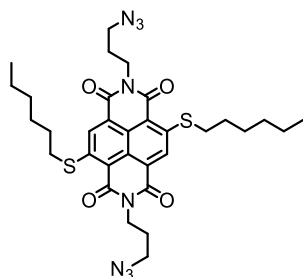
To a suspension of NDI **25** (190 mg, 0.379 mmol, 1 eq.) in dry DMF (16 mL), K_2CO_3 (157 mg, 1.14 mmol, 3 eq.) and hexylthiol (0.213 mL, 1.52 mmol, 4 eq.) was added. The reaction mixture was heated to 50 °C and stirred for 16 h. After cooling to room temperature, the reaction was stopped by the addition of water and extracted with dichloromethane. The combined organic layers were washed with brine, dried over $MgSO_4$ and concentrated under reduced pressure. The crude product was purified by column chromatography (SiO_2, cyclohexane / ethyl acetate 2:1). 2,7-Bis(3-azidopropyl)-4,9-bis(hexylthio)benzo[lmn][3,8]phenanthroline-1,3,6,8(2H,7H)-tetraone (**26**, 64.0 mg, 0.096 mmol, 25 %) was obtained as a red solid.

¹H-NMR (CDCl₃, 400 MHz) δ (ppm): 8.59 (s, 2H), 4.30 (t, $^3J_{H,H}$ = 6.9 Hz, 4H), 3.46 (t, $^3J_{H,H}$ = 6.7 Hz, 4H), 3.20 (t, $^3J_{H,H}$ = 7.4 Hz, 4H), 2.12 – 2.00 (m, 4H), 1.94 – 1.82 (m, 4H), 1.67 – 1.55 (m, 4H), 1.45 – 1.35 (m, 8H), 0.93 (t, $^3J_{H,H}$ = 6.9 Hz, 6H).

¹³C-NMR (CDCl₃, 101 MHz) δ (ppm): 163.4, 162.5, 149.2, 128.5, 125.0, 123.6, 119.0, 49.6, 38.8, 32.5, 29.9, 29.0, 28.0, 27.7, 22.7, 14.2.

MS (MALDI-TOF): m/z = 664.6 ([M]⁻)

TLC (SiO_2, Cyclohexane / ethyl acetate 2:1, UV): R_f = 0.82.

2,7-Bis(3-azidopropyl)-4,9-bis(hexylamino)benzo[lmn][3,8]phenanthroline-1,3,6,8(2H,7H)-tetraone (27)
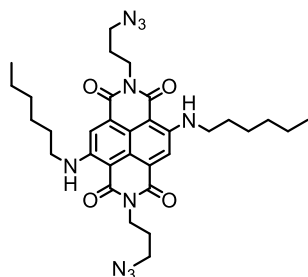
To a suspension of NDI **25** (200 mg, 0.399 mmol, 1 eq.) in dry THF (12 mL), K_2CO_3 (165 mg, 1.20 mmol, 3 eq.) and hexylamine (0.316 mL, 2.39 mmol, 6 eq.) was added. The reaction mixture was heated to 60 °C and stirred for 24 h. The reaction was observed by TLC control, and addition hexylamine was added if necessary. After cooling to room temperature, the reaction was stopped by the addition of water and extracted with dichloromethane. The combined organic layers were washed with brine, dried over $MgSO_4$ and concentrated under reduced pressure. The crude product was purified by column chromatography (SiO_2, cyclohexane / ethyl acetate 2:1). 2,7-Bis(3-azidopropyl)-4,9-bis(hexylamino)benzo[lmn][3,8]phenanthroline-1,3,6,8(2H,7H)-tetraone (**27**, 135 mg, 0.214 mmol, 54 %) was obtained as a blue solid.

^{1}H-NMR (CDCl$_3$, 400 MHz) δ (ppm): 9.14 (t, $^3J_{H,H}$ = 5.1 Hz, 2H), 7.82 (s, 2H), 4.18 (t, $^3J_{H,H}$ = 7.1 Hz, 4H), 3.49 - 3.35 (m, 8H), 2.00 (tt, $^3J_{H,H}$ = 6.9, $^3J_{H,H}$ = 6.9 Hz, 4H), 1.80 (tt, $^3J_{H,H}$ = 7.4 Hz, $^3J_{H,H}$ = 7.3 Hz, Hz, 4H), 1.59 – 1.47 (m, 4H), 1.44 – 1.34 (m, 8H), 0.94 (t, $^3J_{H,H}$ = 6.9 Hz, 6H).

^{13}C-NMR (CDCl$_3$, 101 MHz) δ (ppm): 165.8, 162.7, 148.9, 125.2, 120.7, 118.0, 101.2, 49.6, 43.4, 37.9, 31.7, 29.5, 27.7, 27.0, 22.7, 14.2.

MS (MALDI-TOF): m/z = 630.6 ([M]$^-$)

TLC (SiO$_2$, Cyclohexane / ethyl acetate 2:1, UV): R$_f$ = 0.89.

Surface Click Chemistry
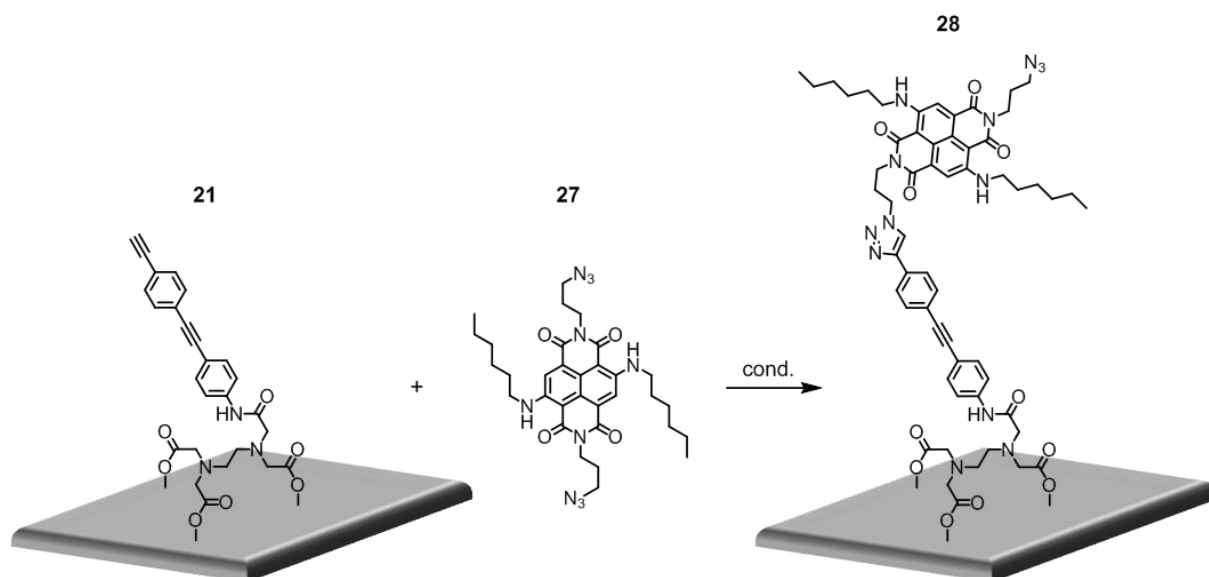
To a solution of Cu(MeCN)₄PF₆ (1.1 mg, 0.003 mmol, 1.0 eq.) and TBTA (1.6 mg, 0.003 mmol 1.0 eq.) in THF (4 mL), a solution of NDI-azide dye **27** (1.9 mg, 0.003 mmol, 1 eq.) in THF (1.5 mL) was added. The wafer with the immobilized alkyne **21** was dipped for 4 h into the reactions solution without stirring. Afterwards, the wafer was sonicated for 2 minutes in a THF bath to wash of non-immobilized residues.

Chapter 2 - Molecular Wires

Molecular Electronics

In 1965, Gordon Moore forecasted the doubling of transistors in dense integrated circuits in an interval of 12 months and reconsidered the length of the interval 10 years later to every 24 months. 50 years later, his prediction has proven to be true as shown in **figure 19**. Currently, the size of a single transistor is below 20 nanometers. Compared to the first used transistors on the microchip Intel 4004 in 1971, the size was decreased by a factor of 500.[107] The size of 20 nm equals the lower boundary of the wavelength of ultraviolet light. The construction of today's transistors and microchips is mainly based on top-down approaches, applying lithographical techniques. The lithography of nanostructures is based on ultraviolet light and therefore limits the top-down approach technique. To scale the dimension of further transistor and microchips, the development of new techniques is essential. By using the recently established extreme ultraviolet (EUV) lithography, the smallest size of commercially used transistor is 10 nm, and the next generation of 7 nm or even smaller chips is being developed.
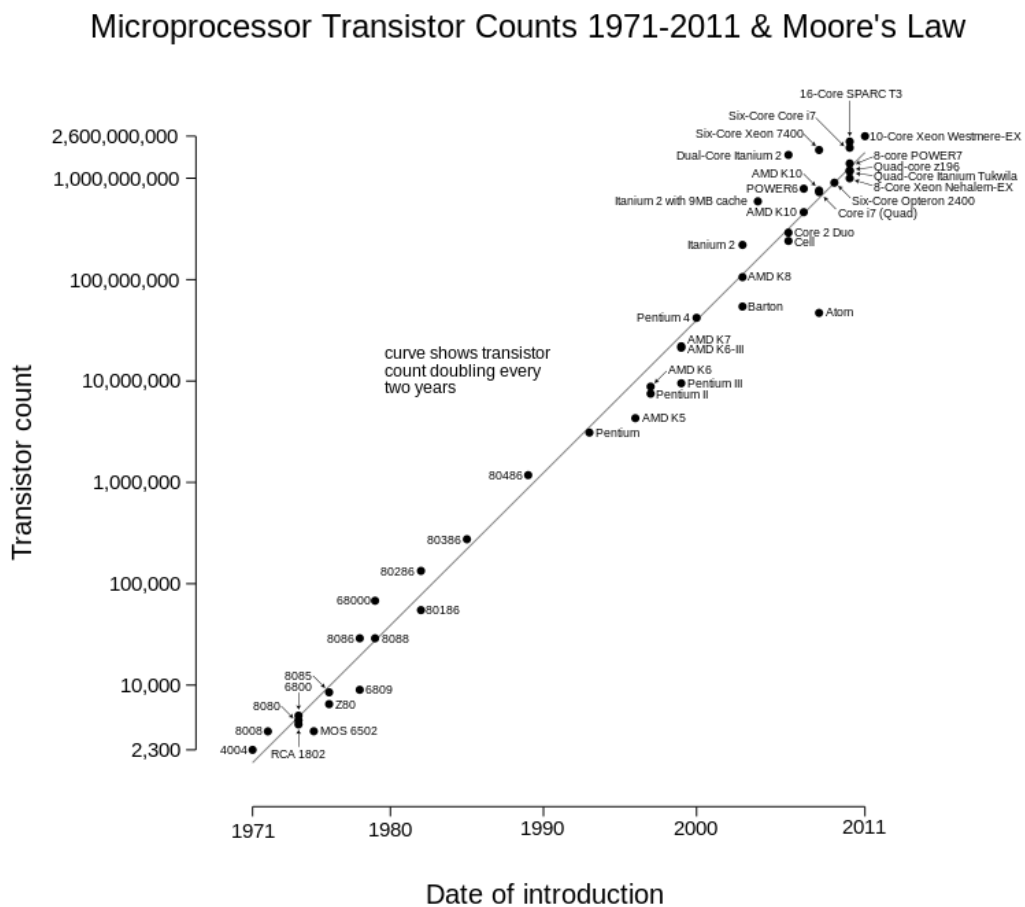
Figure 19. Illustration of Moore's law from 1971 – 2011. Reprinted from Wikipedia[108]

However, enhancement of the existing techniques is only one part of the story. Whereas for the next years, the cost and efficiency of the used top down approaches are the limiting factors, but not the physical barriers, bottom up approaches enable possibilities for novel architectures in molecular electronics, mainly outside of the highly commercialized processor chip and transistor industry. Instead of batch-fabrication processes, such as nanolithography, the production of nanometer-size molecules by chemical synthesis in large quantities is less cost intensive but with the same uniformity. The assembly of molecules possessing the desired electronical configuration by self-assembly techniques allows for the construction of complex systems. Therefore, a deep fundamental understanding of the principles of single molecules as building blocks in molecular electronic is crucial.

To investigate the behavior of electrical circuits on the molecular level, three different type of experiments are typically performed: (i) Molecular break junction measurements, having a single molecule linking two metal electrodes with an applied voltage to measure the conductance.[109] (ii) The metal electrodes are replaced by appropriate molecular electron donor and acceptor building blocks at both ends of a molecular wire. The electron transfer gets induced by a photochemical excitation of the electron accepting building block.[110] The rate of this electron transfer can be observed by a pump-probe experiment. (iii) The third method is based on self-assembled mono layers (SAM) on top of a metal surface, topped by another metal cover. The measured conductance between the two metal surfaces trough the self-assembled monolayer is depending on diameter or thickness of the SAM, leading to a wealth of information. All three types of experiments aim for a better understanding of the electron transfer through single molecules and will enable the ultimate miniaturization of devices to consist of structures at atomic scale.

Molecular Wires

With the tools of organic chemistry, it is possible to arrange atoms in almost every structure and therefore create molecules with the desired characteristics. The electron transport through a single molecule is just the beginning. To minimalize electrical devices to a molecular size, having building blocks with the functionality as molecular rectifier, molecular switch or molecular transistor is essential.[109,111,112] The pioneering work of Aviram and Ratner[113] in a time where conducting polymers and rudimentary organic electronics raised in the community, showed that organic molecules can have a preferred direction of conductance along the molecular axis. The paper was of theoretical nature, but the concept was realized 23 years later by the group of Metzger and coworkers in 1997.[114] Over the last decades, an enormous amount of developed molecular wires, rectifiers, transistors, and switches were reported.[115–118]

Aim of the Work - Molecular Design

The challenge in the future will be the development of a degree of control in molecular electronics with atomic accuracy. To achieve a control over the functionality, the fundamental understanding of charge transport within a molecular wire is crucial. Vonlanthen *et al.*[119,120] showed the conductance dependency of the torsion angle between the two phenyl rings of a biphenyl system. The inter-plane angle of the biphenyl unit was adjusted by alkyl bridges with different lengths. The smaller overlapping of both π-systems resulted in a decreased conductance through the molecule in break junctions experiments. Additionally to the conjugation within the molecule wire, the length of the molecule is an important factor regarding the conductance. In short molecular wires, the charge transport is dominated by direct tunneling in a single step transition and showed an exponential dependency of the length.[121] In longer molecules the hopping process dominates, where the charge is temporarily localized on several molecular sites. Wang and coworkers have shown, with amine-terminated OPE molecular wires, a change in the transport mechanism from a tunneling to the hopping mechanism reaching a molecular length of about 2.75 nm.[121] Only few of the conformation dependent conductance effects have been verified in longer molecular wires.[122] Therefore, we designed, based on the approach of Vonlanthen *et al.*, alkyl-bridge interlinked biphenyl systems, extended by a phenyl ethynyl building block on both sides.
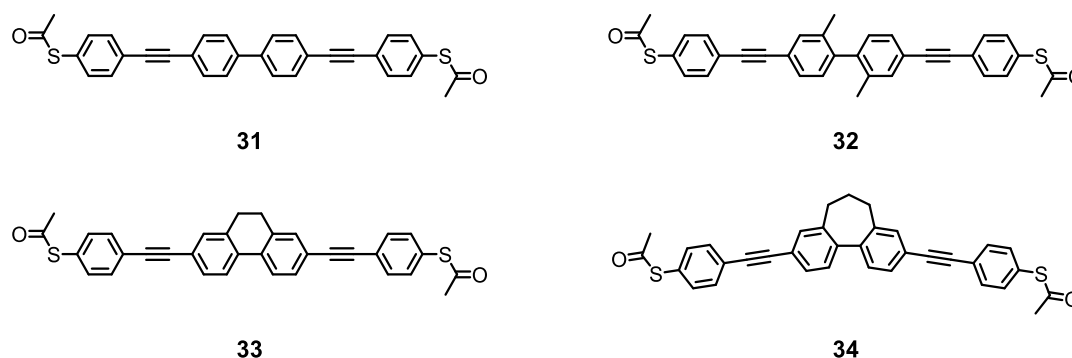
Figure 20. Molecular design of target molecules **31** - **34**. The biphenyl core is in 2,2'-position functionalized either with methyl groups or interlinked by an ethyl bridge or a propyl bridge.

All target molecules have a thioacetyl moiety installed on both ends as anchoring groups. The biphenyl is functionalized in 2,2'-position either with two methyl groups, an ethyl bridge or a propyl bridge. The induced inter-planar angles between the both phenyl rings are 79.7° (**32**), 16,8° (**33**) and 44.7° (**34**), respectively.[119] As reference, the non-functionalized biphenyl derivative **31** was designed. The sulfur to sulfur length in all molecules is around 2.4 nm and

therefore right at the border between a dominating tunneling mechanism and a distinct hopping mechanism.

For the second group of proposed molecules, the inspiration was obtained by the work of Lörtscher *et al.* presenting a reversible and controllable switch functionality of a single-molecule junction.[1] By performing molecular break junction experiments with bipyridyl derivative **B**, hysteresis in conductance at ± 0.9 V were detected. The molecule within the junction switched from an "off" state with lower conductance to an "on" state with higher conduction in the range of 0.9 V. By sweeping the voltage back from 1.5 V to 0 V, a higher conductance was measured in the region between 0.80 V and 0.55 V than during the initial upwards scan. Further decreasing the applied voltage to a range of -1.0 V revealed the back switch to the "off" state.
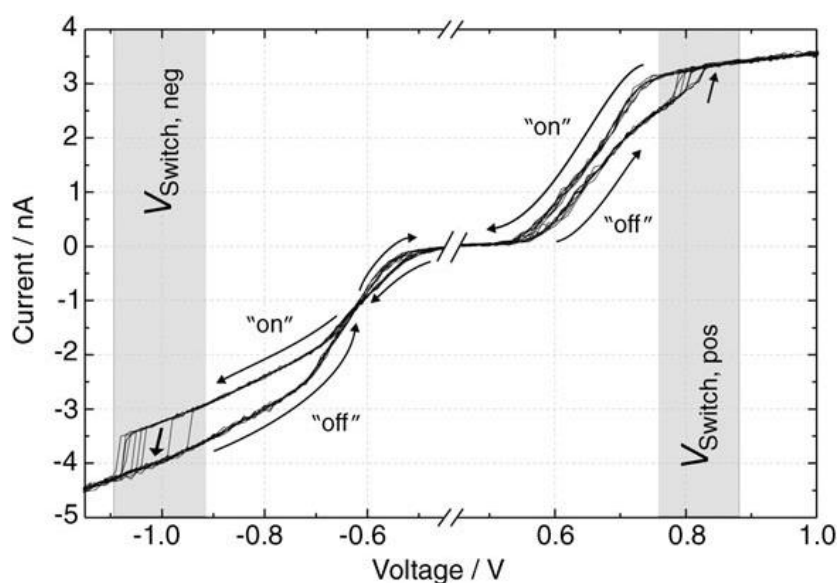
Figure 21. The system switches from the initial "off" state to the "on" state after exceeding a certain positive threshold value ($V_{switch, pos}$). A negative voltage sweep or a pulse below the negative threshold value ($V_{switch,neg}$) resets the molecule again to the initial "off" state. Reprinted with permission from Lörtscher *et al.*[1]

The switch ability was reproducible for several hundred negative and positive sweeps. By applying a potential lower than the required switching potential, the state of the molecule was readable due to the resulting current flow. The nondestructive reading of a tunable state, enables the opportunity to use such a molecule as a memory element. The measurements with the reference structure bipyridyl oligophenylene-ethynylene dithiol **A** did not exhibit a comparable effect. As result, the nitro moiety and its induced intrinsic dipole moment was probably the origin of this switching behavior. To further investigate the influence of electron withdrawing or electron donating effects, a series of test molecules was designed. The 2,2'-bipyridine core was exchanged to a biphenyl unit. As electron withdrawing groups, the trifluoromethyl functionality was selected in compound **36**. To increase the intrinsic dipole

moment within the molecule, an additional electron donating groups was inserted at 5,5'-position. The resulting push-pull system was formed by the combination of the -CF$_3$ group with a methoxy moiety in compound **37** or dimethylamine moiety in compound **38**. Additional, a molecular wire only functionalized with the electron donating methoxy group was designed in molecular wire **35**.
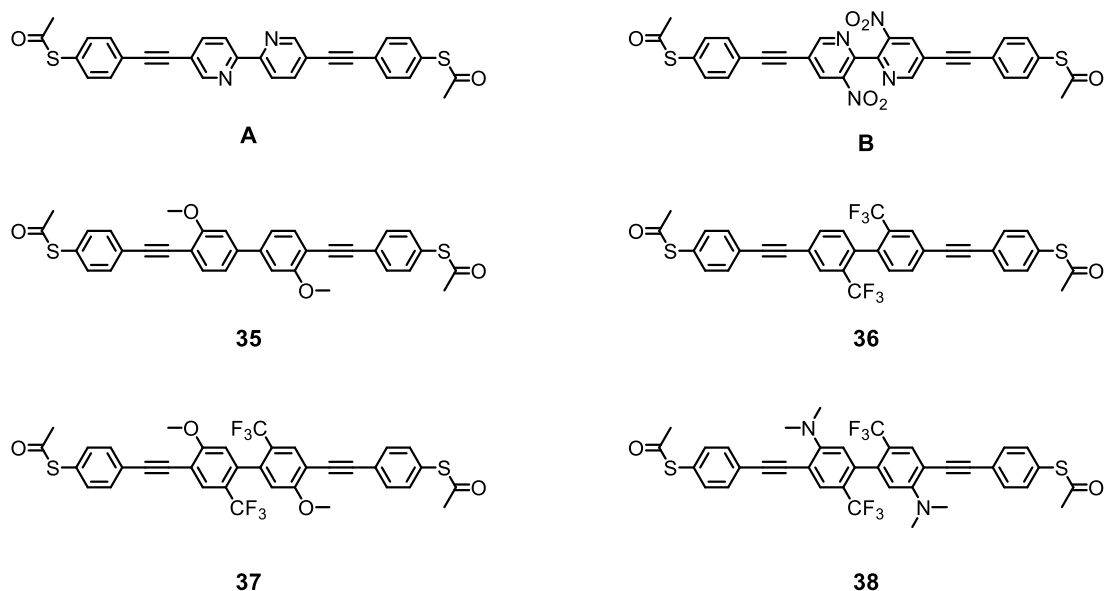
Figure 22. Designed molecular wires with an intrinsic dipole moment. As electron withdrawing substituent, -CF$_3$ moiety was selected. For the electron donating group, either methoxy groups or dimethylamines were used. The biphenyl core was extended by a phenyl ethynyl moiety and thioacetyls were defined as anchoring groups.

Synthetic Pathway

Synthesis of Molecular Wires 31 - 34
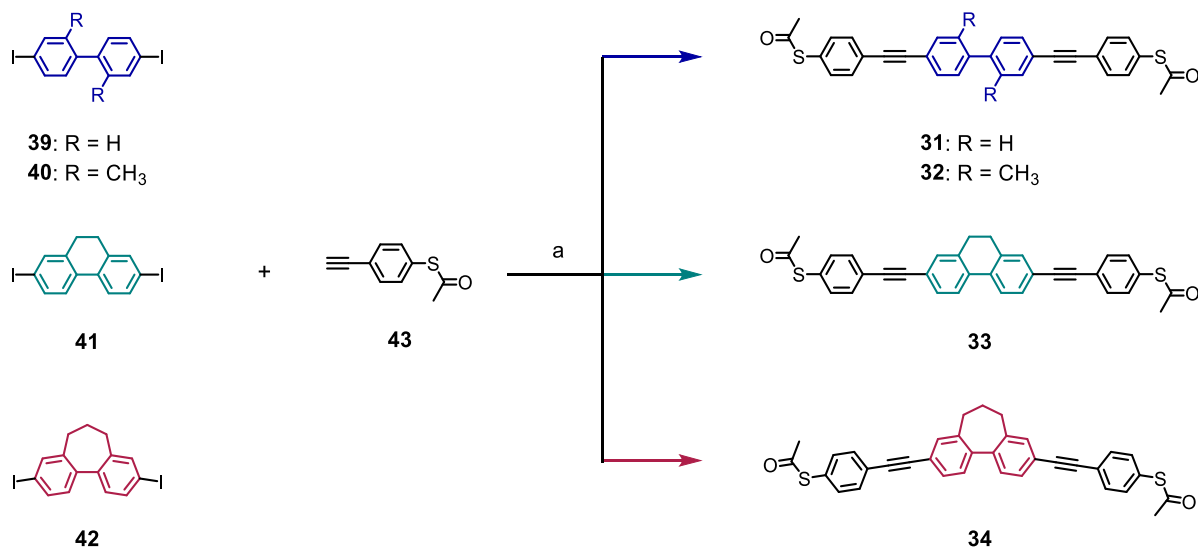
Scheme 11. Synthesis of target structures **31** - **34**. Reaction conditions: a) Pd(PPh3)4, CuI, iPr2NH, THF, 50 °C, 22 h. Yields: **31** (19 %); **32** (55 %); **33** (38 %); **34** (22 %).

To synthesize the molecular wires **31** - **34**, the corresponding diiodobiphenyls **39** - **42** were used as precursors. The synthesis of the bridged biphenyl precursor **41** and **42** is literature known and published by Vonlanthen *et al.*[120] and Shaporenko *et al.*[123], respectively. For the ethyl bridged biphenyl **41**, commercially available 9,10-dihydrophenanthrene was iodinated in 2- and 7-position using elemental iodine and iodic acid in a water / chloroform biphasic solvent system. The synthetic approach for the synthesis of the propyl bridged biphenyl **42** started with the commercially available 2-amino-5-iodobenzoic acid. 4,4'-Diiodo-2,2'-bis(bromomethyl) biphenyl was obtained over three steps.[119] The third bridging carbon atom was introduced by an intramolecular cyclization reaction with the masked formaldehyde (tolylsulfonyl)methyl isocyanide (TosMic)[124] to obtain the corresponding ketone. As last step, the Lewis acid catalyzed reduction of the ketone with polymethylhydrosiloxane (PMHS)[125] provided the propyl bridged diiodobiphenyl **42**. Having all biphenyl derivatives **39** - **42** in hand, the reaction condition for the twofold Sonogashira cross-coupling reaction with S-(4-ethynylphenyl) ethanethioate (**43**) was screened with 4,4'-diiodo-2,2´-dimethylbiphenyl (**40**) (see **table 5**). First, classical Sonogashira cross-coupling conditions were used with Pd(PPh3)2Cl2 and CuI in THF and Hünig's Base (entry 1, **table 5**). The reaction yielded in 13 % of the molecular wire **32**. Since the homo coupled acetylene side product had almost the same polarity as the desired product, the purification was challenging. To avoid the homo coupling, copper-free

Sonogashira cross-coupling conditions[126] were tested (entry 2 and 3, **table 5**) resulting in no conversion to the desired product. The increase of temperature to 50 °C favored the formation of the twofold cross-coupling product to a yield of 40 % (entry 4, **table 5**). By changing the palladium source from $Pd(PPh_3)_2Cl_2$ to $Pd(PPh_3)_4$ the yield could be further increased to 55 %.

Table 5. Screening of the twofold Sonogashira cross-coupling reaction. All reactions were performed under argon atmosphere.

Entry	Cat. System (mol %)	Base	Solvent	Temp. [°C]	Time [h]	Yield [a] [%]
1	$Pd(PPh_3)_2Cl_2$ (5) / CuI (6)	Hünig's base	THF	25	18	13
2	$Pd(PPh_3)_2Cl_2$ (0.5) / $^tBu_3P$(1)	triethylamine	-	60	16	-
3	Pd_2dba_3(0.5) / $^tBu_3P$ (1)	triethylamine	-	60	16	-
4	$Pd(PPh_3)_2Cl_2$ (10) / CuI (12)	Hünig's base	THF	50	22	40
5	$Pd(PPh_3)_4$ (14) / CuI(26)	iPr_2NH	THF	50	15	34
6	$Pd(PPh_3)_4$ (14) / CuI(26)	iPr_2NH	THF	50	22	55

[a] Isolated yields.

The remaining homo coupled alkyne side product was separated by size exclusion chromatography. The optimized reaction conditions were used to synthesize molecular wires **31** - **34** in moderate to good yields. All compounds were fully characterized by ^{1}H-NMR, ^{13}C-NMR and mass spectroscopy.

Synthesis of Functionalized Molecular Wires 35 - 38
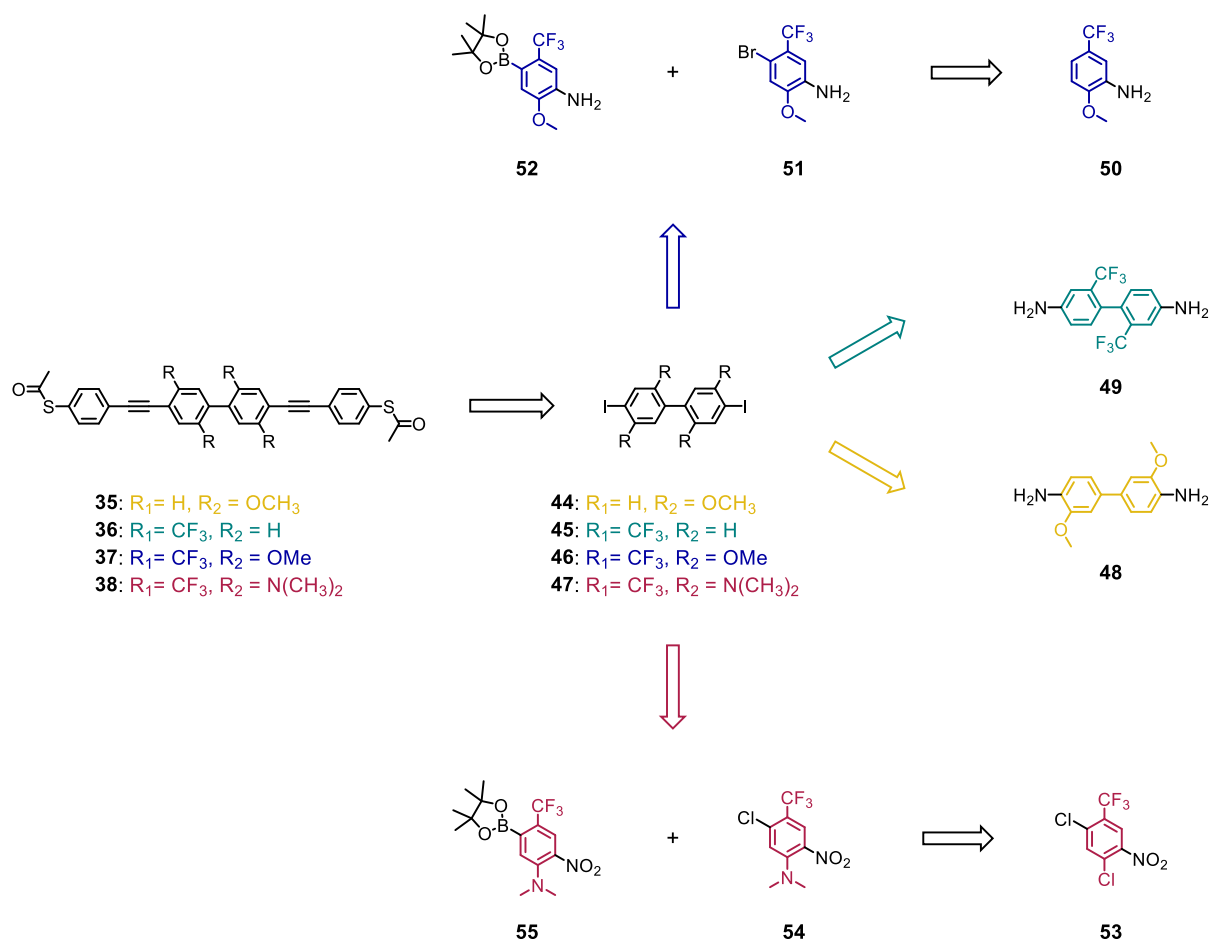
Scheme 12. Retro synthetic analysis of the functionalized molecular wires **35 - 38**. For all four target compounds, the diiodobiphenyls **44 -47** were designed as precursors for the final twofold Sonogashira cross-coupling reaction.

As shown in the previous chapter, the twofold Sonogashira cross-coupling of 4,4'-diiodobiphenyl derivatives with S-(4-ethynylphenyl) ethanethioate (**43**) was performed in moderate to good yields. The synthetic approach for the functionalized molecular wires **35 - 38** is based on the same concept, requiring the synthesis of the corresponding 4,4'-diiodobiphenyl precursors **44 - 47.** For the molecular wires **35** and **36**, the corresponding diamines **48** and **49** are commercially available and can be transformed by classical Sandmeyer type reactions into the diiodobiphenyls **44** and **45**, respectively.

In case of the molecular wires with a push - pull system on the biphenyl core, the challenge was to obtain the phenyl precursors **52** and **55,** with four different functionalities in the required arrangement. Hence, the primary formation of the biphenyl system followed by the controlled insertion of the push - pull system was not beneficial. The electron withdrawing group of the push-pull system had to be in *ortho* - position to the halogen assigned for the formation of the

biphenyl system by a Suzuki Miyaura cross-coupling. In *para* - position to this halogen moiety, a masked halogen was needed to obtain the functionality for the final twofold Sonogashira reaction with S-(4-ethynylphenyl) ethanethioate (**43**). The thioacetyl group is not stable during Sonogashira reactions at higher temperatures and as consequence, an aryl iodide was required to provide an efficient oxidative addition to the palladium catalyst during this last step. Therefore, it was not possible to have a two halogen system and using the advantage of different reactivities regarding the oxidative addition kinetics for the Suzuki and the following Sonogashira reaction. Either an amine or a nitro group was installed as masked iodine in *para* - position of the Suzuki cross-coupling assigned halogen. The nitro group is readily reducible to the amine, which can be converted into the iodine by a Sandmeyer type reaction.

Synthesis of Biphenyl Precursor 46
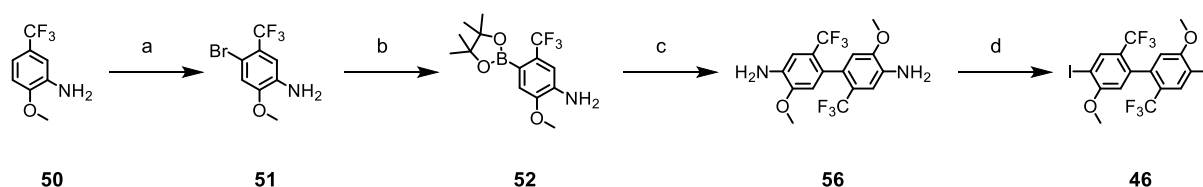
Scheme 13. Synthesis of biphenyl precursor **46**. Reaction conditions: a) NBS, MeCN, -40 °C, 0.5 h, 80 %; b) KOAc, Pd(dppf)Cl$_2$, B$_2$pin$_2$, dioxane, 60 °C, 16 h, 75 %; c) **51**, K$_3$PO$_4$, SPhos Pd G2, THF, H$_2$O, 80 °C, 16 h, 33 %; d) pTsOH, NaNO$_2$, KI, MeCN, H$_2$O, 0 °C, 2 h, 92 %.

The synthesis of diiodobiphenyl **46** started with the bromination of 2-methoxy-5-(trifluoromethyl)aniline (**50**). Whereas the iodination under several condition showed no conversion to the desired product, the bromination of aniline **50** with NBS in acetonitrile yielded 80 % (entry 7, **table 6)**. The key was to perform the reaction at -40 °C to receive the thermodynamically favored product, due to the stronger positive mesomeric effect of the amine group compared to the competing methoxy group. At higher temperatures, the bromination in *ortho* - position to the electron donating methoxy group was considerably increased and the yield of the desired product **51** dropped to 59 % at 0 °C (entry 5, **table 6**).

Table 6. Reaction condition for the halogenation of aniline **50**.

Entry	Reagent	Solvent	Temperature [°C]	Time [h]	Yield [a] [%]
1	I_2, Na_2CO_3 [127]	H_2O / MeCN	25	1	-
2	I_2	DCM	0	18	-
3	NIS	DMSO	25	72	-
4	I_2, $NaHCO_3$	H2O / DCM	40	2	-
5	NBS	MeCN	0	2	59
6	NBS	MeCN	- 20°C	2	72
7	NBS	MeCN	- 40 °C	2	80

[a] Isolated yields

The transformation of bromoaryl **51** to the boronic ester **52** was performed by a palladium catalyzed borylation with bis(pinacolato)diboron using Pd(dppf)Cl$_2$ as catalyst.[128] The obtained boronic ester **52** was used without purification for the subsequent Suzuki-Miyaura cross-coupling with the corresponding bromoaryl precursor **51**. The desired diaminobiphenyl **56** was obtained in a moderate yield of 32 %. However, the following Sandmeyer type reaction using pTsOH and NaNO$_2$ in a water / acetonitrile mixture resulted in an excellent yield of 92 % for the twofold iodine insertion.

Synthesis of Biphenyl Precursor 47
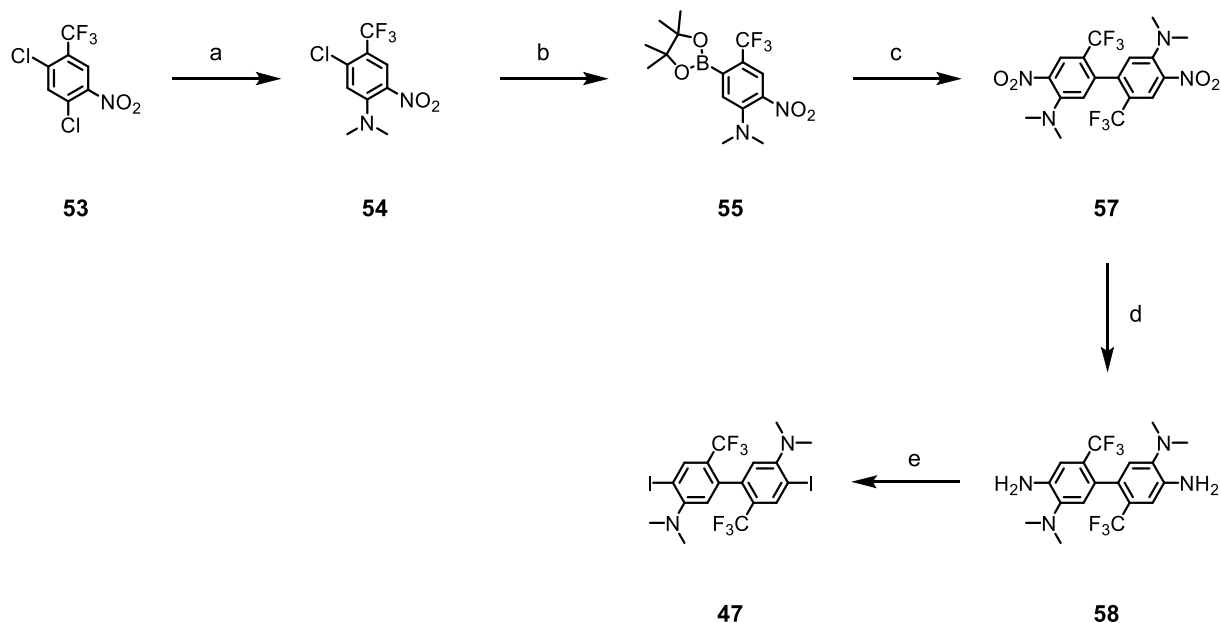
Scheme 14. Synthesis of biphenyl precursor **47**. Reaction conditions: a) Dimethylamine, EtOH, 100 °C, 72 h, 98 %; b) Pd(dba)$_2$, PCy$_3$, B$_2$pin$_2$, dioxane, RT, 30 min.; c) K$_3$PO$_4$. SPhos Pd G2, THF, H$_2$O, 80 °C, 16 h, 57 %; d) SnCl$_2$, EtOH, 80 °C, 16 h, 76 %; e) pTsOH, NaNO$_2$, MeCN, H$_2$O, 0 °C, 2 h, 67 %.

A similar approach was applied for the synthesis of the diiodobiphenyl **47**. The synthetic pathway started with commercially available 1,5-dichloro-2-nitro-4-(trifluoromethyl)benzene (**53**). The insertion of dimethylamine was performed by a nucleophilic aromatic substitution reaction using a procedure by Endeshaw *et al.*[129] to substitute selectively the chlorine in *ortho* - position to the nitro group. The reaction was performed in the microwave using a solution of dimethylamine in ethanol as solvent. As purification step, the formed ammonium chloride salt side-product was crushed out, giving a remarkable yield of 99 % of the desired nitro compound **54** without the need for further purification. Having all four required functionalities in the right arrangement, the borylation and following Suzuki-Miyaura cross-coupling to the biphenyl **57** remained challenging. Although the oxidative addition of aryl chlorides to palladium(0) complexes is slow, the insertion of the boronic ester was achieved using a procedure of Miyaura and coworkers[130] with a catalyst system consisting of Pd(dba)$_2$ and PCy$_3$. The obtained boronic ester **55** was used subsequently without purification for the cross-coupling with the corresponding aryl chloride **54** applying the same conditions as used for the biphenyl **56** synthesis. Dinitrobiphenyl **57** was obtained in a yield of 57 %. The increased yield for the Suzuki Miyaura cross-coupling to the biphenyl **57** compared to the yield of the biphenyl **56** synthesis can be attributed to the electron withdrawing substituent in *para* - position. Aniline **52** had a strong electron donor in *para* - position to the halogen and therefore slowed down

64

the oxidative addition of the palladium(0) species. In the following, both nitro moieties were reduced with tin(II)chloride in ethanol[131] to provide the diaminobiphenyl **58**, which was further transformed to the diiodobiphenyl **47** using the modified Sandmeyer condition as described previously.

Synthesis of the Molecular Wires 35 - 38

The diiodobiphenyls **44** and **45** were both synthesized from the commercially available diamino precursors **48** and **49** by the described modified Sandmeyer reaction in yields of 59 % and 72 %, respectively. For the final twofold Sonogashira cross-coupling, different reaction conditions were used to synthesize the individual molecular wires.

Table 7. Reaction conditions for the twofold Sonogashira cross-coupling reaction to the target molecular wires.
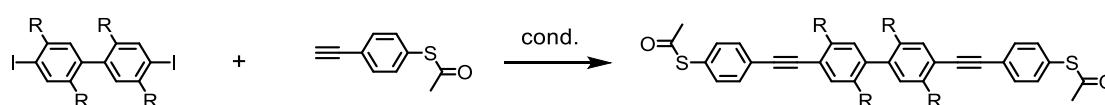
44: R_1= H, R_2 = OCH$_3$ **43**   **35**: R_1= H, R_2 = OCH$_3$
45: R_1= CF$_3$, R_2 = H   **36**: R_1= CF$_3$, R_2 = H
46: R_1= CF$_3$, R_2 = OMe   **37**: R_1= CF$_3$, R_2 = OMe
47: R_1= CF$_3$, R_2 = N(CH$_3$)$_2$ **38**: R_1= CF$_3$, R_2 = N(CH$_3$)$_2$

Entry	Compound	Cat. System (mol %)	Base	Solvent	Temp. / Time [°C] / [h]	Yield[a] [%]
1	**35**	Pd(PPh$_3$)Cl$_2$ (5) / CuI (6)	Hünig's Base	THF	RT / 18	30
2	**36**	Pd(PPh$_3$)Cl$_2$ (5) / CuI (6)	Hünig's Base	THF	RT / 18	53
3	**37**	Pd(PPh$_3$)Cl$_2$ (5) / CuI (0.06)	Hünig's Base	THF	RT / 18	21
4	**38**	Pd(PPh$_3$)$_4$ (14) / CuI 26)	iPr$_2$NH	THF	50 / 22	32

[a] Isolated yields

For the diiodobiphenyls **44** - **47**, a catalyst system of Pd(PPh$_3$)Cl$_2$ and CuI was used with Hünig's Base in THF. The reaction was performed at room temperature over 18 h resulting in moderate yields. For precursor **47** the catalytic system containing of Pd(PPh$_3$)$_4$ and CuI and iPr$_2$NH as a base showed improved conversion to the molecular wire **38**, which was isolated in 32 % yield. The purification was performed by column and size exclusion chromatography.

All target compounds **35 - 38** and their precursor were fully characterized by ^{1}H-NMR, ^{13}C-NMR and mass spectroscopy. For further investigations, all molecular wires were sent to our collaboration partner at the IBM research center in Rüschlikon.

Conclusion

We showed the successful synthesis of a series of new molecular wires and potential molecular switches. All molecules consist of a biphenyl unit as core structure, on both sides elongated with a phenyl ethynyl moiety and a thioacetyl group as anchoring unit. For the first set of compounds, the biphenyl core was functionalized in the 2,2'-positions with methyl groups or alkyl bridges for investigating the conductance dependency of the inter-plane torsion angles in elongated molecular wires. The correlating diiodobiphenyl building blocks **39 - 42** were commercially available or synthesized using published procedures. The following twofold Sonogashira cross-coupling reactions were achieved with Pd(PPh$_3$)$_4$ and CuI as catalytic system in THF at room temperature to conserve the sensitive thioacetyl anchoring group. The molecular wires **31 - 34** were obtained in moderate to good yields.

For the second series of biphenyl derivatives designed as molecular switches, the biphenyl core was functionalized with electron withdrawing groups in 2,2'-position and donating groups in 5,5'-position to obtain an intrinsic dipole moment. As electron withdrawing moiety, the -CF$_3$ functionality was determined and for the electron donating group, either a methoxy or dimethyl amine was installed. As main intermediate for all synthetic strategies of the different molecular switches, the according diiodobiphenyls **44 - 47** were targeted to achieve the desired final compound by a subsequent twofold Sonogashira cross-coupling reaction. The derivatives with solely the methoxy groups in 5,5'-position or the -CF$_3$ ins 2,2'-position were synthesized from the corresponding commercially available diaminobiphenyls by a twofold Sandmeyer reaction, followed by the twofold Sonogashira cross-coupling. For the target compounds with the implemented push-pull system, the key was to synthesize the benzene precursors **52** and **55,** respectively**,** with all four required functionalities in the desired arrangement. A selective dimethylamine insertion by a nucleophilic aromatic substitution reaction of a chlorine yielded compound **54** almost quantitatively. The homocoupling of the benzene building blocks **52** and **55** was achieved by borylation of a halogen functionality and the subsequent Suzuki - Miyaura reaction to the corresponding biphenyl. To obtain the required iodine functionality in 4,4'-position of the biphenyls **46** and **47**, the amine groups, upon reduction from the nitro functionality for compound **58,** were converted to the iodine by Sandmeyer reactions. The final twofold Sonogashira cross-coupling reactions resulted in moderate to good yields for the desired target compounds **35 - 38.**

Experimental Section

General Remarks

Reagent and Solvents: All chemical were used as received without any further purification unless explicitly stated otherwise. Dry Solvents were purchased from *Fluka* or *Accros*. NMR solvent were obtained from *Cambridge Isotope Laboratories, Inc.* (Andover, MA,USA).

[1]H Nuclear Magnetic Resonance (NMR): Bruker DPX-NMR (400 MHz) instrument was used to record all spectra. All chemical shifts are reported relative to trimethylsilane (TMS) or the used solvent. The measurements were performed at room temperature. The multiplicities are written as: s = singlet, d = doublet, t = triplet , dd = doublet of doublets and m = multiplet.

[13]C Nuclear Magnetic Resonance (NMR): Bruker DPX-NMR (101 MHz) instrument was used to record all spectra. All chemical shifts are reported relative to the used solvent. The measurements were performed at room temperature.

GC/MS: For GC/MS analysis a *Shimadzu* GCMS-QP2010 SE gas chromatograph system, with a Zebron 5 MS Inferno column (30 m x 0.25 mm x 0.25 mm), at 1 mL/min He-flow rate (split = 20:1) with a *Shimadzu* mass detector (EI 70 eV) was used.

Mass spectroscopy (MS): MALDI-TOF analyses were performed on a Burker microflex system.

High-resolution mass spectra (HRMS): HR-ESI-ToF-MS were measured with a Maxis 4G instrument from Bruker with the addition of NaOAc.

Column Chromatography: For column chromatography SiliaFlash® P60 from *SILICYCLE* was used with a particle size of 40-63 µm (230-400 mesh), , and TLC was performed on silica gel 60 F254 glass plates with a thickness of 0.25 mm purchased from Merck.

Synthetic Procedures

(4-Iodophenyl) ethanethioate
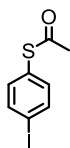
4-Iodophenylsulfonylchloride (1.00 g, 3.31 mmol, 1.0 eq.) was dissolved in dry 1,2-dichloroethane (25 mL) under argon and N,N-diemthylacetamide (0.923 mL, 9.93 mmol, 3.0 eq.) was added. This solution was added dropwise to a suspension of Zn (757 mg, 11.6 mmol, 3.5 eq.) and dichlorodimethylsilane (1.52 g, 11.6 mmol, 3.5 eq.) in dry 1.2-dichloroethane (25 ml) under argon. The reaction mixture was refluxed for 1.5 h. Acetyl chloride (1.25 g, 15.9 mmol, 4.8 eq.) was added and the reaction mixture was stirred 16 h at 25 °C. The solvent was removed under vacuum, the residue was dissolved in DCM, washed with water, dried over $MgSO_4$, filtered and concentrated under reduced pressure. The crude product was purified by column chromatography (SiO_2, cyclohexane / dichloromethane 1:1). (4-Iodophenyl)ethanethioate (828 mg, 2.98 mmol, 90 %) was obtained as white crystals.

^{1}H-NMR (CDCl$_3$, 400 MHz) δ (ppm): 7.74 (d, $^3J_{H.H}$ = 8.4 Hz, 2H), 7.13 (d, $^3J_{H.H}$ = 8.4 Hz, 2H), 2.42 (s, 3H).

^{13}C-NMR (CDCl$_3$, 101 MHz) δ (ppm): 193.2, 138.4, 136.0, 127.8, 95.9, 30.3.

MS (EI, 70 eV): m/z (%) = 278.0 (19), 235.9 (100), 109.1 (45.9).

TLC (SiO$_2$, Cyclohexane / dichloromethane 1:1, UV): R$_f$ = 0.60.

(4-((Trimethylsilyl)ethynyl)phenyl) ethanethioate
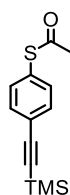
(4-Iodophenyl) ethanethioate (601 mg, 2.16 mmol, 1.0 eq.) and CuI (12.4 mg, 0.06 mmol, 0.03 eq.) was added into a dry 10 ml Schlenk tube under argon atmosphere. Degassed THF (6 mL) and N,N-diisopropylethylamine (2.98 mL, 17.9 mmol, 8.3 eq.) was added and the mixture was degassed for 10 min. Trimethylsilaneacetylene (338 µL, 2.38 mmol, 1.1 eq.) and $Pd(PPh_3)_2Cl_2$ (38.3 mg, 0.054 mmol, 0.025 eq.) was added. The cloudy orange reaction mixture was stirred at room temperature for 16 h. Afterwards, the mixture was directly filtered over celite and concentrated under reduced pressure. The crude product was purified by column chromatography (SiO_2, pentane / ethyl acetate 15:1). (4-((trimethylsilyl)ethynyl)phenyl) ethanethioate (487 mg, 1.96 mmol, 91 %) was obtained as white crystals.

^{1}H-NMR (CDCl$_3$, 400 MHz) δ (ppm): 7.48 (d, $^3J_{H.H}$ = 8.6 Hz, 2H), 7.34 (d, $^3J_{H.H}$ = 8.6 Hz, 2H), 2.42 (s, 3H), 0.25 (s, 9H).

^{13}C-NMR (CDCl$_3$, 101 MHz) δ (ppm): 193.5, 134.2, 132.6, 128.4, 124.5, 104.3, 96.3, 30.4, 0.0.

MS (EI, 70 eV): m/z (%) = 248.0 (16.2), 206.0 (81.3), 191.0 (100).

TLC (SiO_2, Cyclohexane / dichloromethane 1:1, UV): R_f = 0.52.

(4-Ethynylphenyl) ethanethioate (43)
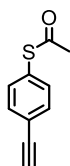
(4-((Trimethylsilyl)ethynyl)phenyl) ethanethioate (189 mg, 0.761 mmol, 1.0 eq.) was dissolved in dry THF (10 ml) under argon atmosphere. Acetic anhydride (144 μL, 1.52 mmol, 2.0 eq.), TBAF in THF (1 M, 921 μL, 0.921 mmol, 1.2 eq.) and acetic acid (87 μL, 1.52 mmol, 2.0 eq.) were added and the reaction mixture was stirred at room temperature for 1.5 h. The reaction mixture was quenched with water and extracted with DCM. The combined organic layers were washed with brine, dried over $MgSO_4$, filtered and concentrated under reduced pressure. The crude product was purified by column chromatography (SiO_2, cyclohexane / ethyl acetate 10:1) (4-Ethynylphenyl) ethanethioate (**43**, 120 mg, 0.681 mmol, 90 %) was obtained as an off-white solid.

^{1}H-NMR ($CDCl_3$, 400 MHz) δ (ppm): 7.52 (d, $^3J_{H.H}$ = 8.5 Hz, 2H), 7.37 (d, $^3J_{H.H}$ = 8.5 Hz, 2H), 3.15 (s, 1H), 2.43 (s, 3H).

MS (EI, 70 eV): m/z (%) = 176.3 (6.8), 134.1 (100), 89.1 (38.3).

TLC (SiO_2, Cyclohexane / ethyl acetate 10:1, UV): R_f = 0.41

4,4'-Diiodo-2,2'-dimethylbiphenyl (40)
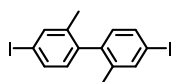
Boron trifluoride etherate (493 μL, 4 mmol, 2.07 eq.) was added to a two-necked round-bottom flask at 0 °C under argon atmosphere. 4,4'-Diamino-2,2'-dimethylamine (550 mg, 1.93 mmol, 1.0 eq.) was dissolved in dry dichloromethane (20 mL) and added dropwise. The reaction mixture turned green and was stirred for 30 min. at 0 °C. *t*-Butyl nitrite (396 μL, 2.97 mmol, 1.54 eq.) was added dropwise and the reaction mixture was stirred at 0 °C for 1 h. KI (447 mg, 2.66 mmol, 1.38 eq.) and I_2 (344 mg, 1.35 mmol, 0.7 eq.) were added all in once and the reaction mixture was stirred at room temperature for 16 h. The reaction was quenched with sat. aq. sodium thiosulfate solution and extracted with dichloromethane. The combined organic layers were washed with brine, dried over $MgSO_4$ and concentrated under reduced pressure. The crude product was purified by column chromatography (SiO_2, pentane). 4,4'-Diiodo-2,2'-dimethylbiphenyl (**40**, 513 mg, 1.18 mmol, 61 %) was obtained as a white solid.

^{1}H-NMR (CDCl$_3$, 400 MHz) δ (ppm): 7.63 (d, $^4J_{H,H}$ = 1.8 Hz, 2H), 7.55 (dd, $^3J_{H,H}$ = 8.0 Hz, $^4J_{H,H}$ = 1.8 Hz, 2H), 6.79 (d, $^3J_{H,H}$ = 8.0 Hz, 2H), 1.99 (s, 6H).

^{13}C-NMR (CDCl$_3$, 101 MHz) δ (ppm): 140.1, 138.9, 138.4, 134.9, 131.0, 93.3. 19.6.

MS (EI, 70 eV): m/z (%) = 434.0 (80.9), 180.2 (39.6), 165.1 (100), 152.2 (11.6), 89.1 (35.5), 76.0 (16.1), 63.0 (12.5).

TLC (SiO_2, Pentane, UV): R_f = 0.54.

4,4'-(4-Ethanethioatephenylethynyl)-2,2'-dimethylbiphenyl (32)
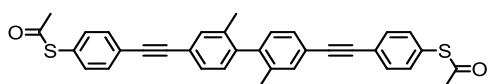
4,4'-Diiodo-2,2'-dimethylbiphenyl (**40**, 130 mg, 0.299 mmol, 1.0 eq.) was placed into a dry 10 mL Schlenk tube under argon atmosphere. 4-Ethynylphenyl-ethanethioate (**43**, 116 mg, 0.658 mmol, 2.2 eq.) was dissolved in dry THF (4 mL) and was added followed by Hünig's Base (0.8 mL), CuI (3 mg, 0.012 mmol, 0.06 eq.) and Pd(PPh$_3$)$_2$Cl$_2$ (10.6 mg, 0.015 mmol, 0.05 eq.). The reaction mixture was stirred for 18 h at room temperature. The mixture was diluted with dichloromethane and filtered over celite. The volatile components were distilled in vacuum. The crude product was purified by column chromatography (SiO$_2$, toluene / dichloromethane 1:1) 4,4'-(4-Ethanethioatephenylethynyl)-2,2'-dimethylbiphenyl (**32**, 20 mg, 0.038 mmol, 13 %.) was obtained as a white solid.

¹H-NMR (CDCl$_3$, 400 MHz) δ (ppm): 7.57 (d, $^3J_{H,H}$ = 8.3 Hz, 4H), 7.48 (s, 2H), 7.44 - 7.39 (m, 6H), 7.10 (d, $^3J_{H,H}$ = 7.8 Hz, 2H), 2.44 (s, 6H), 2.07 (s, 6H).

¹³C-NMR (CDCl$_3$, 101 MHz) δ (ppm): 193.5, 141.4, 136.1, 134.2, 133.1, 132.2, 129.3, 129.0, 128.0, 124.6, 121.9, 91.1, 88.6, 30.3, 19.7.

MS (MALDI-TOF): m/z = 487.3 ([M-C(O)CH$_3$]$^-$)

TLC (SiO$_2$, Toluene / dichloromethane, UV): R$_f$ = 0.40.

2,7-Diiodo-9,10-dihydrophenanthrene (41)
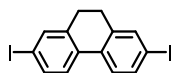
CuI (5.6 mg, 0.030 mmol, 0.05 eq.), NaI (178 mg, 1.18 mmol, 2.0 eq.) and 2,7-dibromo-9,10-dihydrophenanthrene (200 mg, 0.592 mmol, 1.0 eq.) were added in a dry microwave vial under argon atmosphere. 1,4-Dioxane (1 mL) was added followed by TMEDA (7.5 µL, 0.059 mmol, 0.1 eq.). The vial was sealed and the reaction mixture was heated to 110 °C for 20 h. After cooling to room temperature, the reaction was quenched with sat. aq. ammonium chloride solution and extracted with dichloromethane. The combined organic layers were washed with water, dried over $MgSO_4$ and concentrated under reduced pressure. The crude product was purified by a plug filtration (SiO_2, cyclohexane / ethyl acetate 10:1). 2,7-Diiodo-9,10-dihydrophenanthrene (**41**, 202 mg, 0.468 mmol, 79 %) was obtained as white crystals.

MS (EI, 70 eV): m/z (%) = 432.1 (84.7), 178.2 (100), 152.2 (37.0), 127.0 (38.5), 89.1 (42.5), 76.1 (44.2), 63.1 (54.0), 51.1 (44.0).

2,7-(4-Ethanethioatephenylethynyl)-9,10-dihydrophenanthrene (33)
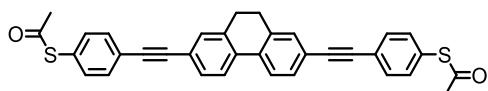
2,7-Diiodo-9,10-dihydrophenanthrene (**41**, 115 mg, 0.266 mmol, 1.0 eq.) was placed into a dry 10 mL Schlenk tube under argon atmosphere. A solution of 4-ethynylphenyl ethanethioate (**43**, 103 mg, 0.585 mmol, 2.2 eq.) in dry THF (4 mL) was added followed by the Hünig's Base (0.8 mL). After degassing for 10 min with argon, CuI (3 mg, 0.016 mmol, 0.06 eq.) and Pd(PPh$_3$)$_2$Cl$_2$ (9.4 mg, 0.013 mmol, 0.05 eq.) was added. The reaction mixture stirred for 18 h at room temperature. The reaction mixture was diluted with dichloromethane and filtered over celite. The volatile components were distilled in vacuum. The crude product was purified by column chromatography (SiO$_2$, toluene / dichloromethane 5:1). 2,7-(4-Ethanethioatephenylethynyl)-9,10-dihydrophenanthrene (**33**, 53 mg, 0.100 mmol, 38%) was obtained as an off white solid.

^{1}H-NMR (CDCl$_3$, 400 MHz) δ (ppm): 7.73 (d, $^3J_{H,H}$ = 8.1 Hz, 2H), 7.57 (d, $^3J_{H,H}$ = 8.0 Hz, 4H), 7.48 (dd, $^3J_{H,H}$ = 8.0 Hz, $^4J_{H,H}$ = 1.7 Hz, 2H), 7.43 (d, $^4J_{H,H}$ = 1.7 Hz, 2H), 7.41 (d, $^3J_{H,H}$ = 8.0 Hz, 4H), 2.89 (s, 4H), 2.44 (s, 6H).

^{13}C-NMR (CDCl$_3$, 101 MHz) δ (ppm): δ 193.6, 137.7, 134.4, 134.3, 132.3, 131.5, 130.6, 128.2, 124.7, 124.1, 122.2, 91.4, 89.6, 30.5, 28.8.

MS (MALDI-TOF): m/z = 485.6 ([M-C(O)CH$_3$]$^-$)

3,9-Diiodo-6,7-dihydro-5H-dibenzo[a,c][7]annulene (42)
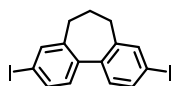
CuI (5.1 mg, 0.027 mmol, 0.1 eq.), NaI (161 mg, 1.07 mmol, 4.0 eq,) and 3,9-diiodo-6,7-dihydro-5H-dibenzo[a,c][7]annulene (94 mg, 0.267 mmol, 1.0 eq.) was added in a dry microwave vial under argon atmosphere. The vial was evacuated and flushed with argon three times. 1,4-Dioxane (1 mL) and TMEDA (6.7 µL, 0.053 mmol, 0.2 eq.) was added. The vial was sealed and the reaction mixture was heated at 110 °C for 20 h. After cooling to room temperature, the reaction was quenched with sat. aq. ammonium chloride solution and extracted with dichloromethane. The combined organic layers were washed with water, dried over $MgSO_4$ and concentrated under reduced pressure. The crude product was purified by a plug filtration (SiO_2, cyclohexane / ethyl acetate 10:1). 3,9-Diiodo-6,7-dihydro-5H-dibenzo[a,c][7]annulene (**42**, 105 mg, 0.235 mmol, 88 %) was obtained as a white solid.

^{1}H-NMR (CDCl$_3$, 400 MHz) δ (ppm): 7.66 (dd, $^3J_{H,H}$ = 8.0 Hz , $^4J_{H,H}$ = 1.9 Hz, 2H), 7.59 (d, $^4J_{H,H}$ = 1.9 Hz, 2H), 7.05 (d, $^3J_{H,H}$ = 8.0 Hz, 2H), 2.43 (t, $^3J_{H,H}$ = 7.0 Hz, 4H)., 2.16 (p, $^3J_{H,H}$ = 7.0 Hz, 2H).

^{13}C-NMR (CDCl$_3$, 101 MHz) δ (ppm): 141.8, 139.8, 137.5, 136.0, 129.9, 93.5, 33.2, 31.0.

MS (EI, 70 eV): m/z (%) = 446.2 (100), 192.2 (61.9), 165.2 (62.5), 127.0 (31.4), 96.2 (25.9), 63.0 (32.8), 82.0 (24.8), 51.2 (37.1).

TLC (SiO_2, Cyclohexane / ethyl acetate 10:1, UV): R$_f$ = 0.95.

3,9-(4-Ethanethioatephenylethynyl)-6,7-dihydro-5H-dibenzo[a,c][7]annulene (34)
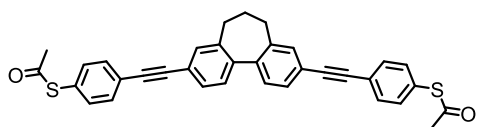
3,9-Diiodo-6,7-dihydro-5H-dibenzo[a,c][7]annulene (**42**, 120 mg, 0.269 mmol, 1.0 eq.) was placed into a dry 10 mL Schlenk tube under argon atmosphere. 4-Ethynylphenyl ethanethioate (**43**, 104 mg, 0.592 mmol, 2.2 eq.) was dissolved in dry degassed THF (4 mL) and was added followed of Hünig's Base (0.8 mL). The reaction mixture was degassed for further 10 min. with argon. CuI (3.1 mg, 0.016 mmol, 0.06 eq.) and $Pd(PPh_3)_2Cl_2$ (9.5 mg, 0.014 mmol, 0.05 eq.) was added. The reaction mixture was stirred at room temperature for 16 h. The mixture as diluted with dichloromethane and was filtered over celite. The volatile components were distilled in vacuum. The crude product was purified by column chromatography (SiO_2, cyclohexane / dichloromethane 1:2). 3,9-(4-Ethanethioatephenylethynyl)-6,7-dihydro-5H-di benzo[a,c][7]annulene (**34**, 32 mg, 0.059 mmol, 22 %) was obtained as a white solid.

^{1}H-NMR (CDCl$_3$, 400 MHz) δ (ppm): 7.58 (d, $^3J_{H,H}$ = 8.4 Hz, 4H), 7.52 (dd, $^3J_{H,H}$ = 7.9 Hz, $^4J_{H,H}$ = 1.7 Hz, 2H), 7.45 (d, $^4J_{H,H}$ = 1.7 Hz, 2H), 7.41 (d, $^3J_{H,H}$ = 8.3 Hz, 4H), 7.37 (d, $^3J_{H,H}$ = 7.8 Hz, 2H), 2.52 (t, $^3J_{H,H}$ = 7.0 Hz, 4H) 2.44 (s, 6H), 2.22 (p, $^3J_{H,H}$ = 6.9 Hz, 2H).

^{13}C-NMR (CDCl$_3$, 101 MHz) δ (ppm): δ 193.6, 141.00, 139.9, 134.4, 132.3, 131.9, 130.2, 128.4, 128.1, 124.7, 122.3, 91.3, 89.2, 33.1, 31.3, 30.4.

MS (MALDI-TOF): m/z = 499.6 ([M-C(O)CH$_3$]$^-$)

TLC (SiO_2, Cyclohexane / dichloromethane 1:2, UV): R_f = 0.38.

4,4'-(4-Ethanethioatephenylethynyl)biphenyl (31)
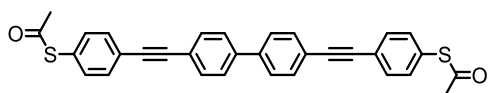
4,4'-Diiodobiphenyl (41.8 mg, 0.103 mmol, 1.0 eq.) was placed into a dry 10 mL Schlenk tube under argon atmosphere. 4-Ethynylphenyl-ethanethioate (**43**, 39.9 mg, 0.227 mmol, 2.2 eq.) was dissolved in dry degassed THF (2.5 mL) and was added followed by Hünig's Base (0.5 mL), CuI (1.1 mg, 0.006 mmol, 0.06 eq.) and Pd(PPh$_3$)$_2$Cl$_2$ (3.7 mg, 0.005 mmol, 0.05 eq.). The reaction mixture was stirred at room temperature for 16 h. The mixture was diluted with dichloromethane and was filtered over celite. The volatile components were distilled in vacuum. The crude product was purified by column chromatography (SiO$_2$, DCM / toluene 1:1). 4,4'-(4-Ethanethioatephenylethynyl)biphenyl (**31**, 10 mg, 0.02 mmol, 19 %) was obtained as a white solid.

^{1}H-NMR (CDCl$_3$, 400 MHz) δ (ppm): 7.62 (s, 8H), 7.58 (d, $^3J_{H,H}$ = 8.6 Hz, 4H) , 7.541 (d, $^3J_{H,H}$ = 8.4 Hz, 4H), 2.44 (s, 6H).

^{13}C-NMR (CDCl$_3$, 101 MHz) δ (ppm): 193.6, 140.4, 134.4, 132.4, 132.3, 128.3, 127.1, 124.6, 122.4, 91.0, 88.8, 30.5.

MS (MALDI-TOF): m/z = 459.5 ([M-C(O)CH$_3$]$^-$)

4-Bromo-2-methoxy-5-(trifluoromethyl)aniline (51)
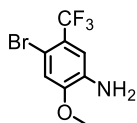
2-Methoxy-5-(trifluoromethyl)aniline (1.15 g, 6.01 mmol, 1.0 eq.) was dissolved in acetonitrile (25 mL) and the solution cooled to - 40 °C. A solution of N-Bromosuccinimide (1.07 g, 6.01 mmol, 1.0 eq.) dissolved in acetonitrile (8 mL) was added dropwise over a half hour. After addition, the reaction mixture was stirred for 30 min. at - 40 °C. The reaction was concentrated under reduced pressure and the crude product was purified by column chromatography (SiO$_2$, Cyclohexane / ethyl acetate 4:1). 4-Bromo-2-methoxy-5-(trifluoromethyl)aniline (**51**, 1.30 g, 4.82 mmol, 80 %) was obtained as brown crystals.

^{1}H-NMR (CDCl$_3$, 400 MHz) δ (ppm): 7.01 (s, 1H), 6.99 (s, 1H), 3.96 (s, 2H), 3.88 (s, 3H).

^{13}C-NMR (CDCl$_3$, 101 MHz) δ (ppm): 149.1, 135.3, 123.4 (q, $^1J_{F,C}$ = 272.3 Hz, 1C), 122.5 (q, $^2J_{F,C}$ = 31.4 Hz, 1C), 116.2, 113.2 (q, $^3J_{F,C}$ = 5.4 Hz, 1C),107.1 (q, $^3J_{F,C}$ = 1.9 Hz, 1C), 56.1.

MS (EI, 70 eV): m/z (%) = 268.9 (100), 253.9 (68.2), 225.9 (44.6), 175.0 (18.7), 147.0 (45.6), 78.0 (14.4).

TLC (SiO$_2$, Cyclohexane / ethyl acetate 4:1, UV): R_f = 0.39.

2-Methoxy-4-(4,4,5,5-tetramethyl-1,3,2-dioxaborolan-2-yl)-5-(trifluoromethyl)aniline (52)
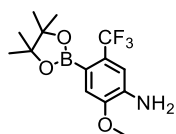
In a dry two-necked round-bottom flask 4-bromo-2-methoxy-5-(trifluoromethyl)aniline (**51**, 322 mg, 1.23 mmol, 1.0 eq.), potassium acetate (244 mg, 2.46 mmol, 2.0 eq.) and bis(pinacolato)diboron (625 mg, 2.46 mmol, 2.0 eq.) was added under argon atmosphere. Dry 1,4-dioxane (10 mL) was added and the mixture was degassed for 10 min with argon. Pd(dppf)Cl$_2$ (50.2 mg, 0.06 mmol, 0.05 eq.) was added under argon counter flow and the reaction mixture was stirred at 60°C for 16 h. After cooling to room temperature, the mixture was diluted with DCM and filtered over a celite plug. The solution was concentrated under reduced pressure. The crude product was purified by column chromatography (SiO$_2$, cyclohecane / ethyl acetate, 1:1). 2-Methoxy-4-(4,4,5,5-tetramethyl-1,3,2-dioxaborolan-2-yl)-5-(trifluoromethyl)aniline (**52**, 291 mg, 0.918 mmol, 75 %) was obtained as white crystals.

^{1}H-NMR (CDCl$_3$, 400 MHz) δ (ppm): 7.11 (s, 1H), 6.99 (s, 1H), 3.90, (s, 3H), 1.34 (s, 12H).

MS (EI, 70 eV): m/z (%) = 317.0 (100), 244 (17.3), 216.0 (28.5). 198.0 (23.0), 176.0 (10.5), 170.0 (10.5), 148.1 (17.6), 133.0 (12.1), 85.0 (15.3), 57.1 (21.3).

5,5'-Dimethoxy-2,2'-bis(trifluoromethyl)-[1,1'-biphenyl]-4,4'-diamine (56)
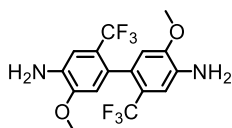
2-Methoxy-4-(4,4,5,5-tetramethyl-1,3,2-dioxaborolan-2-yl)-5-(trifluoromethyl)aniline (**52**, 260 mg, 0.82 mmol, 1.0 eq.) and 4-bromo-2-methoxy-5-(trifluoromethyl)aniline (**51**, 221 mg, 0.82 mmol, 1.0 eq.) were added in a dry two-necked round-bottom flask under argon atmosphere and dissolved in dry THF (5 mL) and water (0.5 mL). The mixture was degassed with argon for 10 min. After the addition of K_3PO_4 (355 mg, 1.64 mmol, 2.0 eq.) and SPhos Pd G2 (5.75 mg, 7.98 µmol, 0.03 eq.), the reaction mixture was heated to 80 °C for 16 h. After cooling to room temperature, the reaction was quenched with sat. aq. NH_4Cl solution and extracted with ethyl acetate. The combined organic layers were washed with brine, dried over $MgSO_4$ and concentrated under reduced pressure. The crude product was purified by column chromatography (SiO₂, cyclohexane / ethyl acetate 2:1). 5,5'-Dimethoxy-2,2'-bis(trifluoromethyl)-[1,1'-biphenyl]-4,4'-diamine (**56**, 102 mg, 0.268 mmol, 33 %) was obtained as a brownish solid.

¹H-NMR (CDCl₃, 400 MHz) δ (ppm): 7.01 (s, 2H), 6.66 (s, 2H), 3.96 (s, 4H), 3.84 (s, 6H).

¹³C-NMR (CDCl₃, 101 MHz) δ (ppm): 147.8, 135.3, 128.3, 124.3 (q, $^1J_{F,C}$ = 271.1 Hz, 2C), 121.5 (q, $^2J_{F,C}$ = 30.1 Hz, 2C), 113.9, 111.8, 55.6.

MS (EI, 70 eV): m/z (%) = 379.9 (100), 364.9 (18.1), 336.9 (28.9), 147.0 (18.0).

TLC (SiO₂, Cyclohexane / ethyl acetate 2:1, UV): R_f = 0.49.

4,4'-Diiodo-5,5'-dimethoxy-2,2'-bis(trifluoromethyl)biphenyl (46)
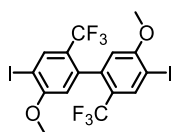
A solution of 5,5'-dimethoxy-2,2'-bis(trifluoromethyl)-[1,1'-biphenyl]-4,4'-diamine (**56**, 52.1 mg, 0.137 mmol, 1.0 eq.) and pTsOH (160 mg, 0.822 mmol, 6.0 eq.) in MeCN (1 mL) was cooled to 0 °C. Maintaining 0 °C, a solution of $NaNO_2$ (37.8 mg, 0.548 mmol, 4.0 eq.) in water (1 mL) was added dropwise and after 5 min. stirring at 0 °C, a solution of KI (115 mg, 0.685 mmol, 5.0 eq.) was added in one portion. The reaction mixture was stirred at 0 °C for 2 h. The reaction was quenched with sat. aq. $Na_2S_2O_3$ and extracted with ethyl acetate. The combined organic layers where washed with water, dried over $MgSO_4$ and concentrated under reduced pressure. The crude product was purified by column chromatography (SiO_2, cyclohexane / ethyl acetate 5:1). 4,4'-Diiodo-5,5'-dimethoxy-2,2'-bis(trifluoromethyl)-1,1'-biphenyl (**46**, 76.0 mg, 0.137 mmol, 92 %) was obtained as a white solid.

¹H-NMR (CDCl₃, 400 MHz) δ (ppm): 8.11 (s, 2H), 6.67 (s, 2H), 3.89 (s, 6H).

¹³C-NMR (CDCl₃, 101 MHz) δ (ppm): 159.6, 138.7, 137.4, 123.1 (q, $^1J_{F,C}$ = 273.4 Hz, 2C), 122.6 (q, $^2J_{F,C}$ = 31.3 Hz, 2C), 113.4, 85.2, 56.8.

TLC (SiO₂, Cyclohexane / ethyl acetate 5:1, UV): R_f = 0.78

4,4'-(4-Ethanethioatephenylethynyl)-5,5'-dimethoxy-2,2'-bis(trifluoromethyl)biphenyl (37)
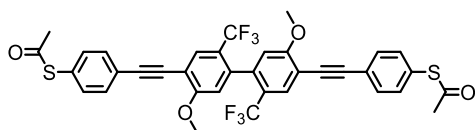
4,4'-Diiodo-5,5'-dimethoxy-2,2'-bis(trifluoromethyl)-1,1'-biphenyl (**46**, 223 mg, 0.37 mmol, 1.0 eq.) and CuI (4.3 mg, 0.022 mmol, 0.06 eq.) was placed into a dry flask under argon atmosphere. (4-Iodophenyl) ethanethioate (**43**, 143 mg, 0.814 mmol, 2.2 eq.) was dissolved in degassed THF and added, followed by the Hünig's Base (2 mL). The solution was degassed for 10 min and Pd(PPh3)$_2$Cl$_2$ (5.0 mg, 0.019 mmol, 0.05 eq.) was added. The reaction mixture was stirred for 18 h at room temperature. After dilution with DCM, the mixture was filtered over a celite plug and concentrated under reduced pressure. The crude product was purified by column chromatography (SiO$_2$, cyclohexane / dichloromethane 1:5). 4,4'-(4-Ethanethioatephenylethylene)-5,5'-dimethoxy-2,2'-bis(trifluoromethyl)-1,1'-biphenyl (**37**, 55 mg, 0.079 mmol, 21 %) was obtained as a white solid.

¹H-NMR (CDCl$_3$, 400 MHz) δ (ppm): 7.87 (s, 2H), 7.61 (d, $^3J_{H,H}$ = 8.5 Hz, 4H), 7.42 (d, $^3J_{H,H}$ = 8.6 Hz, 4H), 6.83 (s, 2H), 3.93 (s, 6H), 2.45 (s, 6H).

¹³C-NMR (CDCl$_3$, 101 MHz) δ (ppm): 193.4, 160.9, 138.9, 134.4, 132.4, 131.6, 128.7, 124.2, 123.8 (q, $^1J_{F,C}$ = 274.0 Hz, 2C), 121.3 (q, $^2J_{F,C}$ = 31.4 Hz, 2C), 113.9, 112.5, 94.4, 85.71, 56.4, 30.4.

MS (MALDI-TOF): m/z = 655.9 ([M-C(O)CH$_3$]$^-$)

TLC (SiO$_2$, Cyclohexane / dichloromethane 1:5, UV): R$_f$ = 0.31.

5-Chloro-N,N-dimethyl-2-nitro-4-(trifluoromethyl)aniline (54)
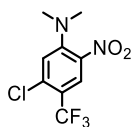
1,5-Dichloro-2-nitro-4-(trifluoromethyl)benzene (772 mg, 2.97 mmol, 1.0 eq.) was dissolved in ethanol (18 mL) and diethylamine in ethanol (2M, 1.06 mL, 5.9 mmol, 2 eq.) was added. The microwave vial was sealed and the reaction mixture was stirred for 72 h in the microwave at 100 °C. Afterwards, the reaction mixture was concentrated under reduced pressure. The residue was dissolved in diethyl ether and the insoluble ammonium salt was filtered off. The solvent was removed under reduced pressure. No further purification was performed. 5-Chloro-N,N-dimethyl-2-nitro-4-(trifluoromethyl)aniline (**54**, 779 mg, 2.90 mmol, 98%) was obtained as a yellow solid.

^{1}H-NMR (CDCl$_3$, 400 MHz) δ (ppm): 8.09 (s, 1H), 7.07 (s, 1H), 2.97 (s, 6H).

^{13}C-NMR (CDCl$_3$, 101 MHz) δ (ppm): 147.7, 136.7 (q, $^3J_{F,C}$ = 1.5 Hz, 1C), 134.5, 127.0 (q, $^3J_{F,C}$ = 5.5 Hz, 1C), 121.6 (q, $^1J_{F,C}$ = 271.6 Hz, 1C), 119.5, 116.1 (q, $^3J_{F,C}$ = 33.3 Hz, 1C), 42.1.

MS (EI, 70 eV): m/z (%) = 268.1 (22.2), 251.1 (60.4), 223.0 (33.5), 206.0 (21.3), 193.1 (100), 179.0 (16.4), 161.1 (12.1), 145.1 (11.4), 118.1 (14.3), 75.1 (11.2).

TLC (SiO$_2$, Cyclohexane / ethyl acetate 3:1, UV): R$_f$ = 0.51.

N,N-dimethyl-2-nitro-5-(4,4,5,5-tetramethyl-1,3,2-dioxaborolan-2-yl)-4-(trifluoromethyl)aniline (55)
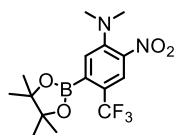
Pd(dba)$_2$ (8.6 mg, 0.015 mmol, 0.03 eq.) and tricyclohexylphosphine (10.4 mg, 0.036 mmol, 0.072 eq.) was placed in a dry flask under argon. 1,4-Dioxane (3 mL) was added and the mixture was stirred for 30 min. at room temperature. Bis(pinacolato)diboron (140 mg, 0.55 mmol, 1.1 eq.), potassium acetate (74 mg, 0.75 mmol, 1.5 eq.) and 5-chloro-N,N-dimethyl-2-nitro-4-(trifluoromethyl)aniline (**54**, 134 mg, 0.5 mmol, 1.0 eq.) was added. The reaction mixture was stirred at 80 °C for 16 h. After cooling to room temperature, the reaction mixture was concentrated under reduced pressure and purified by column chromatography (SiO$_2$, cyclohexane / ethyl acetate 3:1). To obtained mixture of starting material and product was used for the following Suzuki cross-coupling without further purification.

¹H-NMR (CDCl$_3$, 400 MHz) δ (ppm): 8.07 (s, 1H), 7.29 (s, 1H), 2.97 (s, 6H), 1.37 (s, 12H).

MS (EI, 70 eV): m/z (%) = 360.0 (28.4), 343.1 (100), 315.1 (49.0), 285.0 (26.6), 261.0 (37.1), 243.0 (35.4), 227.0 (32.1), 215.0 (43.9), 198.0 (14.3), 185.0 (15.6), 147.1 (13.9), 118.0 (17.8), 83.2 (28.4), 57.1 (37.1).

TLC (SiO$_2$, Cyclohexane / ethyl acetate 3:1, UV): R$_f$ = 0.46.

3,3'-Bis(N,N-dimethylamino)-4,4'-dinitro-6,6'-bis(trifluoromethyl)biphenyl (57)
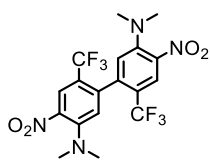
5-Chloro-N,N-dimethyl-2-nitro-4-(trifluoromethyl)aniline (**54**, 81 mg, 0.302 mmol, 1.0 eq.) and N,N-dimethyl-2-nitro-5-(4,4,5,5-tetramethyl-1,3,2-dioxaborolan-2-yl)-4-(trifluoromethyl)aniline (**55**, 108 mg, 0.302 mmol, 1.0 eq.) were placed in a 10 mL two-necked round-bottom flask under argon atmosphere and was dissolved in THF (2 mL) and water (0.2 mL). K_3PO_4 (131 mg, 0.604 mmol, 2.0 eq.) was added and the solution was degassed for 15 min. with argon. After addition of SPhos Pd G2 (6 mg, 0.009 mmol, 0.03 eq.), the flask was closed immediately, heated to 80°C and stirred for 16 h. After cooling to room temperature, the reaction was quenched with sat. aq. NH_4Cl solution and extracted with ethyl acetate. The combined organic layers were washed with brine, dried over $MgSO_4$ and concentrated under reduced pressure. The crude product was purified by column chromatography (SiO_2, cyclohexane / ethyl acetate 2:1). 3,3'-Bis(N,N-dimethylamino)-4,4'-dinitro-6,6'-bis(trifluoromethyl)biphenyl (**57**, 40 mg, 0.086 mmol, 57%) was obtained as a yellow solid.

^{1}H-NMR (CDCl$_3$, 400 MHz) δ (ppm): 8.10 (s, 2H), 6.85 (s, 2H), 2.97 (s, 12H).

^{13}C-NMR (CDCl$_3$, 101 MHz) δ (ppm): 146.3, 140.6, 136.3, 127.4, 123.4 (q, $^1J_{F,C}$ = 272.4 Hz, 2C), 120.2, 117.0 (q, $^2J_{F,C}$ = 32.6 Hz, 2C), 42.3.

MS (EI, 70 eV): m/z (%) = 465.9 (68.9), 448.9 (91.2), 421.0 (29.6), 401.9 (45.6), 388.0 (75.5), 371.9 (65.7), 358.0 (55.6), 344.0 (100), 329.9 (31.3), 315.0 (29.4), 286.0 (23.9), 246.9 (36.1), 218.9 (40.7), 187.0 (56.5), 171.7 (57.5), 158.0 49.5), 69.0 (29.4).

TLC (SiO_2, Cyclohexane / ethyl acetate 3:1, UV): R$_f$ = 0.29.

4,4'-Diamino-3,3'-bis(N,N-dimethylamino)-6,6'-bis(trifluoromethyl)biphenyl (58)
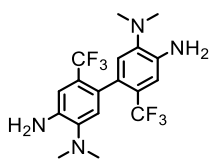
3,3'-Bis(N,N-dimethylamino)-4,4'-dinitro-6,6'-bis(trifluoromethyl)biphenyl (**57**, 250 mg, 0.536 mmol, 1.0 eq.) was dissolved in ethanol (18 mL) and $SnCl_2$ (926 mg, 4.02 mmol, 7.5 eq.) was added. The reaction mixture was stirred at 80 °C for 16 h and after cooling to room temperature concentrated under reduced pressure. The residue was basified with conc. aq. NaOH solution and extracted with toluene. The combined organic layers were washed with water, dried over $MgSO_4$ concentrated under reduced pressure. The crude product was purified by column chromatography (SiO_2, cyclohexane / ethyl acetate 3:1). 4,4'-Diamino-3,3'-bis(N,N-dimethylamino)-6,6'-bis(trifluoromethyl)biphenyl (**58**, 165 mg, 0.406 mmol, 76%) was obtained as reddish crystals.

^{1}H-NMR (CDCl$_3$, 400 MHz) δ (ppm): 7.01 (s, 2H), 6.86 (s, 2H), 4.10 (s, 4H), 2.68 (s, 12H).

^{13}C-NMR (CDCl$_3$, 101 MHz) δ (ppm): 141.7, 140.2, 128.2, 124.4 (q, $^1J_{F,C}$ = 273.6 Hz, 2C), 124.3 (q, $^2J_{F,C}$ = 30.3 Hz, 2C), 123.4, 112.4 (q, $^3J_{F,C}$ = 4.5 Hz, 2C), 43.1.

MS (EI, 70 eV): m/z (%) = 406.0 (100), 341.9 (10.1), 187.0 (10.2).

TLC (SiO$_2$, Cyclohexane / ethyl acetate 3:1, UV): R$_f$ = 0.40.

3,3'-Bis(N,N-dimethylamino)-6,6'-bis(trifluoromethyl)-4,4'-diiodobiphenyl (47)
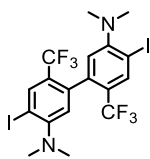
3,3'-Bis(N,N-dimethylamino)-4,4'-dinitro-6,6'-bis(trifluoromethyl)biphenyl (**58**, 167 mg, 0.411 mmol, 1.0 eq.) was dissolved in MeCN (5 mL) and pTsOH (469 mg, 2.47 mmol, 6.0 eq.) was added in one portion. The solution was cooled to 0 °C and a solution of $NaNO_2$ (113 mg, 1.64 mmol, 4.0 eq.) in water (2.5 mL) was added dropwise. After 5 min. stirring at 0 °C, a solution of KI (345 mg, 2.05 mmol, 5.0 eq.) in water (2.5 mL) was added in one portion and the reaction mixture was stirred at 0 °C for 2 h. The reaction was quenched with sat. aq. $Na_2S_2O_3$ and extracted with ethyl acetate. The combined organic layers where washed with water, dried over $MgSO_4$ and concentrated under reduced pressure. The crude product was purified by column chromatography (SiO$_2$, cyclohexane / ethyl acetate 5:1). 3,3'-Bis(N,N-dimethylamino)-6,6'-bis(trifluoromethyl)-4,4'-diiodo biphenyl (**47**, 175 mg, 0.279 mmol, 67 %) was obtained as a white solid.

^{1}H-NMR (CDCl$_3$, 400 MHz) δ (ppm): 8.15 (s, 2H), 6.86 (s, 2H), 2.83 (s, 12H).

^{13}C-NMR (CDCl$_3$, 101 MHz) δ (ppm): 156.7, 138.3, 137.7, 123.9 (q, $^2J_{F,C}$ = 30.9 Hz, 2C), 122.9 (q, $^1J_{F,C}$ = 273.7 Hz, 2C), 122.7, 93.3, 44.3.

MS (MALDI-TOF): m/z = 628.9 ([M]$^+$)

TLC (SiO$_2$, Cyclohexane / ethyl acetate 5:1, UV): R$_f$ = 0.40.

4,4'-(4-Ethanethioatephenylethynyl)-5,5'-bis(N,N-dimethylamino)-2,2'-bis(trifluoromethyl)biphenyl (38)
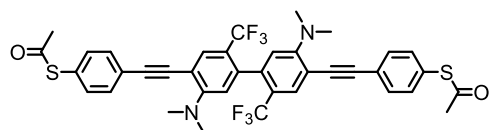
In a two-necked round-bottom flask, (4-ethynylphenyl) ethanethioate (**43**, 105 mg, 0.598 mmol, 2.2 eq.), 3,3'-bis(N,N-dimethylamino)-6,6'-bis(trifluoromethyl)-4,4'-diiodobiphenyl (**47**, 156 mg, 0.272 mmol, 1.0 eq.) and tetrakis(triphenylphosphine)palladium (44 mg, 0.038 mmol, 0.14 eq.) were provided under argon atmosphere. THF (2 mL) and diisopropylamine (3mL) were added and the mixture was degassed for 10 min with argon followed of the addition of CuI (13 mg, 0.071 mmol, 0.26 eq.). The reaction mixture was stirred for 22 h at 50 °C. After cooling to room temperature, the suspension was diluted with DCM and filtered over a celite plug. The crude product was purified by column chromatography (SiO$_2$, cyclohexane / tBME 3:1) 4,4'-(4-Ethanethioatephenylethynyl)-5,5'-bis(N,N-dimethylamino)-2,2'-bis(trifluoromethyl)biphenyl (**38**, 63 mg, 0.087 mmol, 32%) was obtained as a white solid.

^{1}H-NMR (CDCl$_3$, 400 MHz) δ (ppm): 7.80 (s, 2H), 7.57 (d, $^3J_{H,H}$ = 8.3 Hz, 4H), 7.42 (d, $^3J_{H,H}$ = 8.3 Hz, 4H), 6.72 (s, 2H), 3.11 (s, 12H), 2.45 (s, 6H)

^{13}C-NMR (CDCl$_3$, 101 MHz) δ (ppm): 193.5, 154.8, 138.6, 134.5, 133.0, 131.9, 128.4, 124.7, 124.1 (q, $^1J_{F,C}$ = 272.6 Hz, 2C), 119.6 (q, $^2J_{F,C}$ = 31.8 Hz, 2C), 119.3, 111.6, 94.9, 89.8, 42.9.

MS (MALDI-TOF): m/z = 724.5 ([M]$^+$)

TLC (SiO$_2$, Cyclohexane / tBME 3:1, UV): R$_f$ = 0.39.

4,4'-Diiodo-3,3'-dimethoxybiphenyl (44)
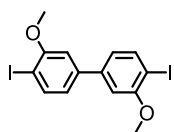
4,4'-Diamino-3,3'-dimethoxybiphenyl (533 mg, 2.39 mmol, 1.0 eq.) was dissolved in acetonitrile (10 mL) and pTsOH (2.80 g, 14.3 mmol, 6 eq.) was added. The mixture was cooled to 0 °C and a solution of $NaNO_2$ (660 mg, 9.56 mmol, 4.0 eq.) in water (5 mL) was added. After 5 min a solution of KI (2.00 g, 12.0 mmol, 5.0 eq.) in water (5 mL) was added and the reaction mixture was stirred at 0 °C for 16 h. The reaction was quenched with sat. aq. $Na_2S_2O_3$ solution and extracted with ethyl acetate. The combined organic layers where washed with water, dried over MgSO4 and concentrated under reduced pressure. The crude product was purified by column chromatography (SiO_2, cyclohexane / dichloromethane 3:2). 4,4'-Diiodo-3,3'-dimethoxybiphenyl (**44**, 662 mg, 1.42 mmol, 59 %) was obtained as a white solid.

¹H-NMR ($CDCl_3$, 400 MHz) δ (ppm): 7.82 (d, $^3J_{H,H}$ = 8.0 Hz, 2H), 6.96 (d, $^3J_{H,H}$ = 2.0 Hz, 2H), 6.83 (dd, $^3J_{H,H}$ = 8.0 Hz, $^4J_{H,H}$ = 2.0 Hz, 2H), 3.95 (s, 6H).

¹³C-NMR ($CDCl_3$, 101 MHz) δ (ppm): 158.6, 142.6, 139.9, 121.4, 109.9, 85.5, 56.6.

TLC (SiO_2, Cyclohexane / dichloromethane 3:2, UV): R_f = 0.53.

4,4'-(4-Ethanethioatephenylethynyl)-3,3'-dimethoxybiphenyl (35)
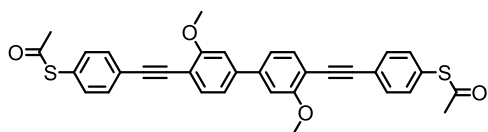
4,4'-Diiodo-3,3'-dimethoxybiphenyl (**44**, 287 mg, 0.616 mmol, 1.0 eq.) and CuI (7 mg, 0.037 mmol, 0.06 eq.) was placed into dry flask under argon atmosphere. (4-Ethynylphenyl)-ethanethioate (**43**, 239 mg, 1.36 mmol, 2.2 eq.) was dissolved in degassed THF (14 mL) and added into the flask, followed by Hünig's Basel (3.3 mL). The mixture was degassed for 10 min. with argon and Pd(PPh$_3$)$_2$Cl$_2$ (21 mg, 0.031 mmol, 0.05 eq.) was added. The reaction mixture was stirred for 18 h at room temperature. After dilution with dichloromethane, the suspension was filtered over a celite plug and concentrated under reduced pressure. The crude product was purified by column chromatography (SiO$_2$, toluene / dichloromethane 3:1). 4,4'-(4-Ethanethioatephenylethynyl)-3,3'-dimethoxybiphenyl (**35**, 103 mg, 0.187 mmol, 30 %) was obtained as a white solid.

^{1}H-NMR (CDCl$_3$, 400 MHz) δ (ppm): 7.60 (d, $^3J_{H,H}$ = 8.3 Hz, 4H), 7.56 (d, $^3J_{H,H}$ = 7.9 Hz, 2H), 7.40 (d, $^3J_{H,H}$ = 8.3 Hz, 4H), 7.19 (dd, $^3J_{H,H}$ = 7.9 Hz, $^4J_{H,H}$ = 1.6 Hz, 2H),), 7.11 (d, $^3J_{H,H}$ = 1.6 Hz, 2H), 4.00 (s, 6H), 2.44 (s, 6H).

^{13}C-NMR (CDCl$_3$, 101 MHz) δ (ppm): 193.6, 160.5, 142.7, 134.3, 134.0, 132.4, 128.1, 125.0, 119.6, 112.0, 109.7, 93.8, 87.5, 56.2, 30.4.

MS (MALDI-TOF): m/z = 519.7 ([M-C(O)CH$_3$]$^-$)

4,4'-Diiodo-2,2'-bis(trifluoromethyl)biphenyl (45)

4,4'-Diamino-2,2'-bis(trifluoromethyl)biphenyl (196 mg, 0.612 mmol, 1.0 eq.) was dissolved in acetonitrile (2 mL) and pTsOH (716 mg, 3.67 mmol, 6.0 eq.) was added. The mixture was cooled to 0 °C and a solution of $NaNO_2$ (169 mg, 2.45 mmol, 4.0 eq.) in water (1 mL) was added. After 5 min a solution of KI (513 mg, 3.06 mmol, 5.0 eq.) in water (1 mL) was added and the reaction mixture was stirred at 0 °C for 2 h. The reaction was quenched with sat. aq. $Na_2S_2O_3$ solution and extracted with ethyl acetate. The combined organic layers where washed with water, dried over MgSO4 and concentrated under reduced pressure. The crude product was purified by column chromatography (SiO_2, cyclohexane / dichloromethane 10:1). 4,4'-Diiodo-2,2'-bis(trifluoromethyl)biphenyl (**45**, 240 mg, 0.443 mmol, 72 %) was obtained as a white solid.

^{1}H-NMR (CDCl$_3$, 400 MHz) δ (ppm): 7.82 (d, $^3J_{H,H}$ = 8.0 Hz, 2H), 6.96 (d, $^4J_{H,H}$ = 2.0 Hz, 2H), 6.83 (dd, $^3J_{H,H}$ = 8.0 Hz, $^4J_{H,H}$ = 2.0 Hz, 2H), 3.95 (s, 6H).

^{13}C-NMR (CDCl$_3$, 101 MHz) δ (ppm): 140.1, 136.0, 135.2, 133.0, 130.5 (q, $^2J_{F,C}$ = 30.8 Hz, 1C), 122.7 (q, $^1J_{F,C}$ = 274.9 Hz, 1C)

TLC (SiO_2, Cyclohexane / dichloromethane 10:1, UV): R_f = 0.73.

4,4'-(4-Ethanethioatephenylethynyl)-2,2'- bis(trifluoromethyl)biphenyl (36)

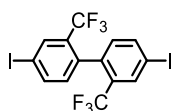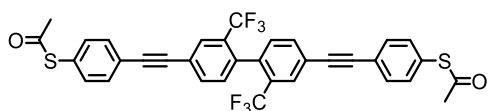4,4'-Diiodo-2,2'-bis(trifluoromethyl)biphenyl (**45**, 208 mg, 0.384 mmol, 1.0 eq.) and CuI (4 mg, 0.023 mmol, 0.06 eq.) was placed into dry flask under argon atmosphere. (4-Ethynylphenyl)-ethanethioate (**43**, 149 mg, 0.845 mmol, 2.2 eq.) was dissolved in degassed THF (10.5 mL) and added in one portion followed by the Hünig's Base (2.1 mL). The reaction mixture was degassed for 10 min. with argon and $Pd(PPh_3)Cl_2$ (13.6 mg, 0.019 mmol, 0.05 eq.) was added. The reaction mixture was stirred for 18 h at room temperature. After dilution with dichloromethane, the mixture was filtered over a celite plug and concentrated under reduced pressure. The crude product was purified by column chromatography (SiO_2, toluene / dichloromethane 3:1). 4,4'-(4-Ethanethioatephenylethynyl)-2,2'-bis(trifluoromethyl)biphenyl (**36**, 130 mg, 0.204 mmol, 53 %) was obtained as a white solid.

^{1}H-NMR (CDCl$_3$, 400 MHz) δ (ppm): 7.93 (d, $^4J_{H,H}$ = 1.6 Hz, 2H), 7.70 (dd, $^3J_{H,H}$ = 7.9 Hz, $^4J_{H,H}$ = 1.7 Hz, 2H), 7.59 (d, $^3J_{H,H}$ = 8.3 Hz, 2H), 7.44 (d, $^3J_{H,H}$ = 8.3 Hz, 2H), 7.30 (d, $^3J_{H,H}$ = 8.0 Hz, 2H).

^{13}C-NMR (CDCl$_3$, 101 MHz) δ (ppm): 193.4, 136.8, 134.4, 133.7, 132.4, 131.8, 129.5, 129.2, 129.0, 123.8, 123.8, 123.4 (q, $^1J_{F,C}$ = 274.1 Hz, 2C), 90.9, 89.2, 30.5.

MS (MALDI-TOF): m/z = 638.1 ([M]$^-$) ; m/z = 595.6 ([M-C(O)CH$_3$]$^-$)

Chapter 3 – High-Triplet State Energy Materials

Introduction

Over the past two decades, organic light emitting diodes (OLEDs) have been studied extensively. The need of light and flexible devices in combination with a low environmental impact motivated the rapid development of optoelectronic device technologies. In 1965, the first investigated organic molecule in the context of electroluminescence were anthracene crystals, by applying a bias voltage of a few hundred volts.[132] Almost 20 years later in 1987, Tang *et al.* described the successful assembly of a first simple OLED.[133] The structure and working principle were improved and introduced a revolution in the display lighting industry.[134] Despite the commercialization, remaining problems demands further investigation in the field of OLEDs.

Principle of Photoluminescence

To understand the working principle, advantages as well as the disadvantages of OLEDs versus LEDs, the terms of photoluminescence has to be understand. Photoluminescence is defined as the light emission of a system by absorption of a photon and the following release of the obtained energy. During the absorption of a photon, the molecule uses the intrinsic energy of said proton to promote an electron into an unoccupied molecular orbital (MO) with a higher energy. The promotion of a lone pair electron into a π*-orbital (n → π*) demands the lowest energy. On the other side, for the transition of a σ-electron into a σ*-orbital, the most energy is required. The transitions can be ordered energetically as follows:[135]

n → π* < π → π* < n → σ* < σ → π* < σ → σ*
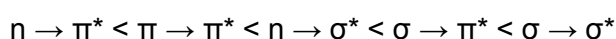
Depending of the energy level of the excited state, the release of the energy can result in the emission of visible light between 400 nm - 800 nm, as the wavelength λ correlates with the energy of the photon, shown in equation **1** as

$$E = \frac{hc}{\lambda} ,$$ **(1)**

where h is the Planck constant and c is the speed of light in vacuum. Most of the organic molecules are in a singlet ground state. During the excitation of a molecule and accordingly the promotion of an electron in an energetically higher molecular orbital, the spin orientation of the electron remains. This principle is defined by the Wigner-Wittmer rule and as consequence, the excited molecule has the same multiplicity as its ground state.[136] The promotion of a molecule from the ground state S_0 to the first excited singlet state S_1, or a higher lying singlet state S_2, is controlled by the energy of the absorbed photon, and therefore of the light source. Additional, to every excited state an almost continuous manifold of vibrational levels exist as shown in **figure 23**.
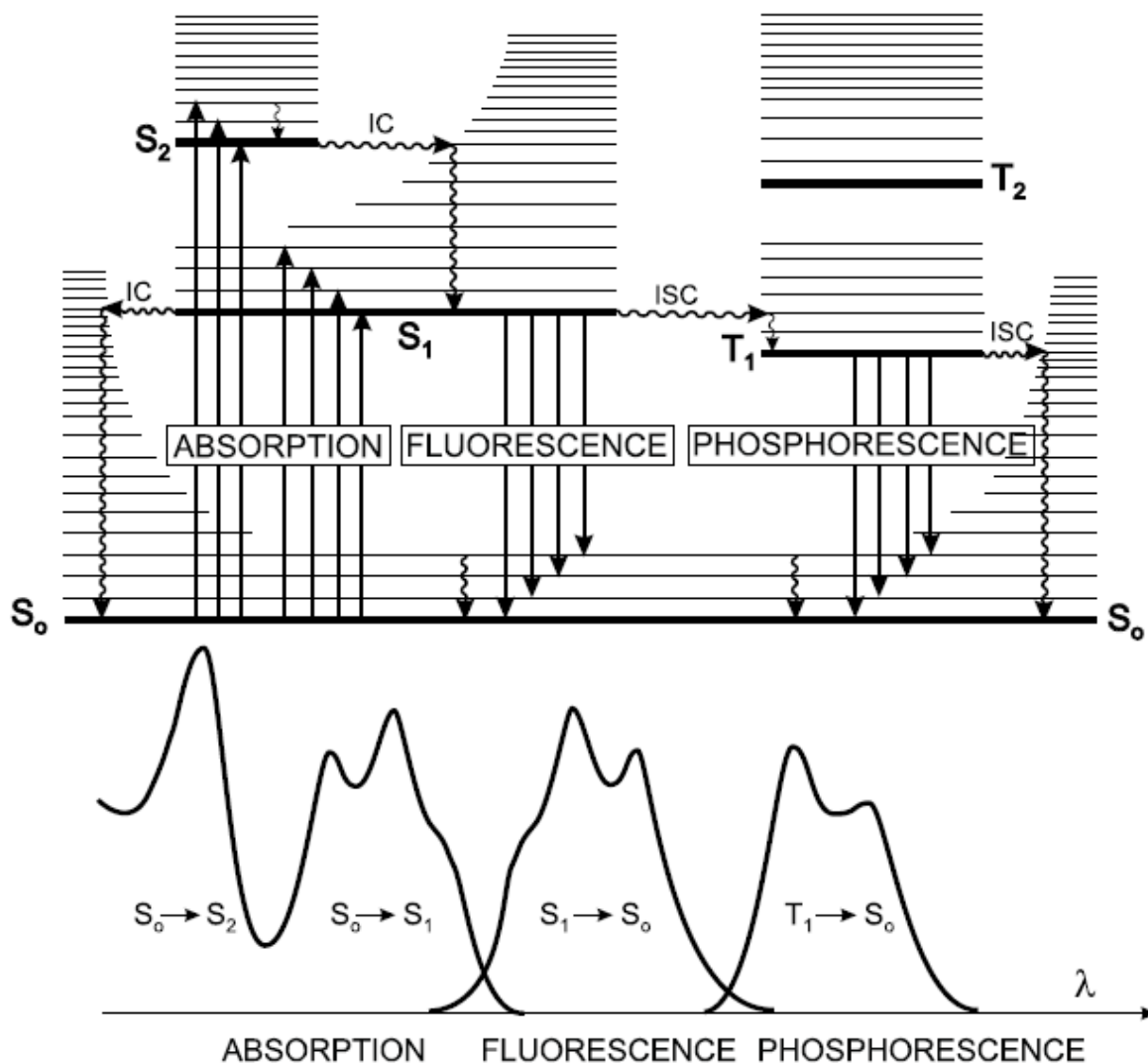
Figure 23. The Jablonksi diagram on top illustrates the different electronic states and their transformations. By photon absorption, an excitation of the electronic ground state S_0 to an excited electronic state S_1 or S_2 occurs. Due to an internal conversion (IC) the system can relax into the S_1 state out of the different vibrational energy levels. The S_1 state can relax by emitting light, called fluorescence, or perform an intersystem crossing (ISC) to end up in an excited triplet state T_1. The radiative de-excitation of T_1 to the S_0 state is called phosphorescence. In the figure below, the corresponding wavelength shifts of the absorption, fluorescence and phosphorescence is illustrated. Reprinted with permission from Valeur, B. and Berberan-Santos.[135]

After excitation to a higher molecular orbital, the relaxation into lower energy states can take place on different and competing ways. First, the relaxation of higher lying vibrational levels towards the S_1 state occurs in a time period of 10^{-12} - 10^{-10} seconds due to collisions with solvent molecules. An excited molecule in a S_1 state can relax by a radiationless deactivation process called internal conversion (IC). This process is more efficient for higher lying excited states than the S_1 state, for example the relaxation from S_2 to S_1. Hence the energy difference is substantially larger between S_1 and the ground state, other processes like fluorescence or intersystem crossing (ISC) can compete.[135] In the case of fluorescence, the S_1 state has a lifetime of 10^{-10} - 10^{-7} seconds before the emission of a photon and therefore the relaxation S_1

94

$\rightarrow S_0$ takes place. The wavelength of the released photon equals the energy difference between the excited state and the ground state, according to equation **1**. As a third competing process, an intersystem crossing can take place in case of fulfilled requirements. During the ISC, the excited electron changes its spin orientation and we observe a transition from a singlet to a triplet state. This nonradiative transition is theoretically forbidden but can occur due to spin-orbit coupling. The terminus spin-orbit coupling describes the admixture of higher lying singlet substate characteristics to the T_1 substate. As consequence, the triplet state has partial singlet state characteristics which makes the transition possible and leads to an increased ISC rate. Hence, the spin-orbit coupling is dependent on the spin of the electron, the angular momentum of the corresponding atom, and the distance between them. An increase of the ISC rate with a dependency of Z^4 is observed, whereas Z is the atomic number.[137,138] The lifetime of excited triplet state is in the range of 10^{-6} - 10 seconds and the radiative de-excitation $T_1 \rightarrow S_0$ is called phosphorescence. This transition is again theoretically forbidden because of the spin flip of the electron, but can still be observed due to spin-orbit coupling.[135]

Multilayer OLED Design

The light emission of traditional LED's relies on the emission of fluorescent light after an excitation by electroluminescence. Considering OLED's, the source of the excitation remains but the principle of the emission changes from fluorescence to phosphorescence in most of the used diodes. The advantages, consequences, and theoretical reasons for this change will be discussed later in this chapter. First, the functionality and build-up of a typical OLED is discussed.

The first described OLED in 1987 by Tang *et al.* consisted of two layers.[133] The hole transporting (HT) and electron transporting (ET) layer. Over the years, the efficiency and the complexity of the build-up increased, but the fundamental working principle remained unchanged. Due to an applied voltage, a chromophore deployed within a multilayer set up between an anode and a cathode is excited. The relaxation of the excited chromophore to its ground state results in the emission of a photon.
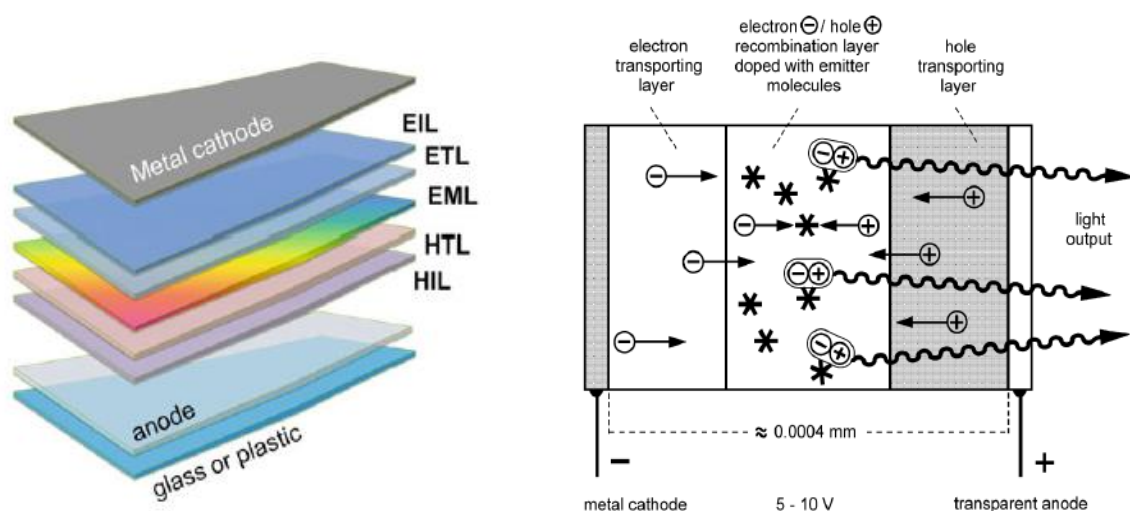
Figure 24. Left: A schematic design of multilayer OLED build up. Right: By applying a voltage, electrons and holes are moving from to cathode to the opposite anode and vice versa. At the recombination layer, the recombination of electrons and holes takes place. The matrix material absorbs the energy from that exciton formation and subsequently excites the dye, which upon relaxation induces the light emitting at a defined wavelength. Reprinted with permission from Giovanella *et al.* and Yersin *et al.*[139,140]

On one side of the OLED, a transparent anode enables the transmission of light. This anode is typically made of indium tin oxide (ITO), which is a mixture of SnO_2 (10 - 20 %) and In_2O_3 (80 - 90 %).[140] Next to the anode, the function of the hole injection layer (HIL) is to facilitate the oxidation of the hole transporting layer (HTL) and therefore has to provide suitable HOMO energy levels (see **figure 25**). The HTL is responsible for an efficient hole transport to the emission layer (EML) and therefore requires a high hole mobility. Additionally, the HOMO energy level has to match the corresponding energy level of the HIL or anode to ensure a low potential barrier for the hole injection, as well as a high LUMO energy level to prevent undesired electron injection from the EML. Furthermore, the triplet energy has to be high enough to block triplet exciton diffusion. The middle of the cell consists of the EML where the recombination of the electrons and the holes takes place. It is made of the host material doped with the light emitting dye. The important interplay of the host material with the dye will be discussed in a later chapter. As for every layer, the matching of the HOMO and LUMO level to the neighboring layers is crucial to ensure a low operating voltage. Between the cathode and the EML, the electron transporting layer (ETL) has to guarantee a high electron mobility. In contrast to the HTL, the ETL gets reduced and therefore the energy level of the LUMO is of interest. To obtain a minimization of the potential barrier for the injection of electrons, an electron injection layer (EIL) can be used. The cathode can consist of aluminum or other oxidizable metals such as calcium, magnesium or indium.[141,142]
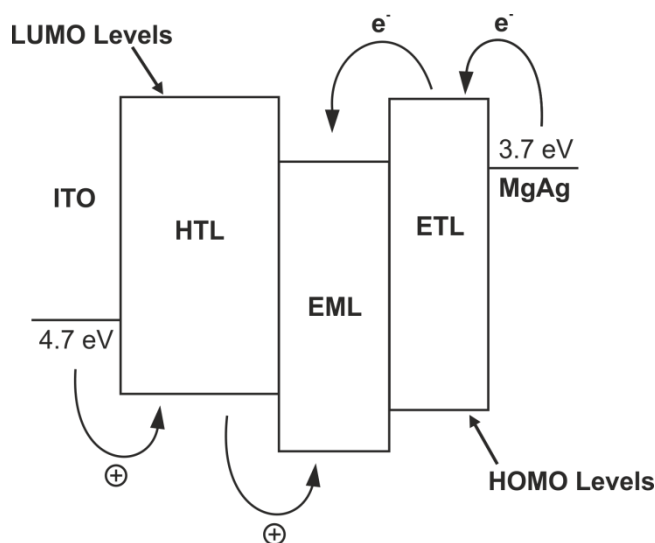
Figure 25. Example for a simple three-layer OLED setup, with respect of the HOMO and the LUMO energy levels. On the left; holes are injected from the ITO anode into the energetically lower lying HOMO of the HTL, transported through the HTL and injected into the EML. On the right; electrons are injected into the ETL. Subsequent electron hopping through the ETL is followed by the injection into the EML.

From a chemical standpoint, the electrochemical properties of the different layers, mainly the energy level of the HOMO and LUMO, are of interest. The energy levels of these orbitals have to be matched to the different layers of the OLED to observe a good electron and hole injection and transport through the cell, especially at the layer interfaces. Carrier accumulation at the interfaces between two layers is a known reason for quenching phenomena and decrease of the overall performance.[141]

The Role of the Emission Layer

The emission layer is where most of the electroluminescence phenomena take place. A crucial step to increase the efficient of OLED was to realize that the light emitting substance is best doped in low concentration in a matrix or host material. Typically, doping concentrations are in the range of 1 – 2 %[143], but there are setups with a doping concentration up to 20 %.[144] To understand the excitation process of the dye, a closer look into the mechanism of the hole-electron recombination is required. After applying a voltage between the cathode and the anode, the ETL is reduced while the HTL is oxidized. Due to the potential, both charges move through the corresponding layers to the EML by a hopping process.[145] In a well-designed OLED, the mobility of the charges and thickness of the different layers ensure the recombination of the holes and electrons in the EML. Due to the negative charge of the electron and the positive charge of the hole, a Coulomb interaction occurs within a critical electron-hole

separation distance R_c.[145] For an attraction, the Coulomb force has to be in a similar range as the thermal heat $k_b T$. Coulomb attraction can be related to the thermal heat by **equation 2.**

$$F(e-h) = \frac{e^2}{4\pi\varepsilon_0 \varepsilon R_c} = k_b T,$$ **(2)**

where e is the electron charge, ε_0 the dielectric constants of the vacuum, ε the dielectric constant of the host material, k_b the Boltzmann constant and T the temperature.[139] Typical setups result in R_c values of about 180 Å. Within this distance an electron and a hole are attracted to each other even if there are several molecules in between them. As the hole and electron are drawing closer together (typically 10 - 15 Å) the wave functions of the electron and the hole start to overlap and form an exciton.[145] This exciton formation is the drawback as well as the advantages of the OLED technique at the same time. The spin orientation of the formed electron after injection into the ETL is random, but remains the same during the hopping process. On the other side, the orientation of the hole is defined by the spin of the residual electron of the HOMO, but is as well not controllable.[139] The linear combination of both wave functions during the recombination and consequent excitation of a molecule leads to four different states: Three triplet states and one singlet state. This ratio is statistically defined due to the independent charge injection on both side of the OLED.[140]
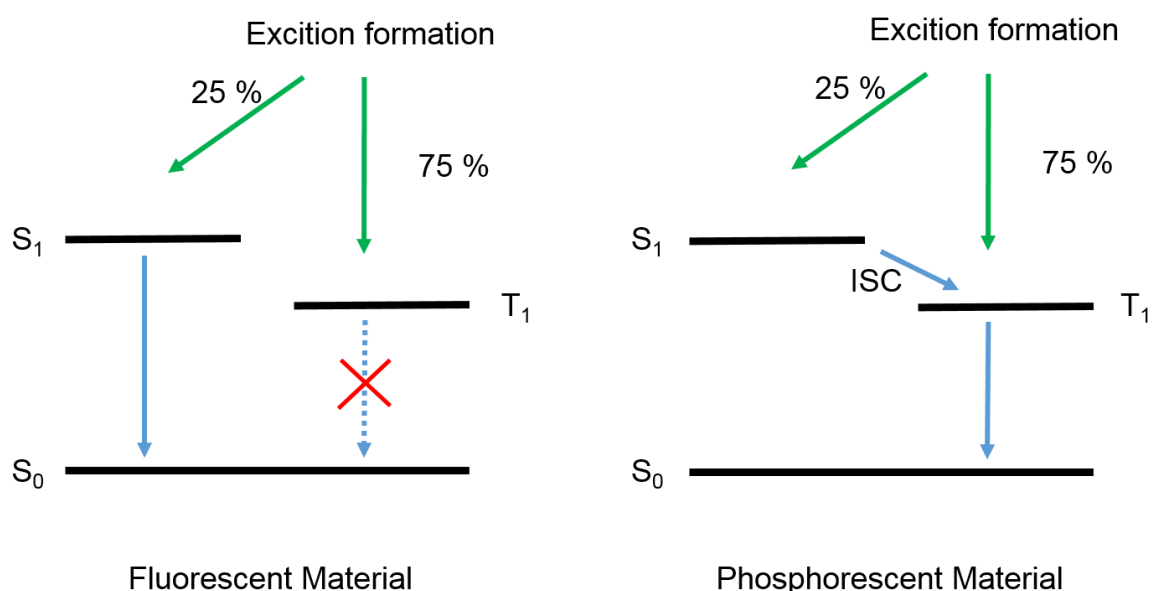
Figure 26. According to spin statistics, only a fourth of the obtained excited states are in a singlet state. Therefore, three quarters of the created excited states are lost by radiationless deactivation, if a fluorescent dye is used. The maximum efficiency with a fluorescent emitter cannot be higher than 25%. The use of a phosphorescence emitter would increase the theoretically efficiency to 100%. The obtained singlet state can be transferred into a triplet state by a fast ISC processes.

As consequence, in fluorescent light emitting diodes, a maximum of 25 % of the formed excited states can produce a photon (see **figure 26**). The resulting triplet states perform a radiationless internal conversion $T_1 \rightarrow S_0$. By using a phosphorescent chromophore, the triplet states can relax into the ground state by emission of phosphorescent light. Furthermore, the singlet states can undergo an ISC to access the energetically lower T_1 state, leading to a theoretically four times higher efficiency.[139,140]

Host – Dye Energy Transfer

Depending on the relative HOMO and LUMO level, the recombination of the electron with a hole can take place either on the host material or on the dye. Therefore, by a carefully combining of an appropriate dye and matrix material, the recombination can be controlled to take place solely on the dye or on the matrix material. Jou *et al.*[144,146] argue that having the recombination on the matrix material followed by an effective host-to-guest energy transfer prevents undesired exciton quenching on the guest molecule. The transfer of the excited state from a host to a guest molecule can happen by two different mechanism.

In the Förster resonance energy transfer (FRET) mechanism, excited singlet states are transferred from the host to the guest molecule (see **figure 27**). The FRET is based on radiationless dipole-dipole interaction that allows the shift of the emission to a lower energy state without a dissipation process. This normally occurs in a two-step process as absorption and re-emission.[140] The energy transfer rate K_{FRET} scales with a $1/R^6$ dependency as shown in **equation 3**.

$$K_{Fret} = t_d^{-1} \left(\frac{R_0}{R}\right)^6, \tag{3}$$

where t_d is the lifetime of the excited singlet state on the host molecule in absence of the guest, R_0 the characteristic Förster distance and R the distance between the host and the guest. The characteristic Förster distance depends on the relative orientation of the host and guest dipole moments, the quantum yield of the host in absence of the guest and the refraction of the medium summarized as factor α in **equation 4.**

$$R_0 = \alpha \int_0^\infty F_d(v)\, \varepsilon_a(v) v^4 dv, \tag{4}$$

F_d (v) and ε_a(v) are the fluorescent spectra of the donor and the molar extinction coefficient of the acceptor.[140] The efficiency of the energy transfer depends on the overlapping of the fluorescent spectra of the host and the absorption spectra of the guest molecules. This means that the energy of the theoretically emitted fluorescent light correlates to the energy which is necessary to excite the guest molecule from a singlet ground state S_0 to an excited singlet state S_1. Typically, distances between host and guest molecule are in the range of 3 - 5 nm, up to 10 nm.[145,147] The overlap between the fluorescence and absorption spectra can be easily examined by UV-Vis measurements. Furthermore, a high molar extinction coefficient of the acceptor is essential.
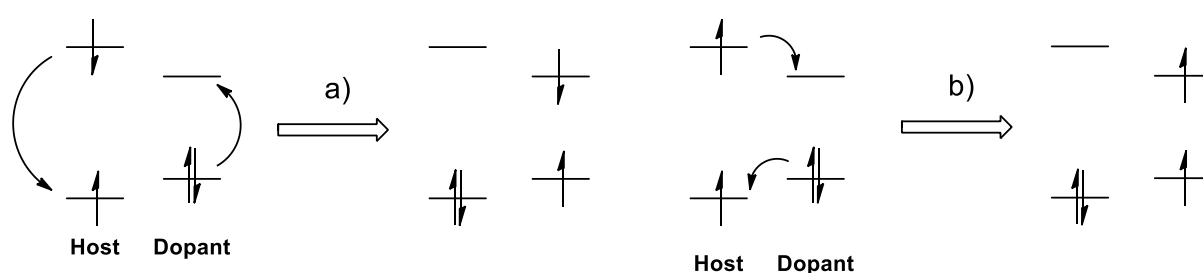
Figure 27. Host - guest energy transfer: a) FRET; an excited singlet state is transferred from the host to the dopant; b) Transfer of the excited triplet state from the host to the guest molecule, known as Dexter energy transfer.

If the distance between the host and the dopant is closer than 1 nm, quantum mechanical effects such as overlapping of the frontier orbitals and tunneling can take place. This leads to a change of the energy transfer mechanism to electron exchange interactions, known as the Dexter energy transfer. As shown in **figure 27**, a singlet - triplet energy transfer via the Förster mechanism is spin forbidden and therefore only observable under very specific conditions.[136] The Wigner-Witmer rule states that the total spin during a process has to remain constant. Therefore both, the singlet - singlet transfer as well as the triplet - triplet transfer are allowed in the Dexter pathway.[136] In combination of both energy transfer mechanisms, the excited host material can transfer its energy to the doped light emitting dye, obtaining the same triplet / singlet ratio. A strong ISC process on the phosphorescence dye to convert the singlet states into the triplet states leads to a high internal phosphorescence quantum yield.

The distance dependency of the two energy transfer mechanism can be used in beautiful designed multi emitter devices for efficient white light emission.[148,149] A fluorescent dye is placed further away from the recombination layer and is therefore only addressable by the long range Förster energy transfer of singlet states. In contrast, a phosphorescence dye is closer to the exciton formation and enables an efficient transfer of all triplet states.

100

Host Material

In summary, host materials for OLEDs have several requirements to fulfil: An efficient energy transfer to the dopant, triplet energy has to be higher than the triplet emitter, good charge transport properties, HOMO and LUMO levels have to be suitable for an efficient hole and electron injection and good thermal, chemical and electrochemical stability. The thermal stability specifically demands a stable film morphology and a high glass transition temperature (T_g).[140,143,145]

The host materials can be classified roughly in two categories: Small organic molecules and polymer materials. The benefits of small molecules are the high triplet energy and the high material purity. On the other side, the poor morphological stability due to low T_g is a drawback. One of the most used host materials is 4,4′-Bis(N-carbazolyl)-1,1′-biphenyl (CBP). Whereas for example carbazole itself would fulfil the requirements of a high triplet energy, the morphological stability requires the use of carbazole as a moiety in more complex molecules. Even in combination with the biphenyl core, CBP has a low T_g of 62 °C[150]. Another drawback is the rather low E_T of 2.56 eV of CBP, which leads to an inefficient triplet state energy transfer to deep blue emitting dyes (E_T > 2.65 eV). Different concepts to improve the thermal stability as well as to increase the triplet energy of CBP were developed. For example, mCP, with two carbazole moieties in meta position of a phenyl core, to minimalize the conjugation within the molecule and therefore increased E_T to 2.9 eV was investigated. However, the thermal stability showed no noteworthy improvement. This problem was addressed by synthesizing spiro or star-shaped moieties as realized in CBF and TCB to increase the glass transition temperature above 160 °C.[151]

| CBP | mCP | CBF | TCB |
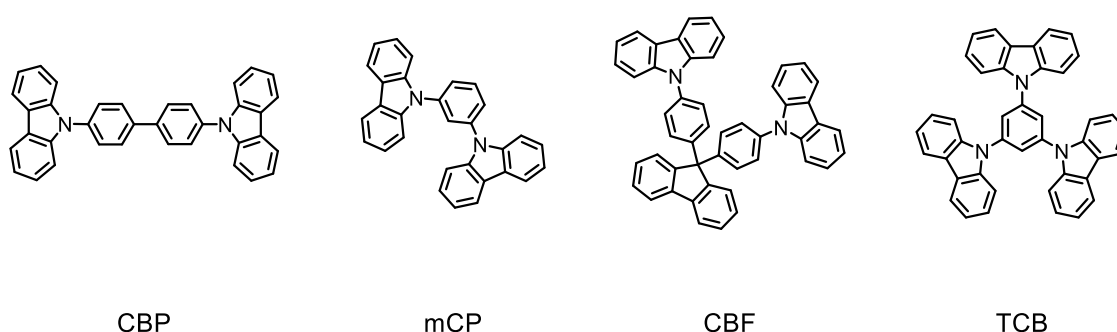
Figure 28. Examples of synthesized host material. CBP as the so far most used host materiel as base structure. Decreasing of the π-conjugation by arrange the both carbazole units in *meta* – position increase the E_T of mCP. By introducing spiro or star-shaped structures in CBF and TCB, increased T_g were achieved.

A different strategy to interrupt the conjugation within the molecule is the insertion of either sp³ hybridized carbon or silicon atoms between the aromatic systems, or sterically demanding

groups to force the alignment of the subunits into a perpendicular arrangement. The insertion of methyl groups in 2,2'-position of the biphenyl in CDBP or 3,3'-position in o-CDBP demonstrates this strategy, leading to triplet state energies of 3.0 eV (CDBP)[152] and 2.7 eV (o-CDBP)[153], respectively. The bulky conformation of SimCP2 fulfils both concepts. The conjugation is interrupted by the sp³ hybridized silicon in the middle and the meta conjugation of the carbazole subunits. The highly sterically demanding groups reflect in the high T_g of 144 °C.[154]
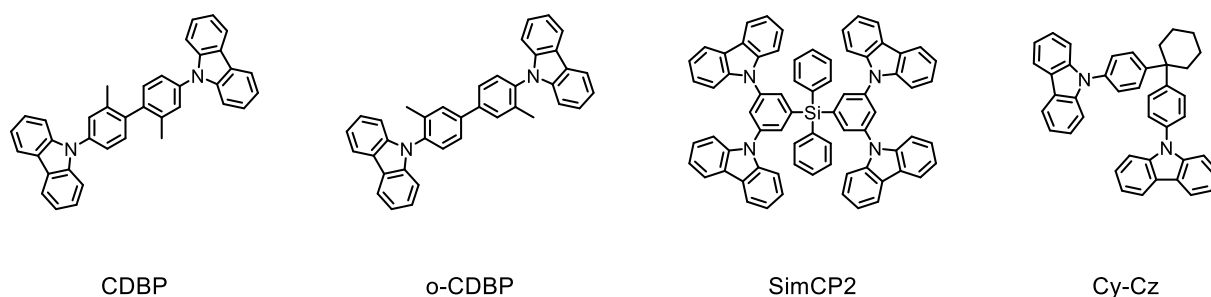
Figure 29. Sterically demanding groups force the individual aromatic systems into a perpendicular alignment. The decreased conjugation within the molecule lead to an increased triplet energy. The same effect can be achieved by introducing sp³ conjugated carbon or silicon atoms as in SimCP2.

Aim of the Work

To further improve the efficiency of OLEDs, understanding the fundamental principle of all factors contributing to the final output is crucial. A main part relies on the emission layer consisting of the host material doped with the emitter dye. Considering the host material, there are several key characteristics to understand:

(i) A high triplet energy is essential to ensure an efficient energy transfer from the host material to the phosphorescence emitter by preventing the back energy transfer and promote the exothermic energy transfer. The most used blue phosphorescent light emitter is bis((4,6-difluorophenyl)-pyridinato-N,C2)picolinate-iridium(III) (FIrpic) with an energy gap between the triplet and the ground state of ΔE ($T_1 - S_0$) = 2.65 eV.[2] Hence, a suitable host material should have a T_1 energy above 2.7 eV relative to the ground state.

(ii) In a multilayer system, the efficiency is strongly dependent on the interplay between the individual layers. Having an optimized alignment of the HOMO and LUMO energy levels is a key factor to achieve a low operating voltage, and therefore a minimalized energy consumption.

(iii) Next to the interplay on the layer interfaces, the ability of charge transport within the host material is crucial. Depending on the design of the OLED setup, the host material needs distinctive charge carrier characteristics, defined by the HTL and ETL. There are three types of host materials considering the charge transport criteria: (a) hole transport type (b) electron transport type (c) bipolar transport type hosts.[2] The most commonly used are host material with good hole transport characteristics or, less frequently, bipolar materials.

(iv) In an operating OLED, the organic material must maintain high temperatures due to Joule heating and the external environment.[155,156] Reaching temperatures above the glass transition temperature (T_g) of the material with the lowest T_g, leads to a diffusion of the different layers. As consequence, a decrease of the luminescence can occur and therefore shows the importance of having host materials with a high T_g.

These four categories illustrate how diverse the required characteristics for future host materials in blue OLEDs are. Whereas some changes of the characteristics, like the HOMO und LUMO adjustment by addition of different functional groups to a known system, are more predictable, others like the correlation of T_g values with the structural

and electronical properties of a molecules are not easily predictable. By synthesizing new CBP derivatives and comparing the measured properties with the theoretically calculated model values, a better understanding of the influences of geometrical and electronical effects to the defined properties can be achieved.

Molecular Design

One of the most used host material in blue OLEDs is 4,4′-Bis(N-carbazolyl)-1,1′-biphenyl. CBP, consisting of two carbazole units, which are known for their high triplet energy, interlinked by a biphenyl backbone. The triplet energy of the basic carbazole molecule is 2.98 eV.[157] Whereas the triplet energy is sufficient for the use in blue OLEDs, the tendency of CBP to crystallize is not compatible with an application in a thin film device. For the use as a host material, the ability to form stable amorphous films is essential. In an amorphous film, the emitting dye is uniformly diluted and therefore minimalizes the effect of concentration quenching.[158] The role of the biphenyl backbone is to improve the solid state behavior, but there is still optimization potential regarding its T_g value of 63 °C.[159] A disadvantage obtained by the biphenyl core is the conjugation of the π-system through the entire molecule, which leads to a decrease of the triplet energy. [2,153,160]

The introduction of sterically demanding groups at the 2,2'-position of the biphenyl leads to a twist of the phenyl rings. By interlinking the biphenyl in 2,2'-position with a bridging alkyl chain, defined torsion angel can be achieved. Single molecule break junction experiments have shown a dependency of the torsion angle and the conductance, and therefore the conjugation through the molecule.[120] Hence, the overlapping of the π-system is reduced or, in case of a torsion angle near 90°, almost nullified. In our system, the aim was to obtain an electronical separation of both carbazole units from the biphenyl core. Substituting the 2,2'-position would not lead to the desired effect. Therefore, to obtain a perpendicular alignment between the carbazole and the biphenyl core, either methyl groups at the 3,3'- and 5,5'-position of the core or in 1,8-position of the carbazole are proposed (compound **59** and **60**, **figure 30**). This modification allows to address the triplet energy and aim for a good charge separation. In the same time, a better solid state behavior can be achieved as the insertion of sterically demanding groups has shown to improve the T_g values.[155]
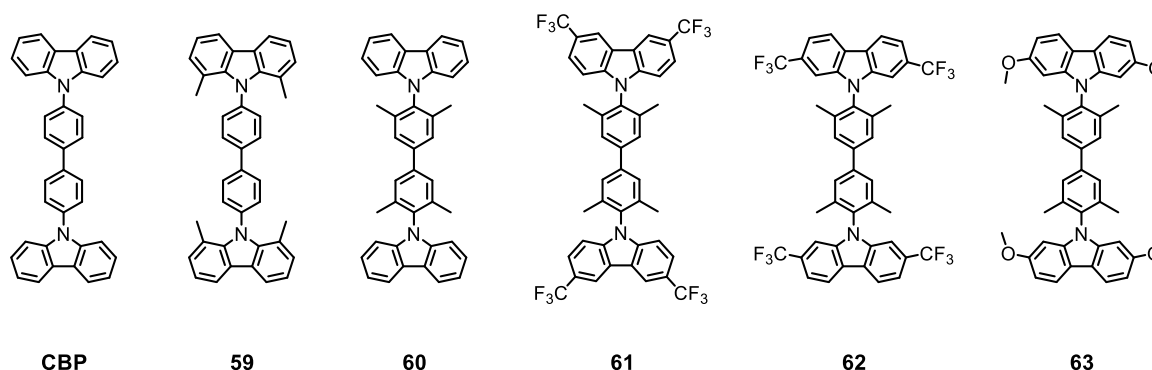
Figure 30. Molecular design of CBP derivatives. Introducing sterically demanding methyl groups to obtain a perpendicular alignment of the carbazole subunit and the biphenyl backbone, as well as the HOMO / LUMO energy level adjustment by the insertion of electron withdrawing or electron donating groups.

105

To investigate the HOMO and LUMO energy level, the carbazole moieties are functionalized with a set of electron donor and electron withdrawing groups. As electron withdrawing groups, trifluoromethyl (-CF$_3$) was chosen and methyl ether (-OMe) as electron donating group. The -CF$_3$ groups were placed either in 3,6-position of the carbazoles in target compound **61** or in 2,7-position for target compound **62**. Target compound **63** was functionalized with methoxy groups in 2,7-position of the carbazoles as shown in **figure 30**. As the most CBP derivatives are known for their good hole transport ability, no direct change to address this characteristics were proposed.

Synthetic pathway

Synthesis of CBP Derivatives 59 and 60
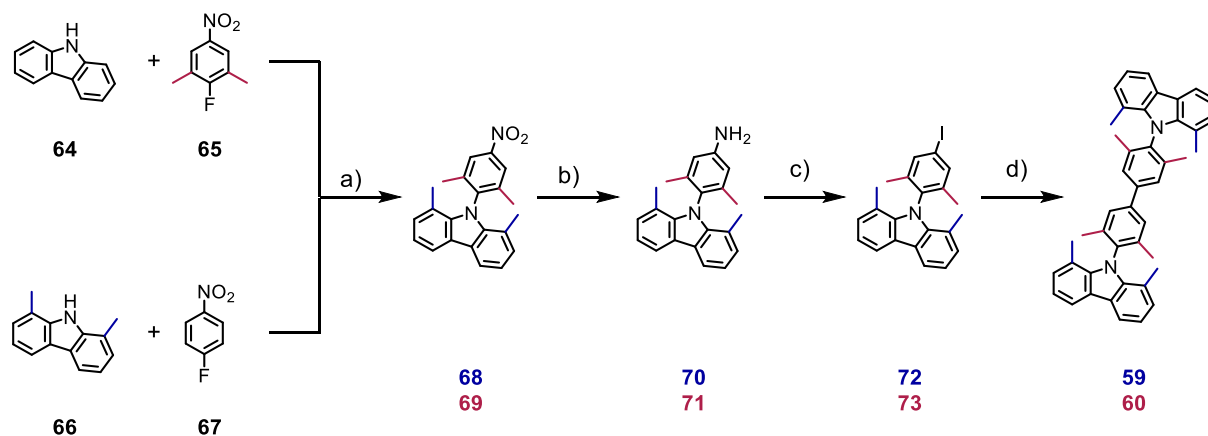
Scheme 15. Synthesis of target structures **59** and **60**. Reaction conditions: a) Cs_2CO_3, DMF, 155 °C, 12 h, **68** (86 %), **69** (87 %); b) $SnCl_2 \cdot 2H_2O$, EtOH, reflux, 4 h, **70** (91 %), **71** (94 %); c) BF_3 Et_2O, ^tBuONO, THF, KI, I_2, MeCN, -10 °C to RT, 12 h, **72** (75 %), **73** (79 %); d) Turbo Grignard, TEMPO, THF, -10 °C to RT , 2 h, **59** (96 %), **60** (97 %).

The key step in the synthesis of compounds **59** and **60** was the formation of the N-C bond between the carbazole and the biphenyl core. The sterically demanding methyl groups, at either one of the building blocks, made the formation via a metal catalyzed cross coupling reaction challenging. After unsuccessful Buchwald-Hartwig reaction conditions, a nucleophilic aromatic substitution reaction (S_NAr) was chosen. Crucial on this concept was the strong electronegativity of the fluorine in *para* - position to a strong electron withdrawing group. The nitro group in *para* - position is known to stabilize the formed Meisenheimer-complex and therefore facilitated the nucleophilic attack. Furthermore, the nitro group provided the required functionality to introduce the iodine for the final homocoupling step by a reduction to the corresponding amine followed by a Sandmeyer reaction.

The synthesis of carbazole **66** was performed by an approach of B. Bedford and M. Betham. [161] Buchwald Hartwig amination followed by a ring closure via C-H activation yielded the desired carbazole in an one-pot microwave synthesis in remarkable 88 % yield. Using classical condition with K_2CO_3 in DMF for the following S_NAr reaction with the commercial available 4-fluoro-nitrobenzene (**67**) showed moderate conversion to the desired product **68**.[162] Considering the +I effect of both methyl groups in ortho position of the amine and the resulting lower acidity of the proton, Cs_2CO_3 as a stronger base was used to obtain nitro compound **68** in 86 % yield.
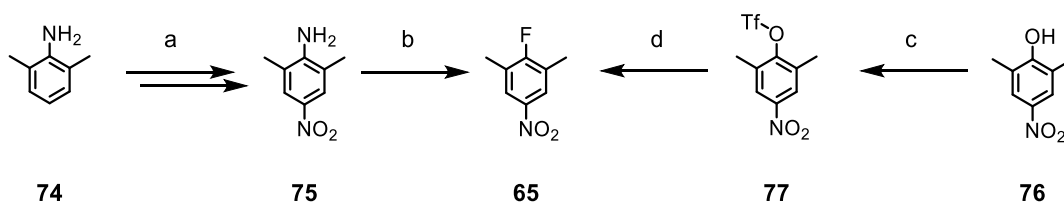
Scheme 16. Synthesis of building block **65**. Reaction conditions: a) (i)) p-TsCl, pyridine, 115 °C, 1.5 h, 93 % (ii) NaNO$_2$, nitric acid, acetic acid, H$_2$O, 90 °C, 4 h, 59 %; (iii) H$_2$SO$_4$, 50 °C, 2 h, 36 %; b) HF-pyridine, NaNO$_2$, -15 °C, 3 h, 88 %; c)Tf$_2$O, pyridine, DCM, 0 °C, 1 h, 98 %; d)[(cinnamyl)$_2$]Pd$_2$, *tert*-BuBrettPhos, CsF, MePh, 110 °C, 24 h, 93 %.

Fluoro compound **65** was first synthesized by a Balz-Schiemann type reaction from the corresponding amine precursor **75** with HF-pyridine.[163,164] The precursor compound had to be synthesized from the commercially available 2,6-dimethylaniline (**74**) by subsequent protection, nitration and deprotection, following the procedure published by Moorthy and Saha.[165] Nevertheless, the large amount of compound **65** required for the formation of target compounds **60 - 63** demanded for a more efficient pathway. The good yields in the small scale reactions dropped enormously during upscaling to an overall yield of 20 % over three step in a gram scale approach. Additionally, the possibility to avoid the work with hydrofluoric acid favored an alternative synthesis. Starting with 2,6-dimethyl-4-nitrophenol (**76**), the hydroxyl group was converted into the triflate **77** by classical conditions. Afterwards, a Pd-catalyzed fluorine insertion reported by Buchwald and co workers[166], using CsF as fluorine source, yielded in excellent 93 % in multigram scale. The subsequent S$_N$Ar reaction with the commercially available carbazole resulted in excellent yield of nitro compound **69**.

With the nitro compounds **68** and **69** in hand, the reduction to the amine was performed with SnCl$_2$ in ethanol in good yields, followed by the transformation to the corresponding iodine compounds by a Sandmeyer type reaction. First, classical conditions with HCl and NaNO$_2$ in a 1:1 mixture of acetonitrile / water to form the diazonium salt were used, before adding an aqueous solution of KI. However, both reactions yielded in moderate yields for compound **72** (63 %) and **73** (61 %), respectively. The poor yields were attributed to the poor solubility of the starting materials. An procedure published by Flatt *et al.*[167] using BF$_3$·OEt$_2$ and ^{t}BuONO to form the air stable diazo-borontetrafluoride salt increased the yields to a satisfying level. The air stable diazo-borontetrafluoride salt was precipitated by the addition of diethyl ether. The filtered salt was dissolved in a solution of KI and I$_2$ in acetonitrile to obtain the iodoaryls **72** and **73**, respectively.

In the final homo coupling reaction, straight forward synthesis as classic Ullmann reaction[168], lithiation and a subsequent Gilman reagent pathway[169] or the use of Cu(II) immobilized on silica[170] as catalyst did not lead to the desirable products. Further screening revealed the use

of Knochel's Turbo Grignard[171] reaction conditions to achieve the oxidative homo coupling to the desired target compounds **59** and **60** in excellent yields of 96 % and 97 %, respectively.

Synthesis of Trifluoromethyl Functionalized Carbazoles
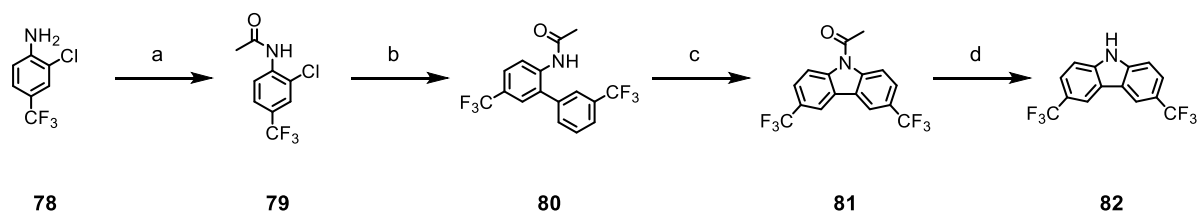
Scheme 17. Synthesis of carbazole **82**. Reaction conditions: a) AcCl, TEA, DCM, RT, 2 h, 91 %; b) SPhos Pd G2, 3-(trifluoromethyl)phenylboronic acid, K$_3$PO$_4$, THF : H$_2$O (20:1), 80 °C, 12 h, 93 %; c) Pd(OAc)$_2$, Cu(OAc)$_2$, MePh, 120 °C, 24 h, 98 %; d) H$_2$SO$_4$ / MeOH (1:5), 80 °C, 0.5 h, 99 %.

Carbazole can be functionalizes in its 3,6-positions directly by an electrophilic aromatic substitution reaction. The +M effect of the amine functionality is strongly directing into both *para* - positions. A twofold iodination of carbazole with NIS is documented in literature[172,173] and resulted in good yields. Nevertheless, after protection of the amine, the subsequent Cu(I) catalyzed -CF$_3$ insertion was challenging, even the reaction is well known in literature.[174,175] The trifluoromethylation with AgF, trimethylsilyl-CF$_3$ and CuCF$_3$ leaded to undesired side products because of multiple insertions of the -CF$_3$ group. The separation of these side products by column chromatography or crystallization was not possible, but only by gel permeation chromatography (GPC) techniques. However, considering the required amounts of carbazole **82**, this technique was not promising. The Buchwald group described a two-step procedure to synthesize similar carbazoles using a Suzuki-Miyaura cross-coupling to form the biphenyl precursor and a subsequent C-H activation to form the C-N bond of the carbazole.[176] For our system, 2-chloro-4-trifluoromethylaniline (**78**) was first acetyl protected in 91 % yield. Afterwards, using classic Suzuki-Miyaura condition with SPhos Pd G2 catalyst lead to biaryl **80** in excellent yields. For the C-N bond formation, a catalytic system consisting of Pd(OAc)$_2$ as precatalyst and Cu(OAc)$_2$ as reoxidant was used and proceeded in good yields in gram scale reactions. The following deprotection of the amine **81** took place in a mixture of sulfuric acid and methanol in an almost quantitative conversion to the desired carbazole **82**.
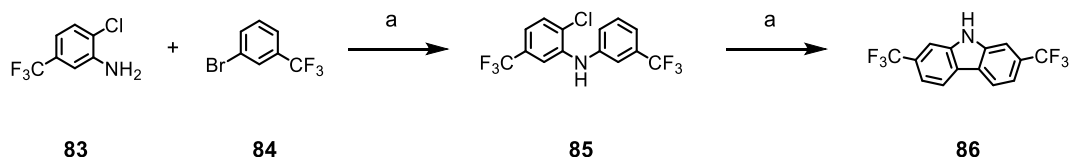
Scheme 18. Synthesis of carbazole **86**. Reaction conditions: a) Pd$_2$(dba)$_3$, *rac*-BINAP, NaO^{t}Bu, MePh, 90 °C, 12 h, 93 %; b) NaO^{t}Bu, [HPtBu$_3$][BF$_4$], Pd(OAc)$_2$, MePh, 160 °C (MW), 3 h, 81 %.

In case of the 2,7-trifluoromethylcarbazole **86**, the same procedure as for the synthesis of 1,8-dimethylcarbzole **66** was tested. The microwave assisted Buchwald-Hartwig amination followed by the intramolecular ring closure via C-H activation in an one-pot synthesis did not result in the desired product. Therefore, the strategy was changed to synthesize carbazole **86** in two steps. First, a classical Buchwald-Hartwig amination with Pd$_2$(dba)$_3$ and *rac*-BINAP as catalyst system in toluene was performed to obtain the secondary amine **85** from commercially available aniline **83** and 3-trifluoromethyl-1-bromobenzene (**84**). As second step, the same conditions as in the one-pot microwave protocol was chosen to close the carbazole via a palladium catalyzed C-H activation. This rout provides the desired carbazole **86** in a yield of 75 % over two steps in large quantities.

Synthesis of CBP Derivatives 61 - 63
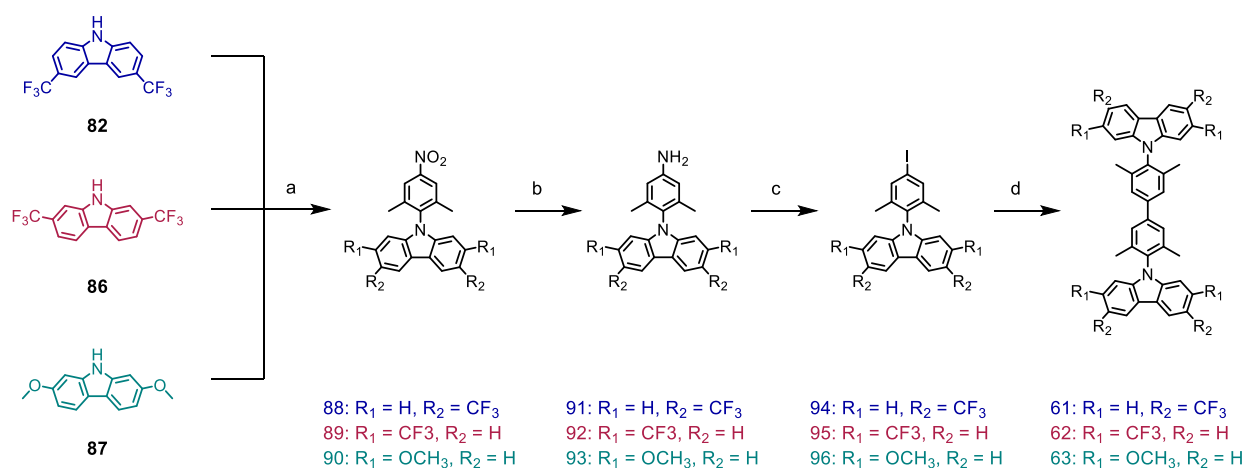
Scheme 19. Synthesis of target structures **61 - 63**. Reaction condition: a) 4-fluoro-3,5-dimethylnitrobenzene (**65**), Cs$_2$CO$_3$, DMF, 12 h, 150 °C, **88** (82 %), **89** (78 %), **90** (86 %); b) SnCl$_2$ · 2H$_2$O, EtOH, reflux, 4 h, **91** (92 %), **92** (93 %), **93** (97 %); c) BF$_3$ · Et$_2$O, ^{t}BuONO, DCM, KI, I$_2$, -10 °C - RT, 12 h, **94** (82 %), **95** (90 %); PTSA, NaNO$_2$, KI, MeCN, H$_2$O, 10 °C, 2 h, **96** (83 %); d) (i) Turbo Grignard, B(O^{i}Pr)$_3$, neopentyl glycol, THF, -10 °C to RT, 12 h; (ii) SPhos Pd G2, K$_3$PO$_4$, THF : H$_2$O (20:1), 60 °C, 12 h, **61** (95 %), **62** (93 %), **63** (97 %) over 2 steps.

Having both trifluoromethylated carbazole **82** and **86** in hand, the last remaining carbazole precursor **87** was synthesized using a protocol published by Bender and coworker[177] in two steps. Suzuki coupling of 1-bromo-2-nitro-4-methoxybenzene and (4-methoxyphenyl)boronic acid followed by a reductive ring-closing reaction promoted by triethylphosphite resulted in the desired carbazole **87**. For all three carbazoles, the reaction condition to achieve the desired target compounds **61** - **63** were kept as close as possible to the developed synthetic strategy of CBP derivative **60**. The S_NAr reaction of the carbazoles with the fluoroaryl **65** provided the 9-*para*-nitrophenylcarbazoles **88** - **90** in good yields in the range of 78 % - 86 %. Furthermore, the reduction of the nitro group to the amine provided the corresponding amines **91** - **93** in almost quantities yields. Subsequently, applying the same conditions for the Sandmeyer reaction as in the synthesis of iodoaryl **73**, the methoxy functionalized aniline **93** revealed no conversion to the corresponding 9-*para*-iodophenylcarbazole derivative **96**. Already the formation of the diazo-borontetrafluoride salt was not observable. A reasonable explanation is the interaction of the $BF_3 \cdot OEt_2$ with the methoxy groups, leading to a deprotection and formation of free phenol species. Alternative conditions using *p*TsOH and $NaNO_2$ in a mixture of water and acetonitrile provided iodoaryl **96** in good yield (83 %).[178] For both trifluoromethyl functionalized anilines **91** and **92**, respectively, the original condition were successfully applied. However, the oxidative homo coupling of iodine compounds **94** and **95** using the Turbo Grignard protocol weren't effective and resulted in poor yields. For the homo coupling of iodoaryl **96** the procedure showed no conversion to target compound **63**. To overcome this issue, the 9-*para*-iodophenylcarbazole derivatives **94** - **96** were first transformed to the corresponding boronic esters[179] and subsequently used for the following Suzuki-Miyaura cross-coupling with one equivalent of the iodoaryl precursor. The target CBP derivatives **61** - **63** were isolated in excellent yields of 93 %, 91 %, and 94 %, respectively.

Results and Discussion

Thermal Properties

In order to determine the thermal stability, differential scanning calorimetry (DSC) measurements of the five CBP derivatives **59** - **63** were performed. Measurements were recorded on a Perkin Elmer DSC Advanced Double-Furnace 8000 using scanning rates of 10 °C min^{-1}, and the glass transition temperature (T_g), crystallization temperature (T_c) and melting point (T_m) were obtained from the second heating scan. Crucial for the applying as a host material in OLEDs is, among others, the T_g value. Below the glass transition temperature, the solid consists of an amorphous state, whereas over the T_g the kinetic energy of the solid is large enough to rearrange to molecules, a so called semi-solid or super cooled liquid.[180] If this state occurs in an OLED, a diffusion of the neighboring layer molecules can occur and as consequence, the overall performance can be affected.[156] Many substances start to crystallize after heating over the T_g. Already at lower temperature formed crystalline embryos can start to grow, caused by the decreased viscosity.[180]   As a reference for our set up, DSC measurements of CBP were performed and compared to literature. Melting point, crystallization and glass transition temperature of CBP and all carbazoles **59** - **63** are summarized in **Table 8**. T_g and T_c do not have an exact thermodynamically defined transition temperature, but are rather occurring over an temperature interval. Therefore, the values are strongly depended of the determination method. Hence, our obtained values for CBP, even not fitting exactly the literature values, are in a good agreement. The improvement of the T_g value for derivative **60** compared to CBP is significant as the value is twice as high with 129 °C. However, for compound **59** no glass transition temperature could be determined, but the enhanced T_c and T_m values indicate a shifting in a comparable range. Compound **61** provided with 202 °C a very high T_g value, whereas compound **62** and **63** are in between with 158 °C and 184 °C, respectively. The increase of the T_g compared to CBP is explainable by the insertion of the methyl groups and the therefore almost perpendicular alignment between the carbazole and the biphenyl backbone. Having additional substituents on the carbazole increases the T_g further, independent of the electron donating or withdrawing effect. This endorses the supposed theory, that the sterically demanding groups disturbs the alignment of the molecules to form a consistent crystal structure. Furthermore, all compounds **59** - **63** showed increased crystallization temperatures. Whereas exceeding the T_g would influence the overall performance of the OLED, crystallization within a layer would lead to a break down. The high T_g and T_c values attest a high thermal stability to all five CBP derivatives and they fulfill the criteria as potential host material in OLEDs.

Table 8. Results of the DSC measurements.

Compound	Melting point, T_m [°C]	Crystallization temperature, T_c [°C]	Glass transition temperature, T_g [°C]
CBP	288; 283 lit.	196; 205 lit.	66; 62 lit.
59	351	246	-
60	293	236	129
61	348	289	202
62	314	199	158
63	299	196	184

Structural Properties

To analyze the effect of the sterically demanding methyl groups to the inter-plane twist angle, X-ray diffraction analysis were performed. Suitable crystals of compound **60**, **61** and **62** were obtained by the slow evaporation method, dissolving the compounds in a 1:1 mixture of dichloromethane and cyclohexane. For compounds **59** and **63**, no crystals were obtained to perform the analysis. Instead, the structure was calculated *in vacuo* with *Spartan´10* by density function theory (DFT) calculations using B3LYP hybrid functional theory with a 6-31G* basis set. Having in mind that the x-ray diffraction analysis considers the effects of intermolecular packing, whereas the calculations only notice the intramolecular repulsion. Nevertheless, we obtained a good idea about the spatial arrangement of the subunits. Of main interest were both inter-plane twist angles between the carbazole subunit and the biphenyl backbone, indicated in **figure 31** as α (between the red and the green plane) and β (between the grey and the blue plane).
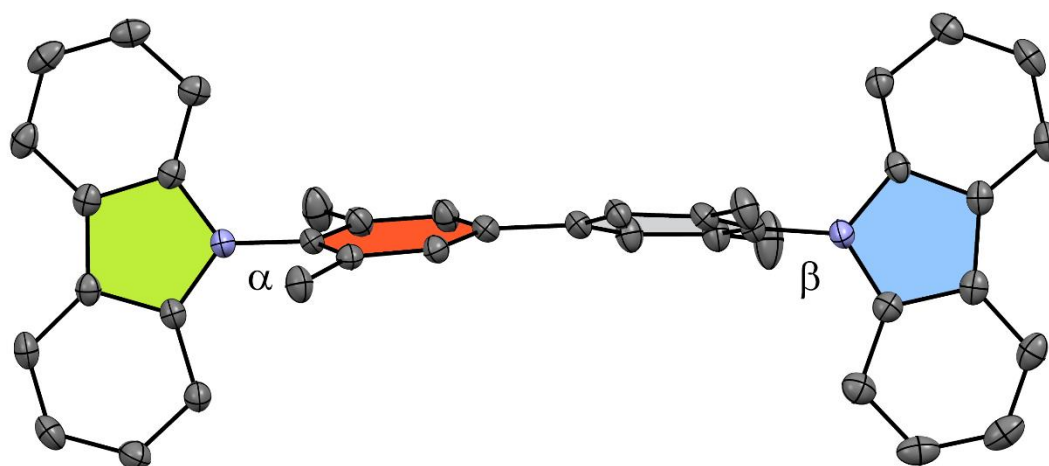
Figure 31. Crystal structure of compound **60**. The inter-plane angles α and β are of major interest to understand the amount of conjugation between the π-system of the carbazole and the biphenyl core.

Crystal system, space group, inter-plane twist angle and lattice parameter a, b and c of carbazole **59** - **63** are summarized in **table 9**. Compound **60**, with the methyl group attached to the biphenyl core, crystallizes in a non-standard monoclinic $P2_1/n$ space group. As a result, the two inter-plane angles differ from each other. Whereas α had an almost perpendicular arrangement of 85.1°, β was slightly less twisted with 75.8°. An almost homogeneity structure showed the DFT calculation of derivative **59** with 90.0° for α and 89.9° for β. The crystal structure of compound **61** with its centro-symmetric orthorhombic space group Fddd, giving for both inter-plane twist angles the same angle of 89.0°. Compound **62** showed slightly decreases inter-plane twists with 79.7° and 76.7°, respectively, and crystallized in the triclinic $P\bar{1}$ space group. All synthesized molecules have inter-plane twist angles above 75° resulting in a very limited conjugation of the π-systems. Having no overlapping of the electron clouds between the carbazoles and the biphenyl indicated a good charge separation after excitation and the original high triplet energy of the carbazoles is maintained.

Table 9. X-ray diffraction analyzing data or DFT calculation using B3LYP hybrid functional theory with a 6-31G* basis set.

Compound	Crystal system	Space group	Inter-plane twist angle(α/β)°	a [Å]	b [Å]	c [Å]
CBP	Monoclinic	P2$_1$/n	49.5/49.5[b]	8.0120(4)	16.0080(7)	10.2428(5)
59	-	-	90.0/89.9[a]	-	-	-
60	Monoclinic	P2$_1$/n	85.1/75.8[b] 82.8/80.1[a]	12.2971(7)	7.6414(5)	31.6860(19)
61	Orthorhombic	Fddd	89.0/89.0[b]	6.9076(3)	25.8233(11)	41.998(2)
62	Triclinic	P$\bar{1}$	79.7/76.7[b]	8.6414 (5)	9.2900(6)	23.1385(15)
63	-	-	90.0/89.5[a]	-	-	-

[a] Data obtained from DFT calculation. [b] Data obtained from x-ray diffraction analyzing.

Photophysical Properties

The absorption and luminescence spectra of compounds **59 - 63** were measured in diluted dichloromethane solution at room temperature. Measurements were recorded on a *Shimadzu* UV spectrometer UV-1800 and on a *Horiba Scientific* Fluoromax-4 spectrofluorometer. The UV-Vis and emission spectra are shown in **figure 32**. The obtained absorption maxima, molar extinction coefficient and further data are reported in **table 10**. As a reference for the discussion about the effects caused by the different substitutions, the absorption and emission spectra of CBP was measured. The region of interest is the absorption in the range of 290 nm to 340 nm. Three prominent bands were observed at 293 nm, 318 nm, and 340 nm. It is possible to assign the bands around 293 nm and 340 nm as ^1L_b (S_1-S_0) and ^1L_a (S_2-S_0) transitions, respectively.[181] Furthermore, the broad absorption around 318 nm can be attributed to a π-π* transition between the carbazole unit and the biphenyl core.[182] The fluorescence spectra of CBP shows a structureless near- ultraviolet emission around 376 nm. Considering the spectra of **59**, the absence of the broad absorption band around 318 nm is crucial. Whereas the carbazole assigned bands at 291 nm and 339 nm were observed, the missing of the band in between can be considered as an electronical separation of the carbazole and biphenyl π-systems.[153,159,183] As consequence, the insertion of the methyl groups in 1,8-position of the carbazole force the inter-plan angle in a perpendicular alignment and results in the loss of conjugation between the two subunits. The absorption spectra of derivative **60** showed the same effect and contained only the bands around 239 nm and 340 nm. In the emission spectra

compound **59** had a bathochromic shift of 40 nm compared to CBP, but the same structureless emission. The shift can be explained by the additional methyl group at the carbazole subunit. In contrast, the emission spectra of derivative **60** showed a hypsochromic shift of 31 nm and a well resolved emission, induced by the addition of the methyl groups at the biphenyl core. As result, the flexibility of the carbazole-biphenyl junction can be limited either by the attachment of the methyl groups in the 1,8-position or in *ortho* - position of the attached phenyl ring. In both cases, the conjugation of the two subunit and their π-system was prevented.
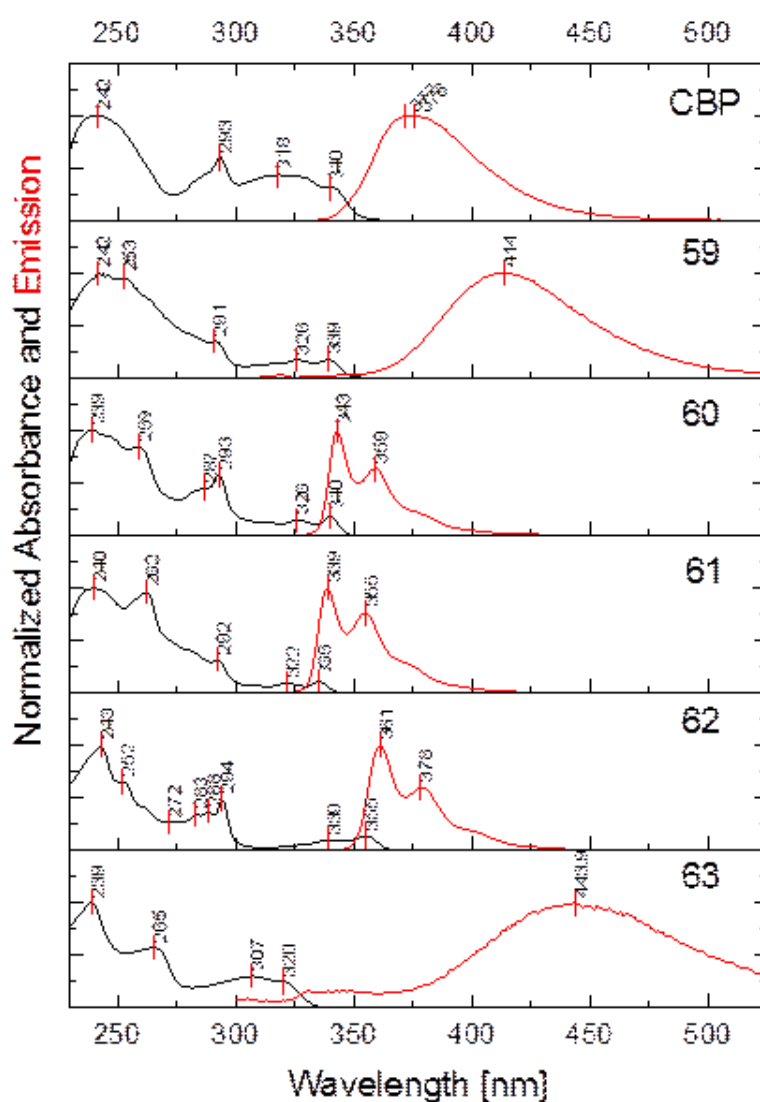
Figure 32. Absorption and luminescence spectra of compounds **59 - 63** and CBP as a reference.

Table 10. Photophysical data from UV-Vis, fluorescence and quantum yield measurements.

	$\lambda_{max, uv}$ [nm]	ε [L·mol^{-1}·cm^{-1}]	$\lambda_{onset, uv}$ [nm]	E_g [eV][a]	$\lambda_{max, emission}$ [nm]	QY [%]
CPB	293	45100	352	3.52	372	78.9
	318	32700				
	340	23800			376	
59	291	35900	348	3.56	414	8.5
	326	17500				
	339	18200				
60	293	44700	347	3.57	343	36.9
	326	11400				
	340	13900			359	
61	292	35300	342	3.63	339	2.6
	335	12000			355	
62	294	83200	364	3.41	361	15.4
	339	17100				
	355	23800			378	
63	265	61700	334	3.71	444	1.0
	307	32500				
	320	27200				

[a] $E_g = 1240 / \lambda_{onset}$

The methylation of the biphenyl is preferred in contrast to methylated carbazole species, since the substitution pattern of the carbazole is thus simplified. In our system, the insertion of the trifluoromethyl groups in 3,6-position for compound **61** and in 2,7-position for compound **62**, respectively. Derivative **61** showed a similar absorption spectrum as parent compound **60** with the two carbazole centered transitions (292 nm and 335 nm) and the significant decreased transition between the carbazole and the biphenyl. Furthermore, the emission spectra showed

only a minimal hypsochromic shift of 4 nm compared to **60**, but the same well resolved emission profile. More effects were visible in the spectra of derivative **62**. The absorption spectrum has an explicit bathochromic shift of the second carbazole centered transition, whereas the first remained at 294 nm. A similar red shift of almost 20 nm was noticeable in the emission spectra. However, the resolved structure persisted the same as seen for compound **60** and **61**, respectively.

The increased effect of the di-trifluoromethane substitution in 2,7-position compared to the 3,6-position might be explained with the higher conjugation over both -CF$_3$ substituents in derivative **61**. A study about connected polycarbazoles in either an 3,6- or 2,7-pattern has shown an extended conjugation in the poly-2,7-carbazole backbone.[184] For compound **63** the -CF$_3$ groups in 2,7-position were changed to two methoxy substituents. In the absorption spectrum, a significant blue shift of the two carbazole centered transition to 265 nm and 320 nm was observed. Furthermore, a broad emission band at 444 nm indicates for an intermolecular charge transfer (ICT) from the excited state centered on the 2,7-dimethoxycarbazole as donor to the biphenyl as acceptor.[185]

Additionally to the absorption and emission spectra, the fluorescence quantum yields (Φ_F) of CBP and all synthesized derivatives were measured. The measurements were performed using a Hamamatsu Quantaurus-QY integrated sphere fluorimeter and the results are reported in **table 10**. CBP has a fluorescence quantum yield of 79 %, whereas derivatives **59** and **60** only reached 9 % and 37 %, respectively. In addition, the -CF$_3$ derivatives **61** and **62** displayed low Φ_F values (15 % and 3 %) indicating an enhanced triplet yield.

As discussed above, one of the main specifications for new compounds used as host material in OLEDs, is a higher triplet energy than the blue phosphorescence light emitting dye **FIrpic,** with a triplet energy of ΔE (T$_1$−S$_0$) = 2.65 eV. Determining the triplet energy of a compound can be carried out by recording the phosphorescence emission spectra, whereas the wavelength of the highest energy peak ($\lambda_{max, phos}$) correlates to the energy of the T$_1$ → S$_0$ relaxation. Phosphorescence spectra were measured in 10^{-5} M aerated and frozen 2-methyltetrahydrofuran solutions at 77 K in gated steady state conditions of all target compounds and with CBP as a reference. The phosphorescence spectra, the data of $\lambda_{max, phos}$ and the calculated triplet energies are listed in **figure 33**. The triplet energy levels were calculated according to E$_T$ = 1240/$\lambda_{max, phos}$.

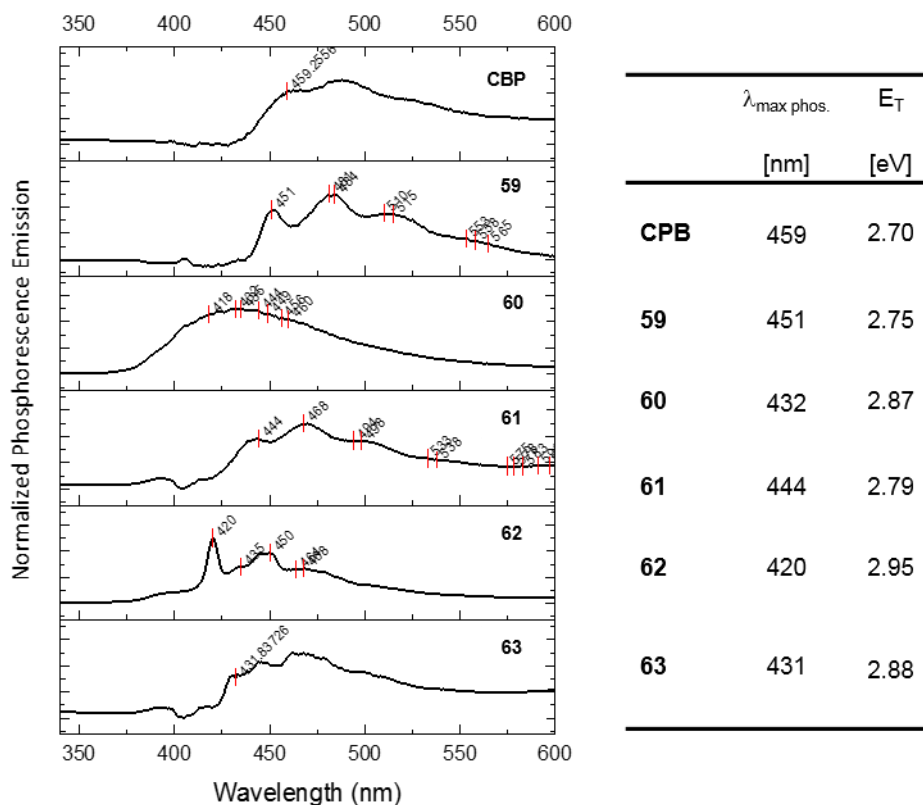|	$\lambda_{max\ phos.}$	E_T
	[nm]	[eV]
CPB	459	2.70
59	451	2.75
60	432	2.87
61	444	2.79
62	420	2.95
63	431	2.88

Figure 33. Phosphorescence emission spectra of compound **59** - **63** and CBP as a reference. The triplet energy was calculated according: ET = $1240/\lambda_{max,\ phos}$.

The observation of phosphorescence in steady state condition is difficult because the emission is usually orders of magnitude smaller than the fluorescence. In our experiment, the phosphorescence emission is coexisting with the fluorescence at 77 K as seen in the example of compound **60** in **figure 34**.

In combination with the decreased fluorescence emission quantum yield observed at room temperature, a clear increase of the triplet yield in both -CF_3 derivatives **61** and **62** was achieved. All new synthesized derivatives have a higher triplet energy compared to CBP in the range of 2.75 eV to 2.95 eV, confirming a decoupled π-system between the carbazoles and the biphenyl core. Comparing N-ethylcarbazole with its triplet energy of 3.1 eV[186] and biphenyl with 2.9 eV[187] as reference, we can conclude that the triplet energy of our compounds is mainly localized on the biphenyl core, due its lower triplet energy. A further evidence for this hypothesis is given as the substitution of the carbazole with -CF_3 groups doesn't affect the triplet energy in a significant manner. However, the hypsochromic shift of the phosphorescence and the resulted higher triplet energy makes these CBP derivatives interesting as host material for OLEDs.
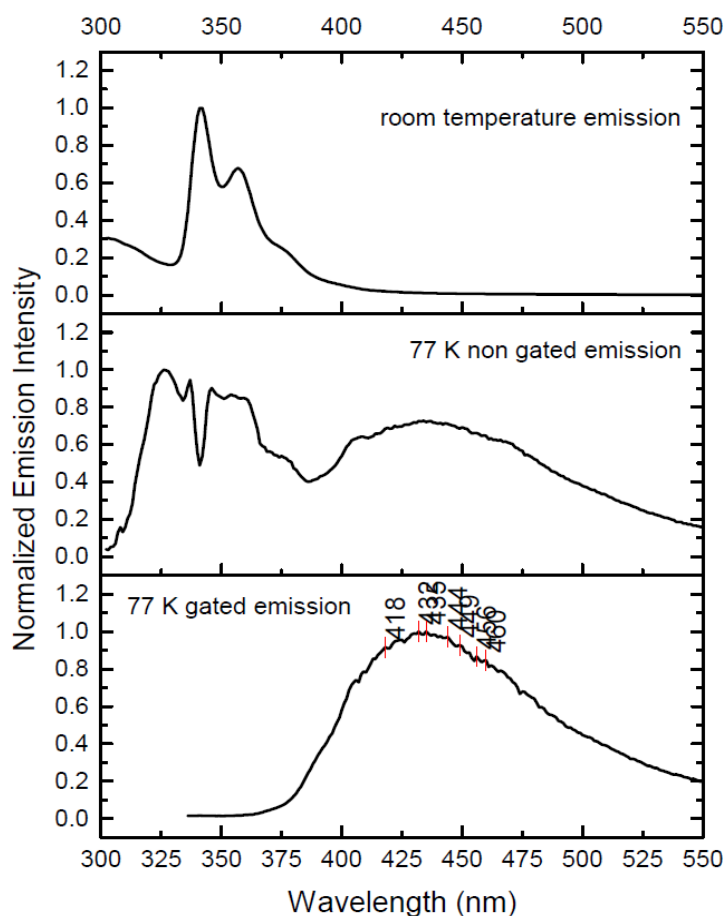
Figure 34. Comparison of gated vs. non gated phosphorescence emission spectra at 77 K of compound **60** 10^{-5} M in 2-MeTHF.

Electrochemical Properties

To study the electrochemical features from CBP derivatives **59** - **63**, cyclic voltammetry measurements were performed. The spectra were obtained from 10^{-3} M solutions in dichloromethane with a conventional three-electrode cell (Platinum working electrode, platinum wire counter electrode, and a saturated calomel reference electrode (SCE)). All compounds showed in the anodic scan an oxidation peak at about 1.5 V vs. *SCE* which is assigned to the oxidation of the carbazole unit. In addition, an irreversible oxidation behavior as shown for compound **60** in **figure 35** was observed.
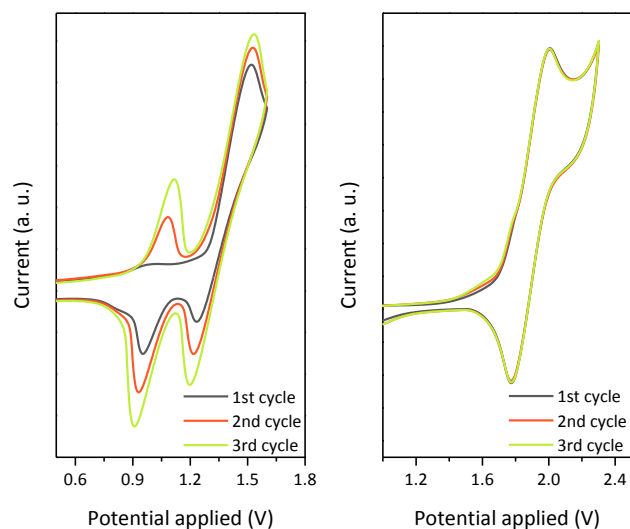
Figure 35. Cyclic voltammogram of compound **60** (left) and compound **61** (right). Three cycles with a scan rate of 100 mV/s were recorded against SCE.

It is known that after the oxidation, the radical cation is stabilized in 3,6-position of the carbazole subunit. This can lead to an undesired intermolecular oxidative coupling (**scheme 20**).[158,188]
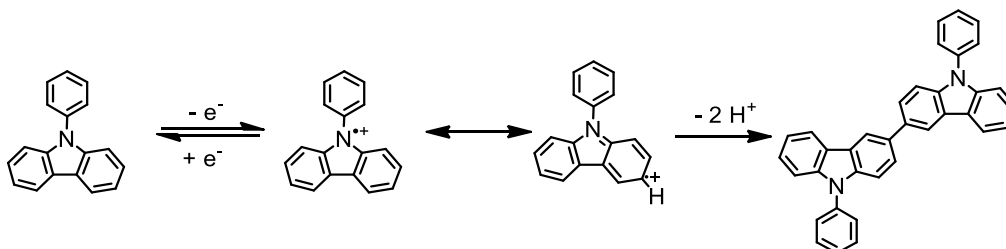
Scheme 20. Oxidation of N-phenylcarbazole followed by the stabilization of the radical cation in 3,6-position and the subsequent oxidative homocoupling.

In the cyclic voltammetry experiment, the dimerization can be observed as an irreversible oxidation. Additionally, the formation and cycle dependent increase, due to accumulation at the platinum electrode, of a new peak after the first cycle in the region of 1.05 V to 1.15 V is observed. Furthermore, in the back scan the well-defined reduction peak at 0.9 V to 1.0 V is observable, which is correlated to the reduction of the newly formed dimerization product. In the case of the 3,6-substituted derivative **61**, the cyclic voltammetry showed a reversible oxidation behavior, which can be attributed to the blocked reactive positions in the carbazole

subunit. For none of the compounds a reduction process was observed within the solvent window. The data is summarized in **table 11**.

Table 11. Data obtained from the CV experiment.

	E_{ox} vs. Fc$^+$/Fc	E_{HOMO}	E_{LUMO}
	[V]	[eV]	[eV]
CPB	0.87	-5.97	-2.45
59	0.80	-5.90	-2.34
60	0.92	-6.02	-2.45
61	1.37	-6.47	-2.85
62	1.36	-6.46	-3.05
63	0.56	-5.66	-1.95

HOMO LUMO Energy Levels

In vacuo calculations of the highest occupied molecular orbitals (HOMO) and the lowest unoccupied molecular orbital (LUMO) with *Spartan´10* using density function theory and a B3LYP 6-31G* basis set, showed a separate localization of both orbitals. The HOMO was localized on the carbazole unit whereas the LUMO is mainly centered on the biphenyl backbone. Such a charge separation provides a basis for a possible adjustment of the HOMO and LUMO independently, by functionalizing either the carbazole or biphenyl unit.
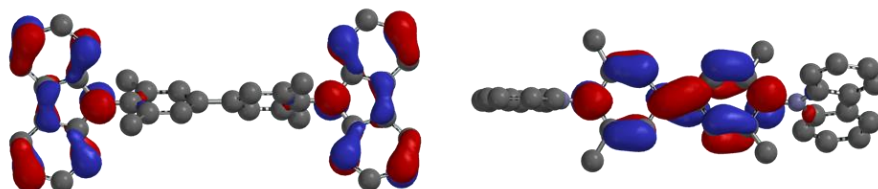

Figure 36. Calculated HOMO and LUMO of **60** using DFT and a B3LYP 6-31G* basis set.

As shown in the previous section, the oxidation potential was measured by DPV experiments. With the obtained data, the calculation of the HOMO energy levels of the synthesized

compounds was performed by their oxidation potentials after correction of the vacuum energy levels (5.1 eV)[189]. Furthermore the LUMO energy level were obtained by adding the optical band gap (E_g), obtained by absorption spectroscopy, to the HOMO level ($E_{LUMO} = E_{HOMO} + E_g$).
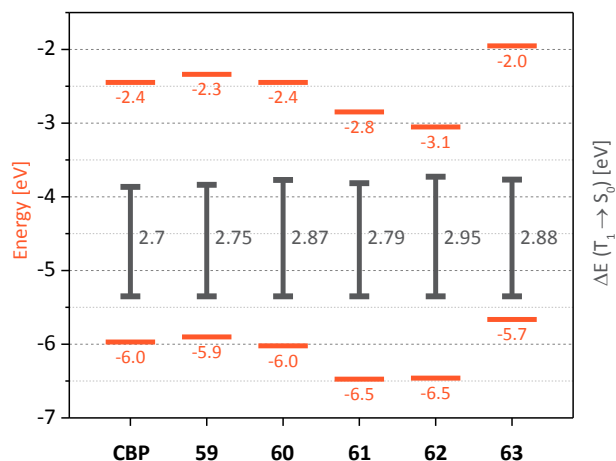

Figure 37. Energy diagram showing the position of the frontier orbitals of the CBP derivatives. The dark grey line displays the position of the triplet energies.

As shown in **figure 36**, the HOMO is located on the carbazole subunit. The functionalization with strong electron withdrawing or electron donating groups took place only on the carbazole. Therefore, the carbazole localized HOMOs are of particular interest. First, the effect of the four methyl groups either on the carbazole unite or on the biphenyl backbone are discussed, compared to CBP. Not surprisingly, the introduction of the methyl groups to the biphenyl core didn't have an effect on the carbazole localized HOMO. In contrast, the positive inductive electron donation effect (+I), by the added methyl groups in compound **59** to the carbazole unit, lead to a slight increase of the HOMO level. The same increase in energy was observed for the LUMO level in spite of the decoupled biphenyl and carbazole subunits. Regarding the -CF$_3$ functionalized compounds **61** and **62**, the expected decrease of the HOMO levels was observed with both substitution patterns. The -I-effect of the trifluoromethyl groups at the carbazole increased the oxidation potential by 450 mV and 440 mV, respectively, compared to compound **60**. Furthermore, the LUMO energy levels of both compounds showed a similar decreasing shift, questioning the proposed hypothesis of individual addressable energy levels of the frontier orbitals. The contrary effect was achieved by the introduction of the methoxy substituents in compound **63**. The positive mesomeric effect (+M) induced through resonance with the electron donating oxygen atom lead to a decreased oxidation potential by 360 mV and therefore, an increased HOMO energy level. Again, a similar shift of the LUMO energy level was observed.

As result of the electrochemistry studies, we can deduce several points. The fine tuning of the HOMO and LUMO levels of CBP derivatives is possible by varying the substituents at the carbazole unit, while the substitution pattern has minor effect. However, the independent addressing of either the HOMO or the LUMO energy level remains challenging. For a multilayer OLED architecture, these fine-tunings are crucial to maintain effective operation voltage. In addition, the functionalization of the 3,6-position of the carbazole units gives electrochemically stable compounds, which would be a certain advantage as radical ions are involved in charge transport within the device.

Conclusion and Future Prospects

Within this thesis five new 4,4'-dicarbazole-1,1'-biphenyl (CBP) derivatives have been successfully synthesized. All compounds have been fully characterized. The concept of decreasing the conjugation of the π-system within the molecule, by introducing sterical demanding methyl groups along the C-N bond, has been showed. The desired rotational restriction of the torsion angle was proofed by absorption and emission spectroscopy. The key step of the synthesis was the formation of the C-N bond and overcoming the sterical hindrance caused by the methyl groups. Using nucleophilic aromatic substitution reaction conditions to obtain the N-*para*-nitrophenyl-carbazole precursors, pushed the synthetic route in the right direction. The required nitro group to stabilize the Meisenheimer complex and therefore enable the nucleophilic attack, was at the same time the functionality for further transformation to the iodine dimerization precursor. Dimerization was achieved by either using oxidative homocoupling condition with Turbo Grignard substrates or Suzuki-Miyaura cross-coupling condition with the corresponding boronic ester derivatives. The structure of CBP derivatives **60**, **61** and **62** were corroborated by X-ray diffractometry, whereas for compounds **59** and **63** DFT calculations were performed. Interlocked torsion angles in a range of 80° to 90° resulted in an almost perpendicular alignment of the biphenyl core and the carbazole subunits. This alignment was further corroborated by the UV-Vis absorption measurements, showing a decreased π-π* transition band between the carbazole and the biphenyl in all compounds. Furthermore, the sterical more demanding configuration disturbed the alignment of the molecules to form a consistent crystal structure, obtaining higher transition glass temperatures and a higher overall thermal stability compared with parent compound CBP. The electrochemical properties revealed the possibility of fine tuning the frontier orbitals by introducing electron withdrawing or electron donating substituents to the carbazole subunit. However, an individual addressing of the HOMO or LUMO orbital remains challenging. Satisfyingly, the most relevant requirement, the triplet energy E_T, was increased within the whole series compared to CBP with a maximal value of 2.95 eV for compound **62**. Therefore an efficient energy transfer from the host to the light emitting dye is provided. Altogether, compounds **61** and **62** showed promising characteristics for the use as host materials in blue organic light emitting diodes.

To address either the HOMO or LUMO in a specific manner, to completely interlock the rotation around the C-N axis is promising. With sterically demanding groups, like the inserted methyl groups, a main orientation of the molecular structure is defined. However, the movement along the C-N axis is not completely prevented and depends on the temperature or energy, respectively. By bridging the carbazole via an alkyl linker to the biphenyl, a defined inter-plane angle depending on the linker length could be obtained. A rigid alkyl linker would prohibit the free movement and rotation around the C-N axis and therefore further decrease the π-

conjugation through the molecule. The obtained decreased communication of the biphenyl core with the carbazole unit could allow an individual adjustment of the HOMO and LUMO energy level by further functionalization.
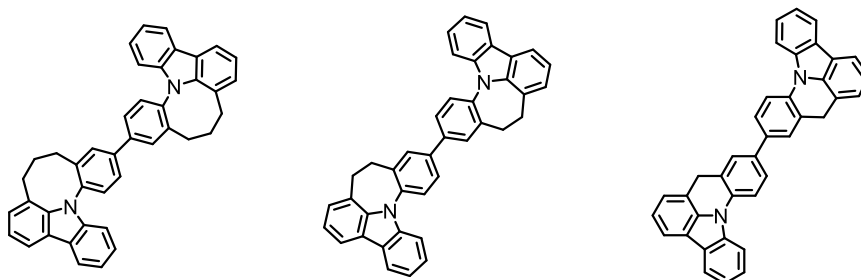

Figure 38. CBP derivatives with the carbazole moiety alky linked to the biphenyl core to prevent the rotation around the C-N axis and obtain a defined inter-plane angle.

Experimental Section

General Remarks

Reagent and Solvents: All chemical were used as received without any further purification unless explicitly stated otherwise. Dry Solvents were purchased from *Fluka* or *Accros*. NMR solvent were obtained from *Cambridge Isotope Laboratories, Inc.* (Andover, MA,USA).

^{1}H Nuclear Magnetic Resonance (NMR): Bruker DPX-NMR (400 MHz) instrument was used to record all spectra. All chemical shifts are reported relative to trimethylsilane (TMS) or the used solvent. The measurements were performed at room temperature. The multiplicities are written as: s = singlet, d = doublet, t = triplet , dd = doublet of doublets and m = multiplet.

^{13}C Nuclear Magnetic Resonance (NMR): Bruker DPX-NMR (101 MHz) instrument was used to record all spectra. All chemical shifts are reported relative to the used solvent. The measurements were performed at room temperature.

GC/MS: For GC/MS analysis a *Shimadzu* GCMS-QP2010 SE gas chromatograph system, with a Zebron 5 MS Inferno column (30 m x 0.25 mm x 0.25 mm), at 1 mL/min He-flow rate (split = 20:1) with a *Shimadzu* mass detector (EI 70 eV) was used.

Mass spectroscopy (MS): MALDI-TOF analyses were performed on a Burker microflex system.

High-resolution mass spectra (HRMS): HR-ESI-ToF-MS were measured with a Maxis 4G instrument from Bruker with the addition of NaOAc.

Column Chromatography: For column chromatography SiliaFlash® P60 from *SILICYCLE* was used with a particle size of 40-63 µm (230-400 mesh), , and TLC was performed on silica gel 60 F254 glass plates with a thickness of 0.25 mm purchased from Merck.

UV-Vis Spectroscopy: The UV-Vis spectra were recorded on a *Shimadzu* UV spectrometer UV-1800 at room temperature.

Emission Spectroscopy: Emission spectra were recorded on a Horiba Jobin-Yvon FluoroMax 4 fluorimeter. Gated emission spectra were recorded in frozen 2-MeTHF solution at 77 K, with a flash delay of 0.05 ms, a sample window of 60 ms and a time per flash of 70 ms. The flash count was set to 20 to increase S/N.

Electrochemistry: The electrochemical measurements were performed with an AutoLab PGSTAT302 potentiostat-galvanostat controlled by resident NOVA 9.1 software using a conventional single-compartment three-electrode cell. A Pt disk of 2 mm ø served as working electrode, as auxiliary a Pt wire was used and the reference electrode was a saturated potassium chloride calomel electrode (SCE). The supporting electrolyte was 0.15 N Bu$_4$NPF$_6$

in dichloromethane. All potentials are quoted relative to SCE with ferrocene/ferrocenium at + 450 mV as internal standard. In all the experiments the scan rate was 100 mV/s for cyclic voltammetry and the pulse frequency was 15 Hz for differential pulse voltammetry (DPV).

Synthetic Procedures

N-(2-Chloro-4-(trifluoromethyl)phenyl)acetamide (79)
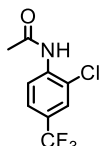
4-Amino-3-chlorobenzotrifluoride (1.00 g, 5.11 mmol, 1.0 eq.) was dissolved in dry DCM (40 mL) in an oven dried argon flushed Schlenk flask. Triethylamine (0.8 ml, 5.62 mmol, 1.1 eq.) was added at room temperature followed by dropwise addition of acetyl chloride (0.41 ml, 5.62 mmol, 1.1 eq.). The yellow solution was stirred for 2 h at room temperature. The reaction was quenched by adding water (100 ml) and DCM (100 ml). The mixture was extracted with dichloromethane (3 x 100ml) and the combined organic layers were washed with brine, dried over $MgSO_4$ and solvent was removed. The crude product was purified by column chromatography (SiO_2, cyclohexane / ethyl acetate, 5:1 – 2:1 gradient). N-(2-Chloro-4-(trifluoromethyl)phenyl)acetamide (**79**, 1.13 g, 4.76 mmol, 93 %) was obtained as white solid.

^{1}H-NMR (CDCl$_3$, 400 MHz) δ (ppm): 8.57 (d, $^3J_{H.H}$ = 8.7 Hz, 1H), 7.74 (s, 1H), 7.64 (d, $^4J_{H.H}$ = 1.7 Hz, 1H), 7.52 (dd, $^3J_{H.H}$ = 8.7 Hz, $^4J_{H.H}$ = 1.7 Hz, 1H), 2.28 (s, 3H).

^{13}C-NMR (CDCl$_3$, 101 MHz) δ (ppm): 168.5, 137.8, 126.5 (q, $^2J_{F,H}$ = 33.5 Hz, 1C), 126.3 (q, $^3J_{F,H}$ = 4.1 Hz, 1C), 125.1 (q, $^3J_{F,H}$ = 3.7 Hz, 1C), 123.4 (q, $^1J_{F,H}$ = 272.0 Hz, 1C), 122.3, 121.2, 25.0.

^{19}F-NMR (CDCl$_3$, 377 MHz) δ (ppm): -62.4.

MS (EI, 70 eV): m/z (%) = 237 (10), 202 (27), 197 (33), 195 (100), 176 (19), 145 (24).

HRMS (ESI): m/z calcd for [C$_9$H$_7$ClF$_3$NO+H]$^+$ 238.0241; found: 238.0238.

N-(3',5-Bis(trifluoromethyl)-[1,1'-biphenyl]-2-yl)acetamide (80)
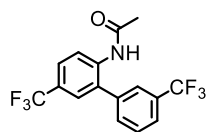
3-(Trifluoromethyl)phenylboronic acid (4.00 g, 21.0 mmol, 2.0 eq.) was added to a solution of *N*-(2-chloro-4-(trifluoromethyl)phenyl)acetamide (**79**, 2.50 g, 10.5 mmol, 1.0 eq.) in a mixture of THF (20 mL) and water (1 mL). To the clear solution K_3PO_4 (4.84 g, 21.0 mmol, 2.0 eq.) was added and degassed for 15min. with argon. SPhos Pd G2 (151 mg, 0.21 mmol, 0.02 eq.) was added and the resulting green suspension was stirred at 80 °C for 12 h. The reaction mixture was cooled to room temperature, *t*BME (50 mL) was added and reaction mixture was filtered over a celite pad. The mixture was extracted with ethyl acetate (3 x 100ml), washed with water (1 x 100ml) and brine (1 x 100ml). The combined organic layers were dried over $MgSO_4$ and the solvent was removed under reduced pressure. The crude product was further purified by column chromatography (SiO_2, cyclohexane / ethyl acetate 2:1 - 1:2 gradient) providing N-(3',5-bis(trifluoromethyl)-[1,1'-biphenyl]-2-yl)acetamide (**80**, 3.30 g, 9.50 mmol, 91 %) as a white solid.

¹H-NMR (CDCl₃, 400 MHz) δ (ppm): 8.45 (d, $^3J_{H,H}$ = 8.6 Hz, 1H), 7.76 - 7.74 (m, 1H), 7.68 - 7.65 (m, 3H), 7.61 - 7.58 (m, 1H), 7.50 - 7.49 (m, 1H), 7.06 (s, 1H), 2.06 (s, 3H).

¹³C-NMR (CDCl₃, 101 MHz) δ (ppm): 168.5, 137.9, 137.8, 132.7, 132.1 (q, $^2J_{F,H}$ = 32.8 Hz, 1C), 130.8, 130.2, 137.76, 127.2 (q, $^3J_{F,H}$ = 3.8 Hz, 1C), 126.7 (q, $^2J_{F,H}$ = 32.2 Hz, 1C), 126.4 (q, $^3J_{F,H}$ = 3.7 Hz, 1C), 126.2 (q, $^3J_{F,H}$ = 3.6 Hz, 1C), 125.7 (q, $^3J_{F,H}$ = 3.8 Hz, 1C), 124.0 (q, $^1J_{F,H}$ = 271.7 Hz, 1C), 123.8 (q, $^1J_{F,H}$ = 272.7 Hz, 1C), 122.1, 24.7.

¹⁹F-NMR (CDCl₃, 377 MHz) δ (ppm): -62.2, -67.7.

MS (EI, 70 eV): m/z (%) = 347 (26), 306 (16), 305 (100), 284 (39), 235 (32), 216 (21).

HRMS (ESI): m/z calcd for $[C_{16}H_{11}F_6NO+H]^+$ 348.0818; found: 348.0817.

3,6-Bis(trifluoromethyl)-9-acetylcarbazole (81)
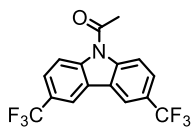
N-(3',5-Bis(trifluoromethyl)-[1,1'-biphenyl]-2-yl)acetamide (**80**, 1.00 g, 2.88 mmol, 1.0 eq.) was added to an oven dried Schlenk flask, followed by finely powdered activated molecular sieve (3Å) and Pd(OAc)$_2$ (12.9 mg, 0.058 mmol, 0.02 eq.). The flask was evacuated and flushed with argon followed by the addition of dry Cu(OAc)$_2$ (106 mg, 0.058mmol, 0.02 eq.). The mixture was suspended in toluene (20 mL). Argon atmosphere was changed into oxygen by applying vacuum and flashing by oxygen using an oxygen filled balloon. This sequence was repeated three times and reaction mixture was lowered in an oil bath and stirred at 120 °C. Every 6 hours, Pd(OAc)$_2$ (12.9 mg, 0.058 mmol, 0.02 eq.) was added until full conversion by TLC was observed. Afterwards the reaction mixture was cooled to room temperature and filtered over a celite pad and diluted with water (100 mL) and ethyl acetate (100 mL). The mixture was extracted with ethyl acetate (2 x 100 mL), washed with brine (1 x 100 mL) and the combined organic layers were dried over MgSO$_4$. The solvent was removed and the crude product was purified by column chromatography (SiO$_2$, cyclohexane / ethyl acetate 5:1) afforded 3,6-bis(trifluoromethyl)-9-acetylcarbazole (**81**, 975 mg, 2.82 mmol, 98 %) as a white solid.

^{1}H-NMR (CDCl$_3$, 400 MHz) *δ* (ppm): 8.36 (d, $^3J_{H,H}$ = 8.9 Hz, 2H), 8.24 (d, $^4J_{H,H}$ = 1.5 Hz, 2H), 7.81 (dd, $^3J_{H,H}$ = 8.9, $^4J_{H,H}$ = 1.5 Hz, 2H), 2.96 (s, 3H).

^{13}C-NMR (CDCl$_3$, 101 MHz) *δ* (ppm): 169.9, 140.9, 126.47 (q, $^2J_{F,H}$ = 33.0 Hz, 1C), 125.44, 125.07 (q, $^2J_{F,H}$ = 3.6 Hz, 1C), 124.19 (q, $^1J_{F,H}$ = 272.0 Hz, 1C), 117.55 (q, $^3J_{F,H}$ = 3.9 Hz, 1C), 116.7, 27.9.

^{19}F-NMR (CDCl$_3$, 377 MHz) *δ* (ppm): -61.5

MS (EI, 70 eV): m/z (%) = 345 (18), 304 (15), 303 (100), 284 (17).

EA: calcd for C$_{16}$H$_9$F$_6$NO: C 55.66, H 2.63 N 4.06; found: C 55.64, H 2.95, N 4.42.

3,6-Bis(trifluoromethyl)-9*H*-carbazole (82)
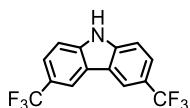
A stock solution was prepared by adding methanol (1 mL) dropwise to a cooled solution of concentrated sulfuric acid (5 mL). 3,6-Bis(trifluoromethyl)-9-acetylcarbazole (**81**, 50 mg, 0.145 mmol, 1eq.) was suspended in 3 ml of the stock solution in a one necked round bottom flask. Resulting suspension was stirred under air at 60 °C for one hour. Sat. aq. Na_2CO_3 solution (20 ml) was added carefully and the product was extracted with methylene chloride (2 x 20 ml). The combined organic layers were washed with brine (1 x 10 ml), dried over $MgSO_4$ and solvent was removed at reduced pressure. Further purification by column chromatography (SiO_2, cyclohexane / ethyl acetate 1:5) yielded 3,6-bis(trifluoromethyl)-9H-carbazole (**82**, 43 mg, 0.142 mmol, 98 %) as white crystalline solid.

^{1}H-NMR (CDCl$_3$, 400 MHz) $δ$ (ppm): 8.42 (s, 1H), 8.37 (d, $^4J_{H,H}$ = 1.9 Hz, 2H), 7.72 (dd, $^3J_{H,H}$ = 8.5, $^4J_{H,H}$ = 1.9 Hz, 2H), 7.53 (d, $^3J_{H,H}$ = 8.5 Hz, 2H).

^{13}C-NMR (CDCl$_3$, 101 MHz) $δ$ (ppm): 141.5, 125.1 (q, $^1J_{F,H}$ = 271.4 Hz, 2C), 123.8 (q, $^3J_{F,H}$ = 3.5 Hz, 2C), 122.9 (q, $^2J_{F,H}$ = 32.5 Hz, 2C), 122.7, 118.4 (q, $^3J_{F,H}$ = 4.2 Hz, 2C)

^{19}F-NMR (CDCl$_3$, 377 MHz) $δ$ (ppm): -60.5

MS (EI, 70 eV): m/z (%) = 304 (16), 303 (100), 302 (11), 284 (33), 253 (20), 234 (13).

HRMS (ESI): m/z calcd for [$C_{14}H_7F_6N$-H]$^-$ 302.0410; found: 302.0412.

2-Chloro-5-(trifluoromethyl)-*N*-(3-(trifluoromethyl)phenyl)aniline (85)
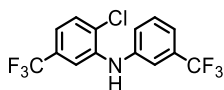
Pd$_2$(dba)$_3$ · CHCl$_3$ (228 mg, 0.220 mmol, 0.01 eq.) and BINAP (419 mg, 0.660 mmol 0.03 eq.), were placed in an oven dried argon flushed Schlenk flask. Degassed toluene (60 mL) was added under counter flow of argon and resulting solution was stirred for 15 minutes. 3-Bromobenzotrifluoride (3.1 ml, 22.0 mmol, 1.0 eq.), followed by NaO^{t}Bu (3.05 g, 30.8 mmol, 1.4 eq.) were added and stirring at room temperature was continued for 30 min. Afterwards, 2-chloro-5-(trifluoromethyl)aniline (3.7 ml, 26.4 mmol, 1.2 eq.) was added dropwise and the Schlenk flask was heated in an oil bath at 90 °C for 12 h. After cooling to room temperature, the reaction mixture was diluted with ^{t}BME (100ml) and filtered over a celite pad. The solution was concentrated under reduced pressure and the crude product was taken up in petroleum ether (75 ml), dried over MgSO$_4$ and filtered over a silica pad affording (**85**, 6.90 g, 20.3 mmol, 92 %) as yellow oil.

^{1}H-NMR (CDCl$_3$, 400 MHz) δ (ppm): 7.51 - 7.45 (m, 3H), 7.40 - 7.39 (m, 1H), 7.37 - 7.34 (m, 2H), 7.12 - 7.39 (m, 1H), 6.31 (s, 1H).

^{13}C-NMR (CDCl$_3$, 101 MHz) δ (ppm): 141.3, 140.2, 132.5 (q, $^2J_{F,H}$ = 32.5 Hz, 1C), 130.6, 130.4, 130.4 (q, $^2J_{F,H}$ = 34.7 Hz, 1C), 125.2, 123.9 (q, $^1J_{F,H}$ = 272.5 Hz, 1C), 123.8 (q, $^1J_{F,H}$ = 272.4 Hz, 1C), 123.3, 120.2 (q, $^3J_{F,H}$ = 3.8 Hz, 1C), 117.7 (q, $^3J_{F,H}$ = 3.9 Hz, 1C), 117.3 (q, $^3J_{F,H}$ = 3.8 Hz, 1C), 112.1 (q, $^3J_{F,H}$ = 3.9 Hz, 1C).

^{19}F-NMR (CDCl$_3$, 377 MHz) δ (ppm): -62.9, -63.0

MS (EI, 70 eV): m/z (%) = 341 (33), 340 (17), 339 (100), 320 (14), 304 (16), 303 (10), 285 (13), 284 (78), 236 (10), 235 (72), 75 (12), 69 (15).

HRMS (ESI): m/z calcd for [C$_{14}$H$_7$F$_6$N-H]$^-$ 338.0177; found: 338.0177.

2,7-Bis(trifluoromethyl)-9*H*-carbazole (86)
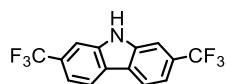
5-(Trifluoromethyl)-*N*-(3-(trifluoromethyl)phenyl)aniline (**85**, 1.00 g, 2.94 mmol, 1.0 eq.), Pd(OAc)$_2$ (66 mg, 0.294 mmol, 0.1 eq.), (^{t}Bu)$_3$PH · BF$_4$ (70.3 mg, 0.235 mmol, 0.08 eq.) and NaO^{t}Bu (728 mg, 7.35 mmol, 2.5 eq.) were placed in an oven dried argon flushed micro wave vial. Three vacuum/argon cycles were performed before the compounds were suspended in degassed toluene (20 mL). Microwave vial was sealed and heated in the microwave for 3 h at 160 °C. After the vial was cooled to room temperature, aq. hydrochloric acid (1M, 20ml) was added and product was extracted with ethyl acetate (2 x 50 ml). The combined organic layers were dried over MgSO$_4$ and after the solvent was removed. The crude product was purified by column chromatography (SiO$_2$, cyclohexane / toluene 2:1) providing 2,7-bis(trifluoromethyl)-9H-carbazole (**86**, 723 mg, 2.38 mmol, 81 %) as white crystalline solid.

¹H-NMR (CDCl$_3$, 400 MHz) *δ* (ppm): 8.38 (s, 1H), 8.20 – 8.18 (m, 2H), 7.76 – 7.75 (m, 2H), 7.55 – 7.53 (m, 2H).

¹³C-NMR (CDCl$_3$, 101 MHz) *δ* (ppm): 139.5, 129.15 (q, $^2J_{F,H}$ = 32.2 Hz, 2C), 125.1, 124.7 (q, $^1J_{F,H}$ = 272.1 Hz, 2C), 121.5, 117.1 (q, $^3J_{F,H}$ = 3.7 Hz, 2C), 108.5 (q, $^3J_{F,H}$ = 4.3 Hz, 2C).
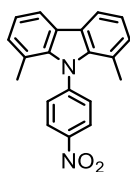
¹⁹F-NMR (CDCl$_3$, 377 MHz) *δ* (ppm): -61.3

MS (EI, 70 eV): m/z (%) = 304 (17), 303 (100), 284 (21), 234 (12).

HRMS (ESI): m/z calcd for [C$_{14}$H$_7$F$_6$N -H]$^-$ 302.0410; found: 338.0412.

Representative procedure of aromatic nucleophilic substitution (68 - 69, 88 - 90)

1,8-Dimethyl-9-(4-nitrophenyl)carbazole (68)

Under argon atmosphere 1,8 - dimethylcarbazole (**66**, 400 mg, 2.05 mmol, 1.0 eq.) was added to a two necked round bottom flask equipped with a reflux condenser. Addition of cesium carbonate (3.36 g, 10.3 mmol, 5.0 eq.) followed by DMF (21 ml) resulted in a suspension, which was stirred for 30 min. at room temperature. Afterwards, 4-fluoronitrobenzene (694 mg, 4.09 mmol, 2.0 eq.) was poured in all in once and reaction mixture was stirred at 155 °C for 12 hours. The black mixture was diluted with water and the crude product was extracted with ethyl acetate (3 x 50 ml). The combined organic layers were dried over $MgSO_4$ and solvent was removed under vacuum. The crude product was purified by column chromatography (SiO_2, cyclohexane / ethyl acetate 10:1). 1,8-Dimethyl-9-(4-nitrophenyl)carbazole (**68**, 557 mg, 1.76 mmol, 86 %) was isolated as yellow solid.

^{1}H-NMR (CDCl$_3$, 400 MHz) δ (ppm): 8.33 (d, $^3J_{H,H}$ = 8.8 Hz, 2H), 7.99 (d, $^3J_{H,H}$ = 7.6 Hz, 2H), 7.66 (d, $^3J_{H,H}$ = 8.8 Hz, 2H), 7.19 (dd, $^3J_{H,H}$ = 7.5 Hz, $^3J_{H,H}$ = 7.5 Hz, 2H), 7.11 (d, $^3J_{H,H}$ = 7.2 Hz, 2H), 1.89 (s, 6H).

^{13}C-NMR (CDCl$_3$, 101 MHz) δ (ppm): 148.6, 147.8, 140.6, 132.3, 129.3, 124.5, 123.6, 121.2, 120.7, 118.3.

MS (EI, 70 eV): m/z (%) = 316 (100), 270 (30).

EA: calcd for $C_{20}H_{16}N_2O_2$: C 75.93, H 5.10 N 8.86; found: C 76.42, H 5.39, N 9.30.

9-(2,6-Dimethyl-4-nitrophenyl)carbazole (69)
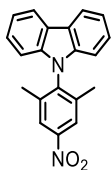
Carbazole (138 mg, 0.786 mmol, 1.0 eq.) yielded 9-(2,6-dimethyl-4-nitrophenyl)carbazole (**69**, 217 mg, 0.686 mmol, 87 %) after column chromatography (SiO$_2$, cyclohexane / ethyl acetate, 10:1).

^{1}H-NMR (CDCl$_3$, 400 MHz) δ (ppm): 8.19 (d, $^3J_{H,H}$ = 7.7 Hz, 2H), 8.17 (s, 2H), 7.41 (dd, $^3J_{H,H}$ = 7.7 Hz, $^3J_{H,H}$ = 7.7 Hz, 2H), 7.32 (dd, $^3J_{H,H}$ = 7.8 Hz, $^3J_{H,H}$ = 7.8 Hz, 2H), 6.89 (d, $^3J_{H,H}$ = 8.1 Hz, 2H), 1.99 (s, 6H).

^{13}C-NMR (CDCl$_3$, 101 MHz) δ (ppm): 147.6, 140.8, 140.4, 139.5, 126.4, 123.6, 123.3, 120.7, 120.2, 109.1

MS (EI, 70 eV): m/z (%) = 316 (100), 255 (38).

EA: calcd for C$_{20}$H$_{16}$N$_2$O$_2$: C 75.93, H 5.10 N 8.86; found: C 75.82, H 5.28, N 9.23.

3,6-Bis(trifluoromethyl)-9-(2,6-dimethyl-4-nitrophenyl)carbazole (88)
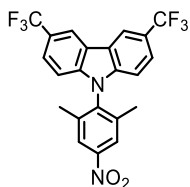
3,6-Bis(trifluoromethyl)-9*H*-carbazole (**82**, 418 mg, 1.38 mmol, 1.0 eq.) yielded 3,6-bis(trifluoromethyl)-9-(2,6-dimethyl-4-nitrophenyl)carbazole (**88**, 512 mg, 1.13 mmol, 82 %) as yellow solid after purification by column chromatography (SiO$_2$, cyclohexane / ethyl acetate 10 : 1).

^{1}H-NMR (CDCl$_3$, 400 MHz) δ (ppm): 8.52 (s, 2H), 8.21 (s, 2H), 7.72 (d, $^3J_{H,H}$ = 8.6 Hz, 2H), 7.02 (d, $^3J_{H,H}$ = 8.6 Hz, 2H), 1.98 (s, 6H).

13C-NMR (CDCl$_3$, 101 MHz) δ (ppm): 148.3, 141.8, 140.3, 139.2, 124.8 (q, $^1J_{F,C}$ = 271.8 Hz, 2C), 124.5 (q, $^3J_{F,C}$ = 3.5 Hz, 2C), 124.1, 123.8 (q, $^2J_{F,C}$ = 32.3 Hz, 2C), 122.7 , 119.0 (q, $^3J_{F,C}$ = 4.0 Hz, 2C), 109.9, 18.0.

19F-NMR (CDCl$_3$, 377 MHz) δ (ppm): -60.5.

MS (EI, 70 eV): m/z (%) = 453 (24), 452 (100), 391 (25), 390 (16), 337 (22), 336 (25).

EA: calcd for C$_{22}$H$_{14}$F$_6$N$_2$O$_2$: C 58.41, H 3.12 N 6.19; found: C 58.08, H 3.74, N 6.64.

2,7-Bis(trifluoromethyl)-9-(2,6-dimethyl-4-nitrophenyl)carbazole (89)

2,7-Bis(trifluoromethyl)-9*H*-carbazole (**86**, 418 mg, 1.38 mmol, 1.0 eq.) yielded 2,7-bis(trifluoromethyl)-9-(2,6-dimethyl-4-nitrophenyl)carbazole (**89**, 488 mg, 1.08 mmol, 78 %) as light yellow solid after column chromatography (SiO$_2$, cyclohexane / toluene, 1:1).
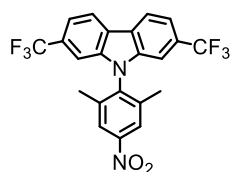
1H-NMR (CDCl$_3$, 400 MHz) δ (ppm): 8.36 - 8.34 (m, 2H), 8.25 - 8.24 (m, 2H), 7.66 - 7.63 (m, 2H), 7.21 - 7.20 (m, 2H), 2.00 (s, 6H).

13C-NMR (CDCl$_3$, 101 MHz) δ (ppm): 148.4, 140.3, 140.0, 139.0, 129.9 (q, $^2J_{F,C}$ = 32.4 Hz, 2C), 125.0, 124.5 (q, $^1J_{F,C}$ = 272.5 Hz, 2C), 124.3, 122.1, 117.9 (q, $^3J_{F,C}$ = 3.6 Hz, 2C), 106.8 (q, $^3J_{F,C}$ = 4.3 Hz, 2C), 18.0.

19F-NMR (CDCl$_3$, 377 MHz) δ (ppm): -61.2.

MS (EI, 70 eV): m/z (%) = 453 (25), 452 (100), 391 (19), 390 (19), 337 (23), 336 (21).

EA: calcd for C$_{22}$H$_{14}$F$_6$N$_2$O$_2$: C 58.41, H 3.12 N 6.19; found: C 58.04, H 3.67, N 6.41.

2,7-Dimethoxy-9-(2,6-dimethyl-4-nitrophenyl)carbazole (90)
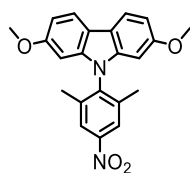
2,7-Dimethoxy-9*H*-carbazole (**87**, 537 mg, 2.36 mmol, 1.0 eq.), yielding 2,7-dimethoxy-9-(2,6-dimethyl-4-nitrophenyl)carbazole (**90**, 761 mg, 2.02 mmol, 86 %) as yellow solid after purification by column chromatography (SiO$_2$, cyclohexane / ethyl acetate 10:1).

^{1}H-NMR (CDCl$_3$, 400 MHz) δ (ppm): 8.18 (s, 2H), 7.93 (d, $^3J_{H,H}$ = 8.5 Hz, 2H), 6.89 (dd, $^3J_{H,H}$ = 8.5, $^4J_{H,H}$ = 2.3 Hz, 2H), 6.28 (d, $^4J_{H,H}$ = 2.2 Hz, 2H), 3.79 (s, 6H), 2.02 (s, 6H)

^{13}C-NMR (CDCl$_3$, 101 MHz) δ (ppm): 158.9, 147.8, 141.1, 140.8, 140.5, 123.9, 120.7, 117.5, 108.4, 93.7, 77.2, 55.9, 18.1

MS (EI, 70 eV): m/z (%) = 377 (24), 376 (100), 361 (39), 315 (10), 121 (11).

HRMS (ESI): m/z calcd for [C$_{22}$H$_{20}$N$_2$O$_4$+H]$^+$ 377.1496; found: 377.1490.

Representative procedure of the reduction (70 - 71, 91 - 93)

4-(1,8-Dimethylcarbazole)aniline (70)

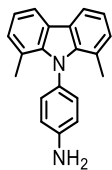1,8-Dimethyl-9-(4-nitrophenyl)carbazole (**68**, 633 mg, 2.00 mmol, 1.0 eq.) and $SnCl_2 \cdot 2H_2O$ (1.69 g, 7.50 mmol, 3.75 eq.) were suspended in ethanol (10 mL). The suspension was stirred at 80 °C for 4 h. Ethanol was removed under reduced pressure. The crude product was taken up in toluene (50 ml) and basified with aq. sodium hydroxide solution (5 M, 30 mL). The organic layer was dried over $MgSO_4$ and filtrate was concentrated in vacuum. The crude product was purified by column chromatography (SiO_2, cyclohexane / toluene 1:1) affording 4-(1,8-dimethylcarbazole)aniline (**70**, 521 mg, 1.82 mmol, 91 %) as slightly orange crystals.

^{1}H-NMR (CDCl$_3$, 400 MHz) δ (ppm): 7.98 (d, $^3J_{H,H}$ = 7.4 Hz, 2H), 7.24 (d, $^3J_{H,H}$ = 8.6 Hz, 2H), 7.13 (dd, $^3J_{H,H}$ = 7.3 Hz, $^3J_{H,H}$ = 7.3 Hz, 2H), 7.08 (d, $^3J_{H,H}$ = 7.3 Hz, 2H), 6.72 (d, $^3J_{H,H}$ = 8.6 Hz, 2H), 3.88 (s, 2H), 1.99 (s, 6H).

^{13}C-NMR (CDCl$_3$, 101 MHz) δ (ppm): 146.9, 140.7, 132.3, 132.0, 128.8, 123.7, 121.8, 119.5, 118.0, 114.3, 19.6.

MS (EI, 70 eV): m/z (%) = 286.1 (100), 287.0 (22.2).

HRMS (ESI): m/z calcd for $[C_{20}H_{19}N_2+H]^+$ 287.1543; found: 287.1541.

4-Carbazole-3,5-dimethylaniline (71)
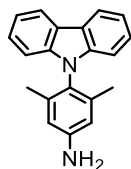
9-(2,6-Dimethyl-4- nitrophenyl)carbazole (**69**, 260 mg, 0.822 mmol, 1.0 eq.) yielded 4-carbazole-3,5-dimethylaniline (**71**, 221 mg, 0.772 mmol, 94 %) as slightly orange crystals after work up and was used without further purification.

138

¹H-NMR (CDCl₃, 400 MHz) δ (ppm): 8.16 (d, $^3J_{H,H}$ = 7.9 Hz, 2H), 7.38 (dd, $^3J_{H,H}$ = 7.7 Hz, $^3J_{H,H}$ = 7.7 Hz 2H), 7.26 (dd, $^3J_{H,H}$ = 7.6 Hz, $^3J_{H,H}$ =7.6 Hz, 2H), 6.99 (d, $^3J_{H,H}$ = 8.0 Hz, 2H), 6.57 (s, 2H), 3.75 (s, 2H), 1.75 (s, 6H).

¹³C-NMR (CDCl₃, 101 MHz) δ (ppm): 146.6, 141.0, 139.2, 126.0, 125.5, 122.9, 120.4, 119.3, 114.9, 109.7, 17.7.

MS (EI, 70 eV): m/z (%) = 286.1 (100), 287.1 (21.2).

HRMS (ESI): m/z calcd for $[C_{20}H_{19}N_2+H]^+$ 287.1543; found: 287.1543.

3,6-Bis(trifluoromethyl)-9-(3,5-dimethylaniline)carbazole (91)
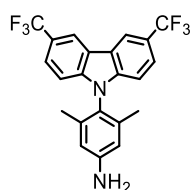
3,6-Bis(trifluoromethyl)-9-(2,6-dimethyl-4-nitrophenyl)carbazole (**88**, 530 mg, 1.17 mmol, 1.0 eq.) yielded after purification by column chromatography (SiO₂, cyclohexane / toluene, 1:1 + 5 % TEA) 3,6-bis(trifluoromethyl)-9-(3,5-dimethylaniline)carbazole (**91**, 454 mg, 1.07 mmol, 92%) as light brownish solid.

¹H-NMR (CDCl₃, 400 MHz) δ (ppm): 8.48 - 8.47 (m, 2H), 7.69 - 7.66 (m, 2H), 7.13 - 7.10 (m, 2H), 6.59 (s, 2H), 3.86 (s, 2H), 1.73 (s, 6H).

¹³C-NMR (CDCl₃, 101 MHz) δ (ppm): 147.4, 143.2, 138.7, 125.2 (q, $^1J_{F,H}$ = 272.5 Hz, 2C), 123.9, 123.9 (q, $^3J_{F,H}$ = 3.8 Hz, 2C), 122.7 (q, $^2J_{F,H}$ = 32.2 Hz, 2C), 122.2, 118.5 (q, $^3J_{F,H}$ = 4.2 Hz, 2C), 115.0, 110.3, 17.6.

¹⁹F-NMR (CDCl₃, 377 MHz) δ (ppm): -60.3.

MS (EI, 70 eV): m/z (%) = 422 (100), 423 (23), 421 (11).

HRMS (ESI): m/z calcd for $[C_{22}H_{16}F_6N_2+H]^+$ 423.1290; found: 423.1294.

2,7-Bis(trifluoromethyl)-9-(3,5-dimethylaniline)carbazole (92)
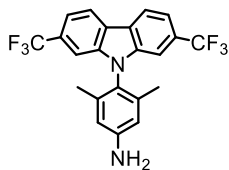
2,7-Bis(trifluoromethyl)-9-(2,6-dimethyl-4-nitrophenyl)carbazole (**89**, 230 mg, 0.508 mmol, 1.0 eq.) afforded 2,7-bis(trifluoromethyl)-9-(3,5-dimethylaniline)carbazole (**92**, 199 mg, 0.47 mmol, 93 %) after purification by column chromatography (SiO$_2$, cyclohexane / toluene 1:1) as light brownish oil, which solidified upon standing.

^{1}H-NMR (CDCl$_3$, 400 MHz) δ (ppm): 8.29 - 8.27 (m, 2H), 7.57 - 7.55 (m, 2H), 7.30 - 7.29 (m, 2H), 6.61 - 6.60 (m, 2H), 3.85 (s, 2H), 1.74 (s, 6H).

^{13}C-NMR (CDCl$_3$, 101 MHz) δ (ppm): 147.4, 141.3, 138.8, 129.3 (q, $^2J_{F,C}$ = 32.1 Hz, 2C), 124.8 (q, $^1J_{F,C}$ = 272.3 Hz, 2C), 124.5, 123.6, 121.6, 116.8 (q, $^3J_{F,C}$ = 3.6 Hz, 2C), 115.1, 107.3 (q, $^3J_{F,C}$ = 4.3 Hz, 2C), 17.6.

^{19}F-NMR (CDCl$_3$, 377 MHz) δ (ppm): -61.0

MS (EI, 70 eV): m/z (%) = 423 (32), 422 (100), 421 (12), 353 (17), 211 (13), 120 (17).

HRMS (ESI): m/z calcd for [C$_{22}$H$_{16}$F$_6$N$_2$+H]$^+$ 423.1490; found: 423.1293.

2,7-Dimethoxy-9-(3,5-dimethylaniline)carbazole (93)
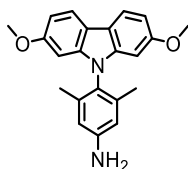
2,7-Dimethoxy-9-(2,6-dimethyl-4-nitrophenyl)carbazole (**90**, 482 mg, 1.28 mmol, 1.0 eq.) afforded 2,7-dimethoxy-9-(3,5-dimethylaniline)carbazole (**93**, 429 mg, 1.24 mmol, 97 %) as light brownish solid after purification by column chromatography (SiO$_2$, cyclohexane / toluene 1:1 + 5 % TEA).

140

¹H-NMR (CDCl₃, 400 MHz) δ (ppm): 7.90 (d, $^3J_{H,H}$ = 8.5 Hz, 1H), 6.83 (dd, $^3J_{H,H}$ = 8.5, $^4J_{H,H}$ = 2.3 Hz, 1H), 6.57 (s, 1H), 6.40 (d, ^4J = 2.3 Hz, 1H), 3.79 (s, 6H), 3.76 (s, 2H), 1.78 (s, 6H).

¹³C-NMR (CDCl₃, 101 MHz) δ (ppm): 158.6, 146.6, 142.5, 139.1, 125.3, 120.2, 117.0, 115.0, 107.8, 93.8, 77.2, 55.8, 17.8.

MS (EI, 70 eV): m/z (%) = 347 (24), 346 (100), 332 (11), 331 (49), 173 (17).

HRMS (ESI): m/z calcd for $[C_{22}H_{22}N_2O_2+H]^+$ 347.1754; found: 347.1755.

Representative procedure of Sandmeyer reaction (Method A) (72 and 73)

9-(4-iodophenyl)-1,8-dimethylcarbazole (72)

Boron trifluoride etherate (0.93 mL, 7.33 mmol, 4.2 eq.) was placed into an argon flushed oven dried two-necked round bottom flask at -30 °C. A solution of 4-(1,8-dimethylcarbazol)aniline (**70**, 500 mg, 1.75 mmol, 1.0 eq.) in THF (5 mL) was added drop wise an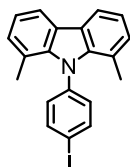d stirred for 20 min. Subsequently, a solution of tert-butyl nitrite (736 mg, 6.43 mmol, 3.7 eq.) in THF (5 mL) was added drop wise and the resulting mixture was allowed to warm to 0 °C. At -5 °C, diethyl ether (10 mL) was added, whereas the diazo salt participated out. The precipitation was filtered off and washed with diethyl ether. In a second flask, KI (412 mg, 2.48 mmol, 1.42 eq.) and iodine (311 mg, 1.22 mmol, 0.7 eq.) were dissolved in acetonitrile (7.5 mL). The diazo salt was added in one portion at 0 °C, the reaction mixture was warmed to room temperature and stirred for 30 min. Afterwards, the black reaction mixture was quenched with sat. aq. Na₂S₂O₃ solution. The product was extracted with ethyl acetate, dried over MgSO₄ and concentrated under reduced pressure. After purification by column chromatography (SiO₂, cyclohexane / DCM 4:1) 9-(4-iodophenyl)-1,8-dimethylcarbazole (**72**, 521 mg, 1.31 mmol, 75 %) was obtained as white solid.

¹H-NMR (CDCl₃, 400 MHz) δ (ppm): 7.98 (d, $^3J_{H,H}$ = 7.3 Hz, 2H), 7.79 (d, $^3J_{H,H}$ = 7.4 Hz, 2H), 7.24 (dd, $^3J_{H,H}$ = 7.4 Hz, $^3J_{H,H}$ = 7,4 Hz, 2H), 7.09 (d, $^3J_{H,H}$ = 7.5 Hz, 2H), 1.93 (s, 6H).

13C-NMR (CDCl$_3$, 101 MHz) δ (ppm): 141.9, 140.4, 137.5, 133.2, 129.0, 124.1, 121.4, 120.1, 118.1, 94.2, 19.8.

MS (EI, 70 eV): m/z (%) = 397 (100), 398 (22), 254 (17).

EA: calcd for C$_{20}$H$_{16}$IN: C 60.47, H 4.06 N 3.53; found: C 60.56, H 4.26, N 3.86

9-(4-Iodo-2,6-dimethylphenyl)carbazole (73)
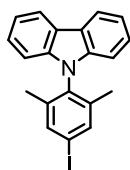
 4-Carbazole-3,5-dimethylaniline (**71**, 200 mg, 0.698 mmol, 1.0 eq.) yielded 9-(4-iodo-2,6-dimethylphenyl)carbazole (**73**, 219 mg, 0.551 mmol, 79 %) as white solid after purification by column chromatography (SiO$_2$, cyclohexane / dichloromethane 4:1).

1H-NMR (CDCl$_3$, 400 MHz) δ (ppm): 8.16 (d, $^3J_{H,H}$ = 7.8 Hz, 2H), 7.64 (s, 2H), 7.39 (dd, $^3J_{H,H}$ = 8.3 Hz, $^3J_{H,H}$ = 7.2 Hz, 2H), 7.28 (dd, $^3J_{H,H}$ = 8.1 Hz, $^3J_{H,H}$ = 7.3 Hz, 2H), 6.93 (d, $^3J_{H,H}$ = 8.1 Hz, 2H), 1.81 (s, 6H).

13C-NMR (CDCl$_3$, 101 MHz) δ (ppm): 140.5, 140.0, 137.7, 134.6, 126.1, 123.0, 120.5, 119.7, 109.3, 94.7, 17.2.

MS (EI, 70 eV): m/z (%) = 397 (100), 268 (34), 255 (68), 254 (60), 127(24).

EA: calcd for C$_{20}$H$_{16}$IN: C 60.47, H 4.06 N 3.53; found: C 61.01, H 4.31, N 3.78.

Representative procedure of Sandmeyer reaction (Method B) (94 and 95):

3,6-Bis(trifluoromethyl)-9-(4-iodo-2,6-dimethylphenyl)carbazole (94)

BF$_3$ diethyletherate (76.0 µL, 0.616 mmol, 2.0 eq.) was placed into an argon flushed oven dried two-necked round bottom flask at - 10°C. 3,6-Bis(trifluoromethyl)-9-(3,5-dimethylaniline)carbazole (**91**, 130 mg, 0.308 mmol, 1.0 eq.) was dissolved in dichlorom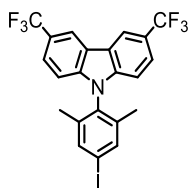ethane (5 mL) and added drop wise to the cooled flask. Subsequently, ^{t}butyl nitrite (61.6 µl, 0.462 mmol, 1.5 eq.) dissolved in dichloromethane (1 mL) and was added carefully via syringe to the beige suspension. Resulting mixture was stirred at 0 °C for 1 h, followed by the addition of potassium iodide (72.3 mg, 0.431 mmol, 1.4 eq.) and iodine (54.8 mg, 0.216 mmol, 0.7 eq.) in one portion. The reaction mixture was lead to warm up over 4 h and was diluted with water (20 mL) and dichloromethane (30 mL). Extraction with dichloromethane (2 x 30 mL), drying over MgSO$_4$ and concentration under reduced pressure afforded a brown product. Further purification by column chromatography (SiO$_2$, cyclohexane / dichloromethane 10:1) yielded 3,6-bis(trifluoromethyl)-9-(4-iodo-2,6-dimethylphenyl)carbazole (**94**, 148 mg, 0.278 mmol, 90 %) as white solid.

^{1}H-NMR (CDCl$_3$, 400 MHz) δ (ppm): 8.51 - 8.49 (m, 2H), 7.72 - 7.70 (m, 4H), 7.08 - 7.06 (m, 2H) 1.82 (s, 6H) ppm.

^{13}C-NMR (CDCl$_3$, 101 MHz) δ (ppm): 142.3, 140.1, 138.2, 133.3, 125.1 (q, $^1J_{F,C}$ = 271.5 Hz, 2C), 124.2 (q, $^3J_{F,C}$ = 3.6 Hz, 2C), 123.1 (q, $^2J_{F,C}$ = 32.4 Hz, 2C) 122.4, 118.7 (q, $^3J_{F,C}$ = 4.1 Hz, 2C), 110.1, 95.9, 17.2.

^{19}F-NMR (CDCl$_3$, 377 MHz) δ (ppm): -60.4.

MS (EI, 70 eV): m/z (%) = 534 (21), 533 (100), 391 (12), 337 (15) 336 (18).

2,7-Bis(trifluoromethyl)-9-(4-iodo-2,6-dimethylphenyl)carbazole (95)
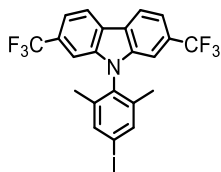
2,7-Bis(trifluoromethyl)-9-(3,5-dimethylaniline)carbazole (**92**, 223 mg, 0.528 mmol, 1.0 eq.) afforded after purification by column chromatography (SiO$_2$, cyclohexane / DCM 10:1) 2,7-bis(trifluoromethyl)-9-(4-iodo-2,6-dimethylphenyl)carbazole (**95**, 230 mg, 0.431 mmol, 82 %) as white solid.

^{1}H-NMR (CDCl$_3$, 400 MHz) δ (ppm): 8.31 - 8.29 (m, 2H), 8.71 (m, 2H), 7.61 - 7.59 (m, 2H), 7.23 - 7.22 (m, 2H), 1.81 (s, 6H).

^{13}C-NMR (CDCl$_3$, 101 MHz) δ (ppm): 140.4, 140.1, 138.4, 133.1, 129.6 (q, $^2J_{F,C}$ = 32.2 Hz, 2C), 124.7, 124.6 (q, $^1J_{F,C}$ = 272.4 Hz, 2C), 121.8, 117.4 (q, $^3J_{F,C}$ = 3.8 Hz, 2C), 107.0 (q, $^3J_{F,C}$ = 4.3 Hz, 2C), 96.0, 17.2.

^{19}F-NMR (CDCl$_3$, 377 MHz) δ (ppm): -61.1.

MS (EI, 70 eV): m/z (%) = 534 (23), 533 (100), 391 (13), 390 (17), 337 (26), 336 (27), 77 (11).

EA: calcd for C$_{22}$H$_{14}$F$_6$IN: C 49.55, H 2.65 N 2.63; found: C 49.83, H 3.20, N 3.12.

2,7-Dimethoxy-9-(4-iodo-2,6-dimethylphenyl)carbazole (96)
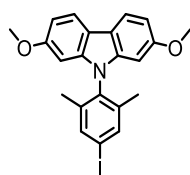
2,7-Dimethoxy-9-(3,5-dimethylaniline)carbazole (**93**, 214 mg, 0.618 mmol, 1.0 eq.) was added to a solution of *p*-TsOH · H_2O (356 mg, 1.85 mmol, 3.0 eq.) in acetonitrile (2.5 mL). The resulting suspension was kept at 10 °C, while a solution of $NaNO_2$ (87 mg, 1.85 mmol, 2.0 eq.) and KI (259 mg, 1.54 mmol 2.5 eq.) in H_2O (0.5 ml) was added drop wise. The reaction mixture was stirred for 10 min. at 10 °C and was than warmed up and stirred for another 2 h at room temperature. The reaction mixture was diluted with water (10 mL) followed by 1 M aq. $NaHCO_3$ until pH 10 was reached. The solution was extracted with ethyl acetate (3 x 20 mL). The combined organic layers were washed extensively with aq. sat. $Na_2S_2O_3$ solution, dried over $MgSO_4$ and concentrated under reduced pressure. The crude product was purified by column chromatography (SiO_2, cyclohexane / toluene, 2:1) yielding 2,7-dimethoxy-9-(4-iodo-2,6-dimethylphenyl)carbazole (**96**, 234 mg, 512 mmol, 83 %) as white solid.

^{1}H-NMR (CDCl$_3$, 400 MHz) δ (ppm): 7.91 (d, $^3J_{H,H}$ = 8.5 Hz, 2H), 7.64 (s, 2H), 6.86 (dd, $^3J_{H,H}$ = 8.5, $^4J_{H,H}$ = 2.3 Hz, 2H), 6.33 (d, $^4J_{H,H}$ = 2.3 Hz, 2H), 3.80 (s, 6H), 1.85 (s, 6H).

^{13}C-NMR (CDCl$_3$, 101 MHz) δ (ppm): 158.7, 141.6, 140.7, 137.9, 134.6, 120.5, 117.2, 108.2, 94.9, 93.7, 55.9, 17.4.

MS (EI, 70 eV): m/z (%) = 458 (25), 457 (100), 442 (36), 330 (13), 272 (10), 228 (11), 121 (11).

HRMS (ESI): m/z calcd for [C$_{22}$H$_{20}$INO$_2$+H]$^+$ 458.0611; found: 458.0602.

Representative procedure of borylation reaction

3,6-Bis(trifluoromethyl)-9-(4-(5,5-dimethyl-1,3,2-dioxaborinan-2-yl)-2,6-dimethylphenyl)carbazole
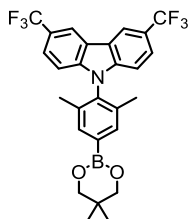
3,6-Bis(trifluoromethyl)-9-(4-iodo-2,6-dimethylphenyl)carbazole (**94**, 50.0 mg, 93.4 µmol, 1.0 eq.) was placed in an oven dried argon flushed Schlenk flask and dissolved in THF (1 mL) and cooled to -10 °C. Turbo Grignard (78.7 µL, 0.102 mmol, 1.1 eq.) was added drop wise and conversion was followed by GC/MS. After full conversion, the addition of triisopropyl borate (25.8 µL, 0.112 mmol, 1.2 eq.) yielded in a milky solution, which was stirred for 2 h at room temperature. Neopentyl glycol (12.7 mg, 0.121 mmol, 1.3 eq.) was added in one portion, solution turned slowly clear and was stirred for 12 h at room temperature. Reaction was quenched with aq. sat. NH₄Cl (5 mL), diluted with water (5 mL) and extracted with ethyl acetate. Combined organic layers were dried over MgSO₄, filtered over a small silica pad and concentrated, yielding crude 3,6-bis(trifluoromethyl)-9-(4-(5,5-dimethyl-1,3,2-dioxaborinan-2-yl)-2,6-dimethylphenyl)carbazole, which was used for the following coupling without further purification.

¹H-NMR (CDCl₃, 400 MHz) δ (ppm): 8.49 - 8.48 (m, 2H), 7.74 - 7.73 (m, 2H), 7.69 - 7.66 (m, 2H), 7.05 - 7.03 (m, 2H), 3.84 (s, 4H), 1.84 (s, 6H), 1.09 (s, 6H).

2,7-Bis(trifluoromethyl)-9-(4-(5,5-dimethyl-1,3,2-dioxaborinan-2-yl)-2,6-dimethylphenyl)carbazole
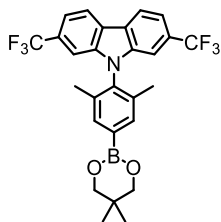
2,7-Bis(trifluoromethyl)-9-(4-iodo-2,6-dimethylphenyl)carbazole (**95**, 87.0 mg, 0.163 mmol, 1.0 eq.) yielded crude 2,7-bis(trifluoromethyl)-9-(4-(5,5-dimethyl-1,3,2-dioxaborinan-2-yl)-2,6-dimethylphenyl)carbazole.

¹H-NMR (CDCl₃, 400 MHz) δ (ppm): 8.31 - 8.29 (m, 2H), 7.76 (m, 2H), 7.58 - 7.56 (m, 2H), 7.22 - 7.21 (m, 2H), 3.85 (s, 4H), 1.84 (s, 6H), 1.09 (s, 6H).

2,7-Dimethoxy-9(4-(5,5-dimethyl-1,3,2-dioxaborinan-2-yl)-2,6-dimethylphenyl)carbazole
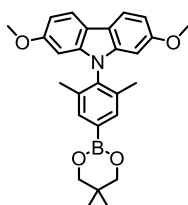
2,7-Dimethoxy-9-(4-iodo-2,6-dimethylphenyl)carbazole (**96**, 75.0 mg, 164 µmol, 1.0 eq.) yielded crude 2,7-dimethoxy-9(4-(5,5-dimethyl-1,3,2-dioxaborinan-2-yl)-2,6-dimethylphenyl) carbazole.

¹H-NMR (CDCl₃, 400 MHz) δ (ppm): 7.91 (d, $^3J_{H,H}$ = 8.5 Hz, 2H), 7.70 (s, 2H), 6.84 (dd, $^3J_{H,H}$ = 8.5, $^4J_{H,H}$ = 2.3 Hz, 2H), 6.32 (d, $^4J_{H,H}$ = 2.3 Hz, 2H), 3.84 (s, 4H), 3.76 (s, 6H), 1.89 (s, 6H), 1.08 (s, 6H).

Representative procedure of homo-coupling reaction (59 and 60)

4,4'-Di(1,8-dimethylcarbazole)1,1'-biphenyl (59)
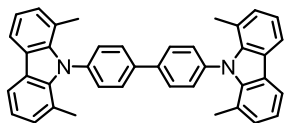
9-(4-Iodophenyl)-1,8-dimethylcarbazole (**72**, 155 mg, 0.391 mmol, 1.0 eq.) and THF (3 mL) was added into a dry Schlenk flask under argon atmosphere. The solution was cooled to -10 °C and turbo Grignard (1.3 M, 0.331 mL, 0.469 mmol, 1.1 eq.) was added. After 1 h, the ice bath was removed and TEMPO (124 mg, 0.777 mmol, 2.0 eq.) was added. The mixture was stirred 1 h at room temperature while a white solid participated. The reaction was quenched with sat. aq. NH$_4$Cl solution. THF was distilled off under reduced pressure and the residue was extracted with dichloromethane. The combined organic layers were dried over MgSO$_4$, filtered and concentrated under reduced pressure. The crude product was purified by column chromatography (SiO$_2$, cyclohexane / dichloromethane 5:1) providing 4,4'-di(1,8-dimethylcarbazole)1,1'-biphenyl (**59**, 101 mg, 0.187 mmol, 96 %) as a white solid.

^{1}H-NMR (CDCl$_3$, 400 MHz) δ (ppm): 8.05 (d, $^3J_{H,H}$ = 7.7 Hz, 4H), 7.85 (d, $^3J_{H,H}$ = 8.3 Hz, 4H), 7.67 (d, ^3J_H8.5, $^4J_{H,H}$ = 2.3 Hz, 2H), 6.33 (d, $^4J_{H,H}$ = 2.3 Hz, 2H), 3.80 (s, 6H), 1.85 (s, 6H).

^{13}C-NMR (CDCl$_3$, 101 MHz) δ (ppm): 141.7, 140.6, 140.4, 131.9, 128.9, 126.8, 124.0, 121.6, 119.9, 118.1, 19.8.

MS (Maldi-TOF): m/z (%) = 540.4 (100), 331.3(8), 310.3 (17).

EA: calcd for C$_{40}$H$_{32}$N$_2$: C 88.85, H 5.97 N 5.18; found: C 88.54, H 6.23, N 5.51.

4,4'-Dicarbazole-3,3'-5,5'tetramethyl-biphenyl (60)
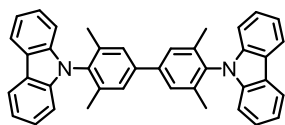
9-(4-Iodo-2,6-dimethylphenyl)carbazole (**73**, 151 mg, 0.378 mmol, 1.0 eq.) afforded 4,4'-dicarbazole-3,3'-5,5'tetramethyl-biphenyl (**60**, 99 mg, 0.183 mmol, 96 %) as a white solid after purification by column chromatography (SiO$_2$, cyclohexane / DCM 5:1).

^{1}H-NMR (CDCl$_3$, 400 MHz) δ (ppm): 8.24 (d, $^3J_{H,H}$ = 7.9 Hz, 4H), 7.62 (s, 4H), 7.46 (dd, $^3J_{H,H}$ = 8.2 Hz, $^3J_{H,H}$ = 7.1 Hz, 4H), 7.34 (dd, $^3J_{H,H}$ = 8.0 Hz, $^3J_{H,H}$ = 7.1 Hz, 4H), 7.07 (d, $^3J_{H,H}$ = 8.1 Hz, 4H), 2.00 (s, 12H).

^{13}C-NMR (CDCl$_3$, 101 MHz) δ (ppm): 140.9, 140.3, 138.6, 134.1, 127.5, 126.0, 123.0, 120.48, 119.5, 109.5, 17.8.

MS (Maldi-TOF): m/z (%) = 540.4 (100), 310.3 (7), 268.3 (20).

EA: calcd for C$_{40}$H$_{32}$N$_2$: C 88.85, H 5.97 N 5.18; found: C 87.49, H 6.28, N 5.32.

Representative procedure of Suzuki-Miyaura reaction (61 - 63)

Bis(3,6-bis(trifluoromethyl)-9,9'-(3,3',5,5'-tetramethyl-[1,1'-biphenyl]-4,4'-diyl)-carbazole) (61)
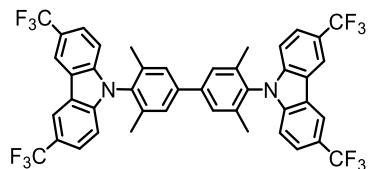
3,6-Bis(trifluoromethyl)-9-(4-iodo-2,6-dimethylphenyl)carbazole (**94**, 44.6 mg, 83.7 μmol, 0.9 eq.), potassium phosphate (40.3 mg, 0.186 mmol, 2.0 eq.) and 3,6-bis(trifluoromethyl)-9-(4-(5,5-dimethyl-1,3,2-dioxaborinan-2-yl)-2,6-dimethylphenyl)carbazole (48.3 mg, 93 μmol, 1.0 eq.) were suspended in THF / water (1 ml, 20:1) and the suspension was degassed for 20 minutes with argon. Subsequently, SPhos Pd G2 (1.34 mg, 1.86 μmol, 0.02 eq.) was added and reaction mixture was stirred at 70 °C for 12 h. After cooling to room temperature, the reaction mixture was diluted with water (5 mL) and ethyl acetate (5 mL). The crude product was extracted with ethyl acetate (2 x 5mL), the combined organic layers were washed with brine and dried over MgSO$_4$. After the solvent was evaporated, crude product was purified by column chromatography (SiO$_2$, cyclohexane / dichloromethane, 10:1) affording bis(3,6-bis(trifluoromethyl)-9,9'-(3,3',5,5'-tetramethyl-[1,1'-biphenyl]-4,4'-diyl)-carbazole) (**61**, 70 mg, 86.1 μmol, 93 % over two steps) as white solid.

^{1}H-NMR (CDCl$_3$, 400 MHz) δ (ppm): 8.54 (s, 4H), 7.75 - 7.72 (m, 4H), 7.62 (s, 4H), 7.17 - 7.15 (m, 4H), 1.97 (s, 12H).

^{13}C-NMR (CDCl$_3$, 101 MHz) δ (ppm): 42.6, 141.7, 138.5, 133.1, 128.1, 125.1 (q, $^1J_{F,C}$ = 271.5 Hz, 2C), 124.1 (q, $^2J_{F,C}$ = 3.3 Hz), 123.1 (q, $^2J_{F,C}$ = 32.3 Hz, 2C), 122.5, 118.7 (q, $^3J_{F,C}$ = 3.9 Hz, 2C), 110.3, 17.8.

^{19}F-NMR (CDCl$_3$, 377 MHz) δ (ppm): -60.3.

MS (Maldi-TOF): m/z (%) = 812.6 (30), 444.8 (100).

Bis(2,7-bis(trifluoromethyl)-9,9'-(3,3',5,5'-tetramethyl-[1,1'-biphenyl]-4,4'-diyl)carbazole (62)
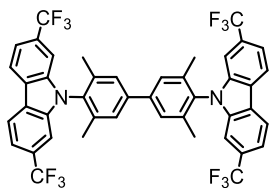
2,7-Bis(trifluoromethyl)-9-(4-iodo-2,6-dimethylphenyl)carbazole (**95**, 78.2 mg, 0.147 mmol, 0.9 eq) afforded bis(2,7-bis(trifluoromethyl)-9,9'-(3,3',5,5'-tetramethyl-[1,1'-biphenyl]-4,4'-diyl) carbazole (**62**, 125 mg, 0.154 mmol, 95 % over two steps) as white solid after column chromatography (SiO$_2$, cyclohexane / dichloromethane, 10:1).

^{1}H-NMR (CDCl$_3$, 400 MHz) δ (ppm): 8.35 (d, $^3J_{H,H}$ = 8.2 Hz, 4H), 7.67 (s, 4H), 7.62 (dd, $^3J_{H,H}$ = 8.2, $^4J_{H,H}$ = 1.6 Hz, 4H), 7.34 (d, $^4J_{H,H}$ = 1.6 Hz, 4H), 1.98 (s, 12H).

^{13}C-NMR (CDCl$_3$, 101 MHz) δ (ppm): 141.8, 140.7, 138.4, 132.8, 129.6 (q, $^2J_{F,C}$ = 32.3 Hz, 2C), 128.4, 124.8, 124.7 (q, $^1J_{F,C}$ = 272.3 Hz, 2C), 121.8, 117.2 (q, $^3J_{F,C}$ = 3.5 Hz, 2C), 107.3 (q, $^2J_{F,C}$ = 4.4 Hz, 2C), 17.9.

^{19}F-NMR (CDCl$_3$, 377 MHz) δ (ppm): -61.1.

MS (Maldi-TOF): m/z (%) = 812.2 (24), 444.6 (100).

EA: calcd for C$_{44}$H$_{28}$F$_{12}$N$_2$: C 65.03, H 3.47 N 3.45; found: C 63.23, H 3.81, N 3.54.

Bis(2,7-dimethoxy-9,9'-(3,3',5,5'-tetramethyl-[1,1'-biphenyl]-4,4'-diyl)carbazole) (63)
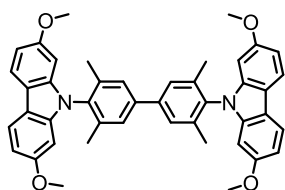
2,7-Dimethoxy-9-(4-iodo-2,6-dimethylphenyl)carbazole (**96**, 65.9 mg, 0.14 mmol, 0.9 eq.) yielded bis(2,7-dimethoxy-9,9'-(3,3',5,5'-tetramethyl-[1,1'-biphenyl]-4,4'-diyl)carbazole) (**63**, 102 mg, 0.154 mmol, 97 % over two steps) as white solid after purification by column chromatography (SiO$_2$, cyclohexane / ethyl acetate 1:10).

^{1}H-NMR (CDCl$_3$, 400 MHz) δ (ppm): 7.95 (d, $^3J_{H,H}$ = 8.5 Hz, 1H), 7.61 (s, 1H), 6.89 (dd, $^3J_{H,H}$ = 8.5, $^4J_{H,H}$ = 2.3 Hz, 1H), 6.44 (d, $^4J_{H,H}$ = 2.3 Hz, 1H), 3.82 (s, 6H), 2.01 (6H).

^{13}C-NMR (CDCl$_3$, 101 MHz) δ (ppm): 58.7, 141.9, 141.0, 138.7, 134.1, 127.7, 120.5, 117.3, 107.9, 94.0, 77.2, 55.9, 18.0.

HRMS (ESI): m/z calcd for [C$_{44}$H$_{40}$N$_2$O$_4$+H]$^+$ 661.3061; found: 661.3055.

Bibliography

[1]   E. Lörtscher, J. W. Ciszek, J. Tour, H. Riel, *Small* **2006**, *2*, 973–977.

[2]   Y. Tao, C. Yang, J. Qin, *Chem. Soc. Rev.* **2011**, *40*, 2943–2970.

[3]   R. J. Holmes, S. R. Forrest, Y.-J. Tung, R. C. Kwong, J. J. Brown, S. Garon, M. E. Thompson, *Appl. Phys. Lett.* **2003**, *82*, 2422–2424.

[4]   M. Gantenbein, M. Hellstern, L. Le Pleux, M. Neuburger, M. Mayor, *Chem. Mater.* **2015**, *27*, 1772–1779.

[5]   T. Govindarajan, R. Shandas, *Polymers* **2014**, *6*, 2309–2331.

[6]   G. Wahl, P. B. Davies, R. F. Bunshah, B. A. Joyce, C. D. Bain, G. Wegner, M. Remmers, F. C. Walsh, K. Hieber, J.-E. Sundgren, et al., in *Ullmanns Encycl. Ind. Chem.* (Ed.: Wiley-VCH Verlag GmbH & Co. KGaA), Wiley-VCH Verlag GmbH & Co. KGaA, Weinheim, Germany, **2000**.

[7]   A. Ulman, *Chem. Rev.* **1996**, *96*, 1533–1554.

[8]   J. C. Love, L. A. Estroff, J. K. Kriebel, R. G. Nuzzo, G. M. Whitesides, *Chem. Rev.* **2005**, *105*, 1103–1170.

[9]   C. D. Bain, G. M. Whitesides, *Science* **1988**, *240*, 62–63.

[10]   G. E. Poirier, E. D. Pylant, *Science* **1996**, *272*, 1145–1148.

[11]   P. E. Laibinis, G. M. Whitesides, D. L. Allara, Y. T. Tao, A. N. Parikh, R. G. Nuzzo, *J. Am. Chem. Soc.* **1991**, *113*, 7152–7167.

[12]   M. M. Walczak, C. Chung, S. M. Stole, C. A. Widrig, M. D. Porter, *J. Am. Chem. Soc.* **1991**, *113*, 2370–2378.

[13]   Z. Li, S.-C. Chang, R. S. Williams, *Langmuir* **2003**, *19*, 6744–6749.

[14]   M. A. White, J. A. Johnson, J. T. Koberstein, N. J. Turro, *J. Am. Chem. Soc.* **2007**, *129*, 4504–4504.

[15]   L. Zhang, R. He, H.-C. Gu, *Appl. Surf. Sci.* **2006**, *253*, 2611–2617.

[16]   C. Yee, G. Kataby, A. Ulman, T. Prozorov, H. White, A. King, M. Rafailovich, J. Sokolov, A. Gedanken, *Langmuir* **1999**, *15*, 7111–7115.

[17]   C. Haensch, S. Hoeppener, U. S. Schubert, *Chem. Soc. Rev.* **2010**, *39*, 2323.

[18]   N. Moitra, P. Trens, L. Raehm, J.-O. Durand, X. Cattoën, M. W. Chi Man, *J. Mater. Chem.* **2011**, *21*, 13476.

[19]   Y. Liu, J. Chen, A. V. Teplyakov, *Langmuir* **2012**, *28*, 15521–15528.

[20]   F. Tian, D. F. Taber, A. V. Teplyakov, *J. Am. Chem. Soc.* **2011**, *133*, 20769–20777.

[21]   Y. Liu, N. RamaRao, T. Miller, G. Hadjipanayis, A. V. Teplyakov, *J. Phys. Chem. C* **2013**, *117*, 19974–19983.

[22]   J. P. Collman, N. K. Devaraj, T. P. A. Eberspacher, C. E. D. Chidsey, *Langmuir* **2006**, *22*, 2457–2464.

[23]   A. A. Salman, T. Heidelberg, *J. Mater. Sci.* **2014**, *49*, 5388–5397.

[24]   H. C. Kolb, M. G. Finn, K. B. Sharpless, *Angew. Chem. Int. Ed.* **2001**, *40*, 2004–2021.

[25]   J. P. Guthrie, *Can. J. Chem.* **1978**, *56*, 962–973.

[26]   R. Huisgen, *Pure Appl. Chem.* **1989**, *61*, DOI 10.1351/pac198961040613.

[27]   R. Huisgen, G. Szeimies, L. M?bius, *Chem. Ber.* **1967**, *100*, 2494–2507.

[28]   W. H. Binder, R. Sachsenhofer, *Macromol. Rapid Commun.* **2007**, *28*, 15–54.

[29]   R. A. Evans, *Aust. J. Chem.* **2007**, *60*, 384.

[30]   F. Himo, T. Lovell, R. Hilgraf, V. V. Rostovtsev, L. Noodleman, K. B. Sharpless, V. V. Fokin, *J. Am. Chem. Soc.* **2005**, *127*, 210–216.

[31]   L. Liang, D. Astruc, *Coord. Chem. Rev.* **2011**, *255*, 2933–2945.

[32]   V. V. Rostovtsev, L. G. Green, V. V. Fokin, K. B. Sharpless, *Angew. Chem. Int. Ed.* **2002**, *41*, 2596–2599.

[33]   C. W. Tornøe, C. Christensen, M. Meldal, *J. Org. Chem.* **2002**, *67*, 3057–3064.

[34]   P. L. Golas, N. V. Tsarevsky, B. S. Sumerlin, K. Matyjaszewski, *Macromolecules* **2006**, *39*, 6451–6457.

[35]   D. V. Partyka, J. B. Updegraff, M. Zeller, A. D. Hunter, T. G. Gray, *Organometallics* **2007**, *26*, 183–186.

[36]   T. Lummerstorfer, H. Hoffmann, *J. Phys. Chem. B* **2004**, *108*, 3963–3966.

[37] J. K. Lee, Y. S. Chi, I. S. Choi, *Langmuir* **2004**, *20*, 3844–3847.

[38] R. Zirbs, F. Kienberger, P. Hinterdorfer, W. H. Binder, *Langmuir* **2005**, *21*, 8414–8421.

[39] D. I. Rozkiewicz, D. Ja?czewski, W. Verboom, B. J. Ravoo, D. N. Reinhoudt, *Angew. Chem. Int. Ed.* **2006**, *45*, 5292–5296.

[40] R. D. Rohde, H. D. Agnew, W.-S. Yeo, R. C. Bailey, J. R. Heath, *J. Am. Chem. Soc.* **2006**, *128*, 9518–9525.

[41] J.-C. Meng, C. Averbuj, W. G. Lewis, G. Siuzdak, M. G. Finn, *Angew. Chem. Int. Ed.* **2004**, *43*, 1255–1260.

[42] Y. Zhang, S. Luo, Y. Tang, L. Yu, K.-Y. Hou, J.-P. Cheng, X. Zeng, P. G. Wang, *Anal. Chem.* **2006**, *78*, 2001–2008.

[43] J. E. Moses, A. D. Moorhouse, *Chem Soc Rev* **2007**, *36*, 1249–1262.

[44] X.-L. Sun, C. L. Stabler, C. S. Cazalis, E. L. Chaikof, *Bioconjug. Chem.* **2006**, *17*, 52–57.

[45] P.-C. Lin, S.-H. Ueng, M.-C. Tseng, J.-L. Ko, K.-T. Huang, S.-C. Yu, A. K. Adak, Y.-J. Chen, C.-C. Lin, *Angew. Chem. Int. Ed.* **2006**, *45*, 4286–4290.

[46] A. Perols, M. Arcos Famme, A. Eriksson Karlström, *ChemBioChem* **2015**, *16*, 2522–2529.

[47] R. Echemendía, O. Concepción, F. E. Morales, M. W. Paixão, D. G. Rivera, *Tetrahedron* **2014**, *70*, 3297–3305.

[48] P. M. E. Gramlich, S. Warncke, J. Gierlich, T. Carell, *Angew. Chem. Int. Ed.* **2008**, *47*, 3442–3444.

[49] Y. Liu, C.-F. Ke, H.-Y. Zhang, J. Cui, F. Ding, *J. Am. Chem. Soc.* **2008**, *130*, 600–605.

[50] D. A. Fleming, C. J. Thode, M. E. Williams, *Chem. Mater.* **2006**, *18*, 2327–2334.

[51] H. J. Levinson, *Principles of Lithography*, SPIE Press, Bellingham, Wash, **2010**.

[52] P. G. M. Wuts, Ed. , in *Greenes Prot. Groups Org. Synth.*, John Wiley & Sons, Inc., Hoboken, New Jersey, **2014**, pp. 1194–1202.

[53] T. A. Gschneidtner, K. Moth-Poulsen, *Tetrahedron Lett.* **2013**, *54*, 5426–5429.

[54] S. M. Weinreb, G. A. Epling, R. Comi, M. Reitano, *J. Org. Chem.* **1975**, *40*, 1356–1358.

[55] K. Lam, I. E. Markó, *Org. Lett.* **2009**, *11*, 2752–2755.

[56] M. Platen, E. Stekhan, *Tetrahedron Lett.* **1980**, *21*, 511–514.

[57] W. S. Yeo, M. Mrksich, *Adv. Mater.* **2004**, *16*, 1352–1356.

[58] K. Kim, H. Yang, E. Kim, Y. B. Han, Y. T. Kim, S. H. Kang, J. Kwak, *Langmuir* **2002**, *18*, 1460–1462.

[59] R. C. Roemmele, H. Rapoport, *J. Org. Chem.* **1988**, *53*, 2367–2371.

[60] C. Goulaouic-Dubois, A. Guggisberg, M. Hesse, *J. Org. Chem.* **1995**, *60*, 5969–5972.

[61] H. J. Jung, H. Min, H. Yu, T. G. Lee, T. D. Chung, *Chem. Commun.* **2010**, *46*, 3863.

[62] J. Engels, *Angew. Chem. Int. Ed. Engl.* **1979**, *18*, 148–149.

[63] R. Zhang, M. Curreli, M. E. Thompson, *ACS Appl. Mater. Interfaces* **2011**, *3*, 4765–4769.

[64] C. Cai, A. Vasella, *Helv. Chim. Acta* **1995**, *78*, 732–757.

[65] A. G. Brook, *Acc. Chem. Res.* **1974**, *7*, 77–84.

[66] L. A. Carpino, S. A. Triolo, R. A. Berglund, *J. Org. Chem.* **1989**, *54*, 3303–3310.

[67] P. S. Guin, S. Das, P. C. Mandal, *Int. J. Electrochem.* **2011**, *2011*, 1–22.

[68] A. A. Kutyrev, *Tetrahedron* **1991**, *47*, 8043–8065.

[69] C. C. Nawrat, C. J. Moody, *Angew. Chem. Int. Ed.* **2014**, *53*, 2056–2077.

[70] L. F. Fieser, M. Fieser, *J. Am. Chem. Soc.* **1935**, *57*, 491–494.

[71] C. Frontana, Á. Vázquez-Mayagoitia, J. Garza, R. Vargas, I. González, *J. Phys. Chem. A* **2006**, *110*, 9411–9419.

[72] R. J. Payne, A. M. Daines, B. M. Clark, A. D. Abell, *Bioorg. Med. Chem.* **2004**, *12*, 5785–5791.

[73] S. Azuma, K. Nishio, K. Kubo, T. Sasamori, N. Tokitoh, K. Kuramochi, K. Tsubaki, *J. Org. Chem.* **2012**, *77*, 4812–4820.

[74] T. E. Long, X. Lu, M. Galizzi, R. Docampo, J. Gut, P. J. Rosenthal, *Bioorg. Med. Chem. Lett.* **2012**, *22*, 2976–2979.

[75] N. Van Tuyen, B. Kesteleyn, N. De Kimpe, *Tetrahedron* **2002**, *58*, 121–127.

[76] R. L. Nyland, M. Luo, M. R. Kelley, R. F. Borch, *J. Med. Chem.* **2010**, *53*, 1200–1210.

[77]   S. G. Mayhew, *Eur. J. Biochem.* **1978**, *85*, 535–547.

[78]   N. Gupta, H. Linschitz, *J. Am. Chem. Soc.* **1997**, *119*, 6384–6391.

[79]   V. Prezhdo, O. Prezhdo, E. Ovsiankina, *Spectrochim. Acta. A. Mol. Biomol. Spectrosc.* **1995**, *51*, 2465–2472.

[80]   Q.-L. Zhang, L.-C. Du, Y.-X. Weng, L. Wang, H.-Y. Chen, J.-Q. Li, *J. Phys. Chem. B* **2004**, *108*, 15077–15083.

[81]   C. Mao, H. Li, F. Cui, Q. Feng, C. Ma, *J. Mater. Chem.* **1999**, *9*, 2573–2582.

[82]   A. Tekiel, J. S. Prauzner-Bechcicki, S. Godlewski, J. Budzioch, M. Szymonski, *J. Phys. Chem. C* **2008**, *112*, 12606–12609.

[83]   U. Diebold, *Appl. Phys. Mater. Sci. Process.* **2003**, *76*, 681–687.

[84]   U. Diebold, *Surf. Sci. Rep.* **2003**, *48*, 53–229.

[85]   H. Alarcón, G. Boschloo, P. Mendoza, J. L. Solis, A. Hagfeldt, *J. Phys. Chem. B* **2005**, *109*, 18483–18490.

[86]   M. Jalali, R. S. Moakhar, A. Kushwaha, G. K. L. Goh, S. K. Sadrnezhaad, N. Riahi-Noori, *J. Appl. Electrochem.* **2015**, *45*, 831–838.

[87]   C. B. Aakeröy, M. Baldrighi, J. Desper, P. Metrangolo, G. Resnati, *Chem. - Eur. J.* **2013**, *19*, 16240–16247.

[88]   A. Krasovskiy, V. Krasovskaya, P. Knochel, *Angew. Chem. Int. Ed.* **2006**, *45*, 2958–2961.

[89]   M. Mayor, R. Scheffold, L. Walder, *Helv. Chim. Acta* **1997**, *80*, 1183–1189.

[90]   A. C. Cardiel, M. C. Benson, L. M. Bishop, K. M. Louis, J. C. Yeager, Y. Tan, R. J. Hamers, *ACS Nano* **2012**, *6*, 310–318.

[91]   R. Cinnsealach, G. Boschloo, S. Nagaraja Rao, D. Fitzmaurice, *Sol. Energy Mater. Sol. Cells* **1999**, *57*, 107–125.

[92]   F. Campus, P. Bonh?te, M. Gr?tzel, S. Heinen, L. Walder, *Sol. Energy Mater. Sol. Cells* **1999**, *56*, 281–297.

[93]   Q. Qu, H. Geng, R. Peng, Q. Cui, X. Gu, F. Li, M. Wang, *Langmuir* **2010**, *26*, 9539–9546.

[94]   N. Vlachopoulos, J. Nissfolk, M. M?ller, A. Brian?on, D. Corr, C. Grave, N. Leyland, R. Mesmer, F. Pichot, M. Ryan, et al., *Electrochimica Acta* **2008**, *53*, 4065–4071.

[95]   P. Bonhôte, E. Gogniat, F. Campus, L. Walder, M. Grätzel, *Displays* **1999**, *20*, 137–144.

[96]   E. L. Unger, S. J. Fretz, B. Lim, G. Y. Margulis, M. D. McGehee, T. D. P. Stack, *Phys Chem Chem Phys* **2015**, *17*, 6565–6571.

[97]   M. Felici, P. Contreras-Carballada, J. M. M. Smits, R. J. M. Nolte, R. M. Williams, L. De Cola, M. C. Feiters, *Molecules* **2010**, *15*, 2039–2059.

[98]   G. J. Kubas, B. Monzyk, A. L. Crumblis, in *Inorg. Synth.* (Ed.: R.J. Angelici), John Wiley & Sons, Inc., Hoboken, NJ, USA, **1990**, pp. 68–70.

[99]   T. R. Chan, R. Hilgraf, K. B. Sharpless, V. V. Fokin, *Org. Lett.* **2004**, *6*, 2853–2855.

[100] F. Doria, A. Oppi, F. Manoli, S. Botti, N. Kandoth, V. Grande, I. Manet, M. Freccero, *Chem Commun* **2015**, *51*, 9105–9108.

[101] S. Erten, Y. Posokhov, S. Alp, S. Icli, *Dyes Pigments* **2005**, *64*, 171–178.

[102] C. Röger, F. Würthner, *J. Org. Chem.* **2007**, *72*, 8070–8075.

[103] P. Allongue, M. Delamar, B. Desbat, O. Fagebaume, R. Hitmi, J. Pinson, J.-M. Savéant, *J. Am. Chem. Soc.* **1997**, *119*, 201–207.

[104] C. H. de Villeneuve, J. Pinson, M. C. Bernard, P. Allongue, *J. Phys. Chem. B* **1997**, *101*, 2415–2420.

[105] M. P. Stewart, F. Maya, D. V. Kosynkin, S. M. Dirk, J. J. Stapleton, C. L. McGuiness, D. L. Allara, J. M. Tour, *J. Am. Chem. Soc.* **2004**, *126*, 370–378.

[106] M.-C. Bernard, A. Chaussé, E. Cabet-Deliry, M. M. Chehimi, J. Pinson, F. Podvorica, C. Vautrin-Ul, *Chem. Mater.* **2003**, *15*, 3450–3462.

[107] F. Fagging, M. E. Hoff, S. Mazor, M. Shima, **1996**.

[108] Wgsimon, **n.d.**

[109] E. Leary, A. La Rosa, M. T. González, G. Rubio-Bollinger, N. Agraït, N. Martín, *Chem Soc Rev* **2015**, *44*, 920–942.

[110] C. Schubert, J. T. Margraf, T. Clark, D. M. Guldi, *Chem Soc Rev* **2015**, *44*, 988–998.

[111] L. D. A. Siebbeles, Ed. , *Charge and Exciton Transport through Molecular Wires*, Wiley-VCH, Weinheim, **2011**.

[112] R. L. McCreery, A. J. Bergren, *Adv. Mater.* **2009**, *21*, 4303–4322.

[113] A. Aviram, M. A. Ratner, *Chem. Phys. Lett.* **1974**, *29*, 277–283.

[114] R. M. Metzger, B. Chen, U. Höpfner, M. V. Lakshmikantham, D. Vuillaume, T. Kawai, X. Wu, H. Tachibana, T. V. Hughes, H. Sakurai, et al., *J. Am. Chem. Soc.* **1997**, *119*, 10455–10466.

[115] W.-Y. Lo, N. Zhang, Z. Cai, L. Li, L. Yu, *Acc. Chem. Res.* **2016**, *49*, 1852–1863.

[116] L. De Cola, C. Chiorboli, Eds. , *Molecular Wires: From Design to Properties*, Springer, Berlin ; New York, **2005**.

[117] D. K. James, J. M. Tour, in *Mol. Wires Electron.*, Springer Berlin Heidelberg, Berlin, Heidelberg, **2005**, pp. 33–62.

[118] D. M. Guldi, H. Nishihara, L. Venkataraman, *Chem Soc Rev* **2015**, *44*, 842–844.

[119] D. Vonlanthen, A. Mishchenko, M. Elbing, M. Neuburger, T. Wandlowski, M. Mayor, *Angew. Chem. Int. Ed.* **2009**, *48*, 8886–8890.

[120] D. Vonlanthen, A. Rudnev, A. Mishchenko, A. Käslin, J. Rotzler, M. Neuburger, T. Wandlowski, M. Mayor, *Chem. - Eur. J.* **2011**, *17*, 7236–7250.

[121] Q. Lu, K. Liu, H. Zhang, Z. Du, X. Wang, F. Wang, *ACS Nano* **2009**, *3*, 3861–3868.

[122] L.-J. Wang, A. Yong, K.-G. Zhou, L. Tan, J. Ye, G.-P. Wu, Z.-G. Xu, H.-L. Zhang, *Chem. - Asian J.* **2013**, *8*, 1901–1909.

[123] A. Shaporenko, M. Elbing, A. Błaszczyk, C. von Hänisch, M. Mayor, M. Zharnikov, *J. Phys. Chem. B* **2006**, *110*, 4307–4317.

[124] O. Possel, A. M. van Leusen, *Tetrahedron Lett.* **1977**, *18*, 4229–4231.

[125] S. Chandrasekhar, C. R. Reddy, B. N. Babu, *J. Org. Chem.* **2002**, *67*, 9080–9082.

[126] V. P. W. Böhm, W. A. Herrmann, *Eur. J. Org. Chem.* **2000**, *2000*, 3679–3681.

[127] P. Hrobárik, V. Hrobáriková, I. Sigmundová, P. Zahradník, M. Fakis, I. Polyzos, P. Persephonis, *J. Org. Chem.* **2011**, *76*, 8726–8736.

[128] P. Su, J. Wang, Y. Shi, X. Pan, R. Shao, J. Zhang, *Bioorg. Med. Chem.* **2015**, *23*, 3228–3236.

[129] M. M. Endeshaw, C. Li, J. de Leon, N. Yao, K. Latibeaudiere, K. Premalatha, N. Morrissette, K. A. Werbovetz, *Bioorg. Med. Chem. Lett.* **2010**, *20*, 5179–5183.

[130] T. Ishiyama, K. Ishida, N. Miyaura, *Tetrahedron* **2001**, *57*, 9813–9816.

[131] Y. C. Chen, G. S. Huang, C. C. Hsiao, S. A. Chen, *J. Am. Chem. Soc.* **2006**, *128*, 8549–8558.

[132] W. Helfrich, W. G. Schneider, *Phys. Rev. Lett.* **1965**, *14*, 229–231.

[133] C. W. Tang, S. A. VanSlyke, *Appl. Phys. Lett.* **1987**, *51*, 913.

[134] C. Adachi, *Jpn. J. Appl. Phys.* **2014**, *53*, 060101.

[135] B. Valeur, M. N. Berberan-Santos, *Molecular Fluorescence : Principles and Applications.*, Wiley-VCH ; Wiley, Distributor], Weinheim [Germany]; Chichester, England, **2012**.

[136] M. Klessinger, J. Michl, *Lichtabsorption und Photochemie organischer Moleküle*, VCH, Weinheim, **1990**.

[137] A. F. Rausch, H. H. H. Homeier, H. Yersin, in *Photophysics Organomet.* (Ed.: A.J. Lees), Springer Berlin Heidelberg, Berlin, Heidelberg, **2010**, pp. 193–235.

[138] B. Minaev, G. Baryshnikov, H. Agren, *Phys Chem Chem Phys* **2014**, *16*, 1719–1758.

[139] H. Yersin, *Transit. Met. Rare Earth Compd.* **2004**, 1–26.

[140] U. Giovanella, M. Pasini, C. Botta, in *Appl. Photochem. Light Meets Mol.* (Eds.: G. Bergamini, S. Silvi), Springer International Publishing, Cham, **2016**, pp. 145–196.

[141] M. G. Helander, G. E. Morse, J. Qiu, J. S. Castrucci, T. P. Bender, Z.-H. Lu, *ACS Appl. Mater. Interfaces* **2010**, *2*, 3147–3152.

[142] U. Mitschke, P. Bäuerle, *J. Mater. Chem.* **2000**, *10*, 1471–1507.

[143] B. Geffroy, C. Prat, *Polym. Int.* **2006**, *55*, 572–582.

[144] J.-H. Jou, S.-H. Peng, C.-I. Chiang, Y.-L. Chen, Y.-X. Lin, Y.-C. Jou, C.-H. Chen, C.-J. Li, W.-B. Wang, S.-M. Shen, et al., *J. Mater. Chem. C* **2013**, *1*, 1680–1686.

[145] Hartmut Yersin, *Highly Efficient OLEDs with Phosphorescent Materials*, WILEY-VCH Verlag GmbH & Co. KGaA, Weinheim, **2008**.

156

[146] J.-H. Jou, C.-J. Wang, Y.-P. Lin, Y.-C. Chung, P.-H. Chiang, M.-H. Wu, C.-P. Wang, C.-L. Lai, C. Chang, *Appl. Phys. Lett.* **2008**, *92*, 223504-223504–3.

[147] X. Gong, J. c. Ostrowski, D. Moses, G. c. Bazan, A. j. Heeger, *Adv. Funct. Mater.* **2003**, *13*, 439–444.

[148] Y. Sun, N. C. Giebink, H. Kanno, B. Ma, M. E. Thompson, S. R. Forrest, *Nature* **2006**, *440*, 908–912.

[149] J. Chen, F. Zhao, D. Ma, *Mater. Today* **2014**, *17*, 175–183.

[150] M.-H. Tsai, Y.-H. Hong, C.-H. Chang, H.-C. Su, C.-C. Wu, A. Matoliukstyte, J. Simokaitiene, S. Grigalevicius, J. V. Grazulevicius, C.-P. Hsu, *Adv. Mater.* **2007**, *19*, 862–866.

[151] L. Xiao, Z. Chen, B. Qu, J. Luo, S. Kong, Q. Gong, J. Kido, *Adv. Mater.* **2011**, *23*, 926–952.

[152] S. Tokito, T. Iijima, Y. Suzuri, H. Kita, T. Tsuzuki, F. Sato, *Appl. Phys. Lett.* **2003**, *83*, 569–571.

[153] J. He, H. Liu, Y. Dai, X. Ou, J. Wang, S. Tao, X. Zhang, P. Wang, D. Ma, *J. Phys. Chem. C* **2009**, *113*, 6761–6767.

[154] D. Sun, X. Zhou, H. Li, X. Sun, Z. Ren, D. Ma, S. Yan, *ACS Appl. Mater. Interfaces* **2015**, *7*, 17802–17810.

[155] S. Yin, Z. Shuai, Y. Wang, *J. Chem. Inf. Comput. Sci.* **2003**, *43*, 970–977.

[156] J. A. McEwan, A. J. Clulow, A. Nelson, N. R. Yepuri, P. L. Burn, I. R. Gentle, *ACS Appl. Mater. Interfaces* **2017**, *9*, 14153–14161.

[157] K. L. Woon, Z. A. Hasan, B. K. Ong, A. Ariffin, R. Griniene, S. Grigalevicius, S.-A. Chen, *RSC Adv* **2015**, *5*, 59960–59969.

[158] P. Schrögel, A. Tomkevičienė, P. Strohriegl, S. T. Hoffmann, A. Köhler, C. Lennartz, *J. Mater. Chem.* **2011**, *21*, 2266.

[159] P. Schrögel, N. Langer, C. Schildknecht, G. Wagenblast, C. Lennartz, P. Strohriegl, *Org. Electron.* **2011**, *12*, 2047–2055.

[160] K. S. Yook, J. Y. Lee, *Adv. Mater.* **2012**, *24*, 3169–3190.

[161] R. B. Bedford, M. Betham, *J. Org. Chem.* **2006**, *71*, 9403–9410.

[162] H. Jian, M. James, *J. Org. Chem.* **2003**, *68*, 5091–5103.

[163] G. Balz, G. Schiemann, *Berichte Dtsch. Chem. Ges. B Ser.* **1927**, *60*, 1186–1190.

[164] C. G. Swain, R. J. Rogers, *J. Am. Chem. Soc.* **1975**, *97*, 799–800.

[165] J. N. Moorthy, S. Saha, *Eur. J. Org. Chem.* **2009**, *2009*, 739–748.

[166] D. A. Watson, M. Su, G. Teverovskiy, Y. Zhang, J. Garcia-Fortanet, T. Kinzel, S. L. Buchwald, *Science* **2009**, *325*, 1661–1664.

[167] A. K. Flatt, Y. Yao, F. Maya, J. M. Tour, *J. Org. Chem.* **2004**, *69*, 1752–1755.

[168] C. Sambiagio, S. P. Marsden, A. J. Blacker, P. C. McGowan, *Chem. Soc. Rev.* **2014**, *43*, 3525–3550.

[169] G. V. Zyryanov, I. S. Kovalev, I. N. Egorov, V. L. Rusinov, O. N. Chupakhin, *Chem. Heterocycl. Compd.* **2011**, *47*, 571–574.

[170] Q. Wu, L. Wang, *Synthesis* **2008**, *2008*, 2007–2012.

[171] A. Krasovskiy, P. Knochel, *Angew. Chem. Int. Ed.* **2004**, *43*, 3333–3336.

[172] Y. Chang, C. Michelin, L. Bucher, N. Desbois, C. P. Gros, S. Piant, F. Bolze, Y. Fang, X. Jiang, K. M. Kadish, *Chem. - Eur. J.* **2015**, *21*, 12018–12025.

[173] B. R. Mullaney, A. L. Thompson, P. D. Beer, *Angew. Chem. Int. Ed.* **2014**, *53*, 11458–11462.

[174] G. E. Carr, R. D. Chambers, T. F. Holmes, D. G. Parker, *J. Chem. Soc. [Perkin 1]* **1988**, 921–926.

[175] M. M. Kremlev, A. I. Mushta, W. Tyrra, Y. L. Yagupolskii, D. Naumann, A. Möller, *J. Fluor. Chem.* **2012**, *133*, 67–71.

[176] W. C. P. Tsang, R. H. Munday, G. Brasche, N. Zheng, S. L. Buchwald, *J. Org. Chem.* **2008**, *73*, 7603–7610.

[177] B. A. Kamino, B. Mills, C. Reali, M. J. Gretton, M. A. Brook, T. P. Bender, *J. Org. Chem.* **2012**, *77*, 1663–1674.

[178] E. Krasnokutskaya, N. Semenischeva, V. Filimonov, P. Knochel, *Synthesis* **2007**, *2007*, 81–84.

[179] C.-Y. Liu, A. Gavryushin, P. Knochel, *Chem. – Asian J.* **2007**, *2*, 1020–1030.

[180] T. Koop, J. Bookhold, M. Shiraiwa, U. Pöschl, *Phys. Chem. Chem. Phys.* **2011**, *13*, 19238.

[181] S. M. Bonesi, R. Erra-Balsells, *J. Lumin.* **2001**, *93*, 51–74.

[182] S. Gong, X. He, Y. Chen, Z. Jiang, C. Zhong, D. Ma, J. Qin, C. Yang, *J Mater Chem* **2012**, *22*, 2894–2899.

[183] L. Deng, X. Wang, Z. Zhang, J. Li, *J. Mater. Chem.* **2012**, *22*, 19700–19708.

[184] G. Zotti, G. Schiavon, S. Zecchin, J.-F. Morin, M. Leclerc, *Macromolecules* **2002**, *35*, 2122–2128.

[185] Y. Zheng, A. S. Batsanov, V. Jankus, F. B. Dias, M. R. Bryce, A. P. Monkman, *J. Org. Chem.* **2011**, *76*, 8300–8310.

[186] G. W. Haggquist, H. Katayama, A. Tsuchida, S. Ito, M. Yamamoto, *J. Phys. Chem.* **1993**, *97*, 9270–9273.

[187] P. J. S. Gomes, C. Serpa, L. G. Arnaut, *J. Photochem. Photobiol. Chem.* **2006**, *184*, 228–233.

[188] J. F. Ambrose, R. F. Nelson, *J. Electrochem. Soc.* **1968**, *115*, 1159–1164.

[189] C. M. Cardona, W. Li, A. E. Kaifer, D. Stockdale, G. C. Bazan, *Adv. Mater.* **2011**, *23*, 2367–2371.

Appendix

Abbreviations

Å	Ångström
c	Speed of light
CAN	Ceric ammonium nitrate
CBP	4,4′-Bis(N-carbazolyl)-1,1′-biphenyl
CuAAC	Cu(I)-Catalyzed Azide-Alkynes Cycloaddition
CV	Cyclic voltammetry
CVD	Chemical vapor deposition
DMF	Dimethylformamide
DMSO	Dimethyl sulfoxide
DFT	Density functional theory
e	Electron charge
ε_a	Molar extinction coefficient of the acceptor
E°	Standard electrode potential
ε	Dielectric constant
ε_0	Dielectric constants of the vacuum
EDTA	Ethylenediaminetetraacetic acid
EIL	Electron injection layer
EML	Emission layer
ETL	Electron transporting layer
F_d	Fluorescent spectra of the donor
FTO	Fluorine-doped tin oxide
FIrpic	Bis((4,6-difluorophenyl)-pyridinato-N,C2)picolinate-iridium(III)
GCMS	Gas chromatography mass spectroscopy
h	Planck constant
HIL	Hole injection layer
HOMO	Highest occupied molecular orbital
HTL	Hole transporting layer
IC	Internal conversion

ICT	Intermolecular charge transfer
ISC	Intersystem crossing
ITO	Indium tin oxide
k_b	Boltzmann constant
λ	Wavelength
LUMO	Lowest unoccupied molecular orbital
K	Kelvin
MALDI	Matrix-assisted laser desorption/ionization
NDI	Naphthalene diimide
NMR	Nuclear magnetic resonance
OLED	Organic light emitting diode
Φ_F	Fluorescence quantum yields
PEG	Polyethylene glycol
PMDTA	Bis(2-dimethylaminoethyl)methylamine
PMHS	Polymethylhydrosiloxane
PVD	Physical vapor deposition
R_0	Characteristic Förster distance
RT	Room temperature
SAM	Self-assemble mono layer
SCE	Potassium chloride calomel electrode
T	Temperature
T_g	Glass transition temperature
TBTA	Tris(benzyltriazolylmethyl)amine
THF	Tetrahydrofuran
TLC	Thin layer chromatography
TMS	Trimethylsilane
TOF	Time of flight
TosMic	(Tolylsulfonyl)methyl isocyanide
UV-Vis	Ultraviolet–visible spectroscopy
V	Volt
Z	Atomic Number

Curriculum Vitae

Personal

Name	Manuel Hellstern
Place and date of birth	Basel / 1st December 1986
Citizenship	Swiss

Education

06/13 – 09/17	University of Basel **PhD in Organic Chemistry** Dissertation: Surface functionalization – a modular approach Supervisor: Prof. Dr. Marcel Mayor
09/10 – 03/13	University of Basel **Master of Science in Chemistry** Master thesis: Rotational restricted carbazole derivatives – towards high energy triplet state matrix materials Supervisor: Prof. Dr. Marcel Mayor
09/07 – 08/10	FHNW Muttenz **Bachelor of Molecular Life Science** Bachelor thesis: Steroid Hormones Modulate the ATPase Activity of the Cystic Fibrosis Transmembrane Conductance Regulator CFTR Supervisor: Prof. Dr. Beat Zehnder, Prof. Dr. Anna Seelig
08/05 – 08/06	GIB Liestal **Berufsmatura** (full-time)
08/02 – 08/05	Clariant Schweiz AG, Muttenz **Apprenticeship as chemical laboratory assistant**

Scientific contribution

Publication	New 4,4'-Bis(9-carbazolyl)–Biphenyl Derivatives with Locked Carbazole–Biphenyl Junctions: High-Triplet State Energy Materials, M. Gantenbein, M. Hellstern, L. Le Pleux, M. Neuenberger, M. Mayor, *Chem. Mater.*, **2015**, 27 (5), 1772.
	How Phosphorylation and ATPase Activity Regulate Anion Flux though the Cystic Fibrosis Transmembrane Conductance Regulator (CFTR), M. Zwick, C. Esposito, M. Hellstern, A. Seelig, *J. Biol. Chem,* **2016,** 291, 14483.
Presentation	SYMOLESCO meeting 2015 Engelberg, *Torsion angle dependent conductibility of extended biphenyl molecular rods*.
Poster presentation	Annual participation at the Regio Symposium, Fall Symposium und Swiss Snow Symposium.

Language

German	Native
English	Good
French	Basic knowledge

Leadership and supervision

Leadership	Supervision and teaching in the organic laboratory course for undergraduate chemistry, biology and pharmacy students.
	Organization, supervision and teaching of the organic laboratory course for nano students.
Supervision	Supervision and tutoring of two successfully completed master theses and three master practical courses.
	Schweizer Jugend Forscht, Boys@science week.